UNIVERSITY OF TRENTO - Italy
Department of Civil, Environmental
and Mechanical Engineering

Doctoral School in Civil, Environmental and Mechanical Engineering
Topic 1. Civil and Environmental Engineering - XXIX cycle 2014/2016

Doctoral Thesis - December 2017

Nadia Zorzi

Managing complexity in high-concentration flow modelling aimed at hazard assessment

Numerical and practical aspects

Supervisor
Giorgio Rosatti
DICAM Department of Civil, Environmental and
Mechanical Engineering, University of Trento

Credits of the cover image: Ernesto Sieff (2017), "Ruin in Val Bregaglia", Indian ink drawing

University of Trento
Doctoral School in Civil, Environmental and Mechanical Engineering
http://web.unitn.it/en/dricam
Via Mesiano 77, I-38123 Trento
Tel. +39 0461 282670 / 2611 - *dicamphd@unitn.it*

Abstract

High-concentration flows are complex phenomena typical of Alpine mountain areas. Essentially, they are free-surface flows with intense sediment transport, often caused by intense rainfall events and involving large volumes of solid material. Because of the amount of sediments moved, the intense erosion and deposition processes typically observed and the quite unexpected character, these phenomena represent a serious hazard in populated mountain areas, where reliable and effective hazard-management and -protection strategies are required.

In mountain-hazard management, high-concentration flows modelling represents a key factor, since it allows to evaluate impacts of possible hazard scenarios and the effectiveness of possible protection and mitigation measures. However, the intrinsic phenomenon complexity makes high-concentration flow modelling and hazard assessment quite challenging. In this thesis, some of the effects of high-concentration flow complexity on modelling are experienced directly and suitable solutions are proposed, to make the phenomenon description more reliable and straightforward.

Among very different modelling approaches present in the literature, this work embraced the quasi-two phase, mobile-bed approach proposed in Armanini et al. (2009b) and in Rosatti and Begnudelli (2013a), which is implemented in the TRENT2D model. TRENT2D is a quite sophisticated model that solves a system of Partial Differential Equations over a Cartesian mesh by means of a finite-volume method with Godunov-type fluxes.

By means of TRENT2D, the back-analysis of a couple of real debris-flow events occurred in Italy was first performed. These applications revealed clearly some troublesome "complexity issues", i.e. modelling issues generated by phenomenon complexity that may affect hazard assessment. Because of the public importance of the subject, four of the "complexity issues" identified were

then faced directly. According to the purpose of this thesis, possible solutions to the issues were proposed, to ensure a proper description of the flow behaviour and possibly limit intricacy in the model use.

The first complexity issue is "operational" and regards the use of the TRENT2D model and, more in general, the amount of work necessary to perform a complete hazard-assessment job about high-concentration flows. Because of the phenomenon complexity and the sophisticated character of the model, the operational chain necessary to assess hazard by means of TRENT2D appears quite demanding. The large efforts required in terms of hand-work, computational charge and resources may divert the user attention from the physical meaning of the hazard-assessment process, possibly leading to inaccurate results. To overcome this issue, a possible solution is proposed, based on the use of a loosely-coupled Service Oriented Architecture approach. The aim is to develop a unique, user-friendly working environment able to support high-quality, cost-effective hazard assessment and, in perspective, the possible development of a Decision Support System for mountain hazard.

The second complexity issue is "geometrical" and "numerical" and concerns morphology representation. Because of the strong interaction between high-concentration flows and bed morphology, these phenomena require bed morphology to be described with the right level of detail, especially where heterogeneity is outstanding. This is typically the case of urbanised mountain areas, with their characteristic terrain shapes, buildings, infrastructures, embankments and mitigation structures. A believable representation of these geometrical constraints may be fulfilled acting on the computational mesh used to solve model equations, preferably avoiding regular Cartesian meshes. In this work, a new version of the TRENT2D model is developed, based on the use of Delaunay, triangular unstructured meshes. To reach second-order accuracy, a MUSCL-Hancock approach is considered, with gradient computation performed by means of the multidimensional method proposed in Barth and Jespersen (1989) for Euler equations. The effects of different gradient limiters are also evaluated, aiming at a proper description of the flow dynamics in heterogeneous morphology contexts.

The third complexity issue is both "geometrical" and "mathematical". It concerns the effects of artificial structures, i.e. artificial geometrical constraints, on the flow dynamics. Among different

structures aimed expressly at controlling the high-concentration flow behaviour, attention was paid to sluice gates, which can be used in channels and hydropower reservoirs to control sediment routing. In the literature, the effects of sluice gates have been studied especially with reference to clear water flows over fixed beds, while knowledge about the influence on high-concentration flows over mobile beds is still limited. Here, a rough, bread new mathematical description is proposed, in order to take into account the 3D morphodynamics effects caused by sluice gates in high-concentration flow modelling.

The last complexity issue is pretty "numerical" and arises from the challenge of numerical models to comply with the phenomenon complexity. Generally speaking, reliable numerical models are expected to catch the main characteristics of the physical processes at both a general and a local spatial scale, although with a certain level of approximation, depending on the numerical scheme. Sometimes it may be hard to close the gap between the local phenomenon complexity and its numerical representation, leading to non-physical numerical results that could affect hazard assessment. In this work, a particular numerical issue is investigated, which was identified through a thorough analysis of TRENT2D model results. In particular, it was observed that the direction of the numerical mixture-mass flux is occasionally opposite to the direction of numerical solid-mass flux, despite the isokinetic approach which the model is based on. This incoherence was studied with a rigorous method, trying to fix the source of the problem. However, the question turned out to be quite tricky, due to the sophisticated character of the model.

These four, deliberately heterogeneous, "complexity issues" allow to perceive clearly the size of complexity effects on high-concentration modelling. Furthermore, they give the measure of how much difficult is reaching the right level of detail in describing and modelling high-concentration flows. The research of solutions that are accurate and as much simple as possible was not straightforward and required a quite large effort. Nonetheless, possible solutions were found in the end for three of the four "complexity issues", therefore the goal of the thesis can be considered as achieved.

Everything should be made
as simple as possible,
but not simpler.

(Albert Einstein)

Acknowledgements

First and foremost, I would like to thank professor Giorgio Rosatti for the opportunity of working on such a relevant and topical subject. Beyond the scientific and technical growth which he guided me through, I would like to thank him for what I learnt about method, constancy and passion. The years I passed working with him were not simply a school of hydraulics but rather a school of life.

Secondly, I would like to thank professor Marian Muste and professor Stefano Sibilla, who were the reviewers of this thesis. I am grateful to them for their careful reading and their relevant observation, which allowed to improve the quality and the contents of this work. A special thanks goes also to professor Luigi Fraccarollo and his co-worker Anna Prati, whose collaboration was essential to develop Chapter 7 of this thesis. Thanks also to professor Michael Dumbser, for the tips about unstructured meshes, to Walter Bertoldi, for the encouragement to reflect about complexity, and to Valentina Cavedon, who (unwittingly) gave me the last little push necessary to opt for this experience.

I would like to thank all my colleagues, or rather friends, who I work with in these years. A special thanks goes to Daniel, who was a constant, reassuring and helpful presence during all this path. Thanks also to Michele, Laura, Daniel, Cristian, Simona, Marta, Erika, Stefano, Alessandro, Andrea and Davide, for sharing with me some steps of the path. I was pleased to work with them, who made me feel at home at any time. Thanks also to Oscar, who was used to remind me that acknowledgements are the most demanding part of the thesis (and he was right).

A particular thanks goes to Elena, who was my mate, friend and confidant. She shared with me any kind of emotion during these years and it was very reassuring to have someone so familiar and faithful just beyond the opposite door. Thanks also to Marialaura, for being an example of determination and optimism.

I want to thank my parents, who were the essential point of reference during these years and accompanied my experience with a lot of encouragements and wise advices. Thanks also because they educate me to perseverance, diligence, patience and uprightness.

A special thanks goes to Fabiano, who was my energy when I was tired, my hope when I was disheartened, my happiness when I was cheerful and my faithful window onto the world. Thanks also to his family, whose warmth is extraordinary. Thanks to my friends of the "Blue van" group, for never giving up to encourage me and remind that true life is made of a lot of little, special moments and intermediate goals. Thanks also to the girls of the "Mater armata", for bringing music, which is a part of my life, inside my office.

Thanks to Ernesto, who created the cover image for me in such a short time. And thanks to all friends, relatives and acquaintances who were close to me in these years, even if just for some seconds, asking me about how this PhD was going. Any of them gave me energy and smile to complete this experience positively.

Contents

List of Figures

List of Tables

List of symbols

α	[°]	Slope angle;
α_{gate}	[°]	Bed slope angle near the sluice gate;
β	[-]	Transport parameter;
β_r	[-]	Reference transport parameter;
Δl	[L]	Characteristic length of mesh cells;
Δt	[T]	Timestep;
Δx	[L]	Cell size along x-axis;
Δy	[L]	Cell size along y-axis;
Δz	[-]	Bed slope height near the sluice gate;
Δz	[L]	Bed step height near the sluice gate;
Δ	[-]	Submerged relative density;
λ	[-]	Linear concentration;
λ_i		i-th eigenvalue;
$\lambda_{\max}$		Maximum eigenvalue;
$\lambda_{\min}$		Minimum eigenvalue;
$\nabla \mathbf{W}_n$		Primitive gradient;
$\mathbf{\Lambda}$		Eigenvalues matrix;
$\mathbf{\Phi}$		Vector of primitive variable limiters;
$\tilde{\mathbf{D}}$		Vector of non-conservative terms;
$\widetilde{\mathbf{W}}_n$		Vector of averaged primitives along n direction;
$\mathbf{A}$		GR-matrix;

$\mathbf{A}_n$		Roe matrix;
$\mathbf{B}$		GR-matrix;
$\mathbf{B}_n$		Roe matrix;
$\mathbf{D}_n$		vector of the non-conservative terms;
$\mathbf{F}$		Vector of the numerical fluxes;
$\mathbf{F}$		Vector of fluxes in x direction;
$\mathbf{F}^{HLL}$		Vector of HLL-fluxes;
$\mathbf{F}^{lat}$		Vector of lateral fluxes;
$\mathbf{F}^{LHLL}$		Vector of LHLL-fluxes;
$\mathbf{F}_n$		Vector of fluxes along the n direction;
$\mathbf{G}$		Vector of fluxes in y direction;
$\mathbf{H}_n$		Matrix of non-conservative terms;
$\mathbf{J}_{\mathbf{F_n}}$		Jacobian matrix of the fluxes $\mathbf{F}_n$;
$\mathbf{J}_{\mathbf{U_n}}$		Jacobian matrix of the conserved variables $\mathbf{U}_n$;
$\mathbf{J}_{\mathbf{F}}$		Jacobian matrix of fluxes;
$\mathbf{M}$		Rotation matrix;
$\mathbf{n}$		Unit normal vector;
$\mathbf{R}$		Eigenvectors matrix;
$\mathbf{R}_i$		i-th eigenvector associated to the i-th eigenvalue;
$\mathbf{t}$		Unit tangential vector;
$\mathbf{T}_n$		Vector of source terms along the n direction;
$\mathbf{U}$		Vector of the conserved variables;
$\mathbf{U}_n$		Vector of conserved variables along n direction;
$\mathbf{W}_n$		Vector of primitive variables along n direction;
$\mathbf{w}_n$		Component of the primitive gradient;
$\mathcal{A}$		Global GR-matrix;
$\mathcal{A}_n$		Roe matrix;
∂A	[L]	Cell perimeter;

ϕ	[°]	Friction angle;
Ψ	[-]	Function for gradient limiter computation;
ρ_m	[ML^{-3}]	Mixture density;
ρ_s	[ML^{-3}]	Solid-phase density;
ρ_w	[ML^{-3}]	Liquid-phase density;
τ_{bc}	[$ML^{-1}T^{-2}$]	Critical bed shear stress;
τ_{bx}	[$ML^{-1}T^{-2}$]	Bed shear-stress in x-direction;
τ_{by}	[$ML^{-1}T^{-2}$]	Bed shear-stress in y-direction;
τ_s	[$ML^{-1}T^{-2}$]	Shear stress of the solid phase;
τ_w	[$ML^{-1}T^{-2}$]	Shear stress of the liquid phase;
$\vec{\tau_b}$	[$ML^{-1}T^{-2}$]	Bed shear-stress vector;
$\vec{u}$	[LT^{-1}]	Depth-average velocity vector;
A	[L^2]	Cell area;
a	[-]	Bagnold constant;
a	[L]	Gate opening;
c	[-]	Depth-average concentration;
c_b	[-]	Maximum bed packaging concentration;
C_c	[-]	Contraction coefficient;
C_q	[-]	Discharge coefficient;
CFL	[-]	Courant coefficient;
D	[L^2T^{-1}]	Coefficient of hydrodynamic dispersion;
D	[LT^{-1}]	Sediment deposition flux;
D	[L]	Deposition depth;
d	[L]	Grain size;
D_0	[L^3T^{-2}]	Bed pressure term;
d_i	[L]	Incircle diameter;
E	[LT^{-1}]	Sediment erosion flux;
E	[L]	Erosion depth;

F_a	[-]	Amplification factor;
g	[LT^{-2}]	Gravitational acceleration;
h	[L]	Flow depth;
h_0	[L]	Undisturbed flow depth;
H_l	[-]	Hazard level;
i	[-]	Intensity;
i_F	[-]	Bed slope;
$i_{F,gate}$	[-]	Bed slope near the sluice gate;
k	[-]	Constant;
Ks	[$L^{1/3}T^{-1}$]	Gauckler-Strickler roughness coefficient;
L	[-]	Subscript for left states or fluxes in a RP;
M		Edge midpoint;
m		Magnitude;
m_0		Threshold magnitude;
P		Intersection of edge and centroid-centroid segment ;
P	[-]	Occurrence probability;
p	[-]	Porosity;
q	[L^2T^{-1}]	Discharge per unit width;
Q_{liq}	[L^3T^{-1}]	Liquid-phase discharge;
Q_{mix}	[L^3T^{-1}]	Mixture discharge;
q_{mix}	[L^2T^{-1}]	Mixture discharge per unit width;
Q_{sol}	[L^3T^{-1}]	Solid-phase discharge;
q_{sol}	[L^2T^{-1}]	Solid-phase discharge per unit width;
R	[-]	Subscript for right states or fluxes in a RP;
S		Wave velocity in a Riemann Problem;
S	[-]	Percentage of saturated basin area;
S_L		$= \min(\lambda_{\min,L}, \lambda_{\min,R})$;

S_R		$= \min(\lambda_{\max,L}, \lambda_{\max,R})$;
t	[T]	Time;
u_c	[LT^{-1}]	Channel velocity;
u_h	[LT^{-1}]	Hillslope velocity;
u_n	[LT^{-1}]	Normal velocity;
u_s	[LT^{-1}]	Velocity of the solid phase;
u_t	[LT^{-1}]	Tangential velocity;
u_w	[LT^{-1}]	Velocity of the liquid phase;
u_x	[LT^{-1}]	x-component of depth-average velocity;
u_y	[LT^{-1}]	y-component of depth-average velocity;
v	[LT^{-1}]	Velocity absolute value;
V_{mix}	[L^3]	Mixture volume;
V_{sol}	[L^3]	Solid-phase volume;
X	[L]	Gate-controlled length along the flow direction;
x	[L]	x-horizontal coordinate;
Y	[-]	Relative submergence;
y	[-]	Dummy variable for limiter computations;
y	[L]	y-horizontal coordinate;
z	[L]	z-vertical coordinate;
z_b	[L]	Mobile-bed elevation;

Chapter 1

High-concentration flow hazard assessment: complexity, simplicity and complicatedness

Natural hazard assessment is a key factor in disaster management. Any efficient protection or mitigation strategy can not be planned without accurate and reliable hazard assessment. However, natural hazard assessment may be not straightforward, for two main reasons: the intrinsic complexity of natural hazardous phenomena and the effects of this complexity on the hazard-assessment procedural chain, which compulsory includes a wide heterogeneity of information and operations.

Undeniable complexity of natural hazards hinders significantly their knowledge and understanding. However, despite the type, the number and the mutual connections of relevant natural entities and processes to be considered, understanding is mandatory to lead reliable hazard assessment, although quite demanding.

Hazard assessment requires phenomena description, therefore natural-hazard understanding must be followed by its quantitative representation. The transition from understanding to describing is anything but easy, given that several science branches, several types of data and information, different levels of uncertainty and long sequences of operations are involved. Certainly, obstacles are significant, nevertheless complexity can not be shunned, but rather faced, making it manageable as much as

possible, i.e. avoiding complicated operations and outcomes.

In this work, this challenge is taken up with reference to a particular class of flow-like hazardous phenomena, characteristic in mountain regions and indicated hereafter as high-concentration flows. These phenomena and their complexity are described in Section 1.2, while Section 1.3 pertains to the effects of complexity over the hazard-assessment process.

However, before discussing about high-concentration flows, it is convenient taking a bearing about the meaning of the word *complexity*, in order to understand properly its nuances and to frame the purpose of this work clearly. For this reason, in Section 1.1, an etymological analysis is proposed, not only about the term *complex*, but also considering other strictly-related terms.

1.1 Some definitions

The concept of *complexity* belongs to the common way of speaking and, at first sight, its meaning appears plain and intuitive. *Complex* is something that is not easily understandable. Similarly, also concepts of *simple* and *complicated* appear plain and intuitive: *simple* is the opposite of *complex*, while *complicated* is often interpreted as a synonym of *complex*.

This is confirmed by the definitions proposed by the Oxford English Dictionary:

- *simple*: easily understood or done;
- *complex*: consisting of many different and connected parts; not easy to analyse or understand;
- *complicated*: consisting of many interconnecting parts or elements.

However, over the years these terms have been used in a number of different ways, not only in the field of environmental sciences but also in physics, informatics, business management, social sciences, policy sciences (Gell-Mann, 1995). For this reason, their etymology is here investigated, in order to disclose some important shades and ensure the right interpretation of these three terms along the entire work.

Simple is the union of the Latin roots *sem-*, which means "only one", and *plex-*, i.e. *plectere*, that means "linking", "intertwine",

connecting". Therefore, *simple* is something that is plain, made of a single part and, so, it can be understood immediately.

Simple shares with *complex* the root *plex-* that, in *complex*, comes after the other Latin prefix *cum-*, which means "together" and implies "many", as clearly explained in Gell-Mann (1995) and in Sun et al. (2016). Therefore, *complex* indicates something that is made of many interconnected parts. What makes something *complex* is not only the quantity of parts, but also their mutual relationships, their links. Something *complex* can not be understood straightforwardly, not only because of the number of parts, but also because of the number of connections. If connections are identified or mapped for the most part, understanding the overall system behaviour could become more accessible. However, a detailed explanation about how each element or connection works remains intrinsically out of reach, since elements and connections they can not be studied separately (Bar-Yam, 1997).

On the other side, *complex* and *complicated* share the common Latin root *cum-* (Sun et al., 2016), but *complicated* is completed by the Latin verb *plicare*, which is similar to *plectere*, but suggests that parts are "folded up" repeatedly. Complicated systems are made of many parts, which are individually simple but collectively entangled. This makes system understanding not straightforwardly. In other words, *complicated* seems to recall some idea of mess, of intricacy. Single parts of a complicated system could be easily and completely understood if considered one at a time, but understanding of the behaviour of the overall system when these parts are put all together could result unreachable.

On the basis of these shades of meaning, the explanation for how the terms *simple*, *complex* and *complicated* are adopted in this work is the following:

- *simple* does not need any additional specification. Its common meaning is suitable also in the context of this work;

- *complex* is used here to indicate systems whose full understanding is out of reach. Natural systems are "undeniably" complex, whether the entire system or its parts are considered, since complexity is strictly linked with the nature of the system. Studying and managing complexity properly can lead to a better understanding of the system or of one of its parts, although an all-encompassing description of the details remains unworkable;

- *complicated* is used to characterise systems that are made of simple parts, i.e. parts that can be individually understood, but appears ravelled when parts are considered all together. A complicated system is twisted and not easily manageable, but, with significant effort, it can be made simple.

Complexity represents the essence of natural systems, therefore it can not be removed. The only things that can be done with complexity are understanding it as much as possible and describing it with proper approaches that are as much simple as possible, avoiding complicatedness. These two aspects are discussed in the next Sections with reference to high-concentration flows, which are complex natural phenomena typical of mountain regions.

1.2 A not-exhaustive account about high-concentration flow complexity

This Section brings into focus complexity of high-concentration flow phenomena, which knowledge is mandatory to develop reliable descriptions to be used in mountain hazard assessment.

Generally, mountain regions are prone to rapid flood events with considerable sediment transport. Such phenomena are indicated here on the whole as high-concentration flows. This term includes flows such as debris flows, debris floods, debris torrents lahars, intense sediment-transport flow, etc. It must be noticed that terminology around high-concentration flows is not univocal. Over the last decades, different classifications have been proposed, varying terms, meanings and discriminating factors (see for example Varnes, 1978; Hutchinson, 1988; Coussot and Meunier, 1996; Hungr et al., 2001; Jakob, 2005a; Takahashi, 2007). However, it is not uncommon to observe phenomena evolving from a class to another during travelling. For instance, *debris flow* is often used to indicate events observed in the upper part of a basin (Armanini, 2015), characterised by high volumetric concentration of sediments, while the propagation of same events in the lower part of the basin is sometimes called *hyperconcentrated flood flow* (Takahashi, 2007), because of its value of concentration, reduced by sediment deposition. In such a case, phenomena classification seems to be too much stiff and a more general description of the whole phenomenon should be preferred. For example, Hungr (2005) suggested the use of the term *debris flow*

to indicate the entire phenomenon, from the initiating slide to the deposition processes on alluvial fans. According to this last approach, in this work the term *high-concentration flow* is used to indicate the whole family of flow-like movements characterised by quite high-concentration values at some point of their space and time evolution. The term *high-concentration flow* is sometimes interchanged with the term *mountain flows*, which is used to indicate the same class of phenomena, but emphasizing the context where they are typically observed, i.e. mountain regions.

This work considers a quite wide range of high-concentration flow-like mass movements, which characteristic sediment concentration can vary roughly from $1-2\%$ to $40-50\%$. Since the focus is set especially on mountain flows observed in the Alps, phenomena with cohesive behaviour, as for example mud flows or clay flow slides, are here excluded (their rheological behaviour is rather different from that of phenomena involving loose, coarse sediments). Mountain flows which this thesis refers to are observed typically in small ($< 5\,\mathrm{km}^2$) and steep basins. They are originated by intense rainfall events (sometimes also snowmelt) over saturated soils, in areas where a certain amount of coarse (but sometimes also fine), loose sediments is available. Such flows are driven by gravity (Takahashi, 2007) and can reach high velocity (up to several meters per second), travelling long distances (Armanini, 2015). All these factors determine a great damaging potential, which becomes evident when mountain flows reach urbanised areas.

Hereafter, some aspects of natural complexity of high-concentration flow are shortly disclosed.

1.2.1 Solid-liquid mixture

Sediment volumes involved in a high-concentration flow can be very large if compared to the solid-transport phenomena typical of floodplains. Because of sediments, the global flow rate of a high-concentration flow can exceed the runoff flow rate even by one order of magnitude. This amplification effect can be easily quantified as shown in (Takahashi, 2007). Indicating with Q_{liq} the runoff discharge and Q_{mix} the total flow rate of a high-concentration flow, the following relation can be set

$$Q_{mix} = F_a Q_{liq} \tag{1.1}$$

where F_a represents the amplification factor, defined as follows (Hashimoto et al., 1978):

$$F_a = \frac{c_b}{c_b - c} \tag{1.2}$$

with c representing the volumetric sediment concentration and c_b representing the maximum packaging concentration of the sediments in the bed. Whenever concentration c approaches c_b, the amplification factor, and therefore the total flow rate, increases significantly. Evidently, such a discharge amplification can not be overlooked when high-concentration flows are studied, even if estimating liquid and total discharges is far from being simple. For this purpose, both hydrological and geological evaluations should be carried out, as described in Sections 1.3.4 and 1.3.5.

However hydrological analyses can be seldom based on observations, since only few mountain basins are instrumented. Typically, instrumentation is installed only if relevant mountain-flows are observed with very high frequency and damaging potential. Therefore, characterising the discharge evolution in time is not free from uncertainty. A few studies (for example Honglian and Xiangxing, 1988; Takahashi, 2007) and experience (personal communication of prof. Aronne Armanini) suggest that precipitation events causing mountain flows can be characterised by a sequence of multiple rainfall peaks, each one with different duration and intensity. However, so far, there is not a univocal characterisation of such peaks.

In addition, total flow rates can be described properly only if also sediment availability is taken into account. For example, a site with long debris-recharge cycles and shallow bedrock is expected to show a scarce availability of loose sediments. In such a case, it is plausible that all the available material contributes to the high-concentration flow discharge. However, because of the scarce quantity of available sediments, discharge amplification is generally limited. On the contrary, a site characterised by high soil fragmentation or short recharge cycles makes available large volumes of sediments. In this case, the amount of solid material involved in the flow depends no more on the total amount of sediments, but rather on the magnitude of the liquid discharge that becomes the limiting factor. Evidently, both liquid and solid phases of a high-concentration flows require to be described properly and no one of them can be neglected.

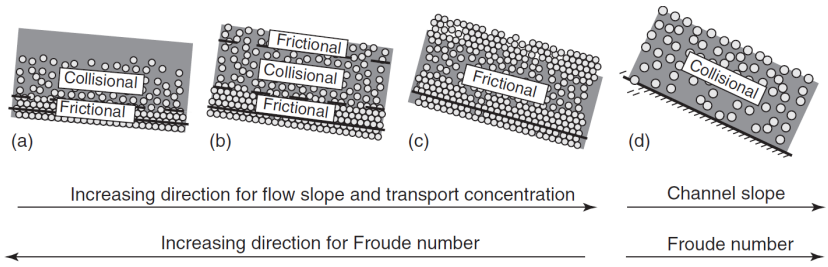

Figure 1.1: Rheological behaviours typical of high-concentration flows (from Armanini et al., 2005): (a) immature or oversaturated flow over loose bed; (b) mature flow over loose bed; (c) unsaturated flow over loose bed; (d) flow over rigid bed.

What is more, the presence of both water and relevant rates of sediments that are poorly-sorted (Takahashi, 2007) requires a proper and detailed description of the rheological behaviour of the solid-liquid mixture. Because of the high sediment concentration, theories and methodologies developed for bed load and suspended load are not suitable for high-concentration flows (especially for debris flows) (Armanini, 2013), since sediments are active players in determining resistance, both frictional and collisional (see Figure 1.1). Then, different and more elaborated approaches have to be resorted to describe properly the two-phase dynamics. This point of discussion is further expanded first in Section 1.3.6 and then in Chapter 2.

1.2.2 Interaction with the bed

Another factor of natural complexity of high-concentration flow is their strong interaction with bed and, in general, with morphology, introducing significant modifications. It must be specified that the term *bed* indicates here the bound at rest coinciding with the surface separating the (moving) flow from the motionless part of the solid-liquid mixture, as explained in Rosatti and Zugliani (2015).

Bed can be either erodible or not. In both cases, significant bed modifications are observed. If bed is erodible, the flow can induce both deposition and erosion processes, while if not only deposition may occur. Erosion and deposition can take place respectively with depths and heights of several meters (see erosion in Figure 1.2). Whatever the bed nature and the modification depth, the exchange of mass and momentum between flow and bed represent a further element of complexity to be suitably managed in the description of the phenomenon dynamics (see Section 1.3.6 and Chapter 2).

Figure 1.2: Erosion due to a debris flow event (Valle Molinara, Italy) Courtesy of the Autonomous Province of Trento.

1.2.3 Time and space scales

As far as morphology is concerned, it must be highlighted that mountain morphology is itself complex, because of the succession of hills, gullies, plains, valleys, geomorphic scars, branched stream networks, alluvial fans, etc. The heterogeneity of mountain morphology has a strong influence on the flow path, whether the flow is confined in a channel or not. Therefore, mountain flows should be studied with a quite detailed representation at the small scale, in order to catch point-wise flow response to the local morphology.

Besides, temporal and spatial scales of the phenomenon itself are quite small if compared with those observed for large rivers or floodplains phenomena. Typically, the order of magnitude of mountain flow duration in Alpine regions is about equal to some hours, while the space scale is limited to some kilometres. This means that time and space resolutions chosen to describe the phenomenon should be fine enough to catch the main processes at a quite short temporal scale and a rather small spatial scale. This implies some operational consequences in hazard assessment, as described in Section 1.3.3, and poses also a problem of hazard management, since typically event duration is not sufficient to activate emergency protection or mitigation procedures.

Figure 1.3: A debris flow over an alluvial fan: Campolongo di Piné, 15th August 2010. Courtesy of the Department for Territory, Agriculture, Environment and Forestry of the Autonomous Province of Trento

1.2.4 A recent history

Evidently, studying high-concentration flows is not an easy task, because of these and also other complexity factors, which are closely related to the nature of the phenomenon. Moreover, it must be noticed also that the history of research around mountain flows is quite short in comparison with that one of large river hydraulics. The interest around mountain flows has become more evident only in the last decades, probably because of increased frequency and size of disastrous consequences in mountain regions (Ammann, 2006). Therefore, mountain-flow knowledge is still quite limited and historical analyses contribute with difficulty to bridge the gap (see Section 1.3.2). Limited knowledge entails limited understanding, which contributes to the perception of mountain-flow complexity as very sizeable.

In mountain regions, and especially on alluvial fans, urbanisation processes have become more frequent only in the last years. Therefore, exposition of people, buildings and infrastructure to relevant levels of hazard is quite recent (Figure 1.3 shows the debris-flow event observed in 2010 in the Molinara Valley (Italy) that damaged the urbanised alluvial fan of Campolongo, which had been uninhabited until the 1950s) and the evaluation of the possible effects of such exposition is still rough.

On the other hand, in some regions, frequency and magnitude of high-concentration flows have been changing as a result of climate change, which is currently modifying rainfall patterns in terms of seasonality and intensity (Stoffel et al., 2014). Therefore,

high-concentration flow prediction and modelling appear uncertain, also because they depend on a variety of rapidly evolving factors, which have been studied only in the last decades.

What is more, several basins show their hazard-prone character not so frequently, i.e. every some decades or even century. This makes difficult both measurements and proofs collection. Besides, low event frequencies lead often to a false sense of security in local citizenry, encouraging then urban development.

1.3 How high-concentration flow complexity affects hazard assessment

High-concentration flow hazard assessment requires in-depth knowledge not only of the phenomenon physics (whose complexity was discussed in the previous Section), but also of the study area and of any past events (when available). Moreover, it should take into account possible future scenarios of hazard and expositions. Describing each on of these elements with the right level of detail may be a challenging and laborious task, sometimes leading to complicatedness. However, avoiding complicatedness is one of the duties in hazard assessment, in order to preserve assessment reliability. Therefore, finding the *right level* of detail in each one of the procedural steps of hazard assessment is mandatory.

In the next Sections, discussion about effects of mountain-flow complexity on the phenomenon description for hazard assessment purposes is divided into topics, following the typical procedure applied to assess high-concentration flow hazard. According to the common practice, this procedure is divided into six steps, as summarised in Figure 1.4, that are namely: historical analyses, morphology representation, geological and geomorphological analyses, hydrological analyses, modelling and hazard evaluation. For each step, in these pages the effect of natural complexity on hazard assessment is discussed, bringing the focus on the necessary trade-off between complexity and simplification. The question about the *right level* of detail to be reached in the description is discussed first in general terms in Section 1.3.1, while in the following Sections it is analysed in depth with reference to each one of the six steps of the hazard assessment procedure.

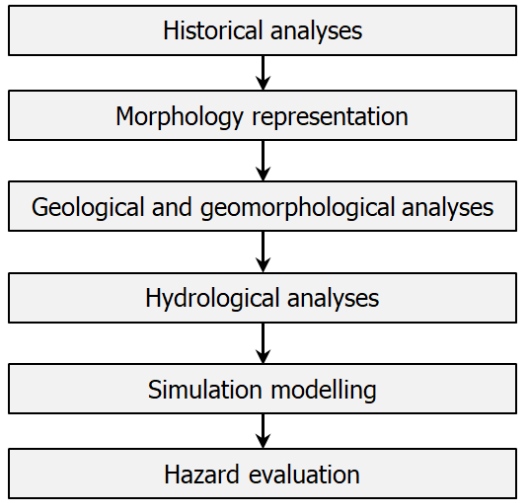

Figure 1.4: Main steps of the procedure typically used in mountain-flow hazard assessment

1.3.1 The question of the *right level* and the Occam's razor principle

It is well-known that, to describe nature, it is necessary to resort to abstraction, i.e. simplification (Favis-Mortlock, 2013) of the real system. Abstraction depends much on human perception (Mulligan and Wainwright, 2013) and, generally, environmental-system complexity is perceived as too large for a thorough mathematical representation, i.e. for extremely detailed quantitative descriptions (Beven, 2009). Therefore, complex natural systems are represented by scientist not exactly, but rather with the *right level* of detail, resorting to suitable simplification when possible.

However, identifying which is the *right level* is far from being simple. If the level is too much low, one runs the risk of working with "spherical cows" (Harte, 1988). Otherwise, if the level is *right* but the steps required to get it are too many and too much intricate, one could end up with unsuitable or incomprehensible descriptions, which are nothing but the outcome of complicatedness.

In order to avoid both these outcomes, often researchers invoke the "Occam's razor" principle. According to this approach, the reference criteria to calibrate explanation capabilities and orientate complexity management is represented by parsimony. Parsimonious descriptions contain sufficient complexity to explain phenomena, but no more (Mulligan and Wainwright, 2013). However, the evaluation of what is sufficient and what is not is

not univocal and depends largely on the goal of the description (Casti, 1979).

In this work, high-concentration flow description is aimed at hazard assessment, which typically involves different natural aspects, several operational issues and different scientific know-hows. In this case, an acceptable trade-off between complexity and simplification should combine enough accuracy in representing the process dynamics and a desirable simplicity in reading results and uncertainty, compulsorily avoiding both oversimplification ("spherical cows") and complicatedness.

Here, the term *description* is mainly referred to modelling, which is intended, broadly speaking, as the totality of operations necessary to reproduce high-concentration flow virtually. Therefore, not only models are considered here, but also field data, data representation, model use, processing efforts. For each one of these elements, undeniable requirements in terms of details and possible compromises in high-concentration flow complexity description are discussed.

It must be noticed that considering all these entities is essential, since a variety of roles (scientists, practitioners, policy-makers, citizenry) is typically involved in hazard assessment. Nowadays, the Transfer of Technology (TOT) from the research community to technicians and decision-makers depends largely on user requirements in terms of skills, knowledge, materials and costs. Therefore, finding the *right level* in representations can not be an issue purely related to the model chosen to perform the representation. Therefore, considering modelling in its broad sense is crucial in determining more or less strong links between the different roles.

This work was developed having in mind exactly this broad approach. The words *managing complexity* that appear in the title of the thesis mean "dealing with natural complexity, trying to keep the *right level* of detail in the phenomenon representation and avoiding complicatedness as far as possible". In other words, *managing complexity in high-concentration flow modelling aimed hazard assessment* means that the *right level* of detail in modelling (in broad sense), is evaluated and managed having in mind a clear purpose, that is assessing high-concentration flow hazard without complicatedness.

1.3.2 Historical analyses

The hazard assessment process should start with historical analyses, oriented to disclose possible information about past events in the study area and, more in general, to acquire in-depth knowledge of high-concentration flow behaviour in the area. For this purpose, records, inventory, pictures, satellite imagery, chronicles, witnesses have to be consulted carefully. In addition, on-site measurements must be collected whenever available.

Historical databases of field measurements, i.e. rain gauged data or discharge measures, are typically rare. They are available only for specific sites (among others, see Zhang, 1993; Berti et al., 2000; Marchi et al., 2002; Bacchini and Zannoni, 2003; Hürlimann et al., 2003; Mathys et al., 2003; Rickenmann and McArdell, 2007; Coe et al., 2008), prone to high-concentration flows on a yearly basis, while, as a rule, not only observations, measures and proofs, but also pictures or eyewitness memorandums are quite uncommon. This scarce availability of past, complete information makes phenomenon prediction and knowledge challenging and hinders hazard assessment.

However, historical analyses should pay attention not only to measurements, but also to site morphology, urbanisation evolution, possible presence of protection and mitigation measures and, not least, the soundness of the available documentation. The job of looking for such information does not appear as much complex, but it may become rather complicated, because of some effort required to find and validate information sources. Often, they are made available by different, not interconnected offices of public administration. Moreover, their level of detail could be not completely satisfying for hazard-assessment purposes, especially if dated documentation is investigated, and sometimes conflicting information is found.

If information is scarce or rough, any hypothesis about possible past and future scenarios is barely stated and any analysis is affected by large uncertainty. This topic was tackled directly in the study proposed in Section 4.2, accounting for the back-analysis of a historic debris-flow event.

1.3.3 Morphology representation

The second step of a high-concnetration flow hazard-assessment job is typically represented by the characterisation of the

site morphology through field surveys. The relevance of a detailed, although complex, representation of the site morphology was already highlighted in the previous Section. Nowadays, detailed representations of morphology are facilitated by the large availability of terrain information, due especially to the rapid diffusion reached in the last two decades by airborne and terrestrial LIDAR techniques (Roering et al., 2013). LIDAR (Light Amplification by Stimulated Emission of Radiation) allows to collect accurate, high-resolution elevation data, covering large areas rapidly and also with rather high frequency. Such elevation data are gathered in Digital Elevation Models (DEMs) and Digital Terrain Models (DTMs), which represent the morphological basis to be used in modelling aimed at hazard assessment. The spatial resolution of recently-surveyed DEMs and DTMs can be quite fine (~ 0.5–1 m), therefore terrain features can be simply recognised with high, point-wise accuracy. DEMs, DTMs and other similar topographic products lighten significantly the fieldwork and allow to improve its quality. However, fieldwork is still necessary, especially to verify the correct representation of some key, complex local areas and to refine accuracy of DEMs and DTMs. For this reason, LIDAR and field surveys should be considered always jointly to ensure the *right level* of detail in the description of terrain elevation. A low level of detail or a bad representation of a heterogeneous mountain morphology could dramatically decrease the level of accuracy and reliability of hazard-assessment jobs.

Typically, LIDAR-based DEMs and DTMs are Cartesian grids with square cells, while spatial information produced by fieldwork could be organised in clouds of not-equally spaced points, which distribution and accuracy depends on the acquisition technique. Besides, anisotropic point clouds could be produced also synthetically, when possible future configurations of the study area are considered, for example to take into account design protection works or to anticipate future urban developments. Merging Cartesian mesh and point clouds is a delicate operation, since typically it is necessary to deal with different reference systems and different sampling. Managing different file formats, performing data roto-translations and interpolation, setting priority levels in merging spatial information update are typical tasks that could lead to complicatedness, if the operational chain is not managed properly. Quality of the spatial description could result lower than desired and hazard assessment outcomes could be signific-

antly conditioned.

Moreover, hazard-assessment analyses could require different levels of detail in different areas, which means that the spatial resolution could be not compulsory constant. Managing such heterogeneous information could be complicated, whether the point of view of model developers or practitioners is assumed. This subject is one of the main topics of this thesis, so its further discussion is postponed until Chapters 5 and 6.

1.3.4 Geological and geomorphological analyses

Next to morphology, also site geology and geomorphology require a proper level of knowledge, in order to ensure a reliable hazard assessment.

Geological investigations are necessary especially to characterise sediments availability in the study basin. Knowing the amount of available loose solid material, its nature and its grain-size distribution, supports the estimate site-specific high-concentration flow magnitude and the discharge amplification, as explained is Section 1.2.1. In general, local authorities of Alpine regions are able to supply detailed description about stratigraphy and localisation of relevant, dormant deposits of loose sediments. However, field surveys are always desirable in order to properly characterise sediments availability.

On the other side, geomorphological analyses can supply very general information about the dynamics of past mountain-flow events. Typically, geomorphological investigations are oriented to recognize so-called "silent witnesses", as for instance U-shaped gullies, well-defined boulder trains or levees, impact marks on trees (Jakob, 2005b). Silent witnesses keep physical memory of past events and can help the hazard-assessment job, contributing to reveal how high-concentration flows typically behave in the study area. Knowledge of the preferential flow paths, of the typical debris diameters or of the locally prevailing processes between erosion and deposition contributes to improve site-specific knowledge of phenomenon dynamics. Certainly, back-analyses of documented past events could contribute more significantly.

1.3.5 Hydrological analyses

Within the hazard-assessment operational chain, hydrological analyses are essential to evaluate high-concentration flow magnitudes properly. Because of the nature of the hydrological processes and their dynamical behaviour, facing with complexity is compulsory also in this case and reaching the *right level* of detail typically appears a challenging purpose.

Basically, hydrological analyses are carried out in order to evaluate two important quantities: the possible duration of a high-concentration flow event and the intensity of its liquid flow-rate. Both these factors depend on basin morphology, hydraulic conductivity, saturation mechanisms and, of course, precipitation. Therefore, their evaluation requires the study of several interconnected processes, typically starting from poor site-specific data. This makes the achievement of *right level* of detail almost unworkable, especially as far as the phenomenon intensity is concerned.

In practice, the duration of a high-concentration flow phenomenon is estimated on the basis of water residence time. GIS processing may help the estimation, since residence time seems to depend particularly on the internal form and structure of the catchment (McGuire et al., 2005). Once the time scale is defined, some significant values of duration are chosen in residence-time neighbourhood and used to depict a certain number of possible precipitation scenarios. Usually, precipitation scenarios are built synthetically, starting from regional IDF (Intensity-Duration-Frequency) curves. Rainfall Intensity is estimated fixing Duration and choosing suitable Frequency values, i.e. return period values. Then, studying how precipitation turns into run-off finally allows to obtain liquid flow-rate intensity.

In such analyses, strong simplifications are generally introduced, with reference to space and time variability of the main hydrological factors (for example about saturation, conductivity, porosity, precipitation). Hereafter, some of them are discussed.

Typically, rainfall intensity is assumed to be constant all over the basin extent. This hypothesis seems to be quite acceptable, because of the small size of mountain-flow prone basins (Rigon et al., 2012). When high-concentration flows generate because of saturation excess, also the hypothesis of basin saturation appears acceptable, on the basis of the rainfall time patterns often observed (see Section 1.2.1). However, some other simplifications are more questionable.

It is well-known that intense rainfall events show a significant spatial variability in mountain regions, because of terrain morphology. Because of this variability, the relevance of regional rain-gauged data decreases dramatically when the distance between the rain-gauge and the study basin exceeds the 5 km (Marra et al., 2016). Therefore, rainfall characterisation on regional basis could be not fully representative, if the extent of the region is too much large. Nevertheless, the regional geostatistical solution is often the only one feasible.

Radar data, when available, can make up for the lack of gauged measurements, supplying the *right level* of detail in describing precipitation over ungauged basins. However, quality of radar data could be scarce, especially in mountain areas where orography shades some sectors and where not only rainfall, but also hail and snowfall are observed. Furthermore, radar data require a quite heavy processing to extract significant historical series. This is the price to pay in order to have meaningful, site-specific rainfall information. In addition, whatever the case, it must be noticed that hydrological analyses for hazard-assessment purposes typically disregard seasonality and climate change.

Although weather and hydrological complexity, once precipitation scenarios are stated, rainfall must be transformed into run-off, i.e. into liquid discharges. Typically, this evaluation is performed by means of rainfall-runoff models. To raise the level of detail, physically-based, distributed models should be considered (Abbott et al., 1986). Since hazard assessment is interested in applications at the event scale, event-based models can be chosen, which typically neglect evaporation and transpiration processes and show a quite small number of parameters.

Despite this reasonable simplification, the hydrological-modelling step remains quite challenging, whenever the description of such hydrological has to be carried out "blindly", i.e. without measurements available. In such cases, a priori values must be chosen for the parameters. This choice can be facilitated by field surveys, although some level of uncertainty remains. Experience suggests that, for each precipitation scenario, a sensitivity analysis should be carried out, in order to increase the reliability of both the rainfall input data and the chosen parameters values. With such an approach, hydrological analyses do not produce a single hydrograph but rather an envelope of hydrographs, i.e. a range of possible discharge scenarios to be used to estimate multiple high-concentration flow scenarios with different magnitudes. The

estimate of these magnitude scenarios, which are synthetic, is typically based on the hypothesis that enough sediments and water are available at the same time. However, the occurrence probability of the synthetic rainfall event could be quite different from the recharge cycle of the sediments, as recalled previously. A more exact description of high-concentration flow phenomena should combine the two probabilities, but, to date, the scarcity of available measurements hinders similar analyses. Therefore, in practice, the occurrence probability of a high-concentration flow with given magnitude is still considered equal to the probability of its triggering rainfall event. Evidently, this is a strong simplification, but different, rigorous solutions are not feasible thus far to represent properly natural complexity Rickenmann (1999).

Once the necessary synthetic magnitude scenarios are stated, the operational procedure for hazard assessment proposed in Figure 1.4 requires that their dynamics is described, i.e. modelled.

1.3.6 Modelling

One of the most critical points in high-concentration flow hazard assessment is the synthetic representation of phenomenon dynamics, i.e. its modelling. By means of modelling, high-concentration flows can be simulated in situations where real-life hazardous phenomena and their damaging consequences should be avoided. Typically, modelling is profitably used in engineering practice to understand past events and predict possible dynamics of hazardous events under different conditions. Clearly, it represents a fundamental resource for hazard assessment.

Modelling can be both physical or mathematical. However, since the costs of the first are generally high, the second is often preferred, especially by practitioners. This is also the case of this thesis, where the focus is set especially on mathematical and numerical modelling.

It must be noticed that only few causes for reflection about modelling are proposed here, since a wider and more thorough analysis is proposed in Chapter 2 and in the subsequent Chapters.

Mathematical models simulating high-concentration flows are typically based on systems of Partial Differential Equations (PDEs) describing the most relevant aspects of the phenomena to be simulated, i.e. its physical nature and its dynamics. Usually, they consist of equations describing mass and momentum conservation and relations accounting for the rheological behaviour of

the flow. For the purpose of describing high-concentration flow physics with the *right level* of detail, at least a 2D, depth-averaged, shallow-flow models should be used, as suggested in Rosatti et al. (2017). In the same paper, it was stated that "quite different 2D models based on this premise are present in the literature. They differ in the basic assumptions regarding the nature of the flow (monophasic or biphasic), in the type of bed over which the flow occurs (fixed- or mobile-bed), and in the type of closure relation concerning the bed evolution, the concentration of sediments and the bed shear stresses". Different assumptions mean different levels of detail and different operational issues, also from a numerical point of view.

However, if models with an acceptable level of detail are chosen, accurate descriptions can be obtained only if accurate input data are supplied. Typically, models require multiple data in different formats, obliging the user to become familiar with multiple software products. Generally, this aspect rises complicatedness in the modelling chain and causes the increase of the overall cost of the analysis, in terms of time, hardware and effort.

Moreover, model results and their relevant uncertainties must be made accessible and easily readable not only to experts, but also to stakeholders and not-technicians in general. Therefore, readability of modelling outcomes must be guaranteed by modellers and users.

These important topics are further expanded and faced in Chapter 5, since only reliable and plain modelling can guide disaster management effectively.

1.3.7 Hazard evaluation

Typically, a hazard-assessment job ends with a quantitative evaluation of the levels of hazard pertaining to the studied phenomenon in a given area.

First, critical interpretation of modelling outcomes should be performed. Critical analyses should concern not only model results, but also of all other information used in the hazard-assessment job, in order to ensure that the *right level* of detail has been taken into account at each step. Outcomes of the critical interpretation depend much on knowledge and experience of the person who carries out the analysis. In the case of mountain flows, reliable results are obtained only if this person is familiar with historical archives, geomatics, geology, geomorphology, hydrology,

high-concentration flow mechanics, mathematical and numerical modelling, hazard management and communications. Such skills and know-how could be not so common and, in any case, require time to be assimilated (Wright and Hargreaves, 2013).

Starting from simulation results, hazard can be evaluated through hazard-level maps editing. Typically, information about point-wise (simulated) behaviour of the phenomenon is converted into more concise, i.e. simplified, information accounting for phenomenon occurrence probability and local intensity. Also in this case, both complicatedness of the transformation procedure and oversimplifications of the hazard-level representation should be avoided, preserving the *right level* of detail in the description, i.e. guaranteeing a suitable correspondence between phenomenon dynamics and its synthetic representation (i.e. without the possibility of bad or wrong interpretation).

For all the reasons highlighted in this and in the previous Sections, reaching the *right level* of detail in hazard evaluation is quite challenging. These difficulties will become still more evident in Chapter 4, where two case studies are presented, and in the subsequent Chapters. There, some of the effects of complexity highlighted in this summary about the procedure high-concentration flow hazard assessment are directly faced and managed.

Chapter 2

Complexity and high-concentration flow modelling

Complexity of high-concentration flows largely affects the hazard-assessment job, as discussed in Section 1.3. One of the most influenced parts of the job is modelling.

As already stated in the previous Chapter, the purpose of modelling is not to reproduce exactly the phenomenon complexity, but rather to describe it with the *right level* of detail. However, the evaluation of which is the *right level*, i.e. the suitable trade-off between accuracy and manageability, is not univocal and depends much on the purpose of the representation.

Representing properly the main processes that govern a high-concentration flow by means of physical laws is one of the main goals for developers of mountain-flow models. Physical laws are expressed in the form of equations, grouped into systems that must be solved, typically by means of numerical methods and with the support of computers. Over the years, several kinds models have been developed, with different constitutive hypotheses, different schemes for equations solving, different efforts in model coding and different amounts of computational burden. In this Chapter, some of the most recent approaches present in the literature about high-concentration flow modelling are analysed, evaluating case-by-case the trade-off chosen as basis for modelling. In particular, Section 2.1 analyses different levels of detail in the mathematical description, taking into account especially approaches that are particularly relevant for the purposes of this

thesis. Then, Section 2.2 discusses some important characteristics required to numerical schemes to properly represent natural complexity. Last, the role of parameters and initial and boundary conditions is shortly analysed in Section 2.3.

2.1 Complexity and mathematical modelling

In the last fifty years, a wide range of mathematical-modelling approaches has been developed for high-concentration flows and, more in general, for flow-like natural processes. These models are intended to describe flow phenomena at a "macroscopic" scale, i.e. at the scale of the phenomenon in its entirety. For this reason, typically they apply a continuum approach. This means that the focus is not on the detail of "micro-scale" phenomena, i.e. on processes at particle size, but rather on the global evolution of the flowing mixture. Therefore, the discussion about the *right level* of detail in the description is carried out here considering consistent time and space scales. Furthermore, according to this approach, both liquid and solid phases can be reasonably treated as fluids.

As a general consideration, Rosatti et al. (2017) notice that 2D models should be preferred to 1D models, in order to take into account properly the phenomenon behaviour and reach an acceptable level of detail. Certainly, three-dimensional models would increase further the level of detail, however they are still subject of research, as far as rheological closures (Armanini, 2015) and numerical schemes (Zugliani, 2015) are concerned. Iverson and Ouyang (2015) stated that depth-average modelling has three main advantages over 3D modelling, since:

- it generates outputs which level of detail is similar to that one of field measurements, facilitating comparisons;
- it embeds the description of bed and free-surface evolution in the governing conservation equation, eliminating the need of solving domain boundaries separately;
- it considers a lower number of degrees of freedom, which reduces computation time.

Therefore, the balance between advantages and burdens introduced by a 3D description seems to be negative. Recalling the "Occam's razor" principle, 2D modelling currently available satisfies the parsimony criteria better than 3D.

Assuming the 2D simplification as acceptable, a wide range of models has been proposed over the years, with each model characterised by different constitutive hypotheses (see Iverson and Ouyang, 2015 for a review). Differences concern mainly how models simulate the nature of the flow, the nature of the bed, the bed evolution and the rheological behaviour of the mixture (Rosatti et al., 2017).

Depending on the approach chosen to describe the nature of the flow, high-concentration flow models can be divided into two main categories: mono-phase models and two-phase models (for sake of brevity, here the family of two-layer models, as for example Fraccarollo and Capart, 2002 or Fernandez-Nieto et al., 2008, is not considered). Both these approaches are discussed in the next Sections, where some relevant aspects are investigated for each category. Analyses are supported by the indication of a reference 1D system of equation, which is intended to support the reader in seizing the level of detail in the description, without getting lost into 2D or 3D terms.

The choice about the approach used in the description influences model accuracy, implementation and use. In general, it can be noticed that the more realistic and accurate is the modelling description, the more sophisticated (and sometimes complicated) is the model-equation solution and understanding.

2.1.1 Mono-phase modelling

In Section 1.2, high-concentration flows have been described as composed by a liquid phase, namely water, and a solid phase, namely sediments. Mono-phase models neglect this distinction between phases and consider the liquid-solid mixture as a unique continuum. This approach seems to be not much fitting whenever cohesionless high-concentration flows are concerned.

Considering the 1D formulation along the x direction, the equations used to describe the mixture dynamics by means of a mono-phase approach are typically written in the following form, where equation 2.1a represents the mixture-mass balance and equation 2.1b is the mixture-momentum balance. Notation is set according to Figure 2.1.

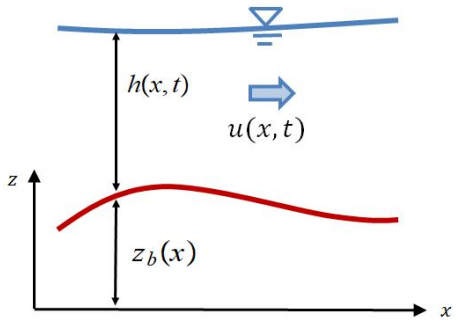

Figure 2.1: Basic notation used to write the 1D, mono-phase model equations

$$\begin{cases} \dfrac{\partial h}{\partial t} + \dfrac{\partial (hu)}{\partial x} = 0 & \text{(2.1a)} \\ \dfrac{\partial (hu)}{\partial t} + \dfrac{\partial}{\partial x}\left(hu^2 + \dfrac{1}{2}gh^2\right) + gh\dfrac{\partial z_b}{\partial x} = -\dfrac{\tau_b}{\rho_m} & \text{(2.1b)} \end{cases}$$

t indicates time, h the flow depth, u the mixture velocity, g the gravitational acceleration, z_b the bed elevation, τ_b the shear stress and ρ_m the (constant) mixture density. Assuming that ρ_m is known, the unknowns of the problem are three: h, u and τ_b. Since the system equations are only two, a further, typically algebraic equations is use to "close" the problem, expressing τ_b as a function of the other variables. A lot of different formulation of τ_b are available in the literature.

This approach shows a high level of simplification and, for this reason, often is preferred to the two-phase approach. However, some of its assumptions appear quite debatable.

The mono-phase approach assumes necessarily that sediment concentration (and therefore density) is constant in space and time, although, in natural high-concentration flows, concentration varies according to hydrodynamics.

Then, mono-phase models do not allow mass exchanges between mixture and bed, therefore neither erosion nor deposition processes can be described properly. The only variation of the bed elevation is considered during the stopping phase, assuming that the bed elevation increases by the flow depth.

Furthermore, the flow stopping stage is simulated typically by means of a threshold criterion. When shear stresses exceed a certain threshold, the mixture, i.e. both sediments and water, stops, even though in natural cohesionless high-concentration flows only the solid phase stops, while the liquid phase flows

away.

For these reasons, the use of such models to simulate two-phase, cohesionless flows appears as an oversimplification, especially if the flow moves over an erodible bed.

Current mono-phase models for mountain-flow simulations can be divided basically into two groups: Cellular-Automata-like models (hereafter CA-like models) and Partial-Differential-Equations-based models (hereafter PDE-based models).

CA-like models are based, partially or totally, on discrete relations approximating conservation principles that are typically expressed as PDEs (Bar-Yam, 1997). Usually, such models divide the study area in discrete cells over a regular grid. Each cell can assume only a finite number of states, depending on how the cell interacts with the neighbours. The cell evolution is evaluated over discrete timesteps according to deterministic rules that depend only on the states of the strictly neighbouring cells (Wolfram, 1984). Such models can be easily implemented, with a limited coding effort and complexity. However, they seem to oversimplify the phenomenon, since the deterministic rules used to evolve cell values are quite basic.

Just for an example, Dottori and Todini (2010) based their CA-model for flood inundations on mass conservation. The continuity equation is written cell per cell, with the inlet and outlet mass fluxes expressed according to the Manning uniform-flow equation. Considering two neighbouring cells, head slope is computed locally as flow-depth slope, while the reference uniform-flow height is the average flow height between the cells. Velocity is assumed to be constant in space and time along directions connecting neighbouring cells.

A similar approach can be found in Gregoretti et al. (2016), where a CA-like model is developed for debris flows. In this case, cell continuity equation includes also the erosion-deposition law proposed by Egashira and Ashida (1987), although written for mono-phase flows. Mass exchange between neighbouring cells is described according to two possible mechanisms: uniform-flow conditions or broad-crested weir flow. In the case of uniform-flow conditions, the Tsubaki equation is considered (Tsubaki, 1972), with the head slope equal to the local bed slope. Only eight possible flow directions are considered (Figure 2.2). This last (non-physical) constraint is quite common in CA-like models describing mountain-flow routing (Hürlimann et al., 2008).

On the contrary, PDE-based models consider conservation

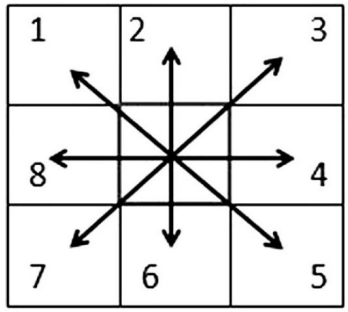

Figure 2.2: Scheme of the eight possible flow directions considered in Gregoretti et al. (2016)

laws expressed in their classical form and solve the system of equations by means of suitable numerical schemes, as explained in detail in Section 2.2. Examples of PDE-based mono-phase models are: the 2D model of O'Brien et al. (1993), which represents the milestone in mono-phase modelling and expresses bed shear stresses as a sum of different contributions (viscous, turbolent, dispersive, coulombian and cohesive); the 1D model of Arattano and Franzi (2003) that uses the relation of Nsom et al. (1998) to describe shear stresses; the 2D model of Medina et al. (2008), which makes available three rheological laws for shear stresses (Bingham, Herschel-Bulkley and Voellmy); the 2D model of Christen et al. (2012) that accounts for Voellmy rheology.

2.1.2 Two-phase modelling

Unlike mono-phase models, two-phase models models consider liquid and solid phases separately (see for example Pitman and Le, 2005; Cao et al., 2006; Wu and Wang, 2008; Armanini et al., 2009b; Greco et al., 2012; Benkhaldoun et al., 2013). However, some models introduce a significant simplification in the description of the two-phase dynamics, assuming that the solid-phase velocity is equal to the liquid-phase velocity. Model developed according to this hypothesis, which is called isokinetic, are addressed as Quasi Two-Phase (QTP) models (Garegnani et al., 2013), to distinguish them from the Fully Two-Phase (FTP) models, that consider each phase with its own velocity. Details about both the approaches are given in the next Sections, where also the other relevant points (nature of the bed, bed evolution, rheological behaviour) are discussed.

With reference to the bed nature, it must be noticed that most available two-phase models work with mobile bed only or with

fixed bed only. However, some studies about time and space transitions from a bed type to the other have been presented recently (Rulot et al., 2012; Rosatti and Zugliani, 2015; Zugliani et al., 2017) and represent an important starting point for further modelling developments.

2.1.2.1 Quasi two-phase modelling

QTP models base the two-phase description of the mixture dynamics on the isokinetic approach, assuming that solid and liquid phases flow with the same velocity. Examples of QTP models are: the 1D models of Cao et al. (2006) and of Wu and Wang (2008); the 2D models of Armanini et al. (2009b) and of Benkhaldoun et al. (2013). Typically, QTP models are PDE-based models.

Evidently, the isokinetic hypothesis is a significant simplification. However, it seems somehow necessary, since a detailed and widely accepted description about how the phases interact, i.e. about inter-phases stresses, is still missing. Furthermore, when concentration is quite high, the isokinetic assumption turns out to be credible.

Most QTP models consider the bed as mobile, giving a proper representation of the typical behaviour of high-concentration flows passing over erodible bed, but failing whenever erosion is simulated where the real bed is fixed. The mobile-bed approach poses the problem of describing how bed and flow interact, i.e. how bed elevation varies according to flow-dynamic variables. The interactions are typically significant, because of the high values of concentration of the mixture, so it is important to describe them properly. Some different approaches can be found in the literature. Here, the two most diffused are discussed. They share the same system of equations, but differ in the approach used to "close" the system.

The reference system of equation in one dimension can be written as follows, with equation 2.2a describing the mass conservation of the mixture, equation 2.2b describing the mass conservation of the solid phase and equation 2.2c representing the mixture momentum balance. Notation is shown in Figure 2.3.

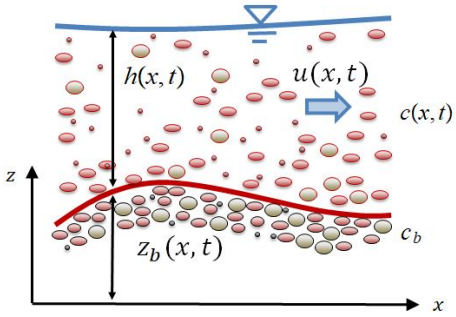

Figure 2.3: Basic notation used to write the 1D, QTP model equations

$$\begin{cases} \dfrac{\partial h}{\partial t} + \dfrac{\partial z_b}{\partial t} + \dfrac{\partial (hu)}{\partial x} = 0 & \text{(2.2a)} \\ \dfrac{\partial (ch)}{\partial t} + c_b \dfrac{\partial z_b}{\partial t} + \dfrac{\partial (chu)}{\partial x} = 0 & \text{(2.2b)} \\ \dfrac{\partial}{\partial t}\left[(1+c\Delta)\, hu\right] + \dfrac{\partial}{\partial x}\left[(1+c\Delta)\left(hu^2 + \dfrac{1}{2}gh^2\right)\right] + (1+c\Delta)\, gh \dfrac{\partial z_b}{\partial x} = -\dfrac{\tau_b}{\rho_w} & \text{(2.2c)} \end{cases}$$

z_b is the bed elevation, c the average volumetric concentration, c_b the maximum packaging concentration ($c_b = 1 - p$, where p is the porosity) and $\Delta = (\rho_s - \rho_w)/\rho_w$, with ρ_w and ρ_s representing the density of the liquid and the solid phase respectively.

The unknowns of the system are five (h, u, z_b, c and τ_b), but only three equations are present in the system. Therefore, two further equations are necessary to "close" it, i.e. to express some unknowns as functions of the other unknowns. These formulae can be either differential or algebraic and, commonly, they concern mixture concentration c (or density), bed-elevation evolution in time $\partial z_b/\partial t$ or shear stresses τ_b.

Several models (see for example Fagherazzi and Sun, 2003; Cao et al., 2006; Wu and Wang, 2008; Benkhaldoun et al., 2013) "close" the problem introducing a differential closure relation for the bed evolution $\partial z_b/\partial t$ and an algebraic relation for the shear stresses τ_b.

Commonly, the expression describing the bed evolution is written in this form:

$$c_b \frac{\partial z_b}{\partial t} = D - E$$

where D represents the sediment deposition flux and E is the bed-sediment entrainment rate. The bed-sediment entrainment rate is often estimated accounting for the Shields parameter value, a reference bed-sediment size and local values of flow depth and velocity. On the other side, deposition fluxes are related to the

local depth-averaged concentration and the settling velocity of a single particle in water at rest. Relations describing D and E are often empirical and difficult to calibrate.

The other necessary closure formula concerns bed shear stresses, which are described sometimes as collisional, sometimes as Coulombian, sometimes as turbulent, sometimes as viscous. Certainly, each rheological approach implies a different "distance" between the phenomenon representation and its natural behaviour, as well as a different computational complexity.

Differently, models such as Armanini et al. (2009b) describe the bed evolution as fully-coupled with the two-phase mixture dynamics, preserving the differential character of the conservation equations. Models applying this approach "close" the system of equations by means of two algebraic closures, one for the bed shear stresses τ_b, as in the previous case, and one for the sediment concentration c. Examples of closure relations used to couple concentration to hydrodynamic variables are:

- the formulation of Meyer-Peter and Müller (1948)

$$c = \frac{8}{\Delta g h u}\left(\frac{\tau_b}{\rho_w} - \frac{\tau_{bc}}{\rho_w}\right)^{3/2}$$

  where τ_{bc} is the critical shear stress for incipient sediment motion;

- the formulation suggested by Takahashi (1987)

$$c = \frac{d}{h}\frac{1 + 5\tan\alpha}{\cos\alpha}\frac{|\tau_b|}{\rho_w g d}\left(1 - k\frac{|\tau_b|}{\tau_{bc}}\right)\left(1 - k\sqrt{\frac{|\tau_b|}{\tau_{bc}}}\right)$$

  where d is the sediment size, α is the slope angle and k a constant;

- the formulation of Armanini (2015)

$$c = 1.54\left(\frac{\sin\alpha}{\Delta}\right)^2\left(\frac{d}{h}\right)^{-5/6}$$

Usually, closure relations are developed for specific ranges of concentrations. For instance, the collisional-regime approach is valid only at quite high concentrations, typical of debris flows, while the turbulent-regime approach is more suitable for bed-load flows (Armanini, 2015). Therefore, the use of an approach

outside of its range of validity could make the description inaccurate. Better results could be obtained using rheology relations valid over a wide range of slopes and concentrations (Armanini, 2015). However, such formulae are still quite rare and their use is expected to increases the effort required for their numerical implementation (personal communication of Giorgio Rosatti).

Anyhow, such an approach appears more general than the previous one, for some reasons. First, differentiability is preserved. Second, no specific parameters are required to describe entrainment and deposition, so hard parameter calibration is avoided. Third, empirical functions used in the previous approach to describe entrainment and deposition rates are obtained typically for low values of sediment concentration and in suspended-load conditions, therefore their application in the high-concentration flow case seems rather imprecise. However, the use of a more general approach obliges the model developer to manage a more sophisticated system of PDEs, with some consequences from a numerical point of view (see Section 2.2).

A further observation concerns sediment size. Only some QTP models (see for example Wu and Wang, 2008) divide moving sediments in size fractions, while the more diffused approach reduces the grain size heterogeneity to a single-size distribution. Giving up to describing the real grain size distributions reduces the level of detail of the phenomenon representation, which is not able to catch processes as for example segregation. However, dealing with more sediment-size fractions could make models excessively sophisticated, generating redundant complicatedness and computational burden. Therefore, for the time being working with single sediment size seems to be an acceptable compromise between natural complexity and modelling manageability, avoiding complicatedness.

2.1.2.2 Fully two-phase modelling

Fully Two-Phase (FTP) models describe each phase with its own velocity. In principle, this approach appears more physically-based than the previous one. 2D models developed by Pitman et al. (2003) and Greco et al. (2012) are two relevant examples of FTP, PDE-based models. They assume the bed respectively as fixed and as mobile.

Fixed-bed FTP models can be traced back to the following 1D system of equations, where equation 2.3a describes the mixture-

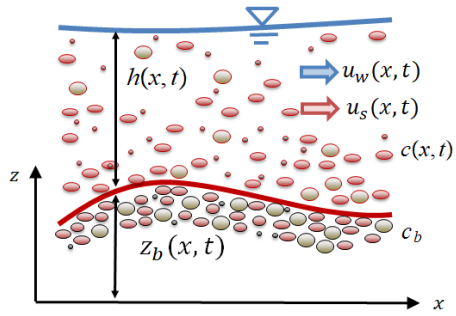

Figure 2.4: Basic notation used to write the 1D, FTP model equations

mass balance, equation 2.3b represents the solid-mass balance, equation 2.3d expresses the momentum conservation of the solid phase and equation 2.3c describes the momentum conservation of the liquid phase. Basic notation used in writing 1D FTP equations is showed in Figure 2.4.

$$\begin{cases} \dfrac{\partial h}{\partial t} + \dfrac{\partial}{\partial x}\left[chu_s + (1-c)hu_w\right] = 0 & \text{(2.3a)} \\ \dfrac{\partial (ch)}{\partial t} + \dfrac{\partial (chu_s)}{\partial x} = 0 & \text{(2.3b)} \\ \dfrac{\partial}{\partial t}\left[(1-c)\,hu_w\right] + \dfrac{\partial}{\partial x}\left[(1-c)\left(hu_w^2 + \dfrac{1}{2}gh^2\right)\right] + (1-c)\,gh\dfrac{\partial z_b}{\partial x} = -\dfrac{\tau_w}{\rho_w} & \text{(2.3c)} \\ \dfrac{\partial}{\partial t}\left(chu_s\right) + \dfrac{\partial}{\partial x}\left[c\left(hu_s^2 + \dfrac{1}{2}\Delta gh^2\right)\right] + c\Delta gh\dfrac{\partial z_b}{\partial x} = -\dfrac{\tau_s}{\rho_s} & \text{(2.3d)} \end{cases}$$

u_s and u_w represent the solid- and the liquid-phase velocity respectively. It must be noticed that the terms τ_s and τ_w collect the both the phase-proper and the inter-phase stresses.

Mobile-bed FTP model equations differ from those presented in system 2.3 essentially for the terms concerning bed evolution. The system of equation can be written as follows:

$$\begin{cases} \dfrac{\partial\left[(1-c)\,h\right]}{\partial t} + (1-c_b)\dfrac{\partial z_b}{\partial t} + \dfrac{\partial}{\partial x}\left[chu_s + (1-c)hu_w\right] = 0 & \text{(2.4a)} \\ \dfrac{\partial (h)}{\partial t} + \dfrac{\partial (chu_s)}{\partial x} = 0 & \text{(2.4b)} \\ \dfrac{\partial}{\partial t}\left[(1-c)\,hu_w\right] + \dfrac{\partial}{\partial x}\left[(1-c)\left(hu_w^2 + \dfrac{1}{2}gh^2\right)\right] + (1-c)\,gh\dfrac{\partial z_b}{\partial x} = -\dfrac{\tau_w}{\rho_w} & \text{(2.4c)} \\ \dfrac{\partial}{\partial t}\left(chu_s\right) + \dfrac{\partial}{\partial x}\left[c\left(hu_s^2 + \dfrac{1}{2}\Delta gh^2\right)\right] + c\Delta gh\dfrac{\partial z_b}{\partial x} = -\dfrac{\tau_s}{\rho_s} & \text{(2.4d)} \end{cases}$$

In both the cases, the systems need to be "closed". However, nowadays widely accepted formulations about how phases reciprocally interact are still missing. Moreover, existing FTP models are typically referred to low-concentration regimes, therefore

they seem to be not suitable for the purposes of this thesis. On the strength of these observations, the expected increase in the level of detail introduced by FTP model seems to be not counterbalanced by a suitable detail in the closure of the problem as far as high-concentration flows are studied. Therefore, QTP model seem to represent a more acceptable compromise between accuracy and robustness in the phenomenon representation.

2.2 Complexity and numerical modelling

Model equations represent "the rules of the game", while "the goal of the game" is to represent time and space evolution of a system. This goal can be reached only applying the rules, i.e. integrating the model equations. However, equation integration is anything but straightforward and requires suitable approaches for discretisation and Riemann Problem solution. In the following paragraphs, significant aspects about integration of high-concentration model equations and solution of relevant problems are presented and discussed.

2.2.1 Hyperbolicity

Typically, 2D, high-concentration flow models are non-linear systems of equations characterized by hyperbolicity. A system is called hyperbolic if its eigenvalues are real and if it shows a complete set of linearly-independent eigenvectors. Hyperbolicity depends not only by the structure of the equations, but also by the relation chosen to "close" the system. For example, Cordier et al. (2011) showed that some bedload transport formula as Meyer-Peter and Müller (1948), Fernandez Luque and Van Beek (1976) or Nielsen (1992) in essentially mono-phase models, (i.e. QTP models where the solid mass balance is essentially the Exner equation) may lead to the lost of hyperbolicity, i.e. to the appearance of complex eigenvalues. Therefore, if hyperbolicity is intended to be preserved, model developers should choose closure relations that are not only physically-based but also avoiding instability.

From a numerical point of view, hyperbolicity represents a profitable property in PDEs systems, since it allows to decompose Riemann Problem solutions in simple waves. Riemann Problems (RPs) are particular Initial-Value Problems (IVPs), where the left and right initial states are two constant values (Toro, 2009) separ-

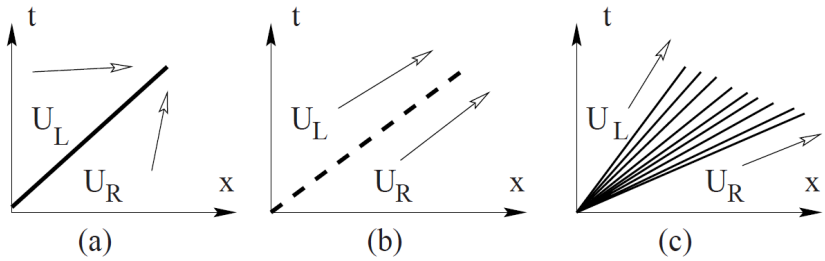

Figure 2.5: From Toro (2009): simple wave solutions of the RP: (a) shock wave, (b) contact wave, (c) rarefaction wave

ated by a discontinuity. A RP for a general non-linear hyperbolic system way can be written as follows:

$$\begin{cases} \dfrac{\partial \mathbf{U}}{\partial t} + \dfrac{\partial \mathbf{F}(\mathbf{U})}{\partial x}, & \text{(2.5a)} \\ \mathbf{U}(x,0) = \begin{cases} \mathbf{U}_L & \text{if } x < 0 \\ \mathbf{U}_R & \text{if } x > 0 \end{cases} & \text{(2.5b)} \end{cases}$$

where $\mathbf{U}$ is the vector of the conserved variables, $\mathbf{F}(\mathbf{U})$ is the vector of the fluxes and $\mathbf{U}_L$ and $\mathbf{U}_R$ are the left and right initial states of the RP. The solution of a RP is made of a number of simple waves equal to the number of eigenvalues of the system. Waves can be either rarefaction waves, shock waves or contact waves.

Rarefaction waves are waves across which there is a smooth transition of the state variables $\mathbf{U}_L$ and $\mathbf{U}_R$ (LeVeque, 1992) and show a typical diverging behaviour (Figure 2.5c). Across the wave, Generalised Riemann Invariants are constant (Toro, 2009).

Shock waves represent jump discontinuities in state variables, with typical compression character (Figure 2.5a). They satisfy the Rankine-Hugoniot and the entropy conditions (Toro, 2009). Both rarefaction and shock waves are associate with genuinely non-linear characteristic field, which means that, if the i-th eigenvalue $\lambda_i(\mathbf{U})$ and the associated eigenvector $\mathbf{R}_i(\mathbf{U})$ are considered,

$$\nabla \lambda_i(\mathbf{U}) \mathbf{R}_i(\mathbf{U}) \neq 0, \ \forall \mathbf{U}$$

On the contrary, contact waves, which are called also contact discontinuities, are associated to linearly-degenerated characteristic fields

$$\nabla \lambda_i(\mathbf{U}) \mathbf{R}_i(\mathbf{U}) = 0, \ \forall \mathbf{U}$$

They satisfy the Rankine-Hugoniot conditions, the constancy of Generalised Riemann Invariants and their characteristics are par-

allel (Toro, 2009) (Figure 2.5b).

Since high-concentration flows often show sequence of impulses, i.e. of discontinuities, the proper representation of shock waves in modelling is essential to reach the *right level* of detail in the description. In this regard, it must be noticed that a wrong representation of a shock may affect a significant part of the modelled flow (Toro, 2001). However, representing properly shocks in non-conservative hyperbolic systems is one of the most challenging topics in numerical modelling and not all the available numerical schemes are suitable for this purpose. Methods able to compute solutions containing discontinuities can be divided essentially into two groups: shock-fitting methods and shock-capturing methods.

Methods applying the shock-fitting approach deal with shocks imposing proper jump conditions only on suitable internal boundary where shocks are observed, while methods suitable for smooth flows are applied elsewhere. In this way, discontinuities are described appropriately. Examples of shock-fitting methods are the front-tracking methods of Chern and Colella (1987) and LeVeque and Shyue (1996) and Glimm et al. (1998). However, the wave interactions inside multidimensional domains make these methods too much complicated (LeVeque, 2002) or impossible to be applied (Toro, 2001).

On the contrary, shock-capturing methods use the same numerical scheme all over the computational domain, in a completely general way. According to these methods discontinuities are simply a part of the solution. The drawback of this approach lies in the representation of shock waves, which are typically smeared over more than one mesh elements. Different shock-capturing methods produce different smearing (Toro, 2001). However, the generality and the remarkable simplicity of this approach make it more attractive than the previous one and definitely more suitable for high-concentration flow modelling. Examples of shock-capturing methods are the HLL solver (Harten et al., 1983) and its derived schemes (Einfeldt, 1988; Toro et al., 1994; Fraccarollo et al., 2003), the Roe-type solvers (Roe, 1981; Harten et al., 1983; Einfeldt et al., 1991; Dubois and Guillame, 1993; Rosatti and Begnudelli, 2013b), the Osher-type solvers (Engquist and Osher, 1981; Osher and Solomon, 1982), the Weighted Averaged Flux WAF method (Toro, 1989; Billett and Toro, 1997), the MUSCL-type (van Leer, 1979) and its high-order versions.

2.2.2 Space and time discretisation

Currently, available numerical approaches can be classified according to the space and time discretisation used. As far as space discretisation is concerned, two main approaches can be identified, i.e. grid-based methods and meshless methods, while according to time discretisation, numerical schemes can be divided into explicit and implicit schemes. Different discretisation choices entail different pros and cons.

Considering space discretisation, grid-based methods base the spatial discretisation of the computational domain on the use of points or cells, which distribution can be both regular or irregular. Such methods are often chosen because they allow to manage space in a quite rational way, especially if regular meshes are used. However, they require some effort for mesh generation, especially when irregular meshes are used. Further details about the different types of mesh and their convenience are reported in Chapter 6. Finite-difference and finite-volume methods belong to this category. However, finite-difference methods, although simple to be implemented, especially if regular grids are considered, allow to catch properly only "strong solutions", i.e. solutions that are smooth enough and can be described by the differential form of the problem, while they are not suitable to describe "weak solutions", i.e. discontinuities. The only way to catch also "weak solutions" is to resort to integral methods, as for example finite-volume methods.

On the other side, meshless methods base their discretisation on particles Smoothed Particle Hydrodynamics (SPH) methods are the most established of this category. These methods are based on a Lagrangian formulation of the governing equations and seem to be particularly suitable to analyse problems with deformable boundary, moving interface and large deformations (Liu and Liu, 2003). SPH methods have the advantage to save time required for meshing.

As far as time discretisation is concerned, explicit methods express the state variables $\mathbf{U}$ at time $t^{n+1} = t^n + \Delta t$ once the state variables at the current timestep t^n are knwon, without solving any system of equations. This makes explicit methods quite easy to be implemented. However, in order to ensure numerical stability a constraint is required on the timestep Δt. This constraint is the Courant-Friedrichs-Lewy (CFL) condition, which is expressed

as follows

$$\frac{\lambda \Delta t}{\Delta l} < CFL$$

where λ represents the maximum speed of the problem, Δl the characteristic length used in the spatial discretisation and CFL is the Courant coefficient, which is typically set equal to 1 in 1D problems.

On the other side, implicit methods obtain the state variables $\mathbf{U}$ at time $t^{n+1} = t^n + \Delta t$ solving a typically non-linear system of equations. This introduces a significant effort at each timestep, but makes stability conditions no more necessary.

2.2.3 One- or two-dimensional schemes

A large number of numerical schemes were developed for 1D problems. However, as stated in the previous Section, at least 2D models should be used for applications in the real world. This means that numerical schemes should be able to work in multi-dimensions.

Often, 1D schemes can be straightforwardly applied also in 2D problems resorting to dimensional splitting. However, sometimes a multidimensional approach is suggested, especially in case of complex morphology. In such conditions, different, more demanding approaches can be used, as shown in Chapter 6.

2.2.4 Bed nature

Another critical point in numerical modelling of high-concentration flows is represented by the bed nature.

First, it must be observed that, if the bed is described as mobile in high-concentration flow models, the system of equation shows both conservative and non-conservative terms. In this case, effort required to solve the model equations is larger than in the fixed-bed case. Moreover, particularly sophisticated schemes are needed, as those developed quite recently by Fraccarollo et al. (2003) or Murillo and García-Navarro (2010), which implementation is quite demanding and introduces high computational costs. However, to date, this is the only way to reach an acceptable level of robustness in reproducing high-concentration flows over mobile bed.

In addition, to reproduce the transition between fixed and mobile bed for models able to deal properly with both the types of

bed, proper numerical solvers are required, as shown in recent studies (Rulot et al., 2012; Rosatti and Zugliani, 2015; Zugliani et al., 2017). In fact, the transition from fixed to mobile bed and viceversa requires the solution of a particular type of Riemann Problem, where not only the state variables, but also the system of PDEs changes from the left side to the right side of the discontinuity. Because of this peculiarity, suitable, more sophisticated RP solvers must be used.

2.2.5 Significant solutions

Whichever are the model-developer choices, it is important that the model is able to catch properly some simple, but essential physical behaviours of the flow. In addition, non-physical solutions must be avoided.

As far as high-concentration flows are concerned, two main conditions must be represented correctly: the water-at-rest condition (C-property) and the steady-state flow condition (well-balancedness). Methods that do not satisfy these two properties should be used carefully.

2.2.6 A trade-off between accuracy and costs

Undoubtedly, natural complexity of high-concentration flows generates significant challenges in numerical modelling, which aims at producing robust solution with the lowest level of approximation possible, though without exceeding in computational costs (hardware, time, number of operations). However, to date this equilibrium seems to be still out of reach.

High level of detail and accuracy mean high costs, as highlighted through the previous analysis, while low costs mean to turn down accuracy. Typically, developers of two-phase PDE-based models prefer reaching an acceptable level of detail, i.e. an enough low level of approximation, bearing high computational costs. To this end, "purely-numerical" model developers are always more oriented towards numerical methods with high-order of accuracy. However, it must be pointed out that the uncertainty in high-concentration flow knowledge is still significant. Therefore, using high-accuracy methods to solve still uncertain equations can look somehow like a waste, clearly failing the parsimony principle.

In these conditions, an acceptable compromise can be represented by second-order methods, which accuracy is comparable with phenomenon knowledge and which computational costs seem reasonable, if compared to methods with higher order of accuracy. Nevertheless, computational costs of second-order methods, although relatively low, can not be neglected. This point generates some drawbacks on model users, who are required to have high-performance hardware available if they want to preserve enough accuracy in model applications. This necessity represents a barrier for the Transfer of Technology. A possible answer to the problem is represented by integrated solutions, as explained in Chapter 5.

On the basis of these observations, this thesis was developed in the framework of grid-based methods with explicit time integration. Finite-volume schemes with Godunov-type fluxes are used, in order to ensure shock-waves capturing, and accuracy is limited to second order.

2.3 Complexity and parameters, initial and boundary conditions

To integrate model equations, not only numerical methods are necessary, but also initial conditions, boundary conditions and parameters values. The level of detail and the reliability of model results depend largely also on these three elements, i.e. on how they are set and managed.

Parameters, initial and boundary conditions are the means of communication between the user and the model, i.e. they are used to adapt the model equations to the specific case study. Choosing right setups is a responsibility of both model developer and user. The developer has to implement suitable strategies to make their understanding and management straightforward, preserving their physical meaning, while the user must choose acceptable values to describe properly what he/she intended to represent.

2.3.1 Parameters

Setting parameter values can be quite challenging and often requires calibration, especially if their physical meaning is not well defined. In general, physically-based parameters can be set reas-

onably also without calibration, while non-physical parameters can be set only on the strength of available empirical suggestions (sometimes gathered in tables), if calibration is not possible.

To better clarify this point, an example is given. The mono-phase model of O'Brien et al. (1993), which is used to simulate both cohesive and cohesionless high-concentration flows, evaluates the yield shear stress τ_y and the flow viscosity η by means of two empirical relations

$$\eta = \alpha_1 \exp(\beta_1 c_v) \quad \text{and} \quad \tau_y = \alpha_2 \exp(\beta_2 c_v) \tag{2.6}$$

where c_v is the volumetric concentration of silt, clays and fine sands, while α_1, α_2, β_1 and β_2 are empirical coefficient. For these coefficients, the authors indicate some relevant values obtained experimentally for some mudflow samples (O'Brien and Julien, 1988). However, it is not clear which value should be chosen depending on the type of application, since no physical handles are available.

On the contrary, the same model requires the specification of the mixture density ρ_m, which physical meaning is straightforward and which value can be easily estimated or measured.

Whenever non-physical parameters are present in a model, sensitivity analysis of parameter values is warmly recommended to avoid improper representations.

In any case, understanding the effect of each parameter on model results is essential to analyse subsequently parameter uncertainty and equifinality and to prevent the forcing of model results.

Similar and more detailed observations can be formulated with reference to initial and boundary conditions.

2.3.2 Initial and boundary conditions

Setting initial and boundary conditions is widely recognised by the model-developers community as one of the most critical points in modelling. However, users are still quite unaware about their key importance and sometimes feed inaccurate or improper data into models, running the risk of a bad representation of reality, even accurate models are used. The reasons of such a possible outcome are mainly two: natural complexity and data-management complicatedness. Both are now discussed, first with reference to initial condition, then to boundary conditions.

Terrain elevation is the most common initial condition of high-concentration flow models. As recalled in Section 1.3, terrain morphology can be represented by means of DTMs, joined with field surveys. Whatever the origin and the format of morphological information, it is important to be aware of its level of accuracy and to choose a proper level of spatial resolution in representing natural complexity. Sometimes, models require also flow depth and velocity values as initial conditions. Also in this case, data accuracy and resolution should be checked. As far as data formats are concerned, model developers should allow users to deal with manageable, not complicated formats and extensions, in order to avoid oversights in terrain and hydrodynamics (and phenomena) representations.

Boundary conditions are as much or even more thorny. For sake of clarity, they are divided here into inlet and outlet boundary conditions.

To simulate high-concentration flows, models require typically the specification of the mixture flow rates incoming into the study area. If two-phase models are considered, time evolution of both solid and liquid discharges must be specified. This information can be set after carrying out the analyses described in Section 1.3, evaluating results carefully. Usually, discharge values need to be transformed into hydrodynamical variables as for example flow height and velocity. This transformation is often performed inside the model, according to physical laws chosen by the developer. Using uniform-flow relations is one of the possibilities. However, it must be noticed that such a choice introduces a significant, arbitrary simplification in the description, since the uniform-flow condition is not necessarily verified at the inlet section of the study domain. Therefore, if this is the developer choice, the user has to identify carefully the inlet section of his/her domain, moving close to the developer hypothesis as much as possible.

Conditions to be considered at the outlet bound of the study domain are often imposed by model developers, although sometimes users are allowed to chose the condition within a set of possible conditions. In both the cases, choosing the right option is essential to represent properly not only boundary processes, but also their influence inside the study domain. Non-reflecting conditions are typical outlet boundary conditions. In this case, the bound is considered transparent outgoing fluxes as computed according to the state variables of the boundary cells. However,

the presence of particular works or devices at the outflow bound (or sometimes inside) the study area could require different, more specific formulations. This is the case of weirs, slit check dams, levees, sluice gates, which behaviour must be properly reproduced in order to catch the real system evolution.

Therefore, developers and users have to face not only intrinsic complexity of the natural processes they describe, but also complexity generated by the interaction between natural flows and artificial elements. This point is further discussed in Chapter 7.

Chapter 3

The TRENT2D model

In this Chapter, the TRENT2D model is shortly presented and its approach to complexity discussed. This model represents the basis of the analyses and the results proposes in the next Chapters of this thesis, therefore its characteristics are reported here with the level of detail necessary to appreciate subsequent analyses.

TRENT2D was firstly developed in 2009 by Armanini et al. and updated in 2013 by Rosatti and Begnudelli, but its development is still continuing due to the work of the research group of prof. Giorgio Rosatti.

TRENT2D is a PDE-based, 2D, shallow flow model developed to describe debris flows and, more in general, high-concentration flows with a quasi two-phase approach. The flow evolution is described applying a QTP (isokinetic) approach over a mobile bed, while the description of the bed evolution is fully-coupled with the flow dynamics, because of the significant values of sediment concentrations typical of high-concentration flows (Garegnani et al., 2013).

Model equations are written in a Cartesian reference system (x, y, z) (see Figure 3.1), where $x-$ and $y-$axes are planar, while the $z-$axis is assumed to be vertical. Equations are then solved over a Cartesian mesh by means of finite-volume shock-capturing methods, with Godunov-type fluxes. Accuracy is second order in time and space.

Modelling and computational complexity of TRENT2D derives mainly from its constitutive hypotheses and regards both the mathematical and the numerical description. Constitutive hypotheses and design choices make the model quite sophisticated to be implemented and managed, although some simplifications

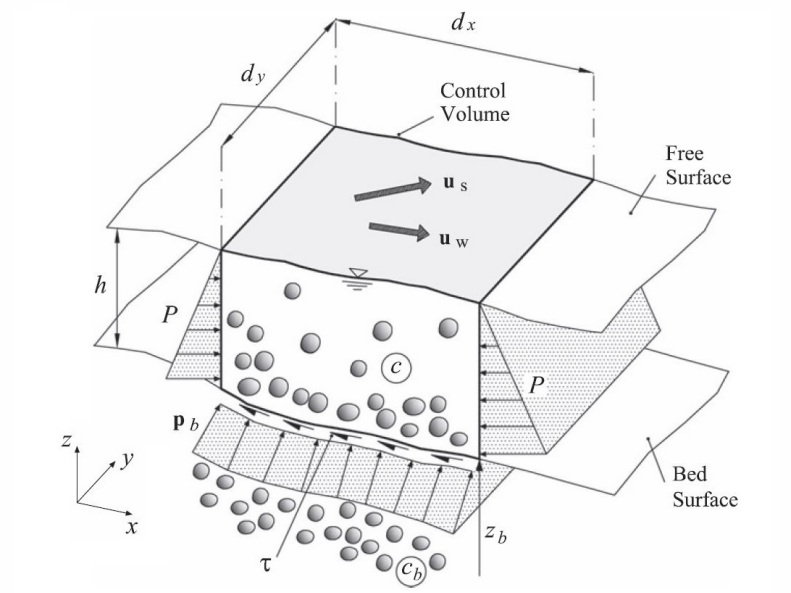

Figure 3.1: Reference system and control volume used to write the TRENT2D model equations (Rosatti and Begnudelli, 2013a)

are present. Such complexity influences somehow also the use of the model. Anyhow, TRENT2D shows a good level of detail in the representation of high-concentration flow complexity, as pointed out by several applications of the model (Stancanelli and Foti, 2015; Rosatti et al., 2015; Lanni et al., 2015; Zasso, 2015; Marchelli et al., 2016; Veronesi, 2017). A couple of them is discussed in the next Chapter.

In order to appreciate different aspects of the TRENT2D model, this Chapter is organised as follows: in Section 3.1 the TRENT2D mathematical model is shortly presented, while Section 3.2 is dedicated to the numerical model; last, in Section 3.3 a short characterisation about model input and output data is proposed. For further detail about the mathematical and numerical model, refer to Armanini et al. (2009b) and Rosatti and Begnudelli (2013a).

3.1 The mathematical model

The mathematical model of TRENT2D is composed of four PDEs, expressing the conservation of the total mass of the solid-liquid mixture (Equation 3.1a), the conservation of the solid-phase mass (Equation 3.1b) and the conservation of the mixture momentum in the x and y horizontal directions (Equations 3.1c and 3.1d). Momentum equations are referred only to the mixture be-

cause of the isokinetic hypothesis.

$$\begin{cases} \dfrac{\partial}{\partial t}(h+z_b)+\dfrac{\partial}{\partial x}(hu_x)+\dfrac{\partial}{\partial y}\left(hu_y\right)=0 & \text{(3.1a)}\\ \dfrac{\partial}{\partial t}(ch+c_bz_b)+\dfrac{\partial}{\partial x}(chu_x)+\dfrac{\partial}{\partial y}\left(chu_y\right)=0 & \text{(3.1b)}\\ \dfrac{\partial}{\partial t}(\delta hu_x)+\dfrac{\partial}{\partial x}\left[\delta\left(hu_x^2+\dfrac{1}{2}gh^2\right)\right]+\delta gh\dfrac{\partial z_b}{\partial x}+\dfrac{\partial}{\partial y}\left(\delta hu_xu_y\right)=-\dfrac{\tau_{bx}}{\rho_w} & \text{(3.1c)}\\ \dfrac{\partial}{\partial t}\left(\delta hu_y\right)+\dfrac{\partial}{\partial x}\left(\delta hu_xu_y\right)+\dfrac{\partial}{\partial y}\left[\delta\left(hu_y^2+\dfrac{1}{2}gh^2\right)\right]+\delta gh\dfrac{\partial z_b}{\partial y}=-\dfrac{\tau_{by}}{\rho_w} & \text{(3.1d)} \end{cases}$$

The unknowns of the system are: the flow depth h, the mobile-bed elevation z_b and the depth-averaged velocity $\vec{u}=\left(u_x,u_y\right)$. t indicates time, g is the gravitational acceleration. c_b is the maximum packaging concentration of the bed sediments, c the depth-averaged concentration of the solid phase in the mixture, $\delta=1+c\Delta$, where $\Delta=(\rho_s-\rho_w)/\rho_s$, ρ_s is the solid-phase density, ρ_w the water density. τ_{bx} and τ_{by} are the bed shear stress components.

In order to close the problem, the model uses two relations describing concentration c and bed shear stresses $\vec{\tau_b}$ as functions of the other hydrodynamic variables. To date, two versions of the mathematical model are available, adopting different closure relations. One version was developed for high-concentration flows with rheological behaviour similar to sediment transport, i.e. for concentration values that are not very high, while the other one was developed specifically for debris flows, which rheological behaviour is different and concentration is higher. The development of two versions was carried out for the purpose of covering somehow a wide range of concentration, until unified closure relations that are also numerically manageable are available.

Both the versions share the same relation to describe concentration c. This relation was proposed in Rosatti and Fraccarollo (2006):

$$c=c_b\beta\frac{|\vec{u}|^2}{gh} \tag{3.2}$$

where β is a dimensionless transport parameter. To be precise, this relation expresses the transport capacity of the flow in uniform-flow conditions. However, the model is based on the hypothesis of immediate adaptation, which allows concentration to be assumed equal to the local and instantaneous transport capacity.

The two versions of the model differ in the formula describing bed shear stresses $\vec{\tau_b}$. Both implement relations developed

for uniform-flow conditions, according to the common practice. Certainly, this is a simplification, since the flow is rarely in equilibrium conditions, however no alternative relations are available, therefore this simplification (which is quite common) must be accepted compulsorily.

TRENT2D^{TS} is the version developed to describe phenomena which average concentration is not extremely high ($c \sim 1 - 10\%$). The relation used to characterise the bed shear stresses is the Gauckler-Strickler formula:

$$\vec{\tau_b} = \rho_m g \frac{|\vec{u}|\vec{u}}{Ks^2 h^{1/3}} \tag{3.3}$$

where Ks is the Gauckler-Strickler roughness coefficient, while ρ_m is the density of the mixture that can be expressed as $\rho_m = \rho_w (1 + c\Delta)$.

TRENT2D^{DF} is the version developed to describe phenomena which average concentration is higher ($c > 5 - 10\%$). These phenomena are indicated hereafter as debris flows and are characterised by a different rheological behaviour (Armanini et al., 2009a). Resistance is no more frictional, but rather collisional. For this reason, the rheological relation proposed by Bagnold (1954) and modified by Takahashi (1978) was considered to describe the grain-inertial regime:

$$\vec{\tau_b} = \frac{25}{4} \rho_s a sin\Phi \frac{\lambda^2}{Y^2} |\vec{u}|\vec{u} \tag{3.4}$$

Φ is the friction angle and a is a constant assumed equal to 0.32 according to Takahashi observations. Y is the relative submergence defined as

$$Y = \frac{h}{d} \tag{3.5}$$

where d is the grain size. In order to limit computational costs and avoid numerical singularities for $h \to 0$, Y is assumed to be constant. In fact, Y is a model parameter, which highest value can be 25 in grain-inertial regime (Julien, 1997). In the relation 3.4 appears also the linear concentration λ, which is defined as follows:

$$\lambda = \frac{c^{1/3}}{{c_b}^{1/3} - c^{1/3}} \tag{3.6}$$

Whatever the TRENT2D version used, it is possible that, locally, concentration goes beyond the concentration range charac-

teristic of the considered version. This means that, locally, both the closure relations could be applied outside the range (for instance, in TRENT2D^{TS} applications concentration could significantly increase whenever deep and diffuse erosion processes are simulated, while in TRENT2D^{DF} applications concentration could significantly decrease whenever intense deposition processes are simulated). However, this limit can not be overcome until relations encompassing the whole range of concentration and numerically manageable are implemented in the model.

3.2 The numerical model

The TRENT2D mathematical model can be written in the following form:

$$\frac{\partial \mathbf{U}}{\partial t} + \frac{\partial \mathbf{F}}{\partial x} + \frac{\partial \mathbf{G}}{\partial y} + \mathbf{H}_x \frac{\partial \mathbf{W}}{\partial x} + \mathbf{H}_y \frac{\partial \mathbf{W}}{\partial y} = \mathbf{T}_x + \mathbf{T}_y \tag{3.7}$$

where

$$\mathbf{U} = \begin{bmatrix} h + z_b \\ ch + c_b z_b \\ (1 + c\Delta) h u_x \\ (1 + c\Delta) h u_y \end{bmatrix}; \qquad \mathbf{W} = \begin{bmatrix} h \\ u_x \\ u_y \\ z_b \end{bmatrix}$$

$$\mathbf{F} = \begin{bmatrix} h u_x \\ c h u_x \\ (1 + c\Delta)\left(\frac{1}{2} g h^2 + h u_x^2\right) \\ (1 + c\Delta) h u_x u_y \end{bmatrix}; \qquad \mathbf{G} = \begin{bmatrix} h u_y \\ c h u_y \\ (1 + c\Delta) h u_x u_y \\ (1 + c\Delta)\left(\frac{1}{2} g h^2 + h u_y^2\right) \end{bmatrix}$$

$$\mathbf{H}_x = \begin{bmatrix} 0 & 0 & 0 & 0 \\ 0 & 0 & 0 & 0 \\ 0 & 0 & 0 & (1 + c\Delta) g h \\ 0 & 0 & 0 & 0 \end{bmatrix}; \qquad \mathbf{H}_y = \begin{bmatrix} 0 & 0 & 0 & 0 \\ 0 & 0 & 0 & 0 \\ 0 & 0 & 0 & 0 \\ 0 & 0 & 0 & (1 + c\Delta) g h \end{bmatrix}$$

$$\mathbf{T}_x = \begin{bmatrix} 0 \\ 0 \\ -\tau_{bx}/\rho_w \\ 0 \end{bmatrix}; \qquad \mathbf{T}_y = \begin{bmatrix} 0 \\ 0 \\ 0 \\ -\tau_{by}/\rho_w \end{bmatrix}$$

This system is highly non-linear, due to the presence of non-

conservative terms, and its solution requires the use of suitable, quite demanding numerical schemes.

Equations are solved over a Cartesian mesh by means of finite-volume, shock-capturing methods based on Godunov-type approach. Two solvers have been used alternatively to solve the PDEs system: the LHLL solver (Fraccarollo et al., 2003), shortly presented in Section 3.2.1, and the Generalised Roe solver (Rosatti and Begnudelli, 2013a) in its two versions (SCGR and CIGR), reported in Section 3.2.2. In both the schemes, accuracy is second order in space and time thanks to the MUSCL-Hancock approach (Harten et al., 1983; Toro, 2001). Both the solvers are applied inside a precise procedure, described in Armanini et al. (2009b) and Rosatti and Begnudelli (2013a) and repeated at each timestep Δt. The procedure is summarised here below. i, j indicate the cell indexes in the x and y directions respectively, n the timestep index, $\Delta x = \Delta y$ the cell dimensions.

1) Non conservative half-step ($t^n \rightarrow t^{n+\frac{1}{2}}$)

   a. *Data reconstruction*: primitive variables $\mathbf{W}^n_{i\pm\frac{1}{2},j}$ and $\mathbf{W}^n_{i,j\pm\frac{1}{2}}$ at the cell bounds are obtained by means of piece-wise linear reconstruction starting from the cell-average values $\mathbf{W}^n_{i,j}$. To avoid oscillations, the minmod limiter is used.

   b. *Solving the non-conservative homogeneous part*: vectors of conserved variables are updated considering only the homogeneous part of the system. Primitive variables $\mathbf{W}$ and fluxes $\mathbf{F}$ and $\mathbf{G}$ are computed by means of their physical expressions, considering reconstructed values $\mathbf{W}^n_{i\pm\frac{1}{2},j}$ and $\mathbf{W}^n_{i,j\pm\frac{1}{2}}$ obtained at the previous point.

$$\begin{aligned}\hat{\mathbf{U}}^{n+\frac{1}{2}}_{i,j} = \mathbf{U}^n_{i,j} \; & -\frac{0.5\Delta t}{\Delta x}\left(\mathbf{F}^n_{i+\frac{1}{2},j} - \mathbf{F}^n_{i-\frac{1}{2},j}\right) \\ & -\frac{0.5\Delta t}{\Delta y}\left(\mathbf{G}^n_{i,j+\frac{1}{2}} - \mathbf{G}^n_{i,j-\frac{1}{2}}\right) \\ & -\frac{0.5\Delta t}{\Delta x}\left[\mathbf{H}_x\right]^n_{i,j}\left(\mathbf{W}^n_{i+\frac{1}{2},j} - \mathbf{W}^n_{i-\frac{1}{2},j}\right) \\ & -\frac{0.5\Delta t}{\Delta y}\left[\mathbf{H}_y\right]^n_{i,j}\left(\mathbf{W}^n_{i,j+\frac{1}{2}} - \mathbf{W}^n_{i,j-\frac{1}{2}}\right)\end{aligned}$$

c. *Source terms*: the ordinary differential equation (ODE)

$$\frac{d\mathbf{U}}{dt} = \mathbf{T}_x + \mathbf{T}_y$$

is solved by means of Euler implicit method:

$$\mathbf{U}_{i,j}^{n+\frac{1}{2}} = \hat{\mathbf{U}}_{i,j}^{n+\frac{1}{2}} + 0.5\Delta t \left([\mathbf{T}_x]_{i,j}^{n+\frac{1}{2}} + \left[\mathbf{T}_y\right]_{i,j}^{n+\frac{1}{2}} \right)$$

and primitives variables $\mathbf{W}_{i,j}^{n+\frac{1}{2}}$ are computed from $\mathbf{U}_{i,j}^{n+\frac{1}{2}}$ solving a non-linear system.

2) Conservative half-step ($t^{n+\frac{1}{2}} \rightarrow t^{n+1}$)

a. *Data reconstruction*: primitive variables $\mathbf{W}_{i\pm\frac{1}{2},j}^{n+\frac{1}{2}}$ and $\mathbf{W}_{i,j\pm\frac{1}{2}}^{n+\frac{1}{2}}$ at the cell bounds are obtained by means of piece-wise linear reconstruction starting from the cell-average values $\mathbf{W}_{i,j}^{n+\frac{1}{2}}$ computed at timestep $t^{n+\frac{1}{2}}$. To avoid oscillations, the minmod limiter is used.

b. *Solving the non-conservative homogeneous part*: vectors of conserved variables are updated considering only the homogeneous part of the system. Intercell non-conservative Riemann Problems (RPs) are solved by means of an approximated solver, considering primitive variables $\mathbf{W}_{i\pm\frac{1}{2},j}^{n+\frac{1}{2}}$ and $\mathbf{W}_{i,j\pm\frac{1}{2}}^{n+\frac{1}{2}}$ obtained at the previous step and computing intercell fluxes $\mathbf{F}_{i\pm\frac{1}{2},j}^{n+\frac{1}{2}}$ and $\mathbf{G}_{i,j\pm\frac{1}{2}}^{n+\frac{1}{2}}$.

$$\begin{aligned}\hat{\mathbf{U}}_{i,j}^{n+1} = \mathbf{U}_{i,j}^{n} \quad & -\tfrac{\Delta t}{\Delta x}\left(\mathbf{F}_{i+\frac{1}{2},j}^{n+\frac{1}{2}} - \mathbf{F}_{i-\frac{1}{2},j}^{n+\frac{1}{2}}\right) - \tfrac{\Delta t}{\Delta y}\left(\mathbf{G}_{i,j+\frac{1}{2}}^{n+\frac{1}{2}} - \mathbf{G}_{i,j-\frac{1}{2}}^{n+\frac{1}{2}}\right) \\ & -\tfrac{\Delta t}{\Delta x}\left[\mathbf{H}_x\right]_{i,j}^{n+\frac{1}{2}}\left(\mathbf{W}_{i+\frac{1}{2},j}^{n+\frac{1}{2}} - \mathbf{W}_{i-\frac{1}{2},j}^{n+\frac{1}{2}}\right) \\ & -\tfrac{\Delta t}{\Delta y}\left[\mathbf{H}_y\right]_{i,j}^{n+\frac{1}{2}}\left(\mathbf{W}_{i,j+\frac{1}{2}}^{n+\frac{1}{2}} - \mathbf{W}_{i,j-\frac{1}{2}}^{n+\frac{1}{2}}\right)\end{aligned}$$

c. *Source terms*: the ordinary differential equation (ODE)

$$\frac{d\mathbf{U}}{dt} = \mathbf{T}_x + \mathbf{T}_y$$

is solved by means of Euler implicit method:

$$\mathbf{U}_{i,j}^{n+1} = \hat{\mathbf{U}}_{i,j}^{n+1} + \Delta t \left([\mathbf{T}_x]_{i,j}^{n+1} + \left[\mathbf{T}_y \right]_{i,j}^{n+1} \right)$$

and primitives variables $\mathbf{W}_{i,j}^{n+1}$ are computed from $\mathbf{U}_{i,j}^{n+1}$ solving an algebraic, non-linear system.

In order to preserve stability, timesteps are limited by the Courant-Friedrichs-Lewy condition (Courant et al., 1928)

$$\frac{\lambda_{max} \Delta t}{\Delta x} < 0.5$$

where λ_{max} is the maximum eigenvalue of the system.

Step 2.b requires the solution of intercell RPs. In the original version of TRENT2D, this operation is carried out by means of the LHLL solver, while in the latest version it is performed through two possible Generalised Roe (GR) solvers: the Specific-Closure GR (SCGR) and the Closure-Independent GR (CIGR). All these three solvers are shortly presented hereafter.

3.2.1 The LHLL solver

The LHLL solver is a HLL solver (Harten et al., 1983) with the addition of a corrective term to discretise properly the non-conservative terms $(1+c\Delta)gh(\partial z_b/\partial x)$ and $(1+c\Delta)gh(\partial z_b/\partial y)$. This solver approximates the solution of a RP with two shock waves, supplemented by a standing central shock, assuming no variation of the primitive variables across it (Rosatti and Fraccarollo, 2006).

Hereafter, L indicates the bound of the cell at the left side of the discontinuity of the RP and R the bound of the cell at the right side. Therefore, considering a discontinuity in the x direction, between cells (i, j) and $(i+1, j)$, the notation can be simplified in this way:

$$\mathbf{W}_L = \mathbf{W}_{\left(i+\frac{1}{2}\right)^-,j}; \quad \mathbf{W}_R = \mathbf{W}_{\left(i+\frac{1}{2}\right)^+,j};$$
$$\mathbf{U}_L = \mathbf{U}_{\left(i+\frac{1}{2}\right)^-,j}; \quad \mathbf{U}_R = \mathbf{U}_{\left(i+\frac{1}{2}\right)^+,j}.$$

If $\lambda_{\min}$ and $\lambda_{\max}$ indicate respectively the minimum and the maximum eigenvalue of the PDEs system, and S_L and S_R are

defined as

$$S_L = \min\left(\lambda_{\min,L}, \lambda_{\min,R}\right); \qquad S_R = \min\left(\lambda_{\max,L}, \lambda_{\max,R}\right);$$

it is possible to write LHLL left and right fluxes as

$$\mathbf{F}_{L,R}^{LHLL}\left(\mathbf{W}_L, \mathbf{W}_R\right) = \mathbf{F}^{HLL}\left(\mathbf{W}_L, \mathbf{W}_R\right) + \mathbf{F}_{L,R}^{lat}\left(\mathbf{W}_L, \mathbf{W}_R\right) \tag{3.8}$$

where

$$\mathbf{F}^{HLL}\left(\mathbf{W}_L, \mathbf{W}_R\right) = \frac{S_R\mathbf{F}\left(\mathbf{W}_L\right) - S_L\mathbf{F}\left(\mathbf{W}_R\right) + S_L S_R\left[\mathbf{U}\left(\mathbf{W}_R\right) - \mathbf{U}\left(\mathbf{W}_L\right)\right]}{S_R - S_L} \tag{3.9}$$

and

$$\mathbf{F}_{L,R}^{lat}\left(\mathbf{W}_L, \mathbf{W}_R\right) = \begin{bmatrix} 0 \\ 0 \\ -\dfrac{S_{L,R}}{S_R - S_L} g \overline{(1 + c\Delta)\, h}\left(z_b^R - z_b^L\right) \\ 0 \end{bmatrix} \tag{3.10}$$

assuming that the RP is along the x direction. $\overline{(1 + c\Delta)\, h}$ is the arithmetic average of $(1 + c\Delta)\, h$ computed between L and R states. For further details about this solver, the reader is addressed to the original paper.

This solver turns out to be simple, robust and cost-effective. However, it has the drawback of being quite diffusive and generating smooth solutions. Therefore, in order to overcome these problems and catch in detail local peculiarities, a different approach was proposed for the newest version of TRENT2D. This approach is shortly presented here below.

3.2.2 SCGR and CIGR solvers

Both SCGR and CIGR solvers were developed starting from the same approach, based on the use of a well-balance Generalised Roe-type solver (Rosatti and Begnudelli, 2013a), which shows negligible numerical diffusion. Both SCGR and CIGR are well-balanced.

Unlike the LHLL solver, Generalised Roe-type solvers consider the exact wave structure of the linearised form of the homogeneous part of the mathematical model.

Resorting to two-dimensional splitting, the homogeneous part

system 3.7 can be rewritten along the generic $n-$direction:

$$\frac{\partial \mathbf{U}}{\partial t} + \frac{\partial \mathbf{F}_n}{\partial n} + \mathbf{H}_n \frac{\partial \mathbf{W}}{\partial n} = 0 \tag{3.11}$$

Generalised Roe-type solvers give the approximated solution of the problem 3.11 obtaining the exact solution of the following linear problem:

$$\frac{\partial \mathbf{U}_n}{\partial t} + \mathcal{A}_n \left(\mathbf{U}_{nL}, \mathbf{U}_{nR} \right) \frac{\partial \mathbf{U}_n}{\partial n} = 0 \tag{3.12}$$

where $\mathcal{A}_n$ represents a suitable, constant matrix, function of the L and R states.

In order to obtain a good matrix, the following constraints must be complied with:

1. *Hyperbolicity*: $\mathcal{A}_n$ must have complete set of real eigenvalues and relevant eigenvectors, so that any flow field can be described composing simple waves.

2. *Differential consistency*: as $\mathbf{U}_{nL} \rightarrow \mathbf{U}_{nR} \rightarrow \mathbf{U}_n$, the linear problem 3.12 must tend to the linearised form of the system 3.11, i.e.
$$\mathcal{A}_n \left(\mathbf{U}_n, \mathbf{U}_n \right) \rightarrow \frac{\partial \mathbf{F}_n}{\partial \mathbf{U}_n} + \mathbf{H}_n \frac{\partial \mathbf{W}_n}{\partial \mathbf{U}_n}$$

3. *Integral consistency*: the integral of the approximated solution must correspond to the integral of the exact solution for a chosen time-space interval. Therefore, integrating problems 3.11 and 3.12 on a time-space interval $[0, 1] \times [-N, N]$, with $-N \leq s_L$ and $N \geq s_R$ (where s_L and s_R are the positions at time 1 of the slowest and fastest waves respectively), this result must be obtained:
$$\mathcal{A}_n \left(\mathbf{U}_{nL}, \mathbf{U}_{nR} \right) \left(\mathbf{U}_{nL} - \mathbf{U}_{nR} \right) = \mathbf{F}_n \left(\mathbf{U}_{nR} \right) - \mathbf{F}_n \left(\mathbf{U}_{nL} \right) - \tilde{\mathbf{D}}_n$$
with $\tilde{\mathbf{D}}_n$ representing the non-conservative term of the pressure exerted over the bed step at the RP interface at time 0.

These constraints can be applied also rewriting the matrix $\mathcal{A}_n \left(\mathbf{U}_{nL}, \mathbf{U}_{nR} \right)$ as a function of primitive variables $\mathbf{W}_{nL}$ and $\mathbf{W}_{nR}$:

$$\mathcal{A}_n \left(\mathbf{U}_{nL}, \mathbf{U}_{nR} \right) = \left[\mathbf{A}_n \left(\mathbf{W}_{nL}, \mathbf{W}_{nR} \right) + \mathbf{H}_n \left(\mathbf{W}_{nL}, \mathbf{W}_{nR} \right) \right] \mathbf{B}_n^{-1} \left(\mathbf{W}_{nL}, \mathbf{W}_{nR} \right)$$

where $\mathbf{A}_n$, $\mathbf{B}_n$ and $\mathbf{H}_n$ are three suitable, unknown matrices, which values must satisfy the following relations, derived from the *integral consistency* condition:

$$\mathbf{A}_n\left(\mathbf{W}_{nL},\mathbf{W}_{nR}\right)\left(\mathbf{W}_{nL}-\mathbf{W}_{nR}\right)=\mathbf{F}_n\left(\mathbf{W}_{nR}\right)-\mathbf{F}_n\left(\mathbf{W}_{nL}\right) \tag{3.13a}$$

$$\mathbf{H}_n\left(\mathbf{W}_{nL},\mathbf{W}_{nR}\right)\left(\mathbf{W}_{nL}-\mathbf{W}_{nR}\right)=-\tilde{\mathbf{D}}_n \tag{3.13b}$$

$$\mathbf{B}_n\left(\mathbf{W}_{nL},\mathbf{W}_{nR}\right)\left(\mathbf{W}_{nL}-\mathbf{W}_{nR}\right)=\mathbf{U}_n\left(\mathbf{W}_{nR}\right)-\mathbf{U}_n\left(\mathbf{W}_{nL}\right) \tag{3.13c}$$

The expressions of the matrices $\mathbf{A}_n$ and $\mathbf{B}_n$ can be obtained starting from the analytical form of the Jacobians of $\mathbf{F}_n$ and $\mathbf{U}_n$, evaluated with reference to the primitive vector $\mathbf{W}_n$. Then, the values of the terms in $\mathbf{A}_n$, $\mathbf{H}_n$ and $\mathbf{B}_n$ need to be calculated in suitable average states $\widetilde{\mathbf{W}_n}$. These average states (the term "average" must be interpreted in a quite broad sense) are expressed as functions of the L and R states

$$\widetilde{\mathbf{W}_n}=\mathcal{F}\left(\mathbf{W}_{nL},\mathbf{W}_{nR}\right)$$

so that

$$\mathcal{F}\left(\mathbf{W}_{nL},\mathbf{W}_{nL}\right)=\mathbf{W}_{nL}$$

Therefore, assuming

$$\mathbf{A}_n\left(\mathbf{W}_{nL},\mathbf{W}_{nR}\right)=\mathbf{J}_{\mathbf{F}_n}\left(\widetilde{\mathbf{W}_n}\right) \tag{3.14a}$$

$$\mathbf{H}_n\left(\mathbf{W}_{nL},\mathbf{W}_{nR}\right)=\mathbf{H}_n\left(\widetilde{\mathbf{W}_n}\right) \tag{3.14b}$$

$$\mathbf{B}_n\left(\mathbf{W}_{nL},\mathbf{W}_{nR}\right)=\mathbf{J}_{\mathbf{U}_n}\left(\widetilde{\mathbf{W}_n}\right) \tag{3.14c}$$

conditions 3.13 become:

$$\mathbf{J}_{\mathbf{F}_n}\left(\widetilde{\mathbf{W}_n}\right)\left(\mathbf{W}_{nL}-\mathbf{W}_{nR}\right)=\mathbf{F}_n\left(\mathbf{W}_{nR}\right)-\mathbf{F}_n\left(\mathbf{W}_{nL}\right) \tag{3.15a}$$

$$\mathbf{H}_n\left(\widetilde{\mathbf{W}_n}\right)\left(\mathbf{W}_{nL}-\mathbf{W}_{nR}\right)=-\tilde{\mathbf{D}}_n \tag{3.15b}$$

$$\mathbf{J}_{\mathbf{U}_n}\left(\widetilde{\mathbf{W}_n}\right)\left(\mathbf{W}_{nL}-\mathbf{W}_{nR}\right)=\mathbf{U}_n\left(\mathbf{W}_{nR}\right)-\mathbf{U}_n\left(\mathbf{W}_{nL}\right) \tag{3.15c}$$

However, thus far expressions of the averaged state $\widetilde{\mathbf{W}_n}$ are still unknown. Finding suitable, manageable expressions of average states that fulfil relations 3.15 and are also manageable is anything but straightforward in the case of quite sophisticated models as TRENT2D. Rosatti and Begnudelli (2013b) suggested a precise procedure in order to obtain the elements of $\widetilde{\mathbf{W}_n}$ without getting

lost in computations:

1) Choose an arbitrary average state vector $\widetilde{\mathbf{W}_n} = \left(\tilde{h}, \tilde{z_b}, \tilde{u_n}, \tilde{u_t}\right)^T$, for example resorting to arithmetic averages between L and R values of the variables.

2) Solve the system of equations 3.15a, which concerns $\mathbf{J}_{\mathbf{F}_n}$, expressing the matrix terms by means of $\widetilde{\mathbf{W}_n}$ values.

   a. Identify equations that are not verified and put them into the set S_A.
   b. Choose a number of Jacobian terms equal to the number of not-verified equations. These terms become the unknowns of the system and are collected into the set M_A. They can be marked with the symbol $\check{}$.
   c. By means of $\widetilde{\mathbf{W}_n}$, evaluate the remaining Jacobian terms that appear in the not-verified equations.
   d. Solve the system for the set of unknowns M_A, obtaining their explicit espressions.

3) Solve the system of equations 3.15c, which concerns $\mathbf{J}_{\mathbf{U}_n}$, expressing the matrix terms by means of $\widetilde{\mathbf{W}_n}$ values.

   a. Identify equations that are not verified and put them into the set S_B.
   b. Choose a number of Jacobian terms equal to the number of not-verified equations. These terms become the unknowns and are collected into the set M_B. They can be marked with the symbol $\check{}$.
   c. By means of $\widetilde{\mathbf{W}_n}$, evaluate the remaining Jacobian terms that appear in the not-verified equations.
   d. Solve the system for the set of unknowns M_B, obtaining their explicit espressions.

4) Solving the system of equations 3.15b for the set of unknowns $M_H = [\ddot{h}, \ddot{u_n}, \ddot{u_t}]$, these expressions can be found:

$$\begin{aligned}
\ddot{h} &= h_k - \frac{|z_R - z_L|}{2} \\
\ddot{u_n} &= u_{nk} \\
\ddot{u_t} &= u_{tk}
\end{aligned}$$

with $k = L$ if $z_L \leq z_R$, $k = R$ otherwise. Unknowns $\dddot{h}$, $\dddot{u_n}$, $\dddot{u_t}$ and their expressions are put into the set M_H.

5) Merge the set of unknowns M_A, M_B and M_H, together with the vector $\widetilde{\mathbf{W}_n}$. Now, elements of the matrices $\mathbf{A}_n$, $\mathbf{B}_n$ and $\mathbf{H}_n$ are all defined.

Because of the multiple possibilities in choosing average states this method is called Multiple Average (MA) approach. Due to the possible variety in choosing average states and unknowns, the method could produce different matrices according to different choices. However, on varying resulting matrices, the solution of the RP problem does not vary significantly.

Once the matrix $\mathcal{A}$ is defined, fluxes at the interface of the RP can be computed as (the notation introduced for the LHLL is used):

$$\mathbf{F}_L^{GR} = \mathbf{F}\left(\mathbf{W}_L^n\right) + \mathcal{A}^-\left(\mathbf{U}_R^n - \mathbf{U}_L^n\right)$$
$$\mathbf{F}_R^{GR} = \mathbf{F}\left(\mathbf{W}_R^n\right) - \mathcal{A}^+\left(\mathbf{U}_R^n - \mathbf{U}_L^n\right)$$

where

$$\mathcal{A}^{\pm}\left(\widetilde{\mathbf{W}_n}\right) = \widetilde{\mathbf{R}}\mathbf{\Lambda}^{\pm}\widetilde{\mathbf{R}}^{-1} \tag{3.18}$$

with $\widetilde{\mathbf{R}}$ representing the matrix composed by the eigenvectors of $\mathcal{A}$ as columns and $\mathbf{\Lambda}^{\pm}$ representing the diagonal matrix of the eigenvalues of $\mathcal{A}$ and defined as follows:

$$\mathbf{\Lambda}^{\pm} = \Lambda_{ii}^{\pm} \tag{3.19}$$

where $\Lambda_{ii}^{\pm} = \frac{1}{2}\left(\tilde{\lambda}_i \pm |\tilde{\lambda}_i|\right)$.

Both SCGR and CIGR methods apply this procedure in order to compute the numerical fluxes at the interface of the RP (Rosatti and Begnudelli, 2013b), however they differ in the way of computing the analytical Jacobians and, therefore, the Multiple Averages.

The CIGR (Closure-Independent Generalized Roe) solver obtains analytical Jacobians considering concentration c as a generic function of h, u_n and u_t. Therefore, about all the Jacobian terms are characterised by the presence of a derivative of c. This choice makes the resulting matrices completely general.

On the contrary, the SCGR (Specific-Closure Generalized Roe) solver obtains analytical Jacobians starting from the expressions of $\mathbf{U}_n$ and $\mathbf{F}_n$ where the concentration term is substituted with the

closure relation 3.2. Therefore, SCGR considers $\mathbf{U}_n$, $\mathbf{F}_n$ and $\mathbf{H}_n$ written in this form:

$$\mathbf{U}_n = \begin{bmatrix} h + z_b \\ c_b\beta\dfrac{u_n^2 + u_t^2}{g} + c_b z_b \\ hu_n + \Delta c_b\beta u_n\dfrac{u_n^2 + u_t^2}{g} \\ hu_t + \Delta c_b\beta u_t\dfrac{u_n^2 + u_t^2}{g} \end{bmatrix}$$

$$\mathbf{F}_n = \begin{bmatrix} hu_n \\ c_b\beta u_n\dfrac{u_n^2 + u_t^2}{g} \\ \left(h + \Delta c_b\beta\dfrac{u_n^2 + u_t^2}{g}\right)\left(\dfrac{1}{2}gh + u_n^2\right) \\ \left(h + \Delta c_b\beta\dfrac{u_n^2 + u_t^2}{g}\right)u_n u_t \end{bmatrix}$$

$$\mathbf{H}_n = \begin{bmatrix} 0 & 0 & 0 & 0 \\ 0 & 0 & 0 & 0 \\ 0 & 0 & 0 & gh + \Delta c_b\beta\left(u_n^2 + u_t^2\right) \\ 0 & 0 & 0 & 0 \end{bmatrix}$$

Avoiding to weigh down the presentation, here no results of the Multiple Average approach are indicated, postponing unknown calculations and matrices expressions to Chapter 8, where they are relevant. At this stage, useful expressions and details can be found also in the original paper (Rosatti and Begnudelli, 2013b), where results obtained by means of both the solvers are compared. For sake of completeness, it must be noticed that differences produced by the two methods are very small, as expected. The advantage of using CIGR lies in its generality, which turns out to be useful in case a different (and hopefully more general) closure relation is used to express the relation between concentration and hydrodynamic variables.

3.3 TRENT2D input and output data

In this Section, input and output data of the TRENT2D model are shortly described, expanding a bit some information included

in papers "A Web service ecosystem for high-quality, cost-effective debris-flow hazard assessment: the WEEZARD system" (Rosatti et al., 2017) and "New technology in debris-flow modelling: a WebGIS integrated solution for TRENT2D" (Zorzi et al., 2016a).

The first input required by TRENT2D concerns the computational domain. It consists in a Cartesian mesh covering the extent of the area where simulated phenomenon is expected to flow. Its dimensions and the size of its cells must be chosen properly, in order to reach a suitable level of detail in the description with acceptable computational costs. Over this grid, initial and boundary conditions must be then provided.

The terrain elevation in pre-event conditions is required as the initial condition, in order to represent the initial morphology of the study domain. This information can be profitably extracted from DTMs and field surveys (see Section 1.3.3). At this step, the use of a GIS tool can turn out to be very convenient.

As the inflow boundary conditions, both geometric and dynamic information is needed. Geometric information consists in the indexes of the cells composing the inflow section and the local average slope. Also this information can be profitably managed by means of GIS tools. Dynamic data are essentially suitable solid and liquid hydrographs, obtained within the hydrological analyses described in Section 1.3.5 and according to the approach presented in Section 1.2.1. This information is then elaborated by the model assuming the local quasi-1D uniform-flow condition at the upper bound of the domain. Details about the exact computation of the upstream boundary condition can be found in Armanini et al. (2009b).

As far as outflow boundary conditions are concerned, two options are available for the user: non-reflecting condition or critical condition. Non-reflecting condition represents the default and implies that the boundary cells assume the same values of the hydrodynamic variables of the relevant upwind cells. However, the user can change settings and impose the critical condition wherever the boundary flow is subcritical. All the boundary cells which indexes were not included in the inflow list are considered potential outflow cells.

To run a simulation, also model parameters must be set. Model parameters are four or five depending on the version of TRENT2D (^{TS} or ^{DF}). For sake of clarity, they are listed in Table 3.1. Except for β, the other parameters are quite common in high-concentration flow modelling and can be easily set.

Parameter	**Symbol**	**Unit**
Maximum packaging concentration	c_b	-
Relative submerged density	Δ	-
Transport parameter	β	-
ONLY IN TRENT2D^{TS}		
Strickler roughness coefficient	K_s	$m^{1/3}s^{-1}$
ONLY IN TRENT2D^{DF}		
Friction angle	Φ	$^\circ$
Relative submergence	Υ	-

Table 3.1: Parameters of the TRENT2D model

With these input data, the model periodically produces a series of output data, which are the grid values of the computed variables ($h, z_b, \Delta z_b, u_x, u_y, c, Fr$), stored in matrix form according to the Cartesian grid of the computational domain. Model results can be displayed and analysed by means of GIS solutions, although data management can become burdensome if performed manually, especially when the number of output files is significant.

Chapter 4

Two case studies highlighting some complexity issues

As shown in the previous Chapters, high-concentration flow complexity may entail very heterogeneous "complexity issues", i.e. hazard-assessment issues generated by natural complexity of the phenomenon. In this Chapter, specific attention is paid to some "complexity issues" that can be typically observed and experienced in hazard-assessment practice whenever a sophisticated model as TRENT2D is used. For convenience, these "complexity issues" can be divided into two main categories, namely: *developer issues* and *user issues*. It is worth noticing that this distinction is not always so stiff and sometimes some *developer issues* could be seen also as *user issues*.

Generally speaking, *developer issues* are generated directly by the purpose of describing the natural high-concentration flow behaviour with the *right level* of detail. The developer issues of utmost importance have been already analysed in the previous Chapters in a quite general frame. Some of them are resumed in this Chapter, assuming the user point of view, though.

On the other side, *user issues* concern both understanding and applying the model. Models should not be used as black box. Users should be aware of modelling hypotheses and uncertainties, especially when sophisticated models are chosen, in order to set proper boundary conditions, parameter values and space discretisation and to avoid misinterpretations of modelling outcomes. Being aware of the relation between modelling and complexity is

essential to give a good measure of the relevance of model-results at decision-making level. However, often users get lost in complicated and laborious pre- and post-processing of model input and output data, loosing focus on modelling itself and taking any modelling result as valid. Avoiding this outcome is a primary responsibility of the user, but also developers can intervene in the problem, resorting to proper modelling solutions, as explained in Chapter 5.

In the next Sections, two applications of the TRENT2D model are introduced. They are two case studies that allow to highlight clearly some "complexity issues" connected to the hypotheses and the use of the model TRENT2D for hazard-assessment purposes. The first case study reported here (Section 4.1) is the back-analysis of a well-documented debris-flow event observed in 2010 in the Italian Alps. This back-analysis was partially presented in a conference paper (Rosatti et al., 2015). The second application (Section 4.2) is represented by the back-analysis of a poorly-documented debris-flow event observed in 1966 in the Italian Alps. This case study was analysed by the MSc thesis of Erika Veronesi (Veronesi, 2017), which was co-tutored by the author of this work. In both cases, *developer* and *user issues* encountered in the job are put into light.

4.1 The debris-flow event of Valle Molinara (Italy)

In 2010, a debris-flow event occurred in Valle Molinara, a small mountain stream in the Eastern Italian Alps (Figure 4.1). During the night between the 14th and the 15th August 2010, an intense precipitation fell over the basin, causing the development of a debris flow that reached the village of Campolongo, damaging buildings and infrastructures.

Shortly after the event, the local agency for Territory, Agriculture, Environment and Forestry of the Autonomous Province of Trento (Italy) produced some records about the event, including field surveys, sediment deposition measurements, aerial pictures, rainfall pattern analyses. These documents were used to perform a back-analysis of the event by means of the TRENT2D^{DF} model in its original version (i.e. with fluxes computed by means of the LHLL solver).

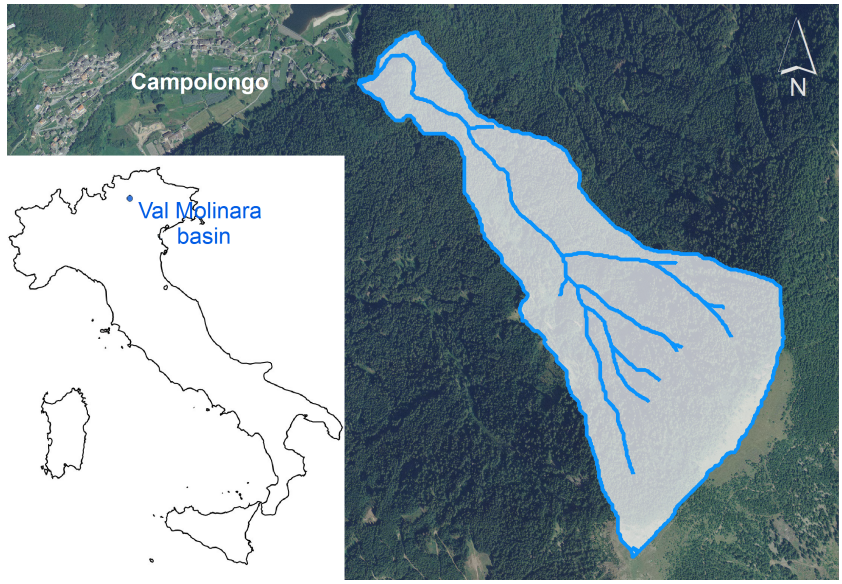

Figure 4.1: The Valle Molinara basin in the Eastern Italian Alps

4.1.1 The study area and the 2010 event

The area of Valle Molinara basin is about equal to 1 km^2. The Valle Molinara stream descends the peak Dosso di Costalta (1955 m) up the Silla stream (988 m), with a length of about 3 km and an average slope of 36%. The village of Campolongo is located on the final part of the Valle Molinara stream, over the alluvial fan. The slope at the fan apex is equal to 21%.

Before August 2010 no evidences of debris flow events had been observed in the basin, not even in years 1882 and 1966, when two disastrous storms occurred in the Eastern Italian Alps, causing a large number of high-concentration flow phenomena (one of them is described in Section 4.2). Therefore, no historical data are available. Moreover, no instrumentation is installed in the basin to measure rainfall heights or flow rates.

Geological analyses carried out by local agency highlighted that, above the altitude 1600 m, a widely fractured formation is present, while the lower part of the basin shows deposits of coarse sediments over low-permeability layers. These surveys suggest that there was a quite large availability of sediments before the event.

Actually, during the night between the 14th and the 15th August 2010, diffuse erosion processes were observed, due to intense rainfall that persisted on the Valle Molinara basin for hours. A comparison between radar measurements and data recorded by

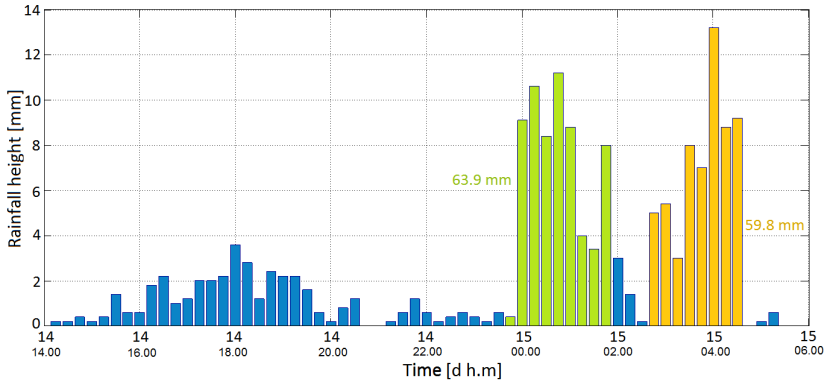

Figure 4.2: Rainfall heights measured by the Sant'Orsola Terme rain gauge from 14th August 2010 2:00 pm to 15th August 6:00 am (UTC+2)

the nearby rain gauge of Sant'Orsola Terme showed that precipitation started during the afternoon of the 14th August with quite weak intensity and then continued during the night, with two cloudburst in succession. Rainfall data gauged in Sant'Orsola Terme are plotted in Figure 4.2. It must be noticed that the Sant'Orsola Terme station is the rain gauge nearest to the study basin (distance is 3.5 km as the crow flies), but it is located on the opposite side of the Dosso di Costalta. Because of the spatial variability of rainfall events in mountain areas, it is not possible to take for a-priori granted the representativeness of Sant'Orsola Terme measurements. Fortunately, in this case, radar measurements showed that these data were significant also for the study basin.

Comparing cumulative rainfall height measured by the Sant'Orsola Terme rain gauge with regional statistics, it can be said that the return period of each cloudburst is about 100 years, while the cumulative rainfall height of the two cloudbursts has a return period of about 200 years. Avoiding discussions concerning the significance of regional statistic, it can be certainly stated that the rainfall event was extreme and quantifiable around 200−500 years (Borga and Zoccatelli, 2010).

It is plausible that starting rainfall increased the basin saturation, while the first cloudburst caused the debris flow beginning. Probably, the debris flow event did not occur as a sudden, impulsive phenomenon, but rather as a long-lasting and continuous high-concentration flow.

Diffused erosion processes were observed along the upper part of the stream, with erosion depths up to 5–6 m, while deposition occurred mainly along the Campolongo fan, with sediment

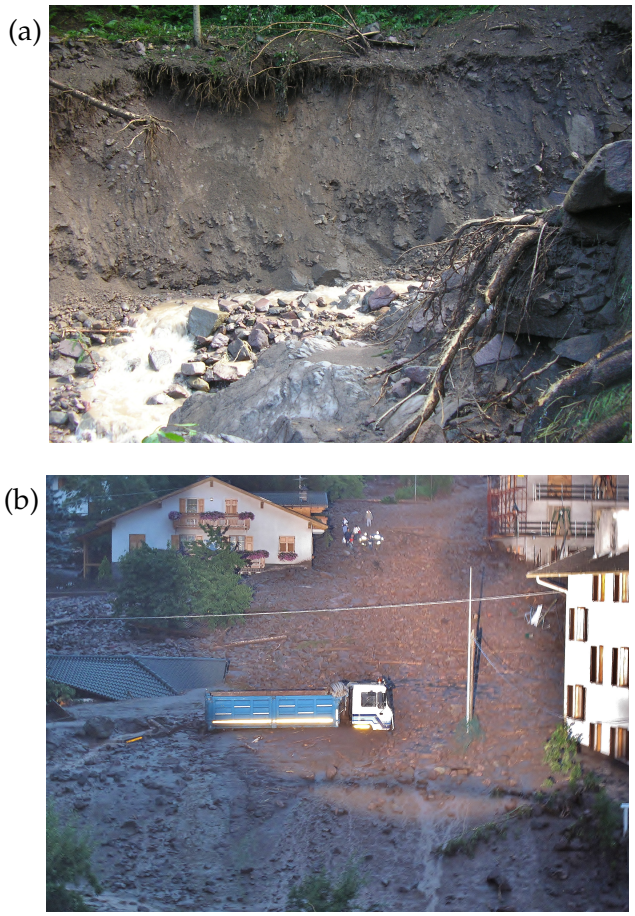

Figure 4.3: (a) Erosion and (b) deposition in Valle Molinara basin after the 2010 debris-flow event. Courtesy of the Autonomous Province of Trento

depth up to 1 m (Figure 4.3). On the whole, the local agency estimated that about 40 000 m^3 of solid material were deposited on and downstream the alluvial fan. This volume becomes equal to 26 000 m^3 net of porosity. As shown in Figure 4.4, five deposition areas were delimited, each one characterised by a different average deposition depth.

However, a comparison between surveyed areas and aerial pictures supplied by the local authority showed how field survey did not cover the whole inundated area. Some zones where deposition depths was small (but not negligible) were not surveyed. Therefore, the perimeter of the deposition area was rearranged in order to include all the deposition areas visible from aerial pictures.

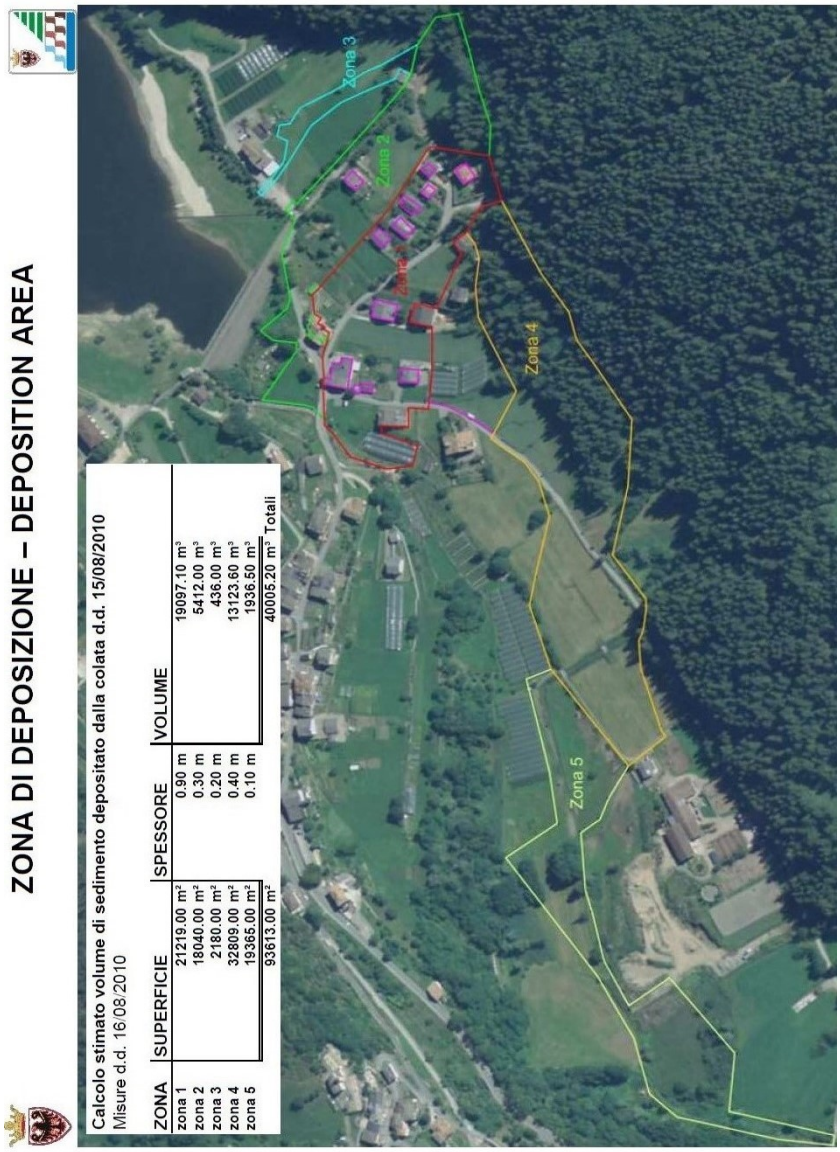

Figure 4.4: Deposition depths and volumes surveyed by the local agency of the Autonomous Province of Trento over the Valle Molinara alluvial fan. Courtesy of the Autonomous Province of Trento.

Parameter		Value
Percentage of saturated area	S	60%
Channel velocity	u_c	2ms^{-1}
Hillslope velocity	u_h	0.02ms^{-1}
Coefficient of hydrodynamic dispersion	D	$1000\text{m}^2\text{s}^{-1}$

Table 4.1: A-priori values chosen for the PeakFlow parameters to study the 2010 debris-flow event of Valle Molinara

4.1.2 Back-analysis through TRENT2D calibration

The back-analysis of the Valle Molinara debris-flow was carried out for the purpose of understanding the possible dynamics of the event. Therefore, starting from post-event available data, TRENT2D^{DF} modelling was performed, paying attention not only to model parameter values, but also to model boundary conditions.

Rainfall data gauged in Sant'Orsola Terme were supplied as input data to a rainfall-runoff model, in order to obtain a suitable liquid hydrograph for the event. For this aim, a semi-distributed GIUH-based rainfall-runoff model was applied "blindly", i.e. without calibration. This approach was necessary since no discharge values were available. The chosen model was PeakFlow (Rigon et al., 2011), an event-based model that takes into account only processes that are relevant on an event time-scale, neglecting for example evaporation or transpiration.

Since the purpose of this Section is the reconstruction of the event in the deposition area, hydrological analyses were carried out closing the basin at the fan apex. Because of the small extent of the basin, rainfall intensity was reasonably assumed to be spatially uniform all over the basin. Then, PeakFlow parameters were set choosing the plausible a-priori values listed in Table 4.1. In particular, the value of saturation percentage was chosen in the light of the fact that precipitation was recorded in the area also during the days before the event.

The liquid hydrograph estimated by means of PeakFlow is plotted in Figure 4.5. Starting from this hydrograph, five mixture hydrographs were obtained, assuming wide availability of loose solid material. Since the debris-flow event was observed during the night between the $14th$ and the $15th$ August, only the sequence of two discharge peaks was taken into account in mixture- and solid-hydrographs computations. According to formulations reported in Section 1.2.1, liquid discharges Q_{liq} were transformed

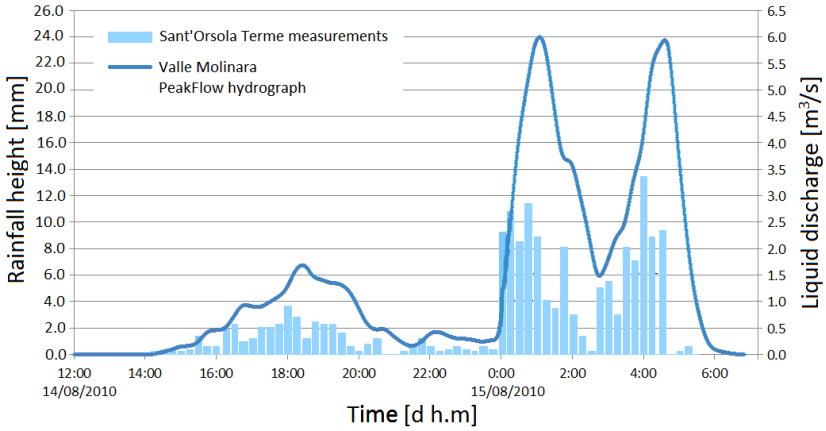

Figure 4.5: Rainfall heights measured by the Sant'Orsola Terme rain gauge from (histogram) and liquid discharges produced by PeakFlow for the Valle Molinara basin closed at the fan apex (UTC+2).

into mixture discharges Q_{mix} as follows:

$$Q_{mix} = F_a Q_{liq}$$

where F_a is the amplification factor defined as

$$F_a = \frac{c_b}{c_b - c}$$

while solid discharges Q_{sol} were obtained as

$$Q_{sol} = c Q_{mix}$$

In these computations, a reasonable value was chosen for c_b ($c_b = 0.65$), together with suitable values of average concentration c, which are summarised in Table 4.2 with some other relevant features of the five scenarios. These concentration values were chosen with the purpose of obtaining solid hydrographs entailing volumes compatible with the solid volume surveyed in the deposition area. These hydrographs represent the inflow boundary condition of the TRENT2D model.

Then, the other data required by the model (see Section 3.3) were specified.

The computational domain was chosen wide enough to include all the Valle Molinara alluvial fan and a segment of the Silla stream. Cell size was chosen equal to 1 m, in order to preserve the level of detail of available information about terrain elevation.

As the initial condition, the DTM produced in 2008 from a

Scenario	c	V_{mix} **(inflow)**	V_{sol} **(inflow)**	Q_{mix} **(max)**	β_0
#1	0.158	96 400 m^3	15 230 m^3	8.0 $m^3 s^{-1}$	0.08
#2	0.193	103 800 m^3	20 000 m^3	8.5 $m^3 s^{-1}$	0.12
#3	0.226	112 000 m^3	24 640 m^3	9.2 $m^3 s^{-1}$	0.17
#4	0.259	121 300 m^3	31 420 m^3	10.0 $m^3 s^{-1}$	0.24
#5	0.293	132 900 m^3	38 940 m^3	10.9 $m^3 s^{-1}$	0.33

Table 4.2: Relevant quantities characterising the five concentration scenarios considered in the Valle Molinara back-analysis

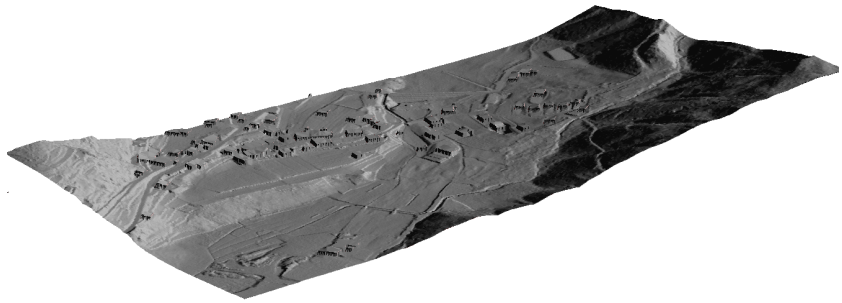

Figure 4.6: 3D representation of the terrain elevation inside the computational domain used in the "blind" reconstruction of the Valle Molinara event

Parameter		**Value**
Friction angle	Φ	38°
Maximum packaging concentration	c_b	0.65
Submerged relative density	Δ	1.65
Relative submergence	Υ	11

Table 4.3: A-priori values chosen for the TRENT2D parameters in the Valle Molinara event reconstruction

LIDAR survey by the Autonomous Province of Trento was considered, in order to take into account the pre-event condition. This datum was then modified locally, in order to represent building encumbrances over the alluvial fan, since flow dynamics is influenced by the presence of relevant obstacles such as for example buildings. Their height was set to be greater than the expected flow depth, in order to keep those cells dry. The resulting 3D-representation of the domain elevation is showed is Figure 4.6.

As the outflow boundary conditions, default conditions were kept. Then, the TRENT2D parameters c_b, Δ, Φ and Υ values were set as specified in Table 4.3, while a starting value of β was chosen for each scenario, as shown in Table 4.2. There, they are marked as β_0.

Among these five scenarios, #1 and #5 were immediately dis-

Parameter set	A	B	C	D	E	F	G
β	$0.5\beta_0$	$0.7\beta_0$	$0.85\beta_0$	β_0	$1.15\beta_0$	$1.3\beta_0$	$1.5\beta_0$

Table 4.4: β values considered in the back-analysis of the Valle Molinara debris flow.

Parameter set	H	I	J	K
Y	8.5	10.0	12.0	13.5

Table 4.5: Y values considered in the back-analysis of the Valle Molinara debris flow.

carded after the first simulations, since significant differences were observed in deposition volumes and areas between surveys and simulations. For the remaining scenarios, further analyses were carried out, varying the values of Y and β. The other parameters were kept constant, since post-event documentation available confirmed the a-priori choice as suitable.

Firstly, only β values were varied, keeping $Y = 11$. For each one of the scenarios #2, #3 and #4, seven parameter sets were identified, varying β according to the rule indicated in Table 4.4. Then, four more parameter set were defined, considering the Y values listed in Table 4.5. In this second family of sets, β was computed according to the uniform-flow hypothesis, applying relations 4.3 and 4.4 with the relevant value of Y. Each set of parameter was then used, with its relevant boundary conditions, to perform a simulation. Among these 33 parameter sets, i.e. 33 simulations (11 for each scenario), the optimal one was chosen according to a couple of criteria:

1) affinity between the surveyed and the simulated deposited volumes;

2) affinity between the extent of the real deposition area (obtained from post-event documentation) and the extent of the simulated deposition area.

The parameter set D applied to the scenario #2 turned out to give the best result, i.e. the lowest error on reconstructed deposited volumes (overestimating real volumes of about 5%) and the highest level of correspondence between areas (79% of real deposition area was covered correctly by simulated deposits), as shown in Figure 4.7, where the simulated area is compared with the real deposition area (delimited according to both field surveys and aerial pictures). Further discussions about the results obtained for this simulation are postponed to Section 4.1.4.

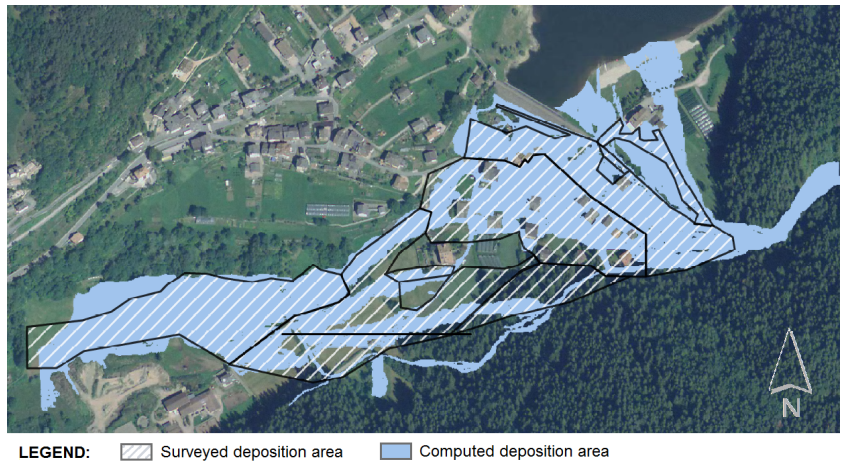

Figure 4.7: Deposition area on the Campolongo fan computed through the TRENT2D back-analysis, compared to the real deposition area, delimited according to field surveys and aerial pictures

4.1.3 A blind simulation of the event

After the back-analysis, a blind simulation of the event was performed by means of TRENT2D^{DF} in the deposition area. The term "blind" indicates here the fact that the model calibration carried out in the previous Section was here totally disregarded and TRENT2D^{DF} was applied considering a-priori boundary conditions and parameters values. This simulation is a kind of what-if test, which considers the typical situation where a model must be applied to back-analyse an event for which only event rainfall data or liquid discharges are available. The purpose is to evaluate the forecast capabilities of the TRENT2D model in such a undefined situation and obtain indications for other model applications where this condition is the only one possible. Therefore, in this context, available post-event measurements and back-analysis results were used only to evaluate the acceptability of the results and not to orientate the analysis.

The starting point of the analysis is the liquid hydrograph obtained in the previous Section (Figure 4.5) by means of the blind application of the PeakFlow model to the rainfall measurements of Sant'Orsola Terme gauge. It is worth remembering that this hydrograph was obtained without calibration, choosing a-priori values for the model parameters.

To transform liquid discharges into mixture and solid hydrographs an estimate of the concentration c was needed. For this purpose, the Takahashi formulation (Takahashi, 1978) was con-

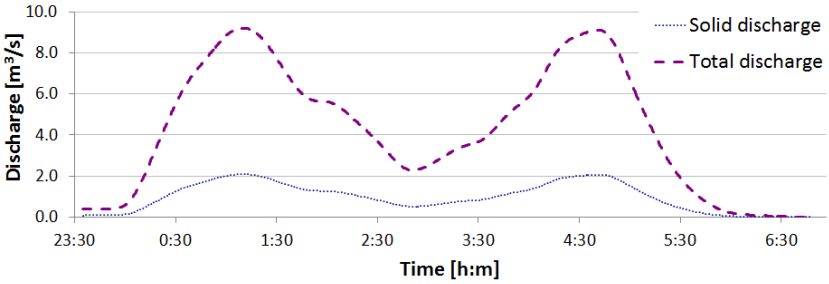

Figure 4.8: Mixture discharges (hatching) and solid discharges (dots) estimated blindly for the Valle Molinara debris-flow event (UTC+2)

Parameter		**Value**
Friction angle	Φ	38°
Maximum packaging concentration	c_b	0.65
Submerged relative density	Δ	1.65
Relative submergence	Υ	11
Transport parameter	β	0.172

Table 4.6: A-priori values chosen for the TRENT2D parameters in the Valle Molinara blind simulation

sidered

$$c = \frac{\tan\alpha}{\Delta\,(\tan\Phi - \tan\alpha)} \tag{4.1}$$

where α represents the terrain slope angle. Reasonable values were used for Δ and Φ, considering loose, coarse grains ($\Delta = 1.65$, $\Phi = 38°$), while α was set according to terrain slope data. Since the simulation focus is set on the alluvial fan, the local slope at the fan apex was considered in concentration computation ($i_F = \tan\alpha = 0.21$). Under these hypotheses, the resulting value for concentration is equal to 0.23. The mixture and solid hydrographs obtained with this value of concentration are plotted in Figure 4.8.

As computational domain and initial condition, the same used in the back-analysis were considered, since they represent the only possible choice also in a blind analysis. Then, TRENT2D parameters values were set (see Table 4.6). In particular, values of c_b, Δ, Φ and Υ were chosen considering reasonable values, while the transport parameter β was computed according to equilibrium assumption, as shown hereafter.

The flow at the upstream cross section of the computational domain was assumed to be quasi-1D and uniform, supposing the inlet slope constant in time. The hypothesis of uniform-flow condition at the inflow section can be translated into the following

system of equations:

$$\begin{cases} \tau_b = (1 + c\Delta)\, g i_F h & \text{(4.2a)} \\ \tau_b = \dfrac{25}{4}(1 + \Delta)\, a \sin\Phi \dfrac{[\lambda(c)]^2}{\Upsilon^2} u^2 & \text{(4.2b)} \end{cases}$$

where the first equation represents the uniform-flow relation deriving from the momentum equation, while the second equation coincides with the closure relation 3.4 for grain-inertial regime. Under the equilibrium assumption, these two expressions can be equalized and a suitable expression for the Froude number $Fr = u^2/(gh)$ can be obtained:

$$\frac{u^2}{gh} = \frac{4}{25} \frac{1 + c\Delta}{1 + \Delta} \frac{i_F}{a \sin\Phi} \frac{\Upsilon^2}{[\lambda(c)]^2} \tag{4.3}$$

Introducing this expression in the concentration closure relation 3.2 and using the relevant concentration value for each scenario, it was possible to quantify the value of β that gives the required concentration in quasi-1D uniform-flow conditions:

$$\beta = \frac{c}{c_b} \left(\frac{u^2}{gh} \right)^{-1} \tag{4.4}$$

The uniform-flow condition at the upper bound of the computational domain is evidently a strong a-priori hypothesis, however it looks like the only one possible to estimate a physically-based value of β within a blind approach.

With these input data, a TRENT2D^{DF} simulation was run and results compared with field surveys and back-analyses results. On the whole, the flooded areas appear quite conform, despite the a-priori assumptions introduced in the reconstruction. The same can be said for the deposited volumes. The post-event surveys estimated a deposited volume of about 40 000 m^3 only in the area covered by the local authority (which is slightly smaller of the real deposition area), while the deposited volume according to the blind simulation was of about 42 000 m^3. A similar comparison can be carried out considering the net solid volume. Surveys estimated a net deposited sediment volume of 26 000 m^3, while the net deposited sediment volume computed by the a-priori reconstruction was about equal to 27 500 m^3.

This result is significant, since the blind simulation coincides

exactly with the run that turned out to be the optimal one within back-analysis. This outcome is not so surprising, since the a-priori values were chosen by means of physically-based hypotheses and considerations, which turned out to be essentially plausible in this case study, as confirmed by the back-analysis.

Such an outcome is extremely relevant, because it suggests that significant TRENT2D simulation can be run for hazard assessment, even if limited data are available and despite phenomenon complexity (recalling Sections 1.2 and 1.3). Certainly, these results can be considered relevant only if also these basic hypotheses (i.e. those used in the a-priori reconstruction) are relevant:

- Rainfall intensity spatially uniform all over the basin;
- Wide availability of loose, coarse sediments in the upper part of the basin;
- Computational domain far enough from the starting point;
- Slope constant in time at the inflow bound of the domain;
- Quasi-1D uniform flow at the inflow section of the domain.

However, the applications described in this and in the previous Section are not free from critical points. In the next Section, some of them are discussed and relevant complexity issues are introduced.

4.1.4 Discussion about complexity issues

Analysing modelling results pointwise, two main inconsistencies are observed between surveys and simulations (even if the optimal back-analysis simulation is considered). They can be clearly recognised in Figure 4.7. The first inconsistency is the excessive extent of the simulated deposition area in the upper right part of the Figure, while the second inconsistency coincides with the missing simulated area in the middle of the Figure.

The first inconsistency is considered not relevant, since the simulated area falling outside the surveyed was characterised by negligible flow and deposition depths. On the contrary, the second inconsistency appears more critical.

An in-depth analysis of the local context allowed to go back to the origin of the inconsistency. Figure 4.9 emphasises the critical point. A bridge was located exactly in the middle of the Figure,

Figure 4.9: A local detail of the optimal simulation

where the simulated flow (coming from right) splits in two. According to the event documentation, the first cloudburst caused the occlusion of the bridge. Since that moment, the mixture was obliged to flow on the top of the bridge and at its sides, crossing the paved (i.e. not erodible) street and continuing straight along the maximum fan slope. However, simulations did not catch the right dynamics of the flow in this particular location, even considering the bridge as clogged up. Since TRENT2D is based on a mobile-bed model approach, it was not possible to reproduce properly the not-erodible character of the street. In that point, erosion processes were simulated and the flow converged along the street, moving across the alluvial fan (upwards in the Figure). This local inconsistency due to the model hypotheses in the description of the bed nature led to a different spatial distribution of the deposition volumes within the whole domain. In particular, the volume of sediments deposited on the alluvial fan was underestimated by 35%, while, in the downstream part of the domain, simulated deposition volumes were concentrated in the lowest areas (see Figure 4.10), instead of being uniformly distributed, as expected and shown by documentation.

However, this second inconsistency can be overcome only once models dealing properly with both fixed and mobile bed are available. Feasible fixed-mobile bed models are proposed in Rulot et al. (2012), Rosatti and Zugliani (2015) and Zugliani et al. (2017), as reported in Chapter 2.

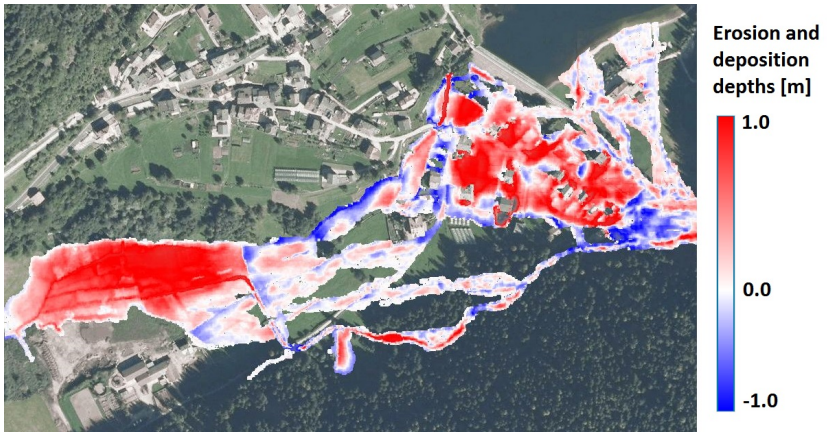

Figure 4.10: Erosion and deposition depths at the end of the optimal simulation reconstructing the Valle Molinara event

Other critical points were identified in the frame of the back-analysis. Among them, four main complexity issues concerning TRENT2D were considered much relevant for the purposes of this thesis, because they allow to analyse effects of complexity from a variety of points of view. These four complexity issues are now shortly disclosed.

The first complexity issue concerns especially the operational side of a hazard-assessment job, i.e. the user, and is extensively tackled in Chapter 5. Because of its nature, this issue is classified here as "operational". On account of high-concentration flow natural complexity, a large number of operations have to be performed in order to carry out a hazard-assessment job. For example, data need to be stored, processed and formatted, their level of detail and reliability analysed, the right hypotheses and the most suitable models chosen. Furthermore, different steps of the job are usually performed with different tools and software and, whether sophisticated models are used, computational costs are typically high. For example, the back-analysis proposed in the previous Section required the use of two models (PeakFlow and TRENT2D^{DF}), a GIS system, CAD software, a spreadsheet, a 3D viewer and a eight Xeon CPU machine, with 8 GB of RAM and a disk of 500 GB. On this machine one of the TRENT2D^{DF} simulations described in the previous Section lasted 7 hours on average, producing approximately 400 output files describing the variables evolution (this is a reasonable number for a simulated event of about 6 hours). From a user point of view, all these elements can be very burdensome. Furthermore, the use of many tools produces a high fragmentation of the work and requires a sig-

nificant percentage of manual work. With all these components, the operational chain can become very complicated and lead to unreliable results because of possible accidental errors. However, complicatedness should be evidently avoided in simulation modelling aimed at hazard assessment, in order to preserve the level of detail and trustworthiness of the description. Furthermore, typically users choose models that can be managed simply, therefore avoiding complicatedness in sophisticated models could also help the Transfer of Technology, moving users closer to model developers. Integrated modelling solutions could represent an answer to this "operational" complexity issue, possibly leading to systems suitable to support decision makers in hazard management. The whole topic is duly expanded in Chapter 5, where also a Web-service ecosystem for high-concentration flow hazard assessment is presented.

The second complexity issue deals directly with natural complexity, in particular with morphological complexity, its influence on high-concentration flow dynamics and the effects of artificial geometrical constraints. These "geometrical" issues are also the main subject of Chapter 6. With reference to the Valle Molinara back-analysis, it was noticed that spatial resolution of 1 m was considered in the back-analysis. This was the original resolution of the terrain datum. However, the section of the Valle Molinara stream is not very large (2–4 m on the alluvial fan), therefore its section is represented only with few cells. Such a representation seems to be quite rough, especially in case not-extreme events are simulated. Typically, events with medium-low intensity are more sensitive to geometrical constraints, therefore a rough representation of the stream sections could produce wrong results. The same line of reasoning can be proposed with reference to buildings or, even more appropriately, dealing with protection structures. Protection structures and, in general, all the artificial structures that modify the natural flow dynamics, require a detailed representation of both their geometry and flow behaviour. As far as geometry is concerned, a more detailed representation of morphology and flow-control structures can be obtained by means of high-resolution Cartesian mesh. However, this solution introduces very high computational costs. Alternatively, variable-resolution structured meshes or unstructured meshes can be used, which allow to limit the computational burden, but introduce computational efforts to be managed by the model developer, as discussed in Chapter 6.

On the other side, the influence of geometrical constraints on the flow behaviour represents the third complexity issue tackled in this work. Its influence should be taken into account properly by the developer not only from a "geometrical" point of view, but also considering their control effect on the flow and bed dynamics, through proper mathematical and numerical descriptions. This complexity issues is better discussed in Chapter 7.

The fourth and last complexity issue faced in this work is pretty "numerical". A local-scale analysis of the numerical results obtained for the Valle Molinara case study highlighted some inconsistency in numerical fluxes that, anyhow, does not produce significant, macroscopic effects. In practice, looking at the local signs of the numerical mass fluxes, it was observed that sometimes the sign of the mixture-mass flux is opposite to the sign of the sediment-mass flux. This result can not be accepted from a physical point of view, since mixture- and sediment-mass fluxes must have the same sign, i.e. the same velocity (on the strength of the isokinetic assumption which the TRENT2D model is based on). Presumably, this issue is related to some mathematical and/or numerical choice introduced in the model to reach an acceptable level of detail in the representation. Since the issue is thorny, Chapter 8 of this thesis is entirely dedicated to scrutinise it from the point of view of the numerical-model developer.

4.2 The 1966 debris-flow event of Rio Lazer (Italy)

At the beginning of November 1966, a large part of North-eastern and Central Italy was damaged by floods and high-concentration flows, causing 118 victims and severe damages and injury (APAT and Agenzie Regionali e delle Province Autonome per la Protezione Ambientale, 2004). Among the different high-concentration flows event observed in 1966, here the debris-flow event of Rio Lazer is back-analysed.

Rio Lazer is a small mountain stream in the Eastern Italian Alps (Figure 4.11), about 40 km away from the Valle Molinara basin (as the crow flies). The event did not caused fatalities, but inundated the village of Siror and its country.

Studying this non-recent event revealed to be a considerable challenge, because of the scarcity of field data and documentation, although a thorough historical analysis was performed before the

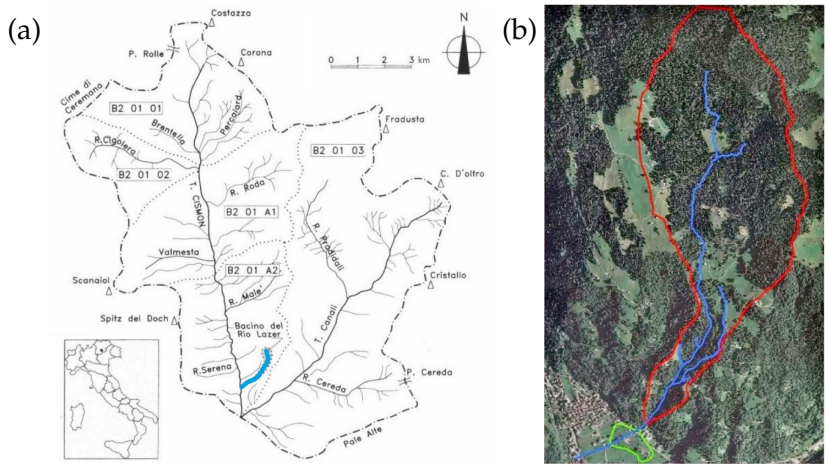

Figure 4.11: (a) Rio Lazer in the basin of the Cismon stream (Lenzi and Paterno, 1997) (b) Perimeter of the Rio Lazer basin (red) and its alluvial fan (green)

modelling stage. For sake of completeness, it must be noticed that a back-analysis of the event had been already performed in Gregoretti et al. (2016). However, the approach used in the reconstruction proposed hereafter is totally different and disregards results obtained in the work of Gregoretti et al. (2016).

In the following Sections, the main outcomes obtained in this back-analysis and some critical points are presented. Some further details can be found in Veronesi (2017).

4.2.1 The study area and the event of Rio Lazer

The Rio Lazer basin is about 1.6 km^2 wide. The Rio Lazer stream descends the Col di Cistri peak (1604 m) and reaches the Siror village (780 m), located on the Rio Lazer alluvial fan. The average slope of the upper part of the basin is about equal to 30%, then it increases up to 50% in the intermediate part and decreases to 12% reaching the alluvial fan. The total length of the stream is about equal to 3.8 km.

Geological analyses carried out by local agencies showed that the whole basin is covered by glacial deposit debris, i.e. coarse, cohesionless gravel and boulders, with high permeability and erodibility. Because of the high values of slope, erosional processes are observed quite frequently in the intermediate part of the basin. For this reason, since 1879, local authorities had been repeatedly involved in the construction of protection and control works. Over the years, they realised: a deposition basin; some slit dams; sequences check dams; a regularisation of the flow sections in the lowest part of the basin. However, works existing in

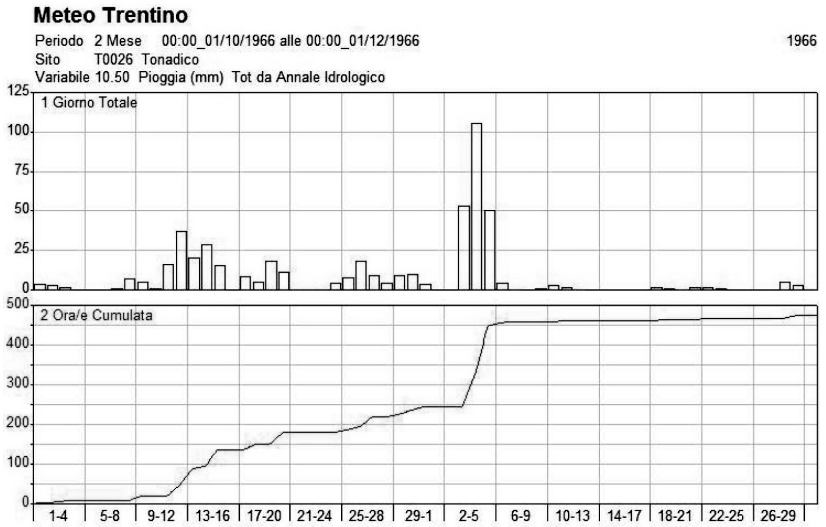

Figure 4.12: Rainfall heights measured by the rain-gauge of Tonadico (Italy) in October and November 1966: daily heights (above) and cumulative heights (below)

1966 were not able to control and stop the debris-flow event, also because of the extreme character of the phenomenon.

A thorough historical analysis showed that about ten flooding events were recorder in the study area in the last two centuries. The debris-flow event of the 4^{th} November 1966 was presumably the worst one. However, historical data describing past events were mainly descriptive and illustrative, while no measurements or field data were found, also because the basin has never been instrumented. Therefore, the back-analysis of the 1966 event was based on little, but cardinal documentation.

During the last days of October 1966 and the first days of November 1966, intense and persisting precipitation events were observed over the whole area of the Province of Trento, where the basin is located. In particular, the return period of the rainfall events registered between 3^{rd} and 4^{th} November all around in Eastern Italian Alps was estimated to be higher than 50 years (De Zolt et al., 2006). Figure 4.12 shows data gauged by the station of Tonadico (placed just 1 km south the alluvial fan of Rio Lazer) during the months of October and November. Analysing the sequence of rainfall events, it is plausible assuming that precipitation until November the 3^{rt} caused the basin saturation, while the peak registered on the 4^{th} leaded to the triggering of the debris flow. Unfortunately, rainfall heights measured in Tonadico were recorded only as daily cumulative rainfall heights (Figure 4.13), therefore no information about the time evolution of the precipitation in the vicinity of Rio Lazer is available.

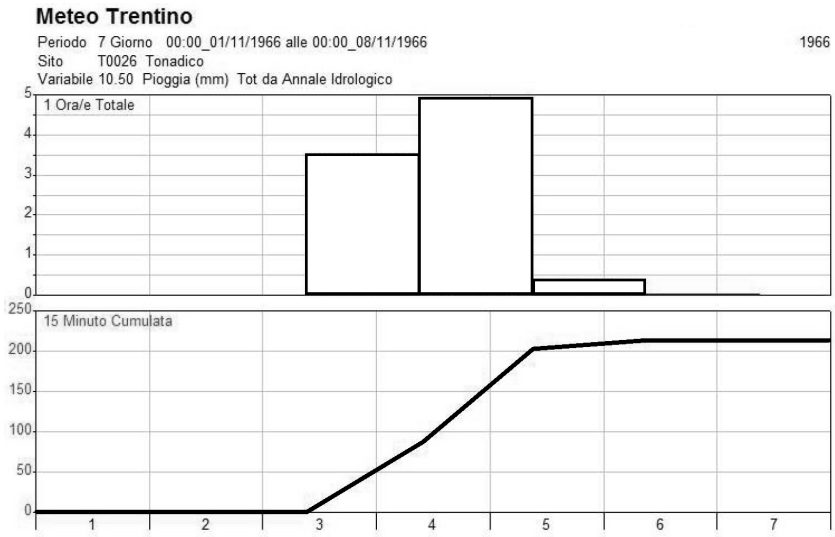

Figure 4.13: Precipitation measured by the rain-gauge of Tonadico (Italy) in between the 1^{st} and the 7^{th} of November 1966: daily average rainfall intensity (above) and cumulative rainfall height (below)

Figure 4.14: Picture representing Rio Lazer and the inundated Siror country just after the 1966 debris flow (Filippi Gilli, 2016)

Other two relevant data were used for the back-analysis of the Rio Lazer event. They are a picture (Figure 4.14), available in Filippi Gilli (2016), and a map of the flooded area extent (Figure 4.15), available in Lenzi and Paterno (1997). The picture (Figure 4.14) shows not only the deposition area, but also some erosion processes on the lateral hills, which contributed to extend slightly the deposition area.

As far as the debris-flow volumes are concerned, Gregoretti et al. (2016) estimated a deposited sediment volume about equal

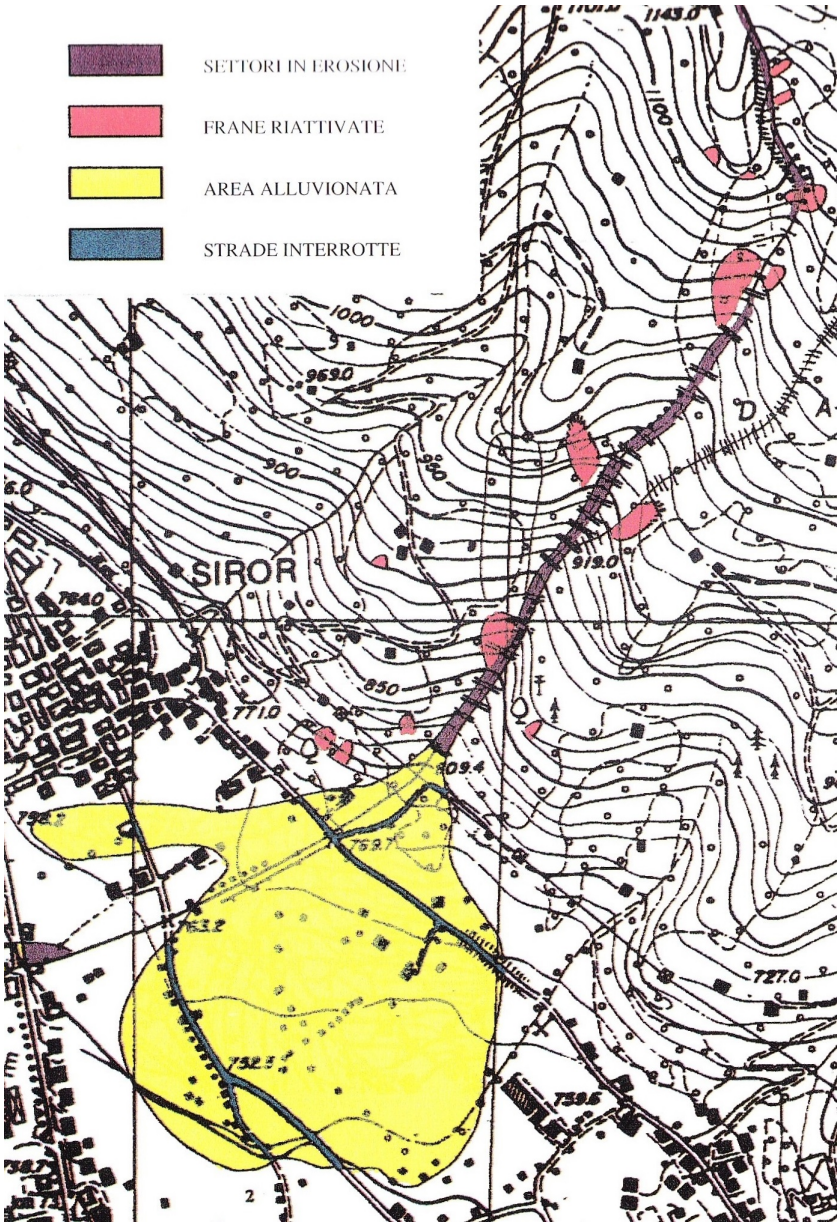

Figure 4.15: Map of areas interested by the 1966 event in the Rio Lazer basin (Lenzi and Paterno, 1997): erosion (purple), reactivated landslides (pink), deposition area (yellow) and interrupted roads (blue)

to 56 000 m^3, which corresponds with a purely-solid volume of about 37 000 m^3 after the deduction of porosity. The origin of this estimate is not very clear, therefore this value is taken into account as an approximated indication about the magnitude of the event.

4.2.2 Back-analysis

Despite the lack of detailed information, a back-analysis was carried out by means of TRENT2D, in order identify a quite limited range of possible event dynamics and also to identify possible critical points in an analysis with poor event-based information.

Because of the low resolution of the gauged data recorded in Tonadico, some a-priori hypotheses were necessarily introduced about the time evolution of precipitation. Assuming that the debris-flow starting was caused by rainfall of the 4^{th} November, hydrological analyses were carried out considering only the cumulative rainfall height measured during this day only (about equal to 100–120 mm) and supposing the basin as fully saturated. According to studies that classify the 1966 floods as extreme, it was assumed that the return period of the Rio Lazer event was quite high. On the basis of the geo-statistical rainfall analyses carried out for the Eastern part of the Autonomous Province of Trento (which are accredited by the Autonomous Province of Trento and first published in Della Lucia et al. (1979)), it was observed that the return period of rainfall with a cumulative height of 100 mm is about equal to 50 – 100 years only if rainfall duration is at most some hours. Therefore, 4^{th} November measurements recorded by the Tonadico rain-gauge must be referred to an interval presumably shorter than one day.

On the strength of these considerations, six synthetic hyetographs were built for the basin, starting from the Intensity-Duration-Frequency (IDF) curves obtained within the region by Della Lucia et al. (1979), for a return period of 100 years. It must be underlined that considering different values of return period (as for example 50 years or 200 years), outcomes do not turn out to be dramatically different.

Different rainfall durations were considered to build the synthetic hyetographs (1, 2, 3, 4, 5 and 6 hours), while rainfall intensity was assumed to be constant in time and space, because of the lack of information and the small extent of the basin.

The rainfall duration that caused the maximum liquid peak discharge in the basin was estimated to be slightly lower than 1 hour. Therefore, on the basis of the rainfall duration chosen, the analysis implicitly assumes that the debris flow was caused by a precipitation event that was not necessarily the one producing the highest discharge peak.

These six hyetographs were used as input data for the Peak-

Parameter		Value
Percentage of saturated area	S	100%
Channel velocity	u_c	$2ms^{-1}$
Hillslope velocity	u_h	$0.02ms^{-1}$
Coefficient of hydrodynamic dispersion	D	$1000m^2s^{-1}$

Table 4.7: A-priori values chosen for the PeakFlow parameters

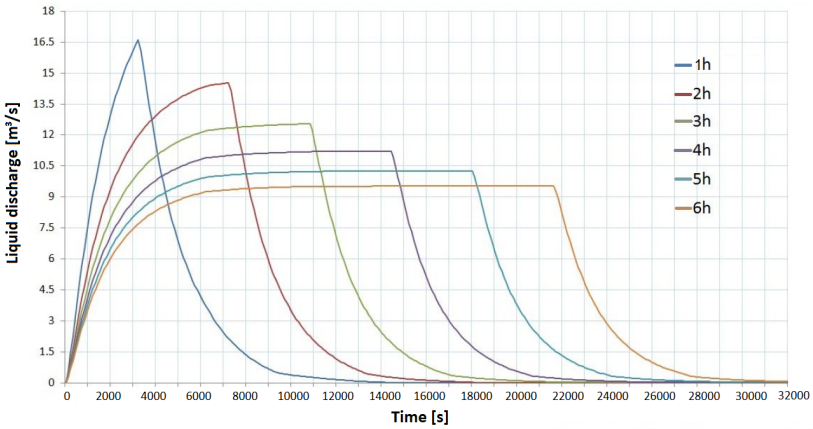

Figure 4.16: Hydrographs hull obtained by means of PeakFlow considering the six synthetic hydrographs produced for the Rio Lazer basin

Rainfall duration	1h	2h	3h	4h	5h	6h
Liquid volumes $[m^3]$	71240	106520	135320	160630	183610	201270

Table 4.8: Liquid volumes of the six liquid hydrographs obtained for the back-analysis of the Rio Lazer event

Flow model (Rigon et al., 2011), in order to obtain a set of possible liquid hydrographs of the event. Since model calibration was not possible, a-priori values were chosen for the parameters. They are summarised in Table 4.7. Hydological modelling was carried out over the basin closed at the fan apex, just upstream the point where stream slope changes, moving from 37% to 12%. Hydrographs obtained with this approach are shown in Figure 4.16, while the total liquid volume of each hydrograph is indicated in Table 4.8.

These hydrographs were turned into mixture hydrographs on the basis of a suitable estimation of the sediment concentration. Because of the presence of the stream-slope variation very close to the point where hydrographs were computed, it was not possible

Table 4.9: Concentration, amplification factor and mixture volume values for the six synthetic hydrographs obtained for the Rio Lazer back-analysis

Rainfall duration	1h	2h	3h	4h	5h	6h
$c[-]$	0.31	0.24	0.21	0.19	0.17	0.16
$F_a[-]$	1.90	1.60	1.46	1.41	1.35	1.33
$V_{mix}[m^3]$	135350	170370	197670	226270	248310	267370

to use the same approach proposed in Section 4.1.3, since the slope value to be introduced in equation 4.1 was not univocal. Therefore, a different approach was applied.

The estimate of the deposited sediment volume computed in Gregoretti et al. (2016) was used as an approximative reference value to quantify the amount of sediments flowing at the fan apex. Since it is not clear if this estimate considers also volumes attributable to erosion on lateral hills or not, it is possible that the deposited volume pertaining to the debris flow is slightly lower than the estimate. Anyhow, the amount of this possible discrepancy is probably comparable to the uncertainty of the estimate. Therefore, considering the uncertainty of the estimate and possible deposition dynamics, it was assumed that the purely-solid volume of the flowing debris-flow at the apex of the alluvial fan about equal to 40 000–45 000 m^3, which becomes 60 000–70 000 m^3 if porosity is taken into account. These values were used, together with the values of the liquid volumes listed in Table 4.8, to estimate suitable values of mixture concentration and amplification factor (Table 4.9). Maximum packaging concentration c_b was reasonably assumed to be equal to 0.65. In this way, six mixture hydrographs were defined.

At this stage, suitable morphological data and reasonable parameters value needed to be defined in order to perform TRENT-2D simulations.

Morphology description was based on the use of a DTM. Since no DTMs were available in 1966, the one surveyed in 2008 by the Autonomous Province of Trento was considered as starting point for the representation (Figure 4.17(a)). However, the 1966 morphology was locally different from the 2008 one. For this reason, a quite long process of editing was performed, in order to make the DTM more accurate with respect to 1966 conditions. As basis of comparison, two historic aerial pictures were considered, one taken in 1963 and one in 1973. These pictures were made available by the authority for Land Planning and Landscape Tutelage

Parameter		Value
Friction angle	Φ	38°
Maximum packaging concentration	c_b	0.65
Submerged relative density	Δ	1.65
Relative submergence	Υ	11

Table 4.10: A-priori values chosen for the TRENT2D parameters in the Rio Lazer back-analysis

of the Autonomous Province of Trento.

First of all, buildings existing in 1966 were added to the 2008 DTM and the obstruction due to the presence of two bridges removed (Figure 4.17(b)). Then, some editing was performed in the upper part of the alluvial fan, where a slit check dam and a deposition basin are present nowadays (Figure 4.17(c)). This modification was introduced trying to reproduce the shape of the deposition basin existing in 1966, which was different to the actual. Lastly, the area lying on the left bank of the deposition basin was suitably rectified. Nowadays, in this area, two buildings are present, over a raised plain. However, since the DTM describes the terrain elevation, it was cleaned from buildings and the result is a quite irregular surface. However, in 1966 neither buildings nor steps raised in that area and the terrain surface declines smoothly towards Siror street. Therefore, DTM was modified in order to make the slope more regular and deleting high steps (Figure 4.17(d)).

In this way, modelling initial and boundary condition were defined, while parameters values were still not. Since no calibration was possible and site-specific information was poor, a-priori value for the TRENT2D parameters were chosen.

As in the previous case study, reasonable values were chosen for c_b, Δ, Φ and Υ (see Table 4.10), while β was estimated according to the uniform flow condition.

In this case, such assumption is presumably mistaken, because of the presence of the slope variations along the stream. Nevertheless, it was accepted since some value for β was anyhow required. β was computed solving the system of equations 4.2a and 4.2b for each on of the six values of concentration. Resulting values are listed in Table 4.11.

Once input data and parameters were all defined, six TRENT2D simulations were run. Comparing model results, no dramatic differences were observed both in the extent of the deposition area and in the erosion and deposition depths (see Figure 4.18).

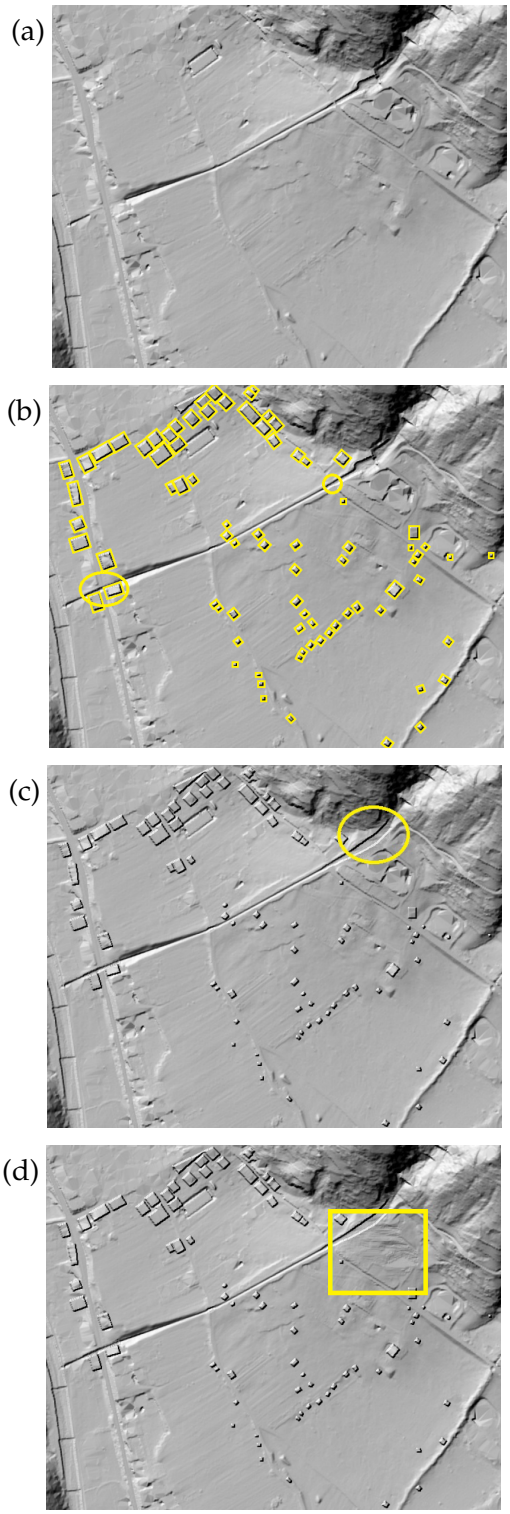

Figure 4.17: DTM modifications over the Rio Lazer alluvial fan: (a) original DTM surveyed in 2008; (b) addition of 1966 buildings p(rectangles) and deletion of the two bridges (circles); (c) editing of the current deposition basin; (d) editing of the plain above Siror street.

Rainfall duration	1h	2h	3h	4h	5h	6h
β[−]	0.44	0.24	0.16	0.135	0.11	0.10

Table 4.11: Values of the transport parameter β for the six synthetic scenarios considered in the Rio Lazer back-analysis

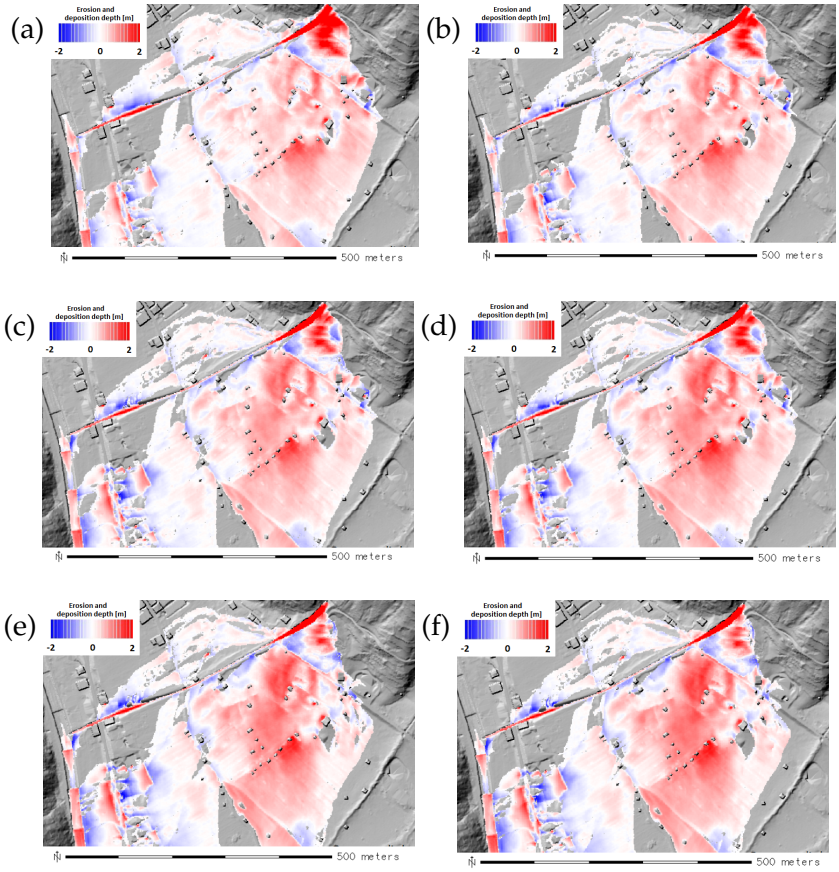

Figure 4.18: Maps of simulated erosion and deposition depths at the end of the simulations with rainfall duration of (a) 1h; (b) 2h; (c) 3h; (d) 4h; (e) 5h; 6h.

Furthermore, the extent of the deposition area is quite similar to the one reported in Lenzi and Paterno (1997). This outcome is displayed in Figure 4.19, where the perimeter of the flooded area is superimposed to the extent of the erosion and deposition area at the end of the 3h simulation. The comparison is quite comforting.

Also the phenomenon dynamics appears quite similar in the whole set of simulations. Therefore, despite the high level of uncertainty, results obtained by means of this approach appear quite univocal.

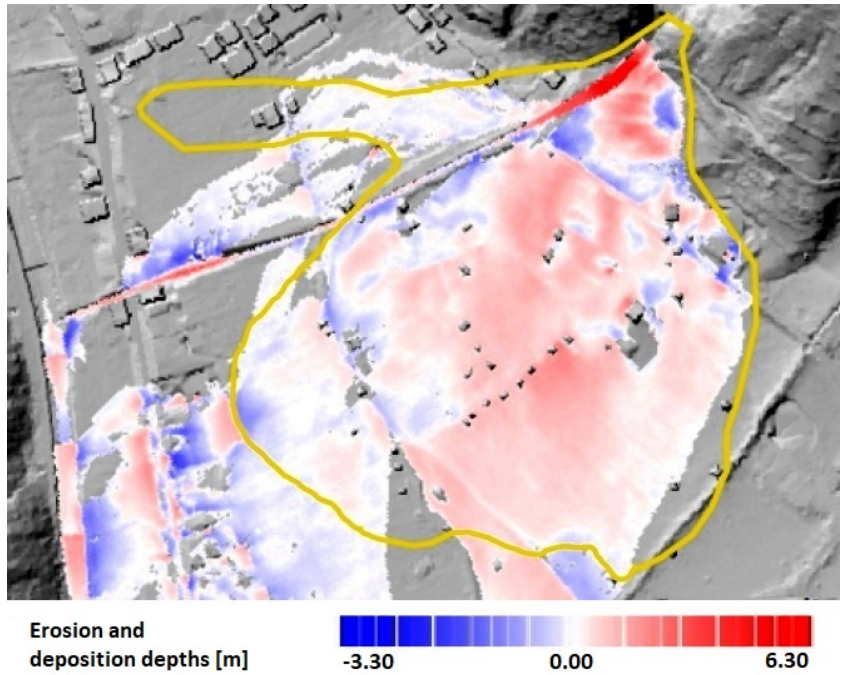

Figure 4.19: Map of erosion and deposition depths at the end of the Rio Lazer simulation, based on a rainfall duration of 3h, over-layered to the perimeter of the flooded area indicated in Lenzi and Paterno (1997).

4.2.3 Discussion about complexity issues

Despite the lack of historic information, especially about precipitation, acceptable results were obtained basing hypotheses and reasoning on physically-based observations as far as possible.

The final result is not a single event reconstruction, but rather a range of possible back-analyses. Uncertainty remains high and further and more detailed analyses should be carried out, in order to evaluate the suitability of assumptions about the hydrological scenarios, the amount of moved sediment volumes, the values of the models parameters, the right representation of morphology in other points of the area. These analyses could be guided by the critical examination proposed here.

For example, the back-analysis results quite imprecise with reference to the branch towards the village of Siror (highlighted in Figure 4.20). It seems that simulated deposition processes were not so extended as expected on the basis of the Gilli's picture. It is plausible that a not very accurate morphology representation conditioned the flow paths, forcing the flow to bend after the leak from the left bank, returning into the channel downstream. This discrepancy could be caused not only by the morphological representation of the Siror fan, but also of the channel banks. Timing

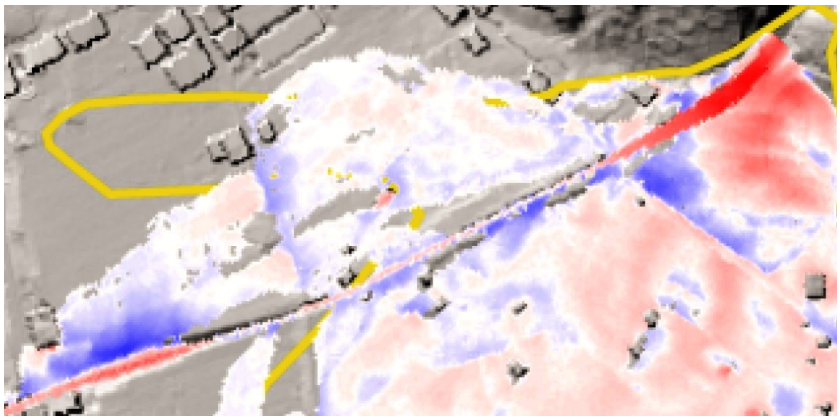

Figure 4.20: Detail of the deposition area on the left bank of Rio Lazer.

of the leak is strongly influenced by the bank elevation. If the banks are represented as too much high, the simulated pouring out of the flow could be delayed with respect to the real event dynamics. On the contrary, too much low channel banks on the right side could have anticipated the pouring out, influencing also the dynamics of the left bank. Furthermore, as in the previous case study, channel sections are very narrow (3–5 m), therefore only a limited number of cells is used to represent cross-section elevations. Also this point could be revealed as critical. As in the previous case, choosing a finer resolution could improve the morphology representation. However, computational costs would increase dramatically. A possible approach to bypass this "geometrical" issue aiming at the *right level* of detail in the morphology description is presented in Chapter 6.

In similar cases, uncertainties in morphology representation are likely to influence simulation outcomes more significantly than uncertainty in discharge evaluations. On the other hand it must be said that historical documentation is not sufficient to solve all the geometrical uncertainty. However, sequences of repeatedly-refined simulations could make up for the lack of information. Clearly, continuous refinements of the morphological description imply a large amount of hand work and suitable software tools. In this case, GIS systems could not represent the most convenient choice, while 3D viewers seem to be more appropriate, because of the small scale of the editing operations. However, 3D viewers could require particular file formats or reference systems, increasing the handwork for the user. Furthermore, in this work, validation of modifications introduced was carried out by means of iterative simulations, which required a continuous trans-

fer from the editing environment to the modelling environment. Also in this case, integrated solutions able to reduce the number of operations and ensure editing accuracy appear extremely desirable. A possible solution to these "operational" issues is presented in Chapter 5.

Last, numerical inconsistency in flux signs was observed locally also in this case. Since the physical basis of the description must be preserved, this "numerical" issue is investigated in Chapter 8.

Chapter 5

WEEZARD: a possible solution to "operational" issues

The case studies presented in Chapter 4 showed tangibly some "operational" issues generated by the hazard-assessment procedural chain presented in Section 1.3. These issues may undermine the reliability of high-concentration flows hazard assessment, although a sophisticated model as TRENT2D is applied. The possible outcome is essentially due to two elements: the amount of data to be managed in order to run a simulation and the number of manual operation to be performed before and after the simulation. Both data and operations introduce in the job a large number of possible sources of mistake and could accidentally divert user attention from the physical meaning of the operations. Such a circumstance could lead unintentionally to a worsening of the level of detail in the description and to a rise in complicatedness.

A similar outcome must be compulsorily prevented by both model developers and users. Users should carry out modelling much carefully and avoiding distraction, while model developers could make available integrated solutions able to reduce handwork burdens and support critical analyses at each step of the procedural chain. If the first remedy pertains mainly to the know-how and the commitment of the user, the second answer appears more effective, although it requires effort in software development.

Integrated solutions could introduce also other significant benefits for the user, if properly designed and developed. For ex-

ample, hardware, software and computational costs could be reduced, accessibility to sophisticated modelling improved, data security ensured, fragmentation avoided, communication simplified.

In this work, an integrated solution is presented for TRENT2D. The model was incorporated into a practical and affordable tool for high-concentration flow hazard assessment, which is called WEEZARD and that was expressly developed for this model. WEEZARD is a Web Service (WS) ecosystem designed and realised to ensure high-quality, cost-effective hazard assessment. These features of WEEZARD appear to fit well the requirements of the UE Flood Directive (UE, 2007) and the USA Disaster Mitigation Act (DMA, 2000) in terms of hazard-protection strategies (*appropriate best practices* should be used, applying *the most cost-effective and efficient technology available*).

In Section 5.1, "operational" issues that led to the development of WEEZARD are shortly summarised. Some of them were already recognised in the previous Chapter, while some others become from experience. Then, Section 5.2 describes the path that led to the development of WEEZARD, while Section 5.3 presents the system architecture. The main functionalities of WEEZARD are illustrated in Section 5.4 and applied in Section 5.5, where hazard-level maps are produced for the Valle Molinara alluvial fan. Last, Section 5.6 discusses forthcoming development and future perspectives of WEEZARD.

It must be noticed that some parts of the following Sections recall or summarise the contents of the paper "A Web Service ecosystem for high-quality, cost-effective debris-flow hazard assessment" by Rosatti et al., recently accepted for publication in Environmental Modelling and Software. Some other information can be found also in Zorzi et al. (2015), Rosatti et al. (2016), Zorzi et al. (2016a) and Zorzi et al. (2016b).

Because of the multi-disciplinary character of the skills necessary to create such an integrated system, WEEZARD has been developed by a team of six researchers and experts, which the author of this thesis belongs to. In particular, the author has been the main responsible of identifying the complexity issues to be faced, planning their management, defining proper strategy for their overcoming and designing concretely the functionalities necessary in the system. Furthermore, the author has taken part actively to all the development steps of the system, paying specific attention to preventing complicatedness and ensuring the

effective overcoming of the complexity issues considered.

5.1 Some "operational" issues of a high-concentration flow hazard-assessment job

In Section 1.3, several complexity issues typical of a high-concentration hazard-assessment job were already disclosed. That discussion was carried out in a quite wide frame, while here the focus is restricted to some of the operational aspects most related to the simulation modelling stage.

These issues were encountered within several TRENT2D applications, included those presented in Chapter 4. Though, they are quite general, i.e. not strictly related to the specific model, and typical, especially if desktop modelling applications are considered.

- **Visualisation and overlaying of geospatial data.** Geospatial data visualisation is essential for both modellers that perform simulations and decision-makers that need to define strategies on the basis of simulation results. Morphology representation, possible thematic layer describing the study area and modelling results need to be displayed in a suitable environment and according to precise reference systems. Generally, these data are visualised by means of GIS tools, but sometimes also with different software products, especially if 3D views or 2D-3D animations are required. This produces work fragmentation and requires that the user is able to deal with different software products. Moreover, each product treats different file formats and, sometimes, different reference systems. This obliges the data user to perform suitable conversions to make data displayable. It must be noticed also that some software products for 2D and 3D view do not allow to perform some kind of processing, as for example draping an orthophoto over a DTM in a 3D view. Furthermore, typically large amounts of geospatial data need to be displayed, which may require significant handwork and time.

- **Editing of geospatial data.** Often, geospatial data, and especially morphology data, require editing, for example to correct inaccurate representation, to merge or to clip layers,

to perform algebraic or logical computing, to change spatial resolution or to add relevant elements as for example designed protection works. Editing can be either punctual or extensive. GIS and CAD tools may support this operation, while 3D viewers can be profitably used to validate the editing operation. Also in this case, work fragmentation may hinder an accurate editing. Furthermore, it could require significant handwork, possibly leading to accidentally imprecise results.

- **Selection of the computational domain.** Typically, models are applied on delimited areas, i.e. computational domains, where the phenomenon is expected to flow. GIS or CAD tools are often used to perform the selection. However, different models require different selection modalities and different formats, which may increase the user effort in data management.

- **Selection of the inflow cross sections.** Usually, mountain-flow models require the specification of the inflow cross sections, i.e. sections where to set upstream boundary conditions. Selection should be made accurately, ensuring that the chosen section is compliant with the hypotheses on which models base boundary-condition setting. To ensure accuracy in the selections, visualisation of the cross section profiles is opportune. This operation requires the use of GIS tools, CAD tools or spreadsheets, increasing work fragmentation once again.

- **Formatting of model input data.** In general, models require input files arranged in specific formats. Therefore, some processing is necessary to prepare proper files and directories concerning initial conditions, boundary conditions and parameters. Such processing increases handwork necessary in the hazard-assessment job and exposes data to additional manipulation, possibly leading to accidental editing. Moreover, formatting is usually performed by means of text editors, which must be added to the list of software products necessary to run a simulation.

- **Storage and retrieval of data.** Simulations require and produce large amounts of data. Therefore, a rigid strategy for data management is required, otherwise data may be lost,

overwritten, mixed up, duplicated, especially when a large number of simulations is performed. Moreover, a lot of time could be necessary to find data, if management is not performed systematically, and space required for storage could turn out to be larger than space strictly necessary. A natural solution could be represented by the use of a registry (database-based or file-based) that must be fed manually at the end of each simulation. However, also this solution does not guarantee data matching as files can be moved or deleted without automatic updating of the database.

- **Need of high-performance hardware.** Whenever hazard-assessment simulations are performed applying sophisticated models in order to reach the *right level* of detail, high-performance hardware is required in order to limit simulation duration. However, users may not have an adequate hardware resource, and costs to get it could turn out to be significant. For this reason, sometimes users move towards more simple, but rough models, according to the "simplification strategy" mentioned in Leskens et al. (2014). In fact, simple models typically are less demanding in terms of hardware and space for data storage.

These operational issues are clear proofs that setting up a simulation with the *right level* of detail by means of sophisticated models requires not only high-concentration flow knowledge and model understanding, but also methodicalness in data management, formatting and displaying and availability of suitable hardware resources. Relaxation of some of these requirements could profitably lead to a wider diffusion of the *best modelling practices*.

5.2 Towards an integrated solution for TRENT2D

The operational issues listed in the previous Section contribute to hinder the Transfer Of Technology between developers and users, especially if sophisticated models are considered. Users are required not only to understand the model, but also to apply it carefully, avoiding operational mistakes and oversights. This demand is often perceived by users as excessive and "spherical cows" are sometimes preferred. This circumstance led to the decision of developing a suitable solution for the TRENT2D model,

able to overcome the largest possible number of operational issues.

The development of the new modelling solution started from the system-concept development and the requirements analysis described in Section 5.2.1. On this basis, the most diffused integrated solution available in the literature were analysed (see Section 5.2.2) in order to choose the most appropriated one to be applied to the TRENT2D model.

5.2.1 System-concept development and requirements analysis

The purposes of the new modelling solution for TRENT2D coincide basically with the overcoming of the operational issues listed in the previous Section. To reach the goal, a system able to perform simulation modelling with limited costs and user efforts in pre- and post-modelling activities was conceived. System requirements were summed up in seven points.

1) **Completeness.** The new system was intended to offer a well-equipped working environment, where not only simulations can be easily run, but also geospatial data management and processing is straightforward. For this reason, the system is intended to integrate the model and other applications in a single solution. The aim is avoiding both possible mess in data processing and fragmentation of operations and tools.

2) **Accessibility.** The system was conceived to be easily accessible in terms of chances for the user, removing the constraint between software and device.

3) **Usability**. The modelling solution was required to be intuitive in its use, i.e. equipped with suitable guided procedure and interfaces. Furthermore, the solution should be suitable also for non-technical communication purposes.

4) **Performance.** The modelling solution was conceived to reduce computational burdens and hardware-resources costs, without intervening on the model itself, but rather on the resources made available to run simulations.

5) **Order.** The system was required to provide automatic and systematic data management strategy, ensuring proper data

storage and retrieval, without weighing on user hardware and software.

6) **Security.** Data security must be ensured, keeping out possible virus attacks, black-outs or physical damages.

7) **Updating.** Periodic system maintenance was intended to reach all the users, in order to ensure continuous improvement of the system and systematic Transfer of Technology.

Section 5.2.2 describes the integrated solutions most diffused in the literature on hydraulic-based phenomena. In light of this analysis, some possible alternative solutions for TRENT2D were supposed and discussed, in order to choose the most suitable one, able to satisfy these seven requirements with reference to high-concentration flow hazard assessment making use of the TRENT2D model.

Because of the trans-disciplinary character of the requirements, the discussion was carried out not only within the research group of prof. Giorgio Rosatti (which the author of this thesis belongs to and which is called hereafter Numerical Kernel Development - NKD group), but also involving Information-Technology experts of the Italian computer company Trilogis. This interdisciplinary collaboration was then carried on also subsequently, along the entire development process. The whole activity was carried on within the frame of three research projects (CLIMAWARE, MHYMESIS and PRIN2015), funded respectively by the University of Trento, the CARITRO Fundation and the Italian Ministry of Education, University and Research.

5.2.2 Which integrated solution?

In the literature, some integrated solutions have been proposed with the purpose modelling flow-like phenomena. However, most of them barely satisfy requirements about completeness, intuitiveness and manageability and rotate only around model running. Anyhow, whichever the general purpose of the integrated solution, it must be noticed that different approaches have been considered and implemented in the literature to integrate multiple components of the operational chains (see Belete et al. (2017) for a general overview about possible integration strategies). In this Section, the most popular approaches are mentioned next to the most promising.

5.2.2.1 Embedded desktop solutions

In an embedded solution, one component constitutes the main desktop environment, while all the others are included in it. In this way, all the components are tightly connected and communication is guaranteed by specific routines.

Either the numerical model or a GIS system can be chosen as main environment. In the first case, the numerical model must be equipped with all the required graphical features, while in the second case, the numerical model becomes a particular library function of the GIS. Using a GIS as the main environment is generally the preferred option (see e.g. Mergili and Fellin, 2007; Wang et al., 2008; Wu et al., 2013; Scheidl and Rickenmann, 2011; Gregoretti et al., 2016), as it can be obtained using an existing system and has a development effort far smaller than a numerical-model-based environment, where the possibility of using of existing libraries, mainly addressed to set up the graphical user interface, is instead more limited. No examples of model-based embedded solutions are known in the field of flow-like phenomena modelling.

The major limitation of an embedded solution derives precisely from its desktop nature. In a GIS-based application, "performance", "order" and "security" are limited by the hardware resources commonly available among users, resources that are adequate to perform classic GIS operations but often inadequate for heavy computing. For this reason, all the models that have been embedded in a GIS so far are CA-like models. Furthermore, because of the desktop nature, typically specific hardware is required to run the application, failing the "accessibility" demand. Moreover, GIS environments do not guarantee an adequate visualization of the outputs, failing the "completeness" requirement. Lastly, disregarding "usability", which varies largely among applications, it must be noticed that also the "update" requirement is not satisfied straightforwardly, since usually maintenance and updates are not automatic, but require installation.

5.2.2.2 Tightly-coupled desktop solutions

In this approach, all the components involving graphical elements are merged together in a single desktop Graphical User Interface (GUI) framework detached from the numerical model, which remains a stand-alone component running in a separate

desktop console environment (see for example Christen et al., 2012). Although they are separate (or decoupled), a strict coupling between the components actually exists, since the GUI works only for that specific numerical model, failing the "completeness" requirement. Moreover, communications commonly occur through exchange of data files.

Separation of environments is at the same time the strongest and weakest point: the typically sophisticated character of the model does not affect the GUI, but communications are not optimized at all. Moreover, this approach is limited by the locally available resources and by the lack of a database management system. Therefore, "performance", "order" and "security" requirements strictly depend on local hardware and storage resources. Furthermore, also in this case, some minimum constraint in terms of hardware resources and operative system is generally introduced, contrary to the "accessibility" requirement. Lastly, it must be noticed that, similarly to the previous solution, satisfaction of the "usability" requirement depends strictly on the individual solution, while the "update" requirement is into the hands of users, which are in charge of updates installation.

5.2.2.3 Loosely-coupled solutions

In a loosely-coupled solution, each of the components has, or makes use of separate components communicating through suitable interfaces. One of the most diffused approach is the Service Oriented Architecture (SOA) (see e.g. Jones (2005) and Shan and Hua (2006)). This approach can be used to build a wide range of solutions that, depending on the degree of interoperability, can range from closed (or essentially closed) to completely open systems.

Closed solutions need to provide all the functionality to perform a given job in a single environment (all-in-one solutions), where the web is used to connect distributed components (client-server solutions) or distributed business modules (Web as a Platform solutions) via customized interfaces. Customized interfaces guarantee high speed communications but limit the interoperability with other systems.

In contrast, completely-open solutions maximize the looseness and the exploitation of the potentiality of the web, allowing a component to be freely accessed through standard interfaces. When the component is a numerical model, a Model Web ap-

proach can be followed as proposed Nativi et al. (2013). This approach, essentially based on the Model as a Service paradigm, is useful when there is a large community that is interested in using the model and incorporating it into their own framework (component chaining). The peculiarity of this approach that offers the model as an independent component is at the same time an advantage and a limitation, because the use of completely general interfaces make communications slower and the GUI less intuitive than in closed solutions.

Whatever the degree of interoperability, SOA solutions present all the best features of the strategies listed in the previous two sections but, at the same time, does not show the limitations previously highlighted. All the operations necessary to perform a mountain flow hazard assessment job can be grouped and efficiently connected in a single environment ("completeness" requirement), while the computational core runs in an environment separate from the GUI, with communications highly optimized. The main difference, and the main advantage, is the possibility of locating all the computational burden on a high-performance cloud server ("performance" requirement). This resource can be shared among many users, so as to make the rental rate easily affordable. Another advantage is that components are not constrained to the same platform, language, operating system, or build environment ("accessibility" requirement) and can be replaced with alternative implementations while maintaining the same service interfaces. Furthermore, any improvement or update of the system is straightforwardly available for all the users ("update" requirement). Also "security" and data storage and retrieval (i.e. "order") can be managed in centralised way. However, these solutions require an effort in system development that may result a bit greater if compared to the that needed to develop desktop solutions.

In the literature, there are several examples of SOA solutions for geospatial data, known as WebGIS. Some have also been equipped with a mathematical model (see e.g. Jia et al., 2009; Kulkarni et al., 2014; Yin et al., 2015; Mure-Ravaud et al., 2016; Tan et al., 2016). However, a solution specifically designed to deal with sophisticated numerical simulations, and particularly in the field of high-concentration flows, is still lacking.

Figure 5.1: Logo and acronym of WEEZARD

5.3 The WEEZARD system

In the light of the system characteristics required (and listed in Section 5.2.1) and the possible integrated solution available (Section 5.2.2), the approach identified as the most convenient was a SOA, partially-open Web Service (WS) ecosystem, which allows the development of highly customized and efficient environments.

The system was called WEEZARD (see Figure 5.1 for the acronym meaning) and was developed according to a multi-tier approach, i.e. with different software components logically grouped together and physically placed on different computers connected by the web (see Section 5.3.1 for a descrition of the system architecture). Some of the components, especially those used in WEEZARD for dealing with geographic information, are based on Free Open Source Software (FOSS), which guarantees a good compromise among quality, security and costs. All the other components were built specifically for the system.

The whole solution was developed according to an iterative and incremental method (see the Manifesto for Agile Software Development of Beck et al., 2001), with recurrent planning, implementation, testing and evaluation, followed by periodic update releases (see Section 5.3.2). This cyclic approach provided a made-to-measure solution for modelling purposes (some of the system functionalities are presented in Section 5.4).

It must be noticed that one of the twelve principle of the Agile Manifesto is simplicity, which recalls observations carried out in Chapter 1. This means that, during system developments life cycles, complicatedness must be avoided compulsorily.

5.3.1 The system architecture

Hereafter, some details about both the logical and the physical architecture of the system are presented.

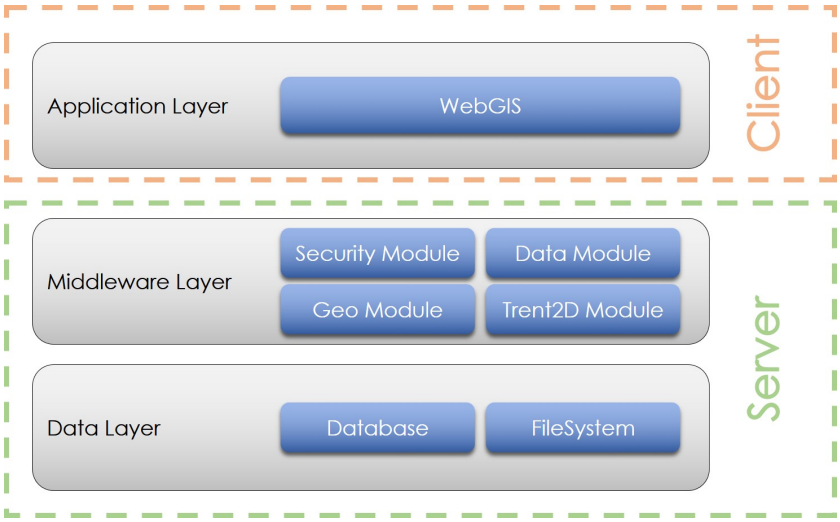

Figure 5.2: Logical architecture of the WEEZARD solution

5.3.1.1 The logical architecture

As shown in Figure 5.2, the system is organized in three layers, namely the Application layer, the Middleware layer and the Data layer, whose functions and software implementations are shortly described below.

- **Application layer**. The application layer represents essentially the web application of the system and looks like a WebGIS. It is loaded on the client machine when the relevant web page is accessed with an internet browser. The main tasks of this layer are to collect user inputs, transforming them into information usable by the WEEZARD WSs (e.g. the TRENT2D model or the data manager); to manage client-server communication; to display the data returned in the form of 2D or 3D maps. The operational load of the client is very limited, and so almost any kind of device with a browser and internet access can be used as a client machine (even a simple smartphone).

- **Middleware layer**. It is the operational core of the system and hosts all the services, supplying system functionalities. The layer consists of several functional elements that were specially developed for this system: the Simple Authentication and Security module for managing user authentication and data security; the TRENT2D core model and relevant

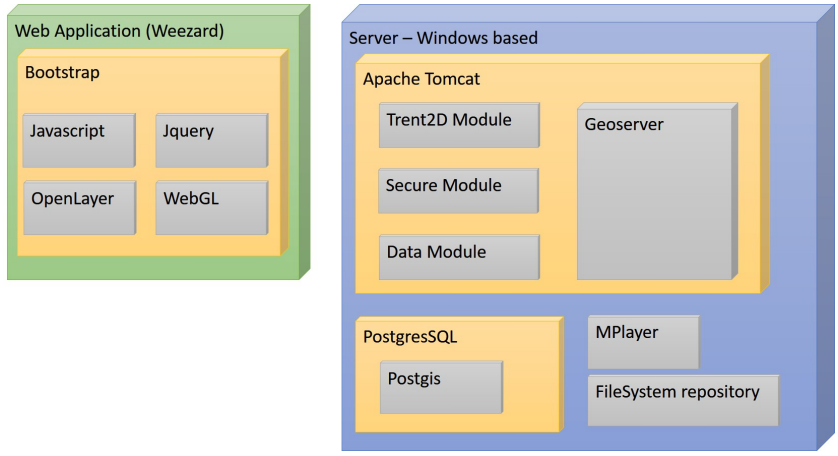

Figure 5.3: Component diagram describing the physical architecture of the WEEZARD solution

auxiliary modules for preparing and harmonizing data; the Data Management module for transferring data back and forth from the middleware layer both to the application and to the data layer; and the geographical information publisher. All these modules are configured as WSs.

- **Data layer**. The data layer is the part of the system that handles data storage and retrieval. Information collected is heterogeneous, varying from user information and model information, to system information and statistical information. The storage strategies are also different, in some cases using the Relational DataBase Management System (RDBMS), with or without spatial schema; in other cases information is stored directly on the filesystem.

Communications between client and server were realised implementing a suitable strategy, similar to the one used in OGC® WPS works, allowing asynchronous processing of requests.

5.3.1.2 The physical architecture

The physical architecture of the system is shown in Figure 5.3, where the component diagram is sketched. In the current implementation it is composed of a client-server structure in which the server is located on a single machine. More complex configurations could be considered in future releases.

The web application is the entry point of the WEEZARD system a looks like a WebGIS webpage. The GUI skeleton was developed by the Trilogis team using HTML5, CSS3 and JavaScript

in the Bootstrap framework, where several GUI controls (e.g. tabs, radio, checkbox and tree) derive from JQuery. OpenLayer library allowed to realise 2D visualizations (maps, sections, etc.), the WebGL library, i.e. a low-level 3D graphics API based on OpenGL exposed through HTML5 (Feng et al., 2011), was used to obtain 3D views.

Following the Infrastructure as a Service (IaaS) principle, middleware services were located on a server rent from an IT cloud provider. The structure of the middleware was designed by the Trilogis team following the Spring Model-View-Controller strategy, a design pattern that allows to build flexible web-based applications, decoupled from the underlying view technologies.

All the modules required in the WEEZARD system were provided by both the NKD group and the Trilogis team as RESTful WSs and hosted in the Apache Tomcat server container. The modules dedicated to geographical data manipulation use Geospatial Data Abstraction Library (GDAL) routines, and geospatial data is shared using the GeoServer with OGC® compliant open standards such as Web Map Service (WMS) and Web Feature Service (WFS). The MPlayer library is used to encode in AVI files animations of the model results.

Finally, the datastore was located by the Trilogis team on the same physical server as the middleware services. In future, it will be located in a cluster of servers and managed by using replication and load balancing strategies. Geospatial data are efficiently managed through the PostgreSQL object-relational database with the PostGIS extension. Simulation output (consisting of many different data points) is stored directly to the filesystem. In some cases, such as in the case of data editing, they are loaded in runtime into the RDBMS.

5.3.2 The system development life cycle

WEEZARD has been developed following an iterative and incremental approach, compliant with the adaptation principle contained into the Agile Manifesto (Beck et al., 2001). The System Development Life Cycle (SDLC) used is made of six steps, as shown in Figure 5.4.

1) **Planning.** Planning represents the first step of the SDLC. It is intended to answer two basic questions: "Which is the problem?" and "Which is the goal to be reached?".

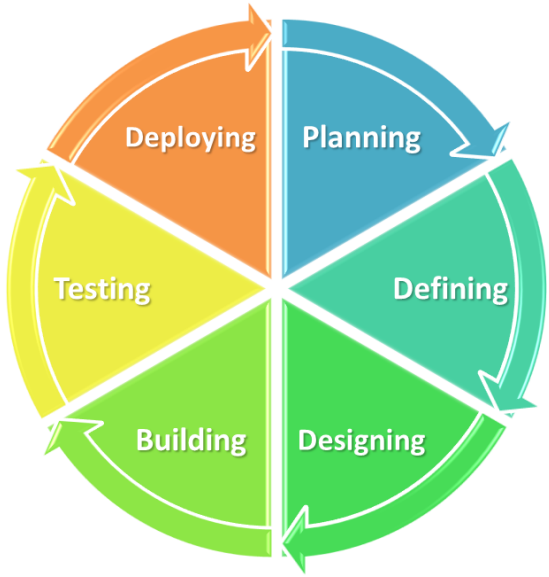

Figure 5.4: System development life cycle applied for the WEEZARD development

2) **Defining.** When problem and goal are clear, the question "Which is the most suitable solution to the problem allowing the goal to be reached?" is posed. To answer, different possible strategies are usually compared, taking into account their requirements in terms of resources, time and know-how.

3) **Designing.** Once the most suitable solution is identified, developers must reply to the question "How to get the solution?". In this step, the solution takes shape on paper, following indications obtained in the *defining* step, i.e. perfecting those too much vague and modifying those unfitting.

4) **Building.** Here, the purely-operational phase begins. The designed solution is implemented according to the final indications. If designing is performed with the *right level* of detail, building should not disclose new problems. However, if this is the case, suitable in-process modifications can be introduced.

5) **Testing.** In this step, the solution is tested in order to verify the goal reaching and to identify possible defects. When defects are easily remediable, they are fixed straightforwardly, otherwise the SDLC is begun again, considering the defect as a problem to be solved.

6) **Deploying.** When defects are fixed and *testing* is completed, the solution is released on the server, so all the user can simultaneously benefit of the solution.

This cycle was used first in the development of the alpha and beta versions of the system and has been repeated whenever an issue or problem required to be tackled, tuning and adjusting the WEEZARD system continuously, typically every two weeks.

Both the NKD group and the Trilogis team have been involved in this process. The NKD group has been the main player in *planning*, *defining*, *designing* and *testing*, while the Trilogis team has been responsible especially of *building* and *deploying*. However, the distinction has been not so Manichaean, especially when the intermediate steps of the cycle (i.e. *defining*, *designing* and *building*) have been faced up. In fact, some of the services closest to the TRENT2D model have been built by the NKD group, while most of the machine-level components have been designed by the Trilogis team.

In particular, the author of this work was responsible of:

- identifying all the operational issues and *planning* the goals to be reached in overcoming each of them;

- *defining* the possible solutions and the requirements to be satisfied, evaluating the opportunity of developing new functionalities or enhancing the existing ones;

- *designing* these solutions, defining how they interact with other existing services and data storage and retrieval, paying special attention to their client implementation, i.e. defining how they appear to the user, creating guided procedures for the most critical operations (creation of the computational domain, preparation of the TRENT2D runs and mapping hazard-level) and ensuring a proper management of user errors;

- *building*, i.e. coding, the services responsible of estimating the β parameter according to the uniform-flow assumption and computing the TRENT2D upstream boundary conditions (see Chapters 3 and 4), in addition to the service aimed at hazard-level mapping;

- alpha and beta *testing* of the designed solutions.

Typically, whenever a new functionality needs to be introduced in the system, the following operations have been implemented:

1) the functionality is identified and characterised;
2) the functionality is subdivided into logical steps, consisting of a number of operations/input data that can fit into a single window layout;
3) each layout is sketched and the operations designed;
4) each layout is implemented, together with the necessary operations;
5) a first validation is performed by the working group: bugs, non-intuitive sequences or operations, and difficulties in using windows are reported and corrected;
6) the functionality is deployed on a beta-testing server
7) a second validation is performed by a beta tester group, made up of people outside the working group; suggestions for possible improvements are collected and, when appropriate, implemented by means of new SDLCs.
8) when the functionality passes the beta testing successfully, it is deployed on the main server.

In this process, particular attention has been paid to giving the GUI an intuitive nature. In order to verify this feature, no detailed user manual has been given to the beta tester group, who had to learn how to use the functionalities with only the support provided by the GUI itself.

In Section 5.4.2, the SDLC of some functionalities is described, making the concepts just presented more clear.

5.3.3 The system availability and accessibility

The WEEZARD system is available on the web since September, 2016 at *http://tool.weezard.eu*.

Since WEEZARD is a web application, the only software product required to access the application is a web browser. Systematic debugging has been performed with Chrome and Firefox, but

the system also works well with other browsers. After registration is completed, a simple login allows the user to access the system.

The hardware demand is also extremely limited. Only the 3D visualization has a minimum hardware requirement, consisting in a video card supporting WebGL and 2GB of system memory. Nowadays, these features are available on the majority of personal computers.

On the server side, the hardware configuration is scalable according to the number of concurrent users. The most demanding element of the system is the numerical kernel. The hardware resources necessary on the server depend on the size of the simulation domain. The current minimum configuration is composed of an eight Xeon CPU machine, with 8 GB of RAM and 500 GB of disk.

5.4 WEEZARD: user categories, functionalities and the GUI

The WEEZARD system is intended to be used for modelling purposes by researchers, students, practitioners and public-agency technicians. Therefore, the GUI and the functionalities have been designed and implemented in answer to their necessities and requests. Singling out the desirable features was accomplished through the systematization both of the observations collected during the development and the practical use of the TRENT2D model, and of informal interviews with the users who employed the desktop code during their work activities.

The present release of the system provides for only two user categories, namely the standard user and the administrative user. A standard user is a person (practitioner, technician, researcher, student) mainly interested in doing simulations and producing suitable representations of outputs, while an administrative user is a researcher of the development group who, besides running simulations for practical use and for testing, also manages some basic aspects of the system. Other user categories, which can be singled out among parties interested in hazard assessment, can be conveniently added.

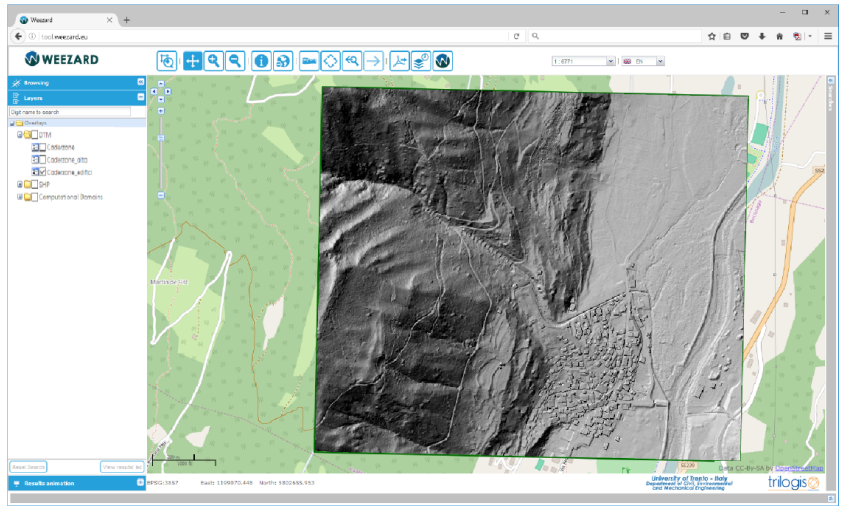

Figure 5.5: Main window of the WEEZARD system

5.4.1 The main environment

Since WEEZARD is mainly intended to host and manage geospatial-related information and functionalities, the main page looks like a WebGIS framework, in which the background map is the worldwide OpenStreetMap®(2016).

After the login procedure, other maps and shapefiles can be overlaid, as shown in Figure 5.5. Their handling is done through a classical Table Of Contents (TOC) layer manager present in the *Layers* accordion menu, located in the *Browsing* side panel. Geospatial data can be either loaded by the user or retrieved from WMSs.

Common GIS functionalities (e.g. pan, zoom, identify, add external sources and search) are available through the quick buttons located at the top of the window. The last two buttons allow access to the *scheduling queue functionality*, which is described in Section 5.4.2.5, and to the WEEZARD main menu (Figure 5.6).

5.4.2 The functionalities for the standard user

All the functionalities are designed with the purpose of carrying out a modelling job in an easy and time-saving way. Several of them perform operations that either cannot be performed through other GIS software or would require a succession of troublesome procedures. In addition, guided paths allow the user to follow chains of tasks in a clear and efficient way.

The WEEZARD button opens the main menu for standard

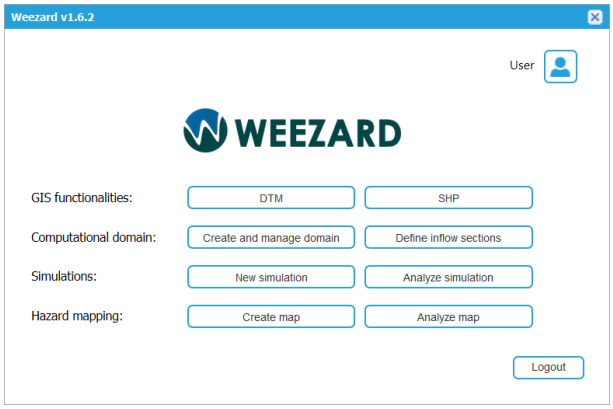

Figure 5.6: Main menu for accessing the WEEZARD functionalities

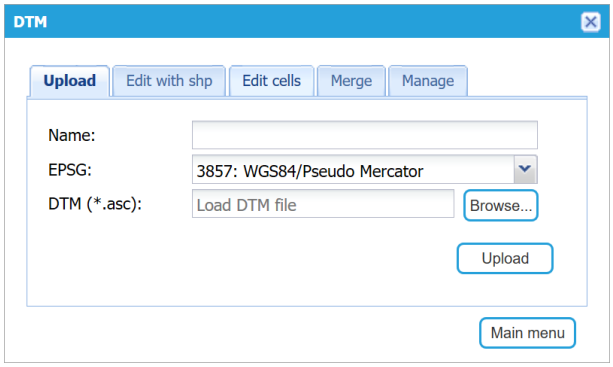

Figure 5.7: Tabs of the *DTM* menu in WEEZARD

users, where functionalities are grouped logically in four categories, namely *GIS functionalities*, *Computational domain* and *Simulations* and *Hazard mapping* (Figure 5.6). The main functionalities will be illustrated in the following Sections, as along with the *scheduling queue functionality*.

5.4.2.1 GIS functionalities

GIS functionalities are collected in two groups: *DTM* and *SHP*.

The *DTM* menu offers some functionalities that appear in the form of tabs (see Figure 5.7). Next to some classical GIS functionalities (i.e. *Upload*, *Merge* and *Manage*), two particular features for DTM editing are available: *edit with shp* and *edit cells*.

Edit with shp allows the user to change the elevation of all the cells inside closed geometries defined in a shapefile. This functionality is particularly useful, for example, when to take into account the presence of buildings.

Edit cells enables easy point-wise modifications of a DTM,

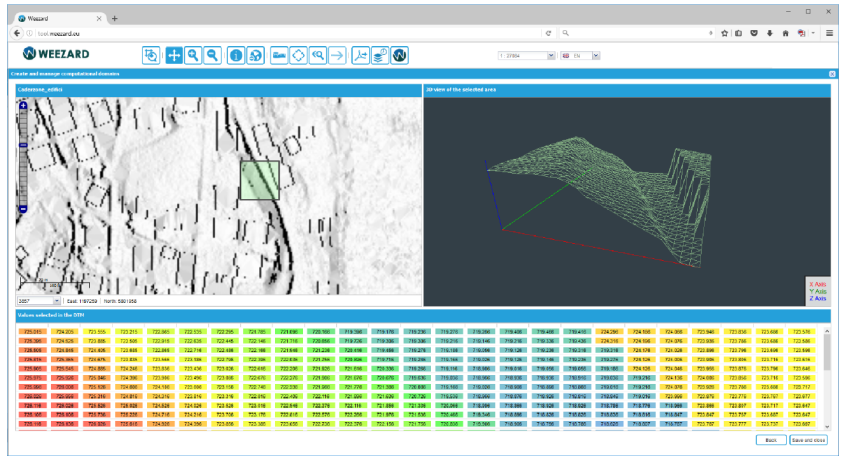

Figure 5.8: Three-panel window of *Edit cells* in WEEZARD

which turn out to be particularly useful to enhance local accuracy of the morphology representation. A three-panel window (see Figure 5.8), showing a 2D view, a 3D view of a zoomed part, and the matrix of the relevant elevations, allows the user to have an immediate perception of possible cell value modifications.

Functionalities contained in the *SHP* menu are classical GIS functionalities of *Uploading* and *Managing*.

5.4.2.2 Computational domain

The *Computational domain* category is intended to prepare input data for TRENT2D simulations. It makes available two groups of functionalities (Figure 5.6): *Create and manage domain* and *Define inflow sections*.

Create and manage domain allows to specify the location in the world and the extent of the computational domain, by means of graphical selection. Over a suitable 2D, georeferenced layout where the DTM is depicted in shaded greyscale, the selection can be performed drawing a rectangle over the desired area (Figure 5.9). The rectangle can be then moved, rotated and resized. The user effort ends here, while the backstage work is just starting. The client sends some data and a request to the server, which performs all the operations necessary to prepare the computational domain as an input file for the model, namely defining the local coordinate system required by the model, determining the number of cells in the computational domain, interpolating cell elevation from the underlying DTM in order to obtain the initial condition for the model, writing files in specific locations and finally registering

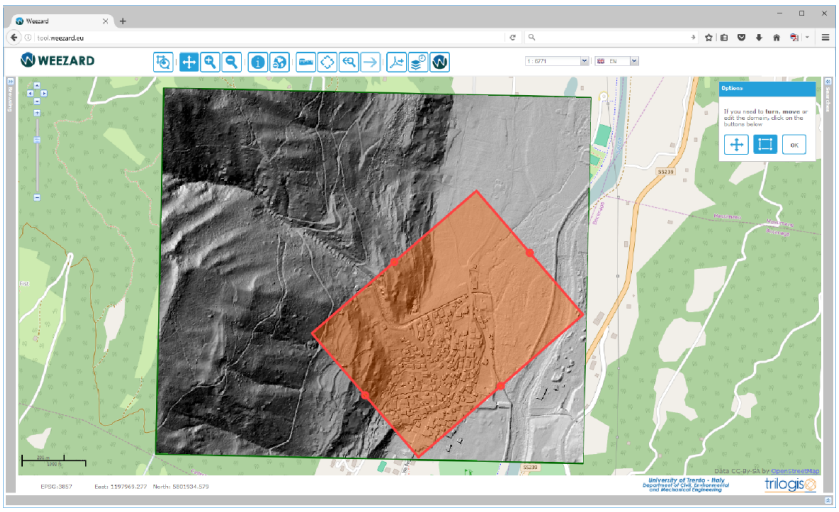

Figure 5.9: Definition of a computational domain in WEEZARD

information into the Datastore.

Define inflow sections allows the user to select the boundary cross section where to apply the upstream boundary conditions of the model. Also in this case a graphical approach is used, both to select the boundary cells (Figure 5.10(a)) and to evaluate the inlet slope (Figure 5.10(b)), used in the estimate of mixture concentration.

5.4.2.3 Simulations

The two groups of tasks of the *Simulation* category are *New simulation* and *Analyze simulation*.

New simulation starts a guided procedure that leads the user through running a TRENT2D simulation. Because of the centrality of the procedure, some highlights about its SDLC (that involved considerably the author of this thesis) are described hereafter, as an example of the approach used in system development.

1) **Planning.** Although geometric input data for the model were already defined, still a large number of operations is required to run a TRENT2D simulation and the user risks to get lost in the operational chain. The procedure required to be simplified, supporting aware user choices and avoiding fragmentation and complicatedness.

2) **Defining.** A guided procedure appeared as the most suitable solution, since it allows to put necessary steps in logical

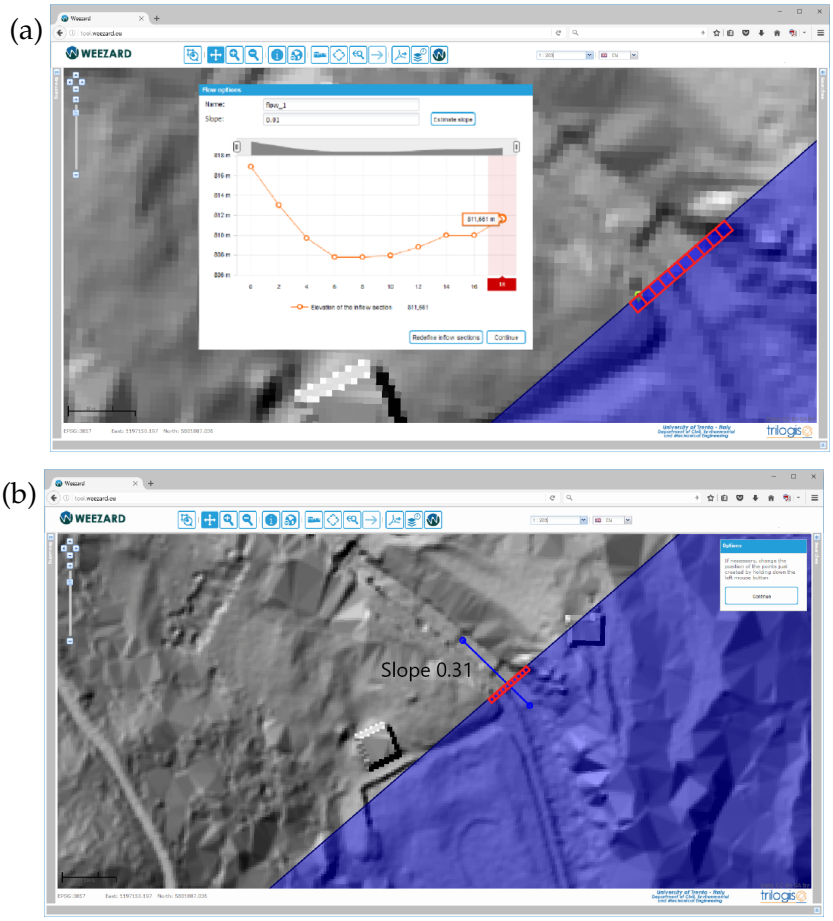

Figure 5.10: Computational domain in WEEZARD: (a) Selection of the input flow section; (b) Estimation of the bed slope across the inflow section

succession, to automate some operations, to introduce suitable checks in order to ensure that user inputs are supplied properly.

3) **Designing.** The procedure was divided into eight steps organised in succession. Clearly, for each step, design regarded functionality implementation, management and appearance. Hereafter, only the essential points are listed, chiefly assuming the client point of view and focusing especially on appearance.

   I. The name of the simulation, the computational domain to be used, the type of high-concentration flow phenomenon to be simulated (i.e. the type of closure to be used for the shear stresses among the two available) are required. As options, the return period characteristic

of the simulation and a short description of what the simulation is intended to represent can be specified.

II. Values for the model parameters are required, except for the parameter β. The system must check that physically-based values are introduced.

III. Input data addressed to boundary-conditions setting are required. The estimate of the inlet slope supplied during the creation of the computational domain must be reported as reference value, but it can be edited. Then, the file of the liquid hydrograph is required. Clear instruction must specify the format of the file and a detailed control analysis must be performed on the file in order to ensure that is well-shaped.

IV. If input data are well made, the procedure can continue with the estimate of the β parameter. An a-priori estimate must be supplied on the basis of the uniform flow hypothesis (see Section 4 and Armanini et al., 2009b). The estimate must be editable.

V. Once the liquid hydrograph and the parameter values are known, boundary-condition concentration can be estimated (see Chapter 4 and Armanini et al., 2009b) and total and solid hydrographs computed automatically. The possibility of supplying directly such hydrographs should be considered too. However, this chance requires a thorough further work on the server side, therefore it is taken out and planned for a later release of the system. Once these hydrographs are defined, they need to be displayed and their volume computed.

VI. The type of boundary condition to be set at the outlet bounds must be chosen. Available possibilities are: non-reflection or critical condition.

VII. The user has to choose the end time of the simulation, the timestep for saving results and the variables to be saved in output.

VIII. A summary window must appear (Figure 5.11), where the user can control and possibly editing supplied input data. Profitably, the same window must show an estimate of the simulation duration and size and the status of the user account, facilitating simulation

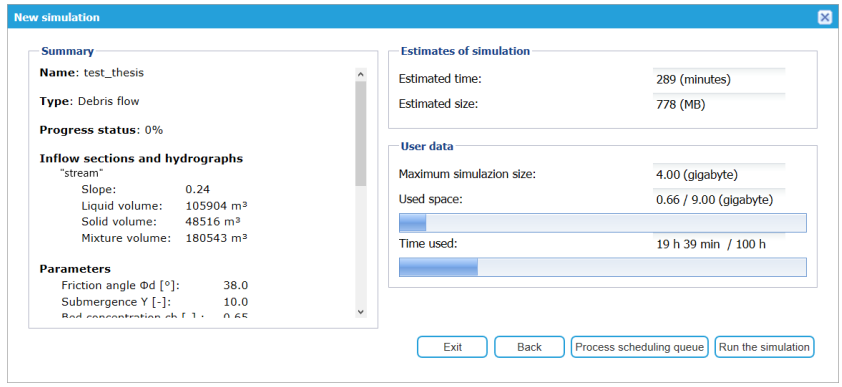

Figure 5.11: Simulation-summary window in WEEZARD

management. Here, the user can choose to start the simulation. The client sends a request to the server, which runs the simulation in background, remaining available for any other client request.

4) **Building.** Without getting into detail about the implementation, it must be noticed that such a procedure requires a significant "backstage" work on the server. Data must be read, checked, processed, displayed, stored and retrieved. All these operations are no more performed manually by the user, but automatically by the system. This implied a considerable developing effort, with the creation of tailored services and routines that involved the whole developers group. However, the result is a much lighter work for the user, which can concentrate especially on the scientific part of the job.

5) **First testing.** The procedure was tested by the working group in a lot of possible conditions, according to the monkey-testing technique, and observed bugs were fixed.

6) **Beta deploying.** The procedure was released on the beta server.

7) **Second testing.** The procedure was tested by the beta testers, which highlighted further bugs and suggested further improvements. Observed bugs were fixed and relevant suggestions taken into account.

8) **Final deploying.** The procedure was released on the main server.

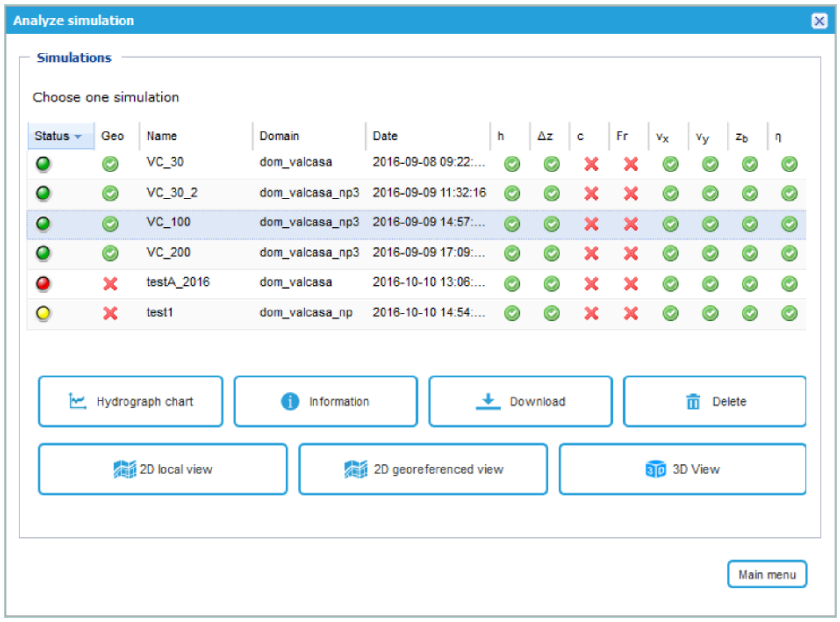

Figure 5.12: *Analyze simulation* panel in WEEZARD

In addition to the *New simulation* group of tasks , the *Simulation* category considers also another group of tasks, which can be accessed through the *Analyze simulation* button.

Thanks to the *Analyze simulation* task group, the user can check the working progress and analyse partial results at any time. As shown in Figure 5.12, *Analyze simulation* consists in a panel where the whole set of simulations is listed, along with the name of the simulations, the computational domain names and the saved model variables. Simulations already performed are labelled with a green traffic light, simulations still running with a yellow light and simulations not yet run with red light.

Once a simulation is selected, different tasks are available depending on the status of the simulation.

The first line of buttons concerns information and management operations, while the second line regards visualisation. Here, three different display frameworks are available, each fulfilling different target requirements.

- **2D local view.** This framework is tailored for in-depth quantitative analyses. Model outputs are displayed in a 2D view, with a local coordinate system (see Figure 5.13). Maps of variables saved can be browsed in time and space and multipoint section profiles can be extracted. The geometrical position of the sections can be stored on the server

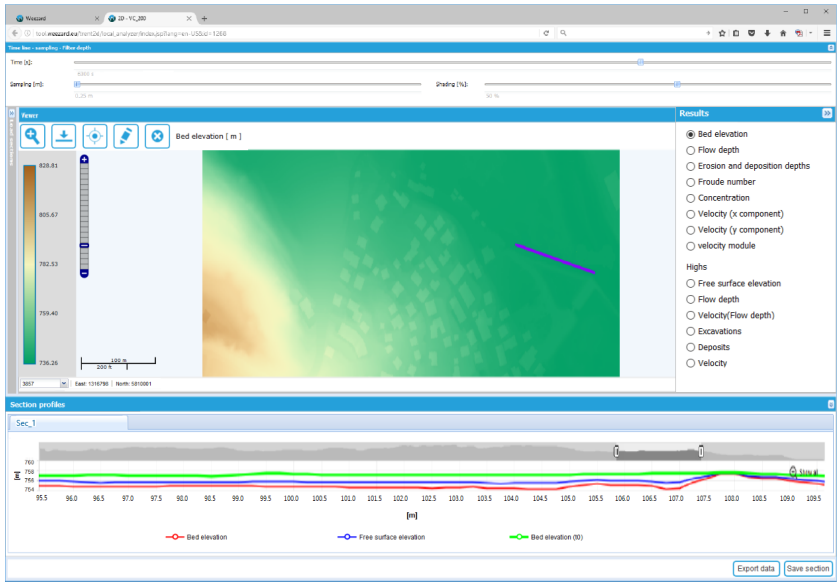

Figure 5.13: 2D local-view framework in WEEZARD

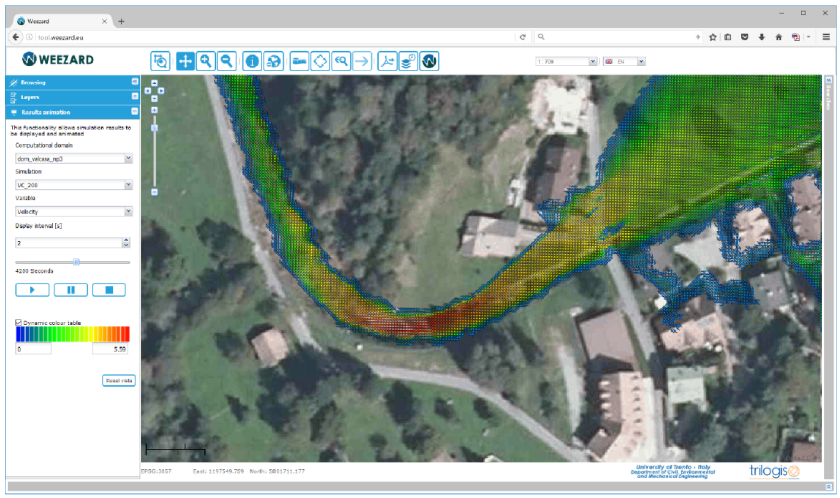

Figure 5.14: 2D georeferenced-view framework in WEEZARD

and used to analyse different simulations on the same computational domain.

- **2D georeferenced view.** This framework allows to contextualize results in the main window. Here (Figure 5.14), the accordion menu *Results animation* in the *Browsing* left panel reveals the relevant management tools. Scalar field maps (or velocity field maps) of the variables can be animated in time over background layers, showing the dynamic development of the simulated phenomenon.

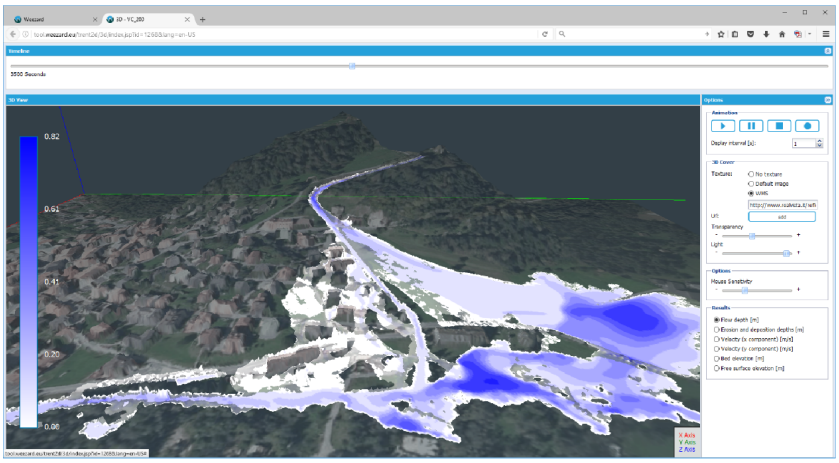

Figure 5.15: 3D-view framework in WEEZ-ARD

- **3D view.** This framework provides realistic 3D representation of a debris-flow simulation and turns out to be particularly useful for communication with non-experts. As pointed out by some authors (Hagemeier-Klose and Wagner, 2009; Albano et al., 2015; Sanders et al., 2016), this element is not a secondary goal in the field of risk management, because the use of advanced web tools can significantly increase citizen awareness and communities resilience. Image orientation and zooming can be controlled with a mouse, while other controls are available in the side panel (Figure 5.15). Dynamic visualisation and video production are supported.

5.4.2.4 Hazard mapping functionalities

The *Hazard mapping* category collects two groups of tasks: *Create map* and *Analyze map*.

Create map allows the user to produce hazard maps by means of the Hazard Mapping service. This is a module developed by the author of this thesis, considering high-concentration flow hazard-mapping regional or national regulation abiding by the BUWAL approach proposed in Heinimann et al. (1998). The module is able to process simulation results, according to hazard-mapping criteria stated by law, and produces hazard-level maps in output. *Create map* is based on a four-step guided procedure, assembled as follows:

I. The name of the hazard map to be created must be specified, together with the nature of the phenomenon represented

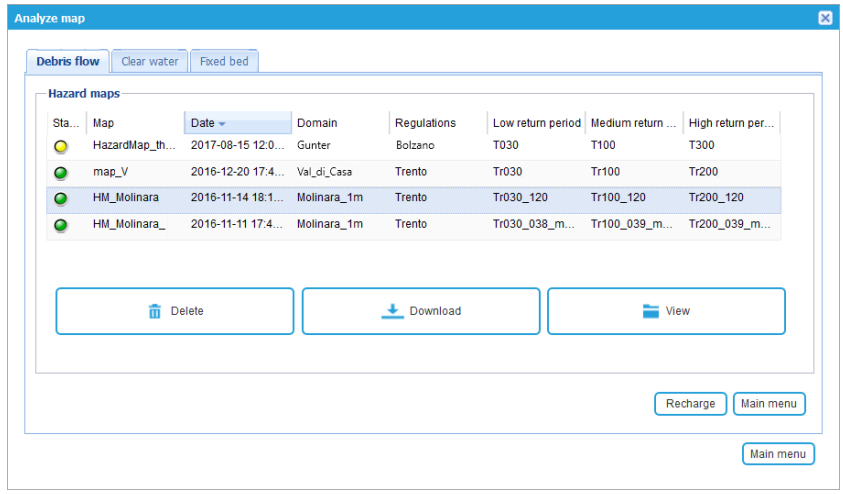

Figure 5.16: *Analyze map* panel in WEEZARD

by the simulation and the regulation (i.e. the classification criteria) to be applied.

II. The domain where to map hazard-level must be chosen. Domains with a number of simulations lower than the minimum number required by law are marked with red traffic lights and can not be selected.

III. Simulations available for the selected domain are listed according to their return period. Traffic lights indicate the status of the simulations. Those to be considered by the Hazard Mapper service are selected within the completed simulations with simple clicks.

IV. Clicking on the *Run* button, Hazard Mapper starts the processing in background and produces hazard-level maps and a lot of other intermediate maps.

Also in this case, a simple procedure hides a considerable "backstage" work on the server, concerning data processing, storage and retrieving.

Once a Hazard Mapper run ends, the user can analyse the outputs of the hazard-mapping procedure by means of the functionality *Analyze map*. This group of tasks (see Figure 5.16) was designed and built similarly to the *Analyze simulation* panel. Hazard maps are here managed, displayed, downloaded or deleted.

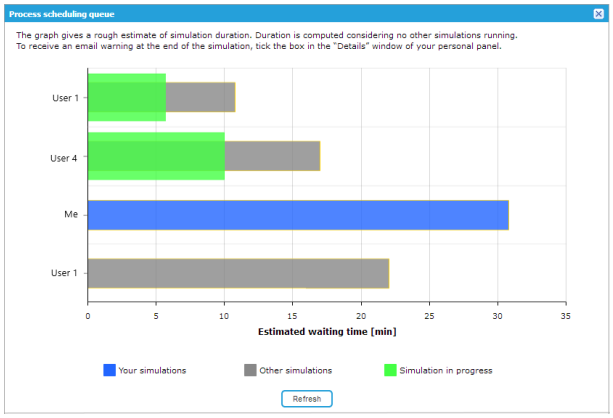

Figure 5.17: Scheduling queue window in WEEZARD

5.4.2.5 Scheduling queue functionality

The multi-user architecture of the system implies that many requests to run simulations can reach the server simultaneously or that a new request may arrive when other simulations are still running. Since only a given number of simulations can conveniently run concurrently (depending on the available computational power of the system), a scheduling queue is necessary to manage the situation.

The scheduling queue functionality provides all the information regarding the progress of a user's run. A window, shown in Figure 5.17, gives a graphical and quantitative overview of: the estimated computational time of each simulation in the queue; the simulations currently running along with their estimated ending time; the position of the user's simulation in the queue.

5.4.3 The functionalities for the administrative user functionalities

Administrative users can access all the standard user functionalities and, in addition, a control panel for the management of some aspects of the system. The panel has four tabs (see Figure 5.18): the first is dedicated to user management; the second gives the simulation list; the third gives a graphical and quantitative overview of the disk usage; the last allows the administrator to set some system options (e.g. timeout values or maximum number of concurrent simulations).

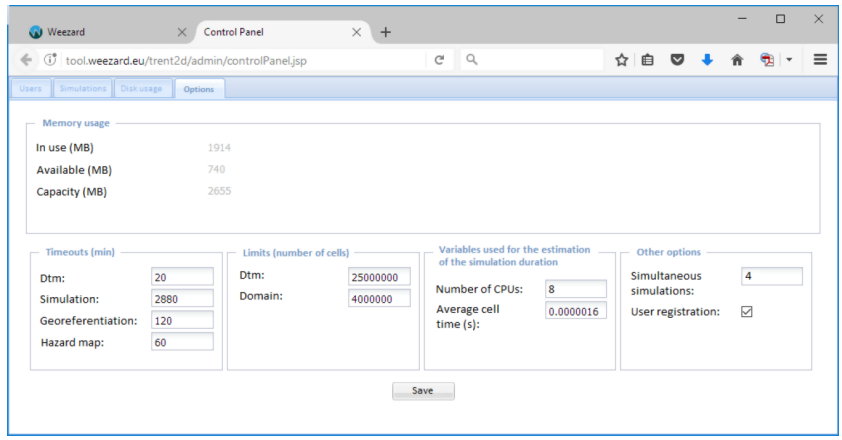

Figure 5.18: WEEZARD administrative panel

5.5 A WEEZARD application: mapping debris-flow hazard-level in Valle Molinara

After the 2010 debris-flow event in Valle Molinara (which back-analysis was reported in Section 4.1), that study area was considered also to carry out some analyses about hazard-level assessment. In particular, the level uncertainty that could characterise an a-priori hazard mapping was scrutinised following the BUWAL approach and applying hazard-mapping regulations of the Autonomous Province of Trento, where the study area is located.

Other, more basic hazard-mapping applications have been presented in Zorzi et al. (2016a) and Zorzi et al. (2016b), but they are not reported here.

5.5.1 A BUWAL-like hazard-mapping approach: regulations in the Autonomous Province of Trento (Italy)

Hazard maps are drawn up to allow technicians, stakeholders and policy-makers to evaluate levels of hazard and take suitable decisions to ensure citizen protection. Because of the different know-how of people involved in hazard management, hazard maps should catch the whole complexity of natural phenomena and summarise it through a simple representation, e.g. through few, coloured hazard levels. Among different approaches available in the literature and in the regulations of Alpine countries, the one proposed in Switzerland by Heinimann et al. (1998) and recalled in Petrascheck and Kienholz (2003) is recognised as the

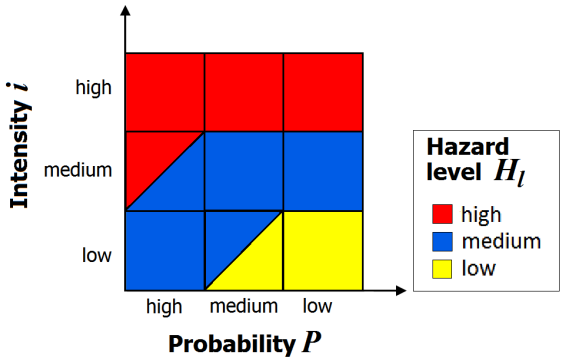

Figure 5.19: BUWAL matrix

most well-validated in Alpine regions, probably also because of its long history (Kunz and Hurni, 2008). This approach was embraced also by the regulation of the Autonomous Province of Trento (Provincia Autonoma di Trento, 2017).

According to this approach, the local hazard level H_l is defined as a function of both the event occurrence probability P and its local intensity i. The concept of hazard level coincides with the one defined in Petrascheck and Kienholz (2003) and recalled in Zimmermann (2005). The function H_l is discretised by the stepwise function shown in Figure 5.19, which is characterised by three possible ordinary hazard levels: high (red), medium (blue) and low (yellow). This discretisation is known as BUWAL matrix, from the name of the Swiss Federal Office for the Environment which Heinimann et al. belong to.

Local hazard levels are assessed on the basis of some suitable "reference events", chosen to represent a significant range of events possibly occurring in the study area. As far as mountain flows are concerned, it must be noticed that there is not an univocal agreement about how these "reference events" should be identified. Typically, they are selected with reference to their return period, or, equally, to the probability $P(m > m_0)$ that their magnitude m does not exceed a certain magnitude threshold m_0 ("magnitude" is used here to indicate the global size of the phenomenon, according to Corominas et al., 2015). However, as far as debris-flow events are concerned, it is not clear which are the most relevant quantities to be considered in evaluating the event magnitude. Possible quantities could be for example the rainfall height causing the debris flow, according to a hydrological approach, or its solid volume, according to a geological approach, or its peak discharge, according to a hydraulic approach. Suitable approaches should consider a compound probability that

Variable	High intensity level	Medium intensity level	Low intensity level
Flow depth	$h > 1\,\text{m}$	$0.5\,\text{m} < h \leq 1\,\text{m}$	$h \leq 0.5\,\text{m}$
	or	*or*	*or*
Flow velocity	$v > 1\,\text{ms}^{-1}$	$0.5\,\text{ms}^{-1} < v \leq 1\,\text{ms}^{-1}$	$v \leq 0.5\,\text{ms}^{-1}$
	or	*or*	*or*
Deposition depth	$D > 1\,\text{m}$	$0.5\,\text{m} < D \leq 1\,\text{m}$	$D \leq 0.5\,\text{m}$
	or	*or*	*or*
Erosion depth	$E > 2\,\text{m}$	$0.5\,\text{m} < E \leq 2\,\text{m}$	$E \leq 0.5\,\text{m}$

Table 5.1: Debris-flow intensity classification criteria provided by the Autonomous Province of Trento (Italy) in the DGP 772/2017

takes into account the occurrence probability referring to both the flowing phases. However, to date, any similar approach does not exist, because of phenomenon complexity (see Section 1.3) and lack of diffused and relevant statistical series. Moreover, it must be noticed that no indication in this respect is stated by law. Therefore, in debris-flow hazard assessment it is quite common to use the rainfall occurrence probability as representative of the debris-flow occurrence probability.

According to regulations of the Autonomous Province of Trento, hazard levels must be assessed considering three "reference events", with return periods T equal to 30, 100 and 200 years respectively, i.e with high, medium and low occurrence probability P.

Once "reference events" are identified, their local intensity i in the study area requires to be quantified and then classified, according to threshold criteria to be applied to some significant variables. Criteria stated by the Autonomous Province of Trento for debris-flow intensity classification are listed in Table 5.1.

As shown by the flowchart in Figure 5.20, these criteria are applied to each "reference event" (intensity-level classification), producing intensity-level maps. Then, for each "reference event", probability and intensity information is merged according to the BUWAL matrix (relative hazard-level classification). Finally, hazard-levels of the three "reference event" are overlaid and the worst local hazard-level is chosen point-wise (hazard-level classification). In this way, two hazard-level maps are obtained, according

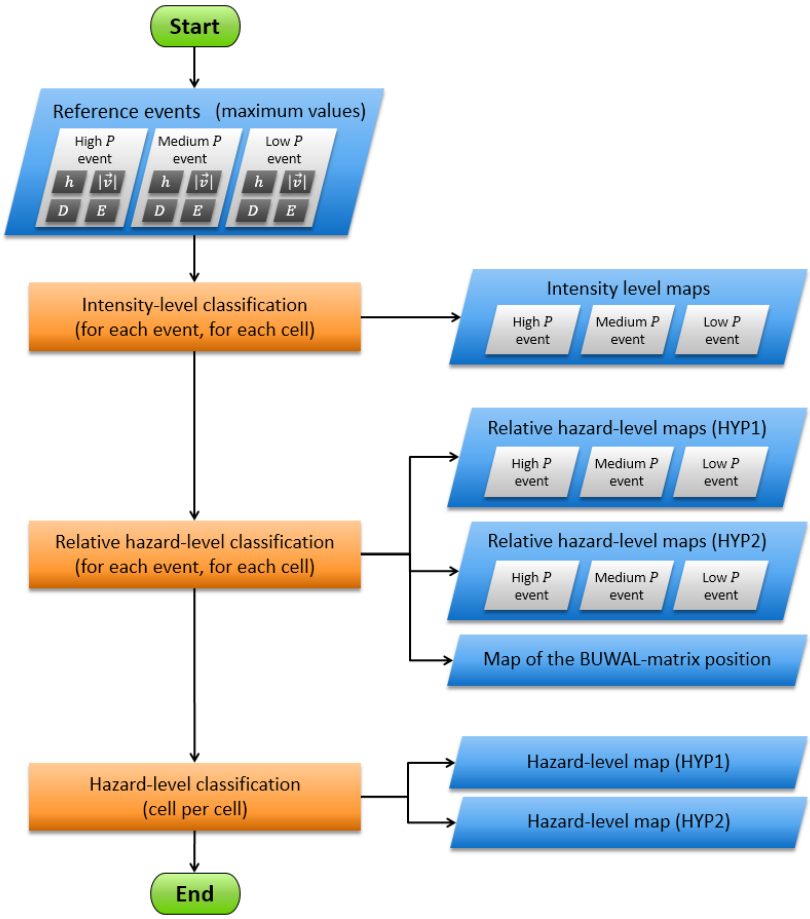

Figure 5.20: Flowchart describing the hazard-level mapping job and the intermediate outputs. In WEEZARD it is performed automatically by the Hazard Mapper module.

to the cut cells present in the BUWAL matrix.

5.5.2 Mapping debris-flow hazard levels on the Valle Molinara alluvial fan

The hazard-mapping approach described in the previous Section was applied to the Valle Molinara site. Analyses reported hereafter belong to a detailed study that the author carried out together with prof. Aronne Armanini and prof. Giorgio Rosatti within the program agreement between the University of Trento and the Autonomous Province of Trento. The complete work is available in Italian in Armanini et al. (2014).

First of all, to map debris-flow hazard three "reference events" were identified. Since no statistical series was available for the site in terms of debris-flow events, the "reference events" were

built with a synthetic approach.

The occurrence probability of these events was considered as coinciding with the probability of the rainfall event causing the high-concentraiton flow event, while sediment availability was considered unlimited. This simplification appeared to be the only possible compromise and in precise agreement with the observations proposed in Section 1.3. The IDF curves relevant for the region (Della Lucia et al., 1979, accredited by the Autonomous Province of Trento) were considered and the necessary hyetographs defined. Following the same sequence of operations described in Sections 4.1.3 and 4.2.2, liquid hydrographs were obtained applying the PeakFlow model with a-priori parameters values. For each return period, the hydrograph showing the highest peak discharge was taken into account. Then, concentration was estimated by means of the Takahashi formulation (equation 4.1), on the basis of the local slope at the fan apex, and total and solid discharges were obtained. The TRENT2D model was then applied under the assumption of uniform flow condition at the upper bound of the domain, making all the necessary "reference events" available.

This synthetic approach is the most common in hazard-mapping practice and requires a sizeable amount of handwork if performed by means of the original version of TRENT2D as desktop application. On the contrary, the same job performed by means of WEEZARD appears really affordable. A test revealed that, performing the same job through the old version of TRENT2D and WEEZARD and being equal the computational power, in the latter case time required to carry out simulations of the all "reference events" was reduced by about two thirds.

At this stage, the "reference events" were defined, leading to the application of the authority classification criteria. Thanks to *Hazard map* functionalities, no processing effort was required to the user in order to perform the operation chain of Figure 5.20, and the final hazard map for the Valle Molinara alluvial fan (Figure 5.21) was obtained in few minutes.

However, the back-analysis of the Rio Lazer event (Section 4.2) showed how significant events are observed not necessarily with the highest peak hydrograph. For this reason, further analyses where carried out on hazard-level mapping, considering different liquid hydrographs, i.e. hydrographs with different durations and peak discharges. Since the rainfall duration giving the highest peak discharge in the Valle Molinara basin was little lower than 1

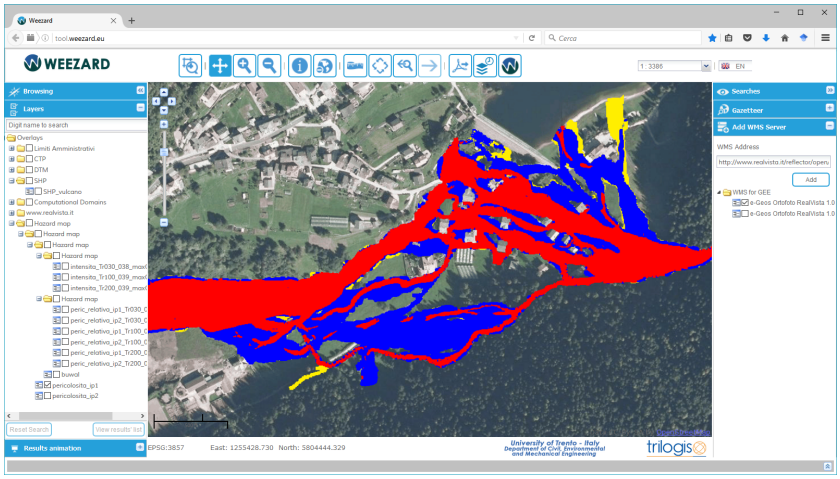

Figure 5.21: Hazard-level map (HYP1) obtained through WEEZARD for the Valle Molinara alluvial fan, considering the liquid hydrographs with the highest peak discharge.

hour, the following rainfall durations were considered: 45, 60, 75, 90, 105 and 120 minutes. Without changing approach and models parameter values, six further, very different "reference events" were obtained for each return period. Differences regarded especially deposition and erosion depths, because of the different liquid and solid volumes at stake.

Then, the procedure was applied six times, one for each rainfall duration and six (twelve if the two drafting hypotheses are considered) hazard-level maps were obtained. However, at a first sight, maps looked pretty much the same and this result was confirmed also by a quantitative comparison between both area extents and hazard levels. As a proof, the hazard-level maps obtained for rainfall durations of 45 and 120 minutes are shown in Figure 5.22. Valle Molinara hazard-level maps appeared to be somehow invariant to rainfall duration and intensity.

This is confirmed also by overlaying these hazard map to the surveyed extension of the 2010 deposition area (Figure 5.23). The hazard maps cover about the whole flooded area, although the maps were obtained considering a single peak hydrograph, while the 2010 event was characterised by two peaks (see Section 4.1).

This supposed invariance depends certainly on the morphology of the alluvial fan, which conditions debris-flow routes significantly. However, although preferential paths of the debris flow over the Valle Molinara fan do not seem to change very much, maps of the maximum values of the governing variables mirror variations in boundary conditions. Nevertheless, this information

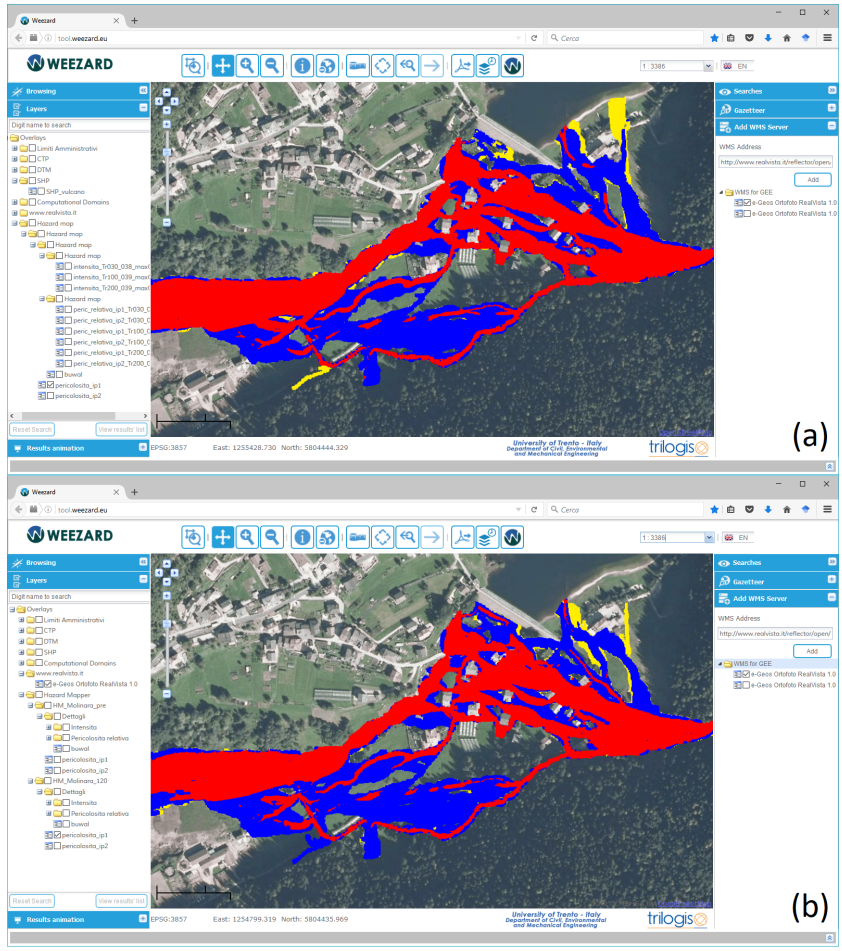

Figure 5.22: Hazard-level map (HYP1) obtained through WEEZARD for the Valle Molinara alluvial fan, considering rainfall durations of (a) 45 minutes and (b) 120 minutes.

disappears then in the intermediate intensity-level maps. Therefore, it seems that variations in "reference events" are smoothed by intensity classification criteria.

Intensity evaluation is based on the local classification of four governing variables (see Section 5.5.1). Each variable may show a different local intensity level, but at the end of the intensity classification, only one intensity level (i.e. the highest among those identified locally) is taken into account. Therefore, point-wise, i.e. for each cell, it is possible to identify one (or more) decision-making variable, i.e. the variable(s) responsible for the choice of the local intensity-level. In order to better scrutinise the map invariance and understand the role of each variable, each simulated "reference event" was classified in terms of decision-making

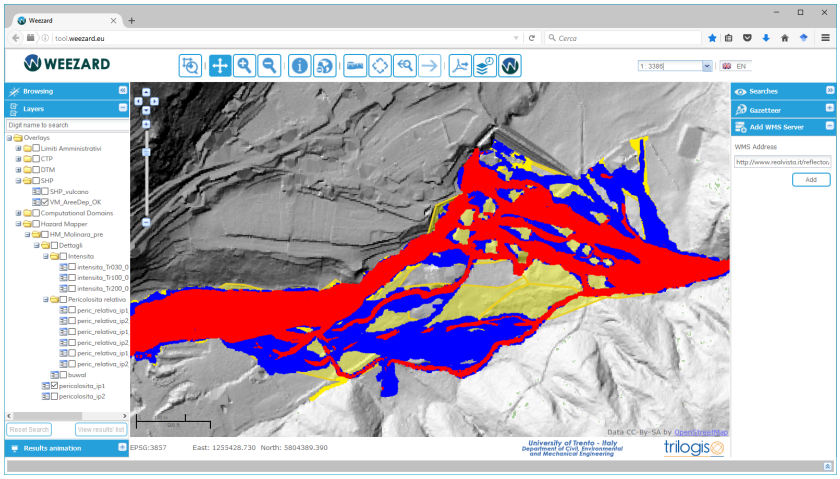

Figure 5.23: Comparison between the extent of the hazard-level map (HYP1) obtained through WEEZARD for the Valle Molinara alluvial fan (rainfall duration of 45 minutes) and the deposition area surveyed after the 2010 event (in light yellow).

variables (by means of a common GIS, outside WEEZARD). The outcome of such a classification was about the same for all the eighteen "reference events". Mixture velocity clearly played the role of prevailing decision-making variable. In particular, high velocity values ($v > 1\,\mathrm{ms}^{-1}$) were observed in a very wide area, often associated with rather low flow depths. The extent of the area governed by the sole velocity ranged from 68% to 73% of the whole mapped area. In this area, the intensity level identified by velocity was seldom equal to the intensity level ascribed to the other governing variables. However, if the analysis includes also those cells where the intensity level identified by velocity was equal to the one identified by at least another governing variable, the percentages increase, reaching values of $97 - 98\%$ in anyone of the eighteen "reference events". This result indicates that, in this case study, intensity levels (and therefore hazard levels) are governed almost exclusively by velocity.

In the light of the these results, a question about the balancing of intensity-classification criteria can be risen considering those areas where high velocity values are associated with rather low values of the other variables. In particular, it should be verified if the destructive potential of the phenomenon is correctly represented and quantified in such conditions. If not, some kind of thresholds revision could be worthwhile.

Without prejudice to this outcome, it must be noticed that the prevailing part of this analysis was carried out without excessive burdens thanks to the WEEZARD system, which allowed to limit

as much as possible the user handwork, leaving considerable time to analyse results and investigate critical points. However, it must be noticed that final processing was supported by tools not included in WEEZARD. This observation opens the way for further developments of WEEZARD, oriented to the integration in the system of further useful functionalities.

5.6 Forthcoming developments and a future perspective for WEEZARD

Assessing high-concentration flow hazard using the best available technology while limiting costs is no longer a "mission impossible" for practitioners and land protection public agencies. The presence of a state-of-the-art high-concentration flow model into an efficient all-in-one, strongly customized environment represent an important result in the field of mountain-flow hazard assessment, as confirmed also by user feedbacks. According to practitioners and technicians that experienced WEEZARD, the system allows a not-negligible reduction in the time and cost of production for a high-concentration flow hazard-assessment job. Simplicity, intuitiveness, accessibility and innovation are the features most appreciated.

However, the version of WEEZARD introduced in this Chapter represents only the starting point towards a more wide, efficient and eclectic system. Next Sections propose some possible future developments (Section 5.6.1) and a long-term perspective for the system (Section 5.6.2).

5.6.1 Possible future developments

Besides the advantages of the chosen technologies with respect to other alternatives, it is necessary also to highlight possible limitations of the system and barriers to its use at the current state of development.

A first issue connected to the TRENT2D model is portability. In order to obtain high computational efficiency, the model Fortran 90 code is compiled with processor-specific optimization in a Windows operating system (OS), therefore it does not have the complete portability of the rest of the system. However, since time necessary to do a simulation job can be quite long, in the initial phase of system development efficiency was prioritised over port-

ability. Anyhow, a LINUX version of the model will be possibly developed in the near future.

As far as data interoperability is concerned, the system is able to use shared data with OGC® WMS standards, while in output, simulation data are not exposed as they are user sensitive and an open access is not advisable. Other forms of data sharing (e.g. FTP; cloud repository; Web Distributed Authoring and Versioning, WebDAV) can be easily activated since the system structure is ready. On the other hand, interoperability with other processing systems has not been pursued so far, because of the type of target users chosen for the system. The orientation of the developers group is to move towards a fully compliant OGC® WPS V. 2.0 in the near future.

Other future developments regard the possibility of equipping WEEZARD with new functionalities and models, in response to user requests and observations. In particular, the following new functionalities will be developed in the next future:

- on the basis of the results presented in Rosatti and Zugliani (2015) and Zugliani et al. (2017), the range of model applicability will be extended with reference to the bed nature. This means that it will be possible to describe high-concentration flow over both fixed and mobile bed, including also dynamic transitions from fixed- to mobile-bed and viceversa;

- the possibility of simulating dense-snow avalanches will be introduced;

- the processing chain available in WEEZARD will be extended also to hydrological analyses, with the integration in the system of a hydrological model. In this way, inflow conditions for the TRENT2D model will be computed in the same working environment;

- further ancillary functionalities will be integrated in the system, in order to better support the analysis stages.

5.6.2 Towards an end-to-end DSS?

In general terms, a Decision Support System (DSS) is a computer-based system developed to aid decision-makers. As referred in Power (1997), someone indicates as DSS any software

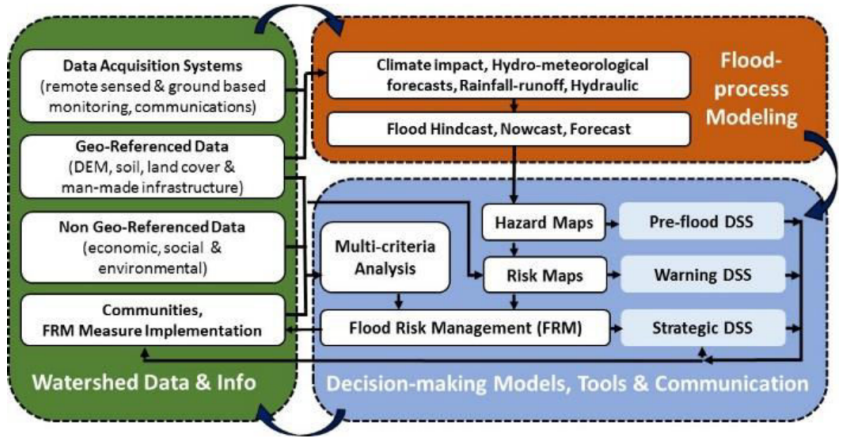

Figure 5.24: Layout of methodologies involved in a end-to-end, generalized DSS and their interactions, from Muste and Firoozfar (2016)

product that runs on a PC and can help managers to make a decision. According to this definition, WEEZARD could be recognised as a DSS.

Many DSS are model-based DSS, i.e. DSS made of simulation models and some techniques for multi-criteria analysis (Giupponi et al., 2011). However, some other DSS categories are identified in Power (2004): data-driven, document-driven, knowledge-driven and communications-driven. A complete DSS should collect these categories all together, giving up specialised DSS and moving towards multi-disciplinarity, interactivity, participation.

This necessity is clearly expressed in Muste and Firoozfar (2016), where such a kind of DSS is addressed as *generalized DSS*. A generalized DSS should support decision in "prevention, mitigation, preparation, response and recovery from impacts with consideration of climate change, socio-economic evolution and stakeholders' input" (Muste and Firoozfar, 2016). Moreover, it should effectively connect different know-how domains and methodologies, as shown in Figure 5.24. In the light of this definition, WEEZARD can not be recognised as a DSS. However, some of its characteristics comply with those typically desirable in a generalized DSS.

The logical structure of the WEEZARD system considers the basic components necessary in a DSS: databases, services, computational algorithms. These components are organised in a advanced cyber-infrastructure, which implies high-performance computing, visualization, digital libraries, databases, distributed systems, middleware, and collaboration technology (Atkins et al., 2003). Therefore, the architecture of the system could represent

the early stage of a DSS architecture. Moreover, the use of several OGC® standards offers wide possibilities in terms of interoperability. For example, the WEEZARD system appears already fitted to share data from public repositories or services, possibly to expose its own data and services and to wrap existing and new services as WPS.

High-performance computing is supported, thanks to a profitable trans-disciplinary collaboration between high-concentration flow scientists and IT experts. Moreover, the system is web-based and supports multi-user activities, as required in Muste and Firoozfar (2016). The web-based character ensures also global accessibility, as required in Zhang (2011).

Making sophisticated models easily accessible is one of the purposes that triggered the development of WEEZARD, according to the "simplification strategy" often requested by practitioners of disaster management (Leskens et al., 2014). Moreover, in WEEZARD some attention was paid also to hazard communication, which importance is often recalled in the literature (Hagemeier-Klose and Wagner, 2009; Albano et al., 2015; Sanders et al., 2016).

Control over model and data is centralised, as required in Zhang (2011). Moreover, other models can (and will) be easily introduced in the system, in order to extend the operational chain available in a single working environment, possibly moving closer to the layout proposed in Figure 5.24.

Another important point is the absence of spatial limitation, hoped in Zhang (2011). In practice, WEEZARD can be used to assess high-concentration flow hazard all over the world.

On the other side, to date WEEZARD is specialised only on high-concentration flow modelling, i.e. it lacks of the other most important component of a end-to-end DSS. However, it is not excluded that the continuous activity of system update and growth could be orientated towards the development of a generalised DSS. Certainly, the work would be long and challenging, but premises seem to be comforting.

Another possibility for WEEZARD is its integration in other existing, end-do-end DSS. This solution seems to be more reachable in the short term if compared with the previous one. However, just like the previous one, it requires a strict multi-disciplinary collaboration not only with IT experts, but also with public agencies, practitioners, hydrology scientists, data managers, stakeholders, politicians, economists, sociologists, ecologists.

Chapter 6

Complex morphology: the TRENT2D-UTG model

In Chapter 4, the importance of a proper description of the site morphology was highlighted by means of two case studies. There, morphological complexity issues were named concisely "geometrical" issues.

The key point in morphology description seems to be its spatial representation or, more precisely, its discretisation. Often, in modelling, spatial discretisation is performed by means of Cartesian, i.e. regular, meshes. This choice relies on the fact that a large number of models base the morphology description on the use of DTMs, which are typically supplied as Cartesian grids. However, sometimes they appear too much rigid to obtain everywhere the *right level* of detail in morphology representation. On the contrary, other types of meshes appear more suitable to reach the goal, as for example unstructured meshes.

In this Chapter, this particular family of meshes is taken into account in order to improve morphology representation and to develop a new of the TRENT2D model. This new version, called TRENT2D-UTG (Unstructured Triangular Grid) was addresses to overcome possibly the "geometrical" issues previously identified.

TRENT2D-UTG solves the TRENT2D equations over a triangular, Delaunay-type mesh by means of the LHLL solver developed by Fraccarollo et al. (2003). In order to preserve second-order accuracy in space and time, the same numerical algorithm developed for the original model is used. The main difference is represented by the technique used to perform the primitive variables reconstruction at the cell bounds. In the original version of

TRENT2D, gradient of the variables is obtained via dimensional splitting, while the minmod function was chosen as the slope limiter. On the contrary, in TRENT2D-UTG, gradients are computed and limited by means of the multidimensional approach of Barth and Jespersen (1989). In the latter case, not only the original approach was taken into account, but also different expressions of the limiter, which are compared with the original formulation of Barth and Jespersen (1989).

In Sections 6.1 and 6.2, detailed motivations about the choice of considering unstructured, Delaunay-type grids are presented. Then, Section 6.3 describes the modifications necessarily introduced in the numerical core in order to manage unstructured meshes properly. Finally, Sections 6.4 and 6.5 show some numerical tests performed applying TRENT2D-UTG respectively to simple Riemann Problems and to a realistic case study.

6.1 Which spatial discretisation?

Most of the 2D, PDE-based models simulating high-concentration flow dynamics and applying finite-volume methods were developed over Cartesian, i.e. regular, meshes (see for example Laigle, 1997; Medina et al., 2008; Pelanti et al., 2008; Greco et al., 2012). These grids allow to organise cells and variables rationally and functionally, ensuring a simple management of (not only) morphological information. However, Cartesian meshes imply a necessary trade-off between accuracy in the representation and simulation costs. Typically, coarse Cartesian meshes, i.e. with large cells, allow to limit computational costs, but give a rough morphological representation (Figure 6.1(b)). On the other side, fine Cartesian meshes, i.e. with smaller cells, reproduce better the site morphology and in general the flow dynamics (Figure 6.1(c)), but have the drawback of multiplying computational costs, raising machine requirements and efforts in geo-spatial data management. Moreover, Cartesian meshes give staircase representation whenever a curved boundary or constraint is present. This is clearly an approximation, which relevance is as much high as much coarse is the mesh.

The need of representing morphology and flow dynamics with an acceptable resolution but with reasonable costs generated a different approach to the problem, based on the use of adaptive meshes. Adaptive meshes allow a smarter representation of the

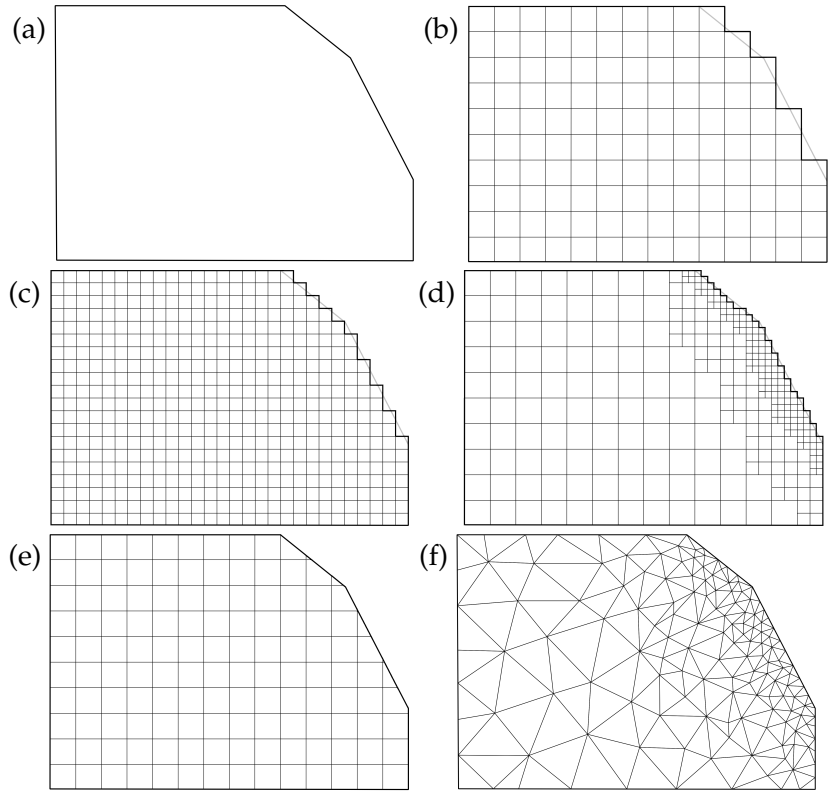

Figure 6.1: Meshes: (a) domain to be meshed; (b) coarse Cartesian mesh; (c) fine Cartesian mesh; (d) block-structured mesh; (e) cut-cell mesh; (f) unstructured mesh

system, increasing spatial resolution where necessary (i.e. in the expected key points) and decreasing it where the level of detail is not required to be very high. Clearly, adaptive meshes allow to represent spatial heterogeneity with a larger flexibility. However, such a choice entails larger costs in model development and in spatial data management.

Within adaptive-mesh methods, both structured and unstructured meshes are used in mountain-flow modelling (see for example George and Iverson, 2014 and Benkhaldoun et al., 2013).

Adaptive, block-structured meshes keep the advantages of Cartesian meshes and allow to reduce computational costs. They turn out to be particularly suitable to represent linear-type constraints that are aligned with the Cartesian axes, while they give staircase representation whenever constrained are oblique or curved (Figure 6.1(d)). Moreover, they require a careful management of those areas where different mesh refinements are in touch.

Since modellers showed the desire of applying hydraulic models also to geometries not constrained to be rectilinear (Wright and

Hargreaves, 2013), cut-cell methods and unstructured grid-based methods were developed in answer to this need.

In general, cut-cell methods (Figure 6.1(e)) are addressed to fit geometrical constraints at bounds, while the rest of the domain is described with a structured grid (see for example Ingram et al., 2003).

On the other side, unstructured meshes (Figure 6.1(f)) are characterised by a larger flexibility in the spatial representation of the whole computational domain, containing computational costs (Benkhaldoun et al., 2013), but introducing more demanding mesh generation and management. However, for sake of completeness, it should be noticed also that unstructured mesh can be easily displayed by means of software product or routines that are quite diffused among modellers and practitioners. On the contrary, cut-cell grids, and also block-structured meshes, require the development of customized visualisation tools. Therefore, in the latter cases, a further development effort must be addressed to this task.

Whichever the choice, the problem formulation appears significantly affected and, therefore, requires efforts in managing the logical structure necessary to describe cells connectivity properly (LeVeque, 2002). Accepting this increased demand in model development, the unstructured-mesh approach (Figure 6.1(f)) was chosen to improve the TRENT2D capabilities in representing significant morphological constraints and their effects on high-concentration flows.

6.2 Unstructured meshing by means of Delaunay triangulation

Over the years, several meshing methods have been developed to produce unstructured grids. The most popular make use of cells with a specific shape (for example triangles, hexagons, tetrahedra), however some techniques were developed also to manage cells of different shapes in a single grid (Mavriplis, 1997). In this work, grids with only triangular cells are considered, in order to avoid excessive costs in grid generation and management.

Generating an unstructured mesh could appear as a simple task. However, any mesh is not compulsorily a suitable mesh. Hydrodynamic simulations require quality meshing, i.e. mesh-generation algorithms able to design grids that are fine enough,

boundary-conform and characterised by well-shaped cells (Bern et al., 1994). Moreover, automatic and robust design-algorithms are required (Mavriplis, 1997).

The most popular meshing technique is the method of Delaunay triangulation, which appears to be powerful and richly based on mathematical theory (Barth, 1990). Basically, it adopts an optimisation criterium that allows to maximise the minimum angle of the cell. However, also other techniques have been developed over the years, each one considering a different optimisation criterium. For example, the alorithm for Greedy triangulation (explained in Preparata and Shamos, 1985) continually adds triangle faces avoiding face crossing. Data-dependent triangulations assume vertexes number and positions as constraints (see for example Dyn et al., 1990). Other techniques abide by the minimisation of the maximum edge length (Edelsbrunner and Tan, 1993) or of the maximum edge lengths sum (Eppstein, 1994). Further algorithms have been produced, based on different constraints, however accounting for them is not the purpose of this thesis.

Because of the nice properties of the generated meshes, only the Delaunay triangulation algorithm is considered here. Given a cloud of planar points, Delaunay triangulation can be performed applying the empty circumcircle criterion. This means that no point of the cloud must lie into the circumcircle associated to each triangle, as shown in Figure 6.2(a). Whenever a further point is added to the cloud, a new Delaunay triangulation must be performed, i.e. all the existing triangle whose circumcircles contain the new point are deleted and a new local triangulation is carried out (Mavriplis, 1997).

The empty circumcircle property makes Delaunay triangles "well-shaped", i.e. triangles with large internal angles are preferred to those with small angles. Therefore, the minimum internal angle is maximised, which leads to more accurate results in equations solutions (Bern et al., 1994). Because of this property, which is called equiangular, the Delaunay triangulation is often indicated as the MinMax triangulation (Barth, 1990). Furthermore, Delaunay triangulation is unique and leads to the connection of the nearest neighbour points. The dual mesh of a Delaunay grid is a Voronoi diagram (Figure 6.2(b)).

In this work, Delaunay triangulation is performed by means of Triangle, an open-source tool developed by prof. Jonathan Shewchuk (Shewchuk, 1996). This software allows to build both

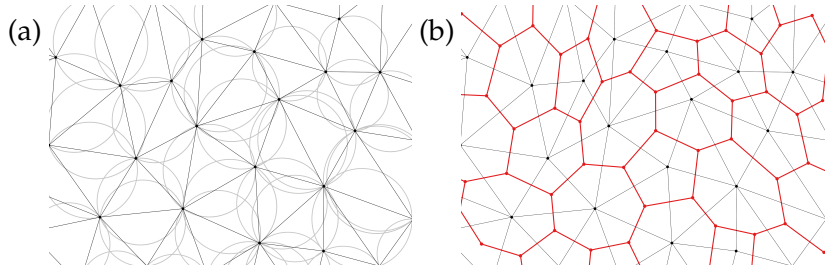

Figure 6.2: (a) Circumcircle property (b) Voronoi diagram

constrained and conformed triangulations. If a polyline is given inside or bounding the points cloud, a (data-)constrained triangulation produces triangle whose edges are forced to coincide with polyline segments. In this case, triangles could not be Delaunay. On the contrary, a conformed triangulation permits the addition of further points, called Steiner points, along the polyline segments, in order to produce triangles that preserve the Delaunay properties. For the purposes of this thesis, only this second option was used. Therefore, unstructured triangular meshes were produced only with Delaunay properties.

Furthermore, Triangle allows to force grid cells to be smaller than a given area. In this way, the "nominal" resolution of the mesh is defined where no other limiting constraints are applied.

Triangle provides also an algorithm for mesh refinements that maintains Delaunay properties (Shewchuk, 2002). This tool is extremely useful since it allows to study key area with a higher resolution without generating a new mesh starting from scratch.

6.3 Second-order accuracy

TRENT2D-UTG solves the TRENT2D model equations 3.1 over unstructured, Delaunay triangular meshes by means of the same approach used for the original version of TRENT2D. Only the LHLL solver was implemented here, because of its simplicity. However, less-diffusive solvers will be implemented in the future, in order to enhance the representation.

Second-order accuracy is reached thanks to the MUSCL-Hancock approach, applied following the procedure described in 3.2 and suitably adapted.

The indexes used in the notation are displayed in Figure 6.3, where i and j indicate the considered cell and its neighbour and k is the local index of common edge. $\mathbf{n}_{i,k}$ is the unit vector perpen-

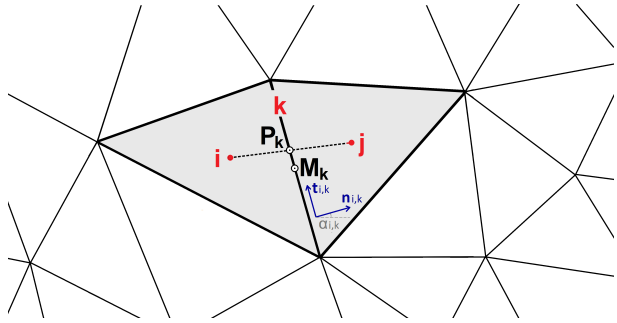

Figure 6.3: Notations and conventions used in the unstructured mesh management

dicular to the $k-$th edge and pointing outward the $i-$th cell, while $\mathbf{t}_{i,k}$ is the unit vector tangential to the $k-$th edge.

Having in mind this notation, the procedure is modified as follows:

1) Non conservative half-step ($t^n \rightarrow t^{n+\frac{1}{2}}$)

   a. *Data reconstruction*: primitive variables $\mathbf{W}^n_{i,k}$ at the k-th cell bounds are obtained by means of multidimensional linear reconstruction, starting from the cell-average values $\mathbf{W}^n_i$. In order to avoid oscillations, the $i-$th cell gradient $\nabla\mathbf{W}^n_i = \left[(\mathbf{w}_x)^n_i, \left(\mathbf{w}_y\right)^n_i\right]$ and its limiter $\mathbf{\Phi}^n_i$ are estimated according to Barth and Jespersen (1989). Techniques to compute the gradient and its limiter are extensively presented in Sections 6.3.1 and 6.3.2.

   b. *Solving the non-conservative homogeneous part*: vectors of conserved variables are updated considering only the homogeneous part of the system. Fluxes $\mathbf{F}$ are computed by means of their physical expressions, considering reconstructed values $\mathbf{W}^n_{i,k}$ obtained at the previous point.

$$\begin{aligned}\hat{\mathbf{U}}^{n+\frac{1}{2}}_i = \quad & \mathbf{U}^n_i - \frac{0.5\Delta t}{A_i}\sum_{k_i=1}^{3} L_{i,k}\mathbf{F}^n_{i,k}\cdot\mathbf{n}_{i,k} \\ & -0.5\Delta t\,[\mathbf{H}_x]^n_i\left[\mathbf{\Phi}^n_i \circ (\mathbf{w}_x)^n_i\right] \\ & -0.5\Delta t\left[\mathbf{H}_y\right]^n_i\left[\mathbf{\Phi}^n_i \circ \left(\mathbf{w}_y\right)^n_i\right]\end{aligned}$$

   where A_i indicates the $i-$th cell area, $L_{i,k}$ the length of the $k-$th edge of the $i-$th cell and $\mathbf{F}^n_{i,k}$ the vector of the fluxes computed with the primitive variables $\mathbf{W}^n_{i,k}$ reconstructed at the $k-$th edge of the $i-$th cell.

c. *Source terms*: the ordinary differential equation (ODE)

$$\frac{d\mathbf{U}}{dt} = \mathbf{T}$$

is solved by means of Euler implicit method and primitives variables $\mathbf{W}_i^{n+\frac{1}{2}}$ are computed from $\mathbf{U}_i^{n+\frac{1}{2}}$ solving a non-linear system.

2) Conservative half-step ($t^{n+\frac{1}{2}} \rightarrow t^{n+1}$)

a. *Data reconstruction*: primitive variables $\mathbf{W}_{i,k}^{n+\frac{1}{2}}$ at $k-$th cell bounds are obtained by means of linear reconstruction starting from the cell-average values $\mathbf{W}_i^{n+\frac{1}{2}}$ computed at timestep $t^{n+\frac{1}{2}}$. To avoid oscillations the $i-$th cell gradient $\nabla\mathbf{W}_i^n$ and its limiter $\mathbf{\Phi}_i^n$ are estimated according to Barth and Jespersen (1989).

b. *Solving the non-conservative homogeneous part*: vectors of conserved variables are updated considering only the homogeneous part of the system. Intercell non-conservative Riemann Problems (RPs) are solved by means of the LHLL approximated solver, considering primitive variables $\mathbf{W}_{i,k}^{n+\frac{1}{2}}$ and $\mathbf{W}_{\mathbf{j,k}}^{\mathbf{n+\frac{1}{2}}}$ obtained at the previous step for the neighbouring cells i and j at the common edge.

$$\begin{aligned}\hat{\mathbf{U}}_i^{n+1} = \quad & \mathbf{U}_i^n - \frac{\Delta t}{A_i}\sum_{k_i=1}^{3} L_{i,k_i}\mathbf{F}_{i,k_i}^{n+\frac{1}{2}}\cdot\mathbf{n}_{i,k} \\ & -\Delta t\,[\mathbf{H}_x]_i^{n+\frac{1}{2}}\left[\mathbf{\Phi}_i^{n+\frac{1}{2}}\circ(\mathbf{w}_x)_i^{n+\frac{1}{2}}\right] \\ & -\Delta t\left[\mathbf{H}_y\right]_i^{n+\frac{1}{2}}\left[\mathbf{\Phi}_i^{n+\frac{1}{2}}\circ\left(\mathbf{w}_y\right)_i^{n+\frac{1}{2}}\right]\end{aligned}$$

c. *Source terms*: the ordinary differential equation (ODE)

$$\frac{d\mathbf{U}}{dt} = \mathbf{T}$$

is solved by means of Euler implicit method and primitives variables $\mathbf{W}_i^{n+1}$ are computed from $\mathbf{U}_i^{n+1}$ solving a non-linear system.

It must be noticed that, under the assumption that the PDEs system is rotationally invariant, the scalar product $\mathbf{F}_{i,k_i} \cdot \mathbf{n}_{i,k}$ can be expressed also by means of the following transformation matrix $\mathbf{M_{i,k}}$:

$$\mathbf{M}_{i,k} = \begin{bmatrix} 1 & 0 & 0 & 0 \\ 0 & 1 & 0 & 0 \\ 0 & 0 & \cos\alpha_{i,k} & \sin\alpha_{i,k} \\ 0 & 0 & -\sin\alpha_{i,k} & \cos\alpha_{i,k} \end{bmatrix} \tag{6.1}$$

where $\alpha_{i,k}$ is the angle between the unit vector $\mathbf{n}_{i,k}$ and the $x-$axis (see Figure 6.3). This matrix allows to rotate the reference system, compute 1D-fluxes in according to the $\mathbf{n}_{i,k}$ direction and then counter-rotate the result:

$$\mathbf{F}_{i,k}\left(\mathbf{W}_{i,k}\right) \cdot \mathbf{n}_{i,k} = \mathbf{M}_{i,k}^{-1}\left[\mathbf{F}_{i,k}\left(\mathbf{M}_{i,k}\mathbf{W}_{i,k}\right)\right] \tag{6.2}$$

In order to preserve stability, timesteps are limited by the CFL condition. Since the algorithm for the update of the conserved variables is unsplit, i.e. it deals with both directions n and t at the same time, the CFL condition is set as

$$\frac{\lambda_{\max}\Delta t}{d_i} < 0.5 \tag{6.3}$$

where $\lambda_{\max}$ is the maximum eigenvalue of the system and d_i is a characteristic length, representative of the mesh-cell dimension. Here, it was set equal to the minimum incircle diameter, as for example in Dumbser et al. (2010) or Balsara et al. (2014).

6.3.1 Gradient computation

In order to reach second-order accuracy, piece-wise constant values of the cell variables are substituted by means of a linear piece-wise reconstruction. Starting from the cell-average values of the variables, i.e. the values at the cell center, suitable slopes must be computed in the x and y directions. Then, the reconstruction of the value of any variable Q at any location (x, y) inside the cell (x_0, y_0) is performed as follows:

$$\begin{aligned} Q(x,y) &= Q_0 + \nabla\mathbf{Q}(x_0,y_0) \cdot \triangle\mathbf{x} \\ &= Q_0 + q_x(x-x_0) + q_y(y-y_0) \end{aligned} \tag{6.4}$$

where Q_0 is the cell-average value $Q(x_0, y_0)$, $\nabla\mathbf{Q}(x_0, y_0) = \left[q_x, q_y\right]$ is the gradient of Q computed for the considered cell and $\triangle\mathbf{x} =$

$[(x - x_0), (y - y_0)]^T$ is the vector of the distance between the cell center (x_0, y_0) and the desired location (x, y). In this work, piecewise linear reconstruction is applied to the vector of the primitive variables $\mathbf{W}$, therefore the previous relation becomes

$$\mathbf{W}(x, y) = \mathbf{W}_0 + \nabla\mathbf{W}(x_0, y_0) \cdot \triangle\mathbf{x} \tag{6.5}$$

where $\nabla\mathbf{W} = \left[\mathbf{w}_x, \mathbf{w}_y\right]$.

Since unstructured meshes are considered, slopes computation can not be performed by means of N-dimensional splitting. So-called multidimensional techniques must be used, which should follow the reconstruction design criteria listed in Barth and Fredrickson (1990):

1) *Conservation of the mean*. Indicating with W any component of the vector $\mathbf{W}$ and with A the cell area, this constraint can be expressed as follows:

$$W(x_0, y_0) = \frac{1}{A} \int_A W(x, y)\, dA \tag{6.6}$$

2) *k-exactness*. A reconstruction is $k-exact$ if the reconstruction operator computes exactly the variables gradient in case the space variations are described by a polynomial of degree k. For instance, if a variable varies linearly in space, the reconstruction is $1-exact$ whenever it reproduces exactly this variations.

3) *Compact support*. The gradient computation should depend only on a relatively small neighbourhood around the cell (x_0, y_0). The amount of cells included in the neighbourhood should be at least equal to $(k+1)(k+2)/2$, but not excessively large, in order to limit computational costs and to preserve accuracy, since faraway data could be not representative of the processes observed in the cell (x_0, y_0). In this work, since we consider linear reconstruction with $k = 1$, at list 3 cells should be considered in the gradient computation.

4) *Efficiency*. Since the reconstruction is performed more than once in each cell, it is important to implement the gradient computation efficiently, avoiding repeated computations of the non-varying quantities.

Moreover, Barth and Jespersen (1989) require that the gradient computation is possible for any arbitrary mesh, since this constraint makes the gradient-computation algorithm robust and general.

In this work, the gradient computation and also the limiter evaluation are performed according to the technique proposed by Barth and Jespersen (1989). Although it was the first truly-multidimensional technique, it is recognised to be the most popular and successful for at-least second-order accuracy numerical schemes implemented over unstructured meshes, probably because of its simplicity (Darwish and Moukalled, 2003).

This technique abides by the constraints previously listed and bases the gradient computation of the Green-Gauss integration, commonly used unstructured grid-based schemes. According to the Green theorem, it is possible to express the volumetric integral of the gradient of a function as the surface integral of the function along the bounding surface. Applying the theorem to the primitives-gradient computation, it is possible to obtain:

$$\int_A \nabla \mathbf{W} dA = \oint_{\partial A} \mathbf{W}\mathbf{n} ds \tag{6.7}$$

where A is the area of the control volume, i.e. the compact support, considered in the computation, ∂A is its bound and $\mathbf{n}$ is the outward pointing unit vector, orthogonal to ∂A at the s location, where s represents the coordinate along the hull perimeter. Equation 6.7 leads to the following expression:

$$\nabla \mathbf{W} = \frac{1}{A} \oint_{\partial A} \mathbf{W}\mathbf{n} ds \tag{6.8}$$

Now, the point is which suitable control volume A, i.e. which surface ∂A, has to be chosen in order to compute the gradient. In Barth and Jespersen (1989), three alternatives are proposed, however, only the third satisfies the aforementioned design criteria including also the constraint about robustness and generality. For this reason, the alternative implemented in TRENT2D-UTG coincides with the most demanding proposed by Barth and Jespersen (1989). According to this choice, the surface ∂A corresponds with the centroid-centroid path including the hull made of the non-adjoining neighbour cells that share with the central cell i at least one node. Figure 6.4 displays the hull and its perimeter ∂A. The integral along ∂A is computed via trapezoidal rule.

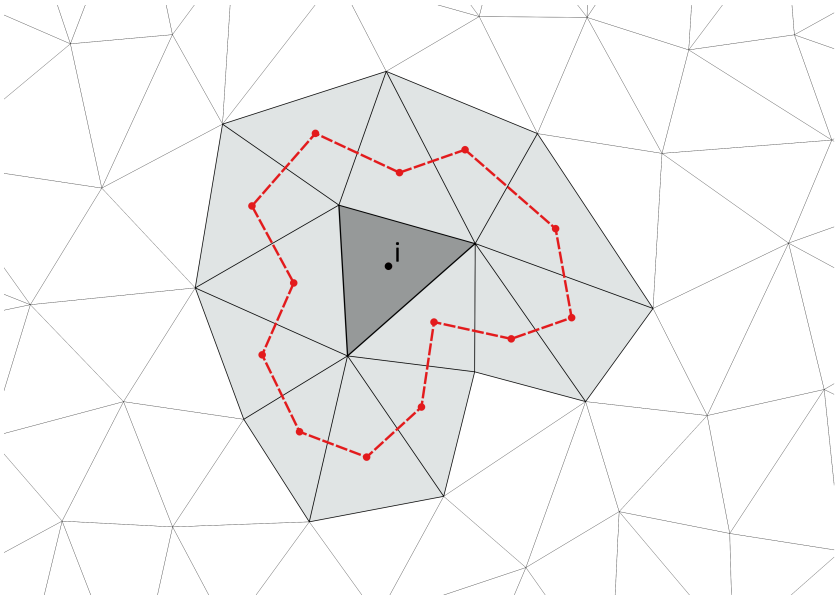

Figure 6.4: Compact support used to compute the gradient according to Barth and Jespersen (1989)

6.3.2 Gradient limiters

Variables reconstruction must fulfil also another important constraint that is the monotonicity principle. According to monotonicity, no new local extrema can be created by reconstruction. This means that reconstructed values must not exceed the maximum and minimum values set at the cell center of the neighbouring cells:

$$\min\left(W_j, W_i\right) \leq W_i\left(x, y\right) \leq \max\left(W_j, W_i\right) \tag{6.9}$$

where W_i and W_j represent the cell-center values of any primitive variable W in the considered cell and in its neighbours respectively, while $W_i\left(x, y\right)$ represents the reconstructed value at any location (x, y) inside the i-th cell.

In order to satisfy this requirement, the gradient is multiplied by a limiter $\mathbf{\Phi}_i$, which reduces the value of the gradient when necessary. The limited form of the variable reconstruction appears as follows:

$$\mathbf{W}\left(x, y\right) = \mathbf{W}_0 + \mathbf{\Phi}_i \nabla \mathbf{W}\left(x_0, y_0\right) \cdot \triangle \mathbf{x} \tag{6.10}$$

$\mathbf{\Phi}_i$ is a non-linear limiter that should avoid spurious oscillations in the solution of the model equations. The challenge is to find the largest $\mathbf{\Phi}_i$ admissible, in order to limit the reconstruction the bare minimum.

6.3.2.1 The Barth and Jespersen formulation

Barth and Jespersen (1989) proposed a formulation of $\mathbf{\Phi}_i$ suitable for solving the Euler equations, which was later applied by Anastasiou and Chan (1997) to 2D Navier-Stokes equations. Here, the same formulation is applied to a more sophisticated system of equations. The Barth-Jespersen method takes into account values of the variables computed at the i-th cell-center, at the j-th neighbour cell-centres and at the m-th vertex of the i-th cell. In detail:

- W_{i0} represents the cell-centred value of the variable W in the cell i;
- W_{j0} represents the cell-centred value of the variable W in the three cells j adjacent the cell i;
- $W_{i,m}$ represents the value of the variable W computed at the three vertexes m of the $i-$th cell without limitations.

As far as the neighbour cells are considered, assuming that

$$W_i^{\min} = \min\left(W_{i0}, W_{j0}\right) \quad \text{and} \quad W_i^{\max} = \max\left(W_{i0}, W_{j0}\right)$$

with $j = 1...3$, the following quantities can be computed:

$$\Delta W_i^{\min} = W_i^{\min} - W_{i0} \quad \text{and} \quad \Delta W_i^{\max} = W_i^{\max} - W_{i0} \tag{6.11}$$

Similarly, with regard to the reconstructed values at vertices

$$W_{i,m} = W_i\left(x_{i,m}, y_{i,m}\right) = W_{i0} + \left(w_x\right)_i \left(x_{i,m} - x_{i0}\right) + \left(w_y\right)_i \left(y_{i,m} - y_{i0}\right)$$

the following quantity can be computed

$$\begin{aligned} \Delta W_{i,m} &= W_{i,m} - W_{i0} \\ &= \left(w_x\right)_i \left(x_{i,m} - x_{i0}\right) + \left(w_y\right)_i \left(y_{i,m} - y_{i0}\right) \end{aligned} \tag{6.12}$$

The Barth-Jespersen limiter is based on the use of a simple, non-differentiable function indicated here as Ψ:

$$\Psi\left(y\right) = \min\left(1, y\right) \tag{6.13}$$

where y is a dummy variable.

Defining

$$y_{i,m}^{\max} = \frac{\Delta W_i^{\max}}{\Delta W_{i,m}} \quad \text{and} \quad y_{i,m}^{\min} = \frac{\Delta W_i^{\min}}{\Delta W_{i,m}}$$

the Barth-Jespersen limiter can be computed as

$$\Phi_{i,m} = \begin{cases} \Psi\left(y_{i,m}^{\max}\right), & \text{if} \quad \Delta W_{i,m} > 0 \\ \Psi\left(y_{i,m}^{\min}\right), & \text{if} \quad \Delta W_{i,m} < 0 \\ 1, & \text{otherwise} \end{cases} \tag{6.14}$$

for each vertex. Then, the most restrictive value of $\Phi_{i,m}$ computed for the variable W of the cell i is used all over the cell, that is

$$\Phi_i = \min\left(\Phi_{i,m}\right) \tag{6.15}$$

This procedure ensures the fulfil of the monotonicity principle anywhere within the cell. However, Barth and Jespersen (1989) observed that reconstructed values of the primitive variable are required only in some specific locations and not at any point within the cell. This allows to relax the constraint at vertices, imposing that the monotonicity principle must be satisfy only in some relevant locations, where the reconstruction is being actually performed.

According to Buffard and Clain (2010), two suitable locations can be considered to compute reconstructed values: the edge midpoint M and the intersection P between the edge and the segment connecting the cell i and its neighbour j, both shown in Figure 6.3. Considering alternatively these two locations in place of the cell vertexes, the following quantities can be computed

$$\Delta W_{M_k} = (w_x)_i \left(x_{M_k} - x_{i0}\right) + \left(w_y\right)_i \left(y_{M_k} - y_{i0}\right) \tag{6.16a}$$

$$\Delta W_{P_k} = (w_x)_i \left(x_{P_k} - x_{i0}\right) + \left(w_y\right)_i \left(y_{P_k} - y_{i0}\right) \tag{6.16b}$$

and replaced to the term $\Delta W_{i,m}$ appearing in $y_{i,m}^{\max}$, $y_{i,m}^{\max}$ and $\Phi_{i,m}$. In the first case, a less restrictive expression of the Barth-Jespersen limiter is obtained, following Hubbard (1999). In the latter, a new, slightly restrictive formulation is reached. All the three alternative formulations (at vertexes m, at midpoints M_k, at intersections P_k) were implemented in TRENT2D-UTG and compared in Section 6.4.

6.3.2.2 The Venkatakrishnan formulation

The Barth-Jespersen original limiter is not the only one developed for solving unstructured-meshes-based methods (see for example Durlofsky et al., 1992; Lambert et al., 1996; Bruner and Walters, 1997, to name but a few). In this work, the Venkatakrishnan limiter (Venkatakrishnan, 1995) is considered as a further option in the TRENT2D-UTG. This limiter was chosen since it was developed starting from the work of Barth and Jespersen (1989), but overcoming the convergence problems found with the limiter (Darwish and Moukalled, 2003). Venkatakrishnan (1995) replaced the original expression of the function Ψ with the following one:

$$\Psi(y) = \frac{y^2 + 2y}{y^2 + y + 2} \tag{6.17}$$

In this case the computation of the limiter is performed considering alternatively the reconstruction locations M_k and P_k. Some results obtained by means of the Venkatakrishnan limiter are shown in Section 6.4.

6.4 Numerical tests

In order to validate the TRENT2D-UTG model and compare the different limiters, some simple test cases were carried out.

First, the model was tested in order to verify that some simple, but essential, physical behaviours of the flow are properly caught, without generating non-physical results (Section 6.4.1), according to observation proposed in Section 2.2.5.

Second, some 1D Riemann Problems were solved and compared with their exact solution (Section 6.4.2).

Last, a circular dam-break is simulated, in order to verify symmetry (Section 6.4.3).

6.4.1 Steady-state tests

The first test performed was about the water-at-rest condition, in order to verify the *C*-property, i.e. the exact balance of fluxes in case of no motion. This condition was verified over both a flat bed and a single-step bed. In both cases, it was satisfied with any of the limiters.

Then, another steady-state test case was considered, because of its importance in free-surface flows modelling. The quasi-1D uniform flow condition was analysed in channel 400 m long, with rectangular, 20 m wide cross section and slope $i_F = 0.05$. The channel was supplied with a constant discharge. This test was performed considering both the closure relations available in TRENT2D to describe bed shear stresses, however for brevity only the results obtained by means of the Gauckler-Strickler formulation (equation 3.3) are presented here.

In the steady-state test discussed hereafter, a mixture discharge equal to Q_{mix} =20.672 83 m^3s^{-1} was considered, with a concentration $c = 0.021155$. Model parameters values were chosen as follows: $c_b = 0.65$, $\Delta = 1.65$, K_s =30 $m^{1/3}s^{-1}$ and $\beta = 0.01$. With these values, the uniform flow depth was evaluated to be equal to h =0.322 246 m, while the velocity in the flow direction was evaluated be equal to u =3.207 613 8 ms^{-1}. The test was performed over a Delaunay, triangular mesh made of 12393 elements, with areas at most equal to 1 m^2. End time of the simulation was set equal to 5 s.

In Figures 6.5, 6.6 and 6.7, results obtained by means of the different limiters are shown for 390 m$\leq x \leq$400 m. All the cells whose barycenter is located in this x-range are represented, with the cell values located in the cell barycenter.

As far as different locations are considered in computing the limiter with the Barth and Jespersen (1989) approach, different results are obtained, with different levels of accuracy. In particular, vertices computation (Figure 6.5(a)) resulted as the most imprecise, as highlighted in Figure 6.6(a), while midpoint computation appears more regular but with some point-wise spikes (Figures 6.5(b) and 6.6(b)). These outcomes are due to the excessive limitation introduced by these two computations, which do not allow to obtain proper reconstructed values at cell bounds. Differently, computation of the limiters at points P (i.e. at intersections between cell edges and segments connecting neighbour cell centers) allow to compute the expected primitive values at cell bounds.

A very similar result is obtained considering the Venkatakrishnan (1995) limiter computed alternatively at midpoints M and intersections P (see Figure 6.7).

On the strength of these results, next applications of the model are carried out preferring the limiter computation at intersections.

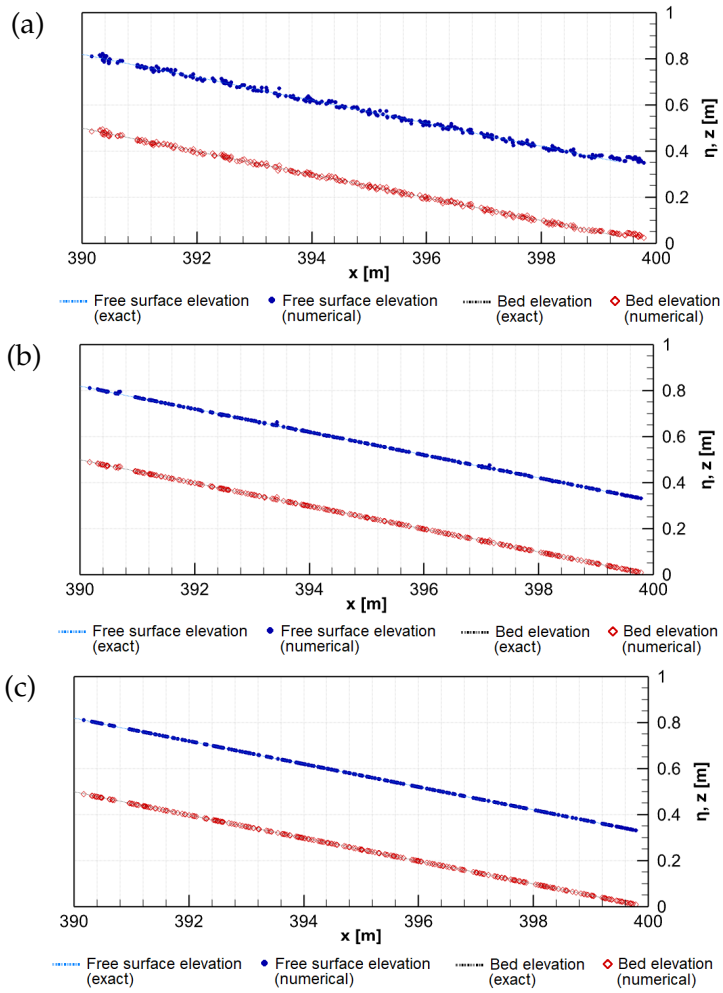

Figure 6.5: TRENT2D-UTG uniform-flow test with Barth and Jespersen (1989) limiter computed at (a) vertices m (b) edge midpoints M (c) intersections P

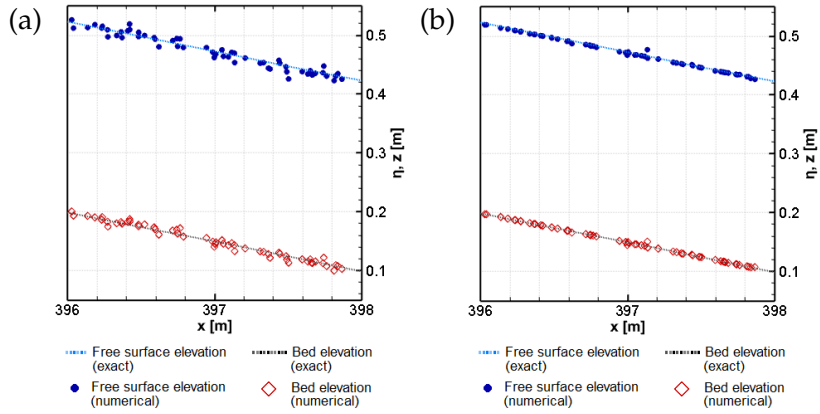

Figure 6.6: Zoom of TRENT2D-UTG uniform-flow test with Barth and Jespersen (1989) limiter computed at (a) vertices m (b) edge midpoints M

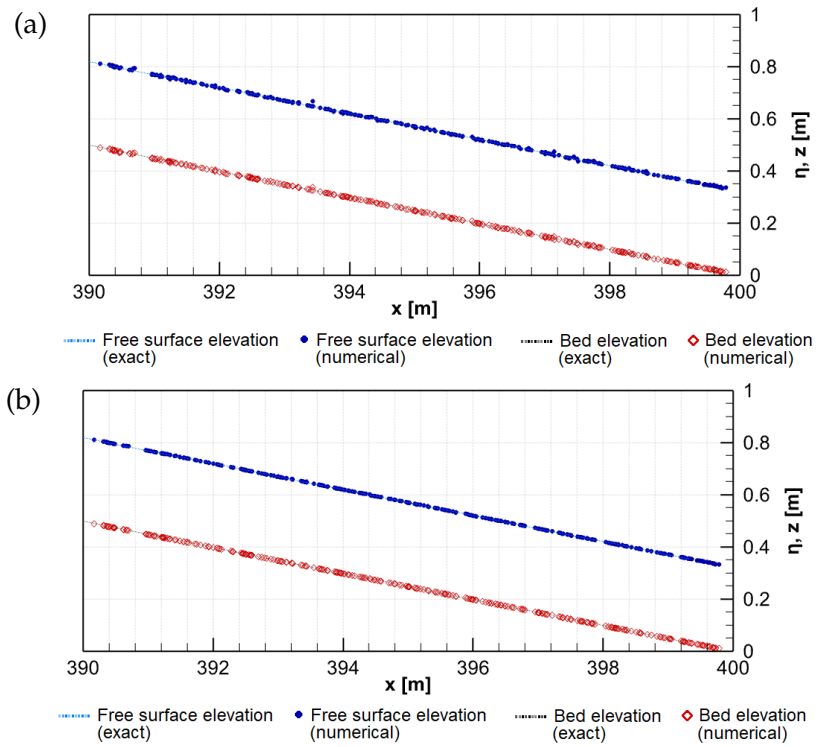

Figure 6.7: TRENT2D-UTG uniform-flow test with Venkatakrishnan (1995) limiter computed at (a) edge midpoints M (b) intersections P

6.4.2 1D Riemann Problems

Two 1D Riemann Problems (RP) are then solved considering only the homogeneous part of the PDEs system and assuming the x-direction as the main flow direction.

6.4.2.1 Three rarefaction waves

The first test case is a 1D RP, which solution involves only rarefaction waves. The domain is square and its edges are 80 m long. It counts 51200 cells, whose maximum area is equal to 0.125 m^2. Left L and right R initial values are set as follows: h_L =2.0 m, h_R =1.725 95 m, z_{bL} =1.0 m, z_{bR} =1.124 05 m, u_{xL} =0.0 ms^{-1}, u_{xR} = 2.671 75 ms^{-1}, u_{yL} =0.0 ms^{-1}, u_{yR} =0.0 ms^{-1}. The following model parameters values were used: c_b = 0.65, Δ = 1.65, β = 1.0. The end time is set at 5 s.

Figure 6.8 shows results obtained by means of the Barth and Jespersen (1989) limiter computed at intersections P. Very similar results are obtained also by means of the other approaches, except for the Barth and Jespersen limiter computed at vertices, whose

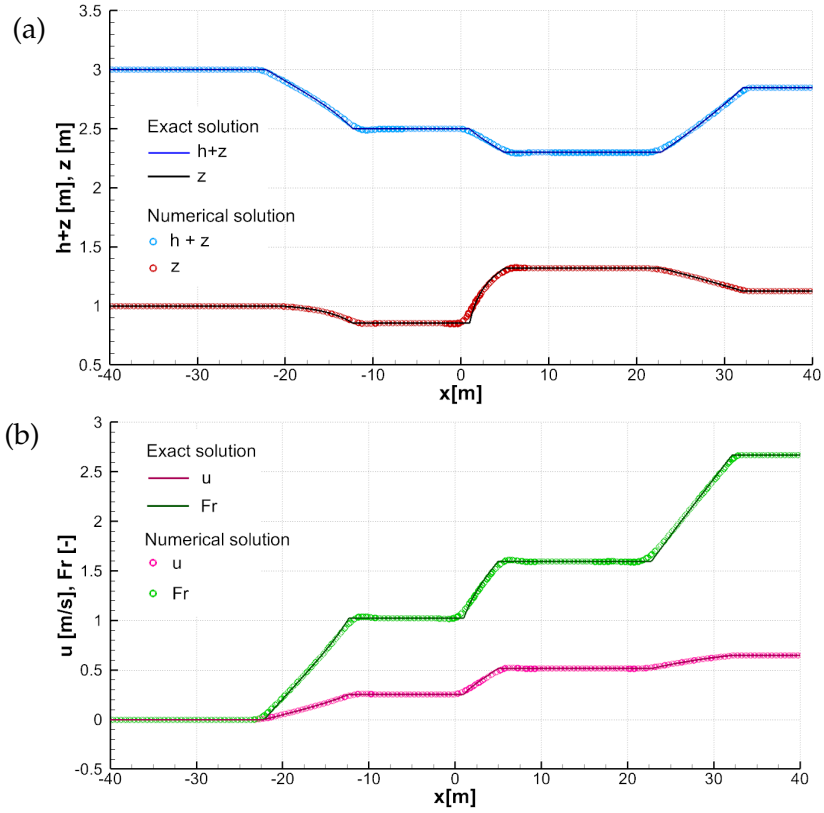

Figure 6.8: Results obtained through TRENT2D-UTG for the test with three rarefaction waves, applying the Barth and Jespersen (1989) limiter computed at intersections P over a mesh of 51200 cells: (a) free surface and bed elevation; (b) velocity along the main flow direction x and Froude number

accuracy appears slightly lower. However, the model is able to reproduce correctly the structure of the solution with any of the limiter approaches.

Still considering the same RP, a comparison of the different limitation approaches is shown if Figure 6.9. It was obtained by means of the same grid.

As shown by the zoom on the central rarefaction (Figure 6.10), limiters computed at midpoints and intersections give pretty much the same result, while computation of the Barth and Jespersen limiter at vertexes is more imprecise.

Finally, the intersection computation of the Barth and Jespersen limiter was used to solve the same RP over six meshes with different resolutions (i.e. numbers of cells equal to 800, 3200, 12800, 51200, 204800 and 819200). As expected, accuracy increases with the mesh refinement (Figures 6.11 and 6.12). This is confirmed also by the computation of the L_1 norms for the flow depth h (results are summarised in Table 6.1).

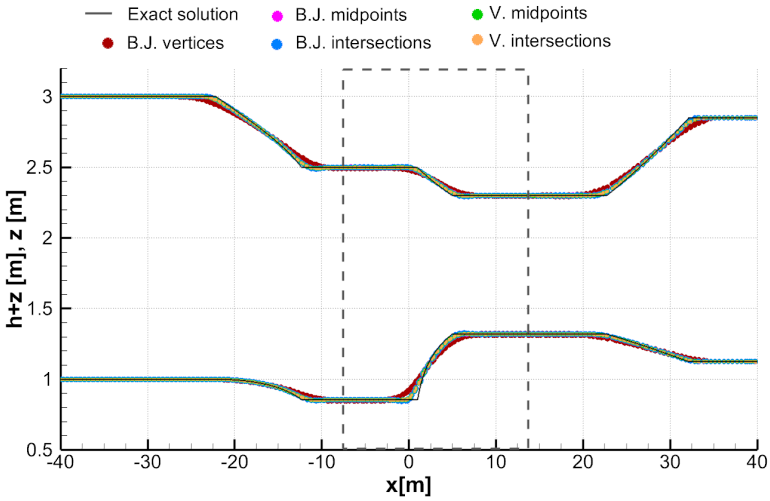

Figure 6.9: Comparison of the five different approaches available in TRENT2D-UTG for limiter computation, considering the three-rarefaction test and a grid with 51200 cells

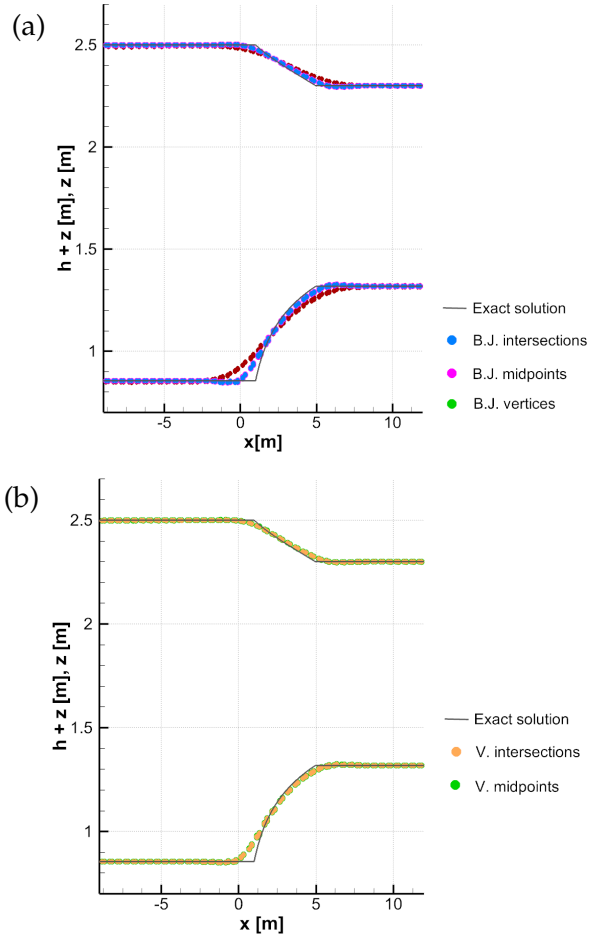

Figure 6.10: Zoom on results obtained through TRENT2D-UTG for the test with three rarefaction waves, applying the different limiter computations over a mesh of 15492 cells: (a) Barth and Jespersen (1989) approach; (b) Venkatakrishnan (1995) approach

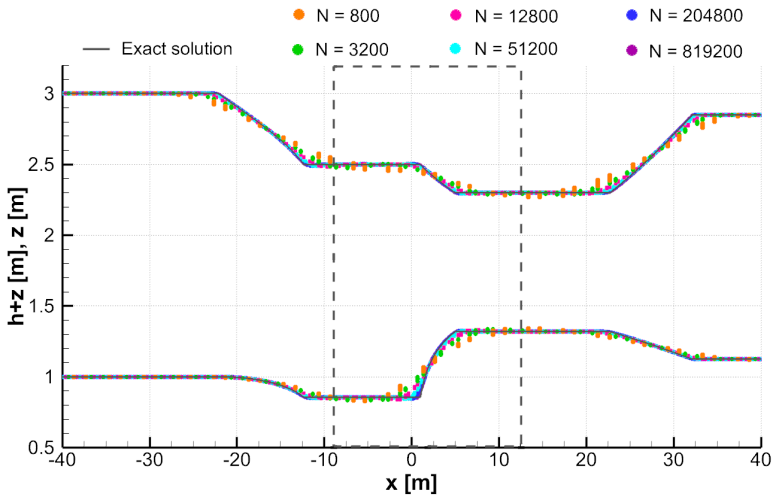

Figure 6.11: Comparison of results obtained by means of TRENT2D-UTG with the Barth and Jespersen limiter computation at intersections, considering the three-rarefaction test and six different meshes

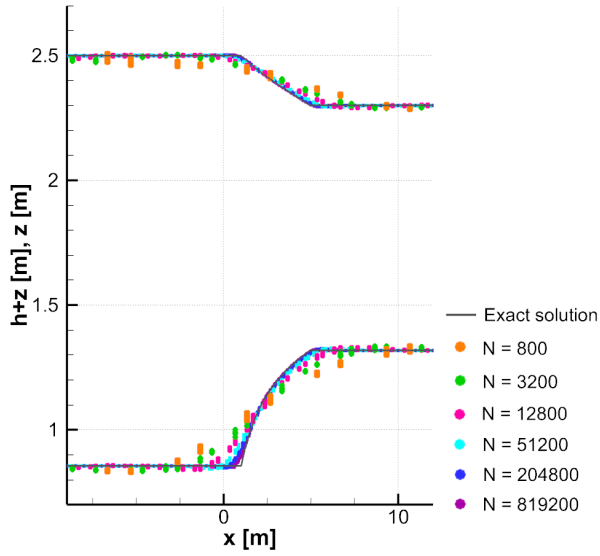

Figure 6.12: Zoom on the comparison of results obtained by means of TRENT2D-UTG with the Barth and Jespersen limiter computation at intersections, considering the three-rarefaction test and six different meshes

Number of cells	$L_1(h)$	Order
800	$8.38E-02$	
3200	$2.40E-02$	1.805
12800	$6.05E-03$	1.988
51200	$1.52E-03$	1.991
204800	$3.76E-04$	2.018
819200	$9.21E-05$	2.027

Table 6.1: Numerical convergence results obtained for the three-rarefaction test with TRENT2D-UTG and the Barth and Jespersen limiter computation at intersections.

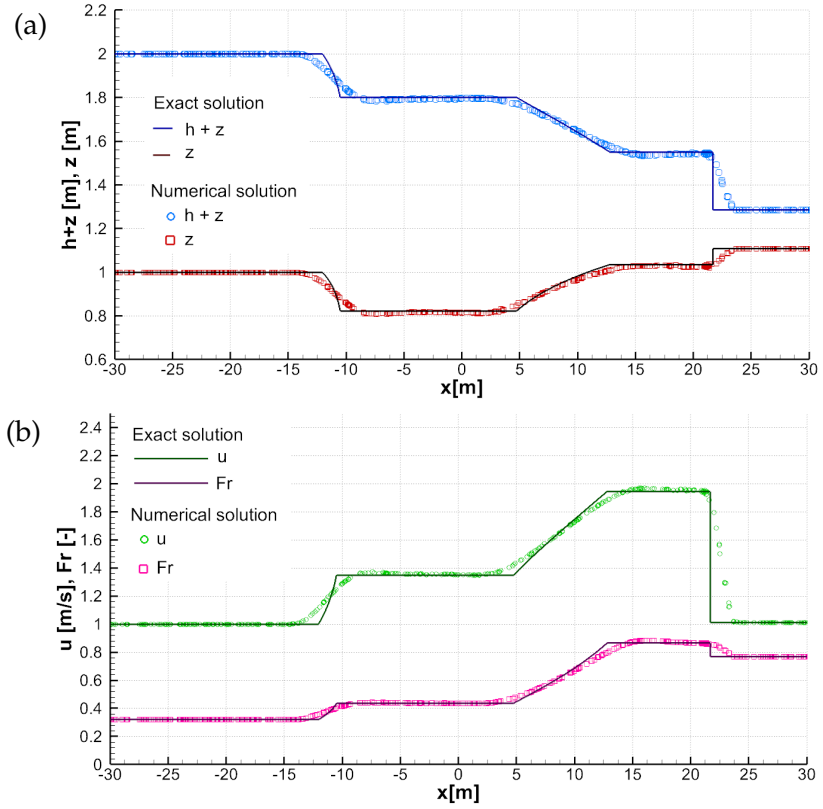

Figure 6.13: Results obtained through TRENT2D-UTG for the test with two rarefaction waves and one shock, applying the Barth and Jespersen (1989) limiter computed at intersections P over a mesh of 1549 cells: (a) free surface and bed elevation; (b) velocity along the main flow direction x and Froude number.

The L_1 norm was computed because it appears more suitable for conservation laws than the L_2 norm and, anyhow, usually it gives results that are much similar to the L_2 norm LeVeque (2002).

6.4.2.2 Two rarefaction waves and a shock

The second test case is a 1D problem, whose solution is made of two rarefaction waves and a shock. The computational domain is square, with edges 100 m long. The domain counts 15492 cells and maximum cell area is 1 m^2 wide. Left and right initial values are set in this way: h_L =1.0 m, h_R =0.18 m, z_{bL} =1.0 m, z_{bR} =1.108 m, u_{xL} =1.0 ms^{-1}, u_{xR} =1.012 ms^{-1}, u_{yL} =0.0 ms^{-1}, u_{yR} =0.0 ms^{-1}. Parameter values were kept equal to those used in the first test. The end time of the test is set at 7 s.

Figure 6.13 shows results obtained considering the Barth and Jespersen (1989) limiter computed at intersections P. The model is able to catch quite well the two rarefaction waves, while is not able to reproduce the shock as a sharp discontinuity (the shock appears to be quite smoothed). The cause of this result is the

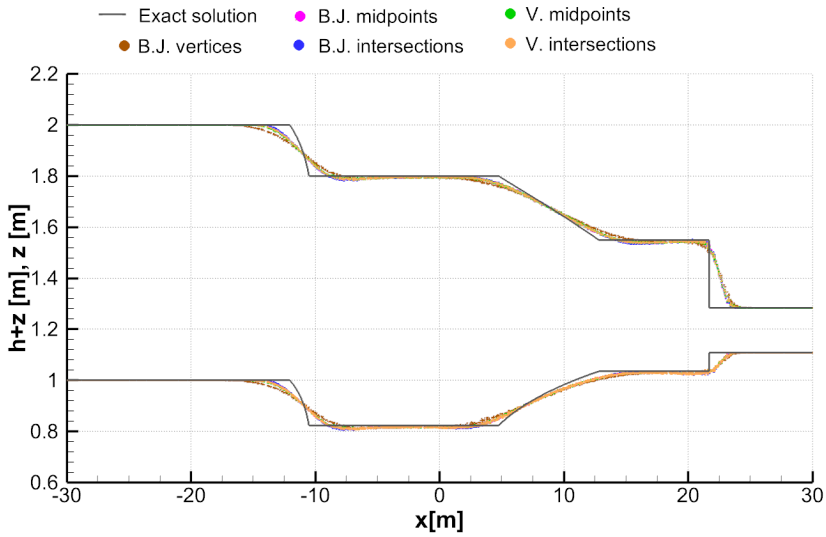

Figure 6.14: Comparison of the five different approaches available in TRENT2D-UTG for limiter computation, considering the two-rarefaction waves + one shock test and a grid with 15492 cells

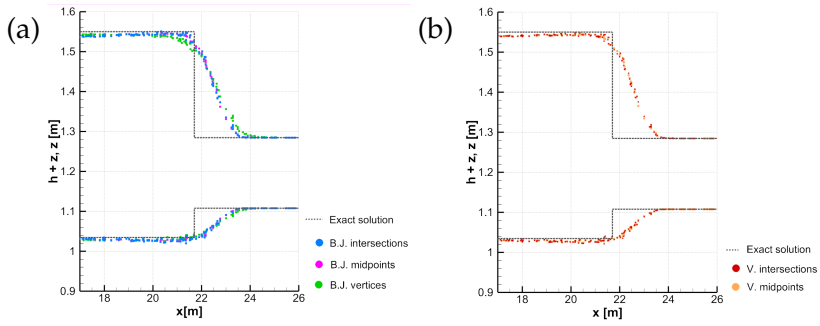

Figure 6.15: Zoom on the shock representation obtained through TRENT2D-UTG for the test with two rarefaction waves and one shock, applying the different limiter computations over a mesh of 15492 cells: (a) Barth and Jespersen (1989) approach; (b) Venkatakrishnan (1995) approach

numerical diffusion (Rosatti and Fraccarollo, 2006), which is very high in the LHLL solver.

Similar results are obtained also considering the other approaches in the limiter computation, as shown in Figure 6.14. As expected, the Barth and Jespersen limiter computed at vertexes gave the worst results.

The inaccuracy in the shock representation is highlighted in Figure 6.15 considering the whole set of limiter-computation approaches.

6.4.2.3 Unstructured VS Cartesian

A further test case was considered in order to compare results obtained with the UTG version of TRENT2D and those achieved applying the original version of TRENT2D, i.e. TRENT2D over a structured mesh.

For this purpose, a three-rarefaction RP was considered with the following left and right initial values: h_L =2.0 m, h_R =2.87 m, z_{bL} =1.0 m, z_{bR} =0.63 m, u_{xL} =0.5 ms^{-1}, u_{xR} =3.41 ms^{-1}, u_{yL} =0.0 ms^{-1}, u_{yR} =0.0 ms^{-1}. Model parameters were set equal to: c_b = 0.65, Δ = 1.65, β = 1.0.

The problem was solved both with first- and second-order accuracy, as shown in Figures 6.16 and 6.17. At second order, TRENT2D-UTG was applied with the Barth and Jespersen limiter computed at intersections. Results obtained with TRENT2D-UTG second-order accuracy are very close, and locally more accurate, to those obtained with TRENT2D (i.e. over a Cartesian mesh with resolution comparable to that one of the unstructured mesh) with the same accuracy. The same observation can be deduced for the first-order accuracy. Small differences introduced by the two models are due only to the different approaches in gradient computation and limitations.

6.4.3 Circular dam-break

A further test was performed considering a circular dam break. To simulate this problem a square grid with edges 50 m long was considered, with 62055 cells, whose maximum area is equal to 0.0625 m^2. As initial condition, the following values were considered: h_{in} =4.0 m, h_{out} =1.0 m, $z_{b,in}$ =1.0 m, $z_{b,out}$ =2.0 m, $u_{x,in} = u_{x,out}$ =0.0 ms^{-1}, $u_{y,in} = u_{y,out}$ =0.0 ms^{-1}. Model parameters were set equal to: c_b = 0.65, Δ = 1.65, β = 0.1. This test was performed considering also bed shear stresses via Gauckler-Strickler formulation. For this purpose, the roughness coefficient K_s was set equal to 20 m$^{1/3}$s^{-1}.

Results obtained by means of the Barth and Jespersen computed at locations P are shown in Figures 6.18 and 6.19 at time t =3 s. They do not show any comparison with an analytical solution, which is not available, but account for symmetry, which is the essential requirement in similar problems. The result obtained appears acceptable with reference to both free-surface and bed elevation.

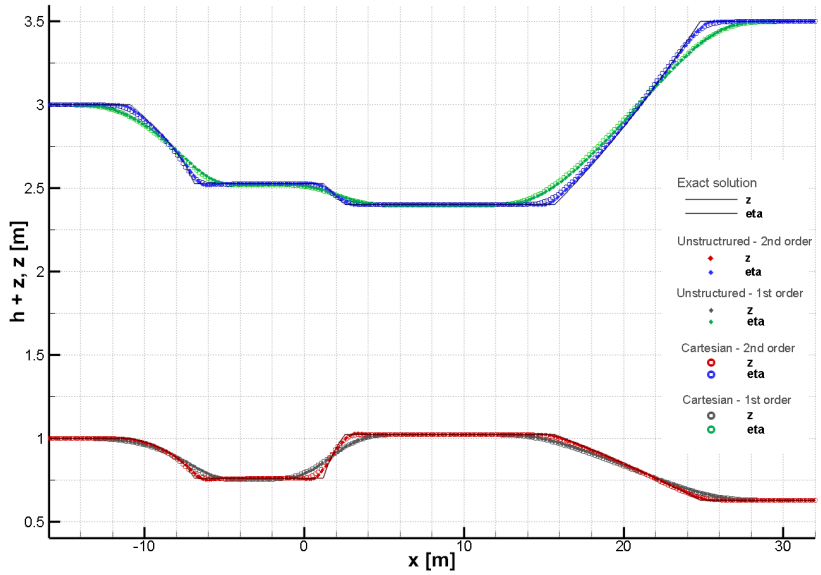

Figure 6.16: Comparison of results obtained for the same RP by means of TRENT2D and TRENT2D-UTG considering grids with the same number of cells

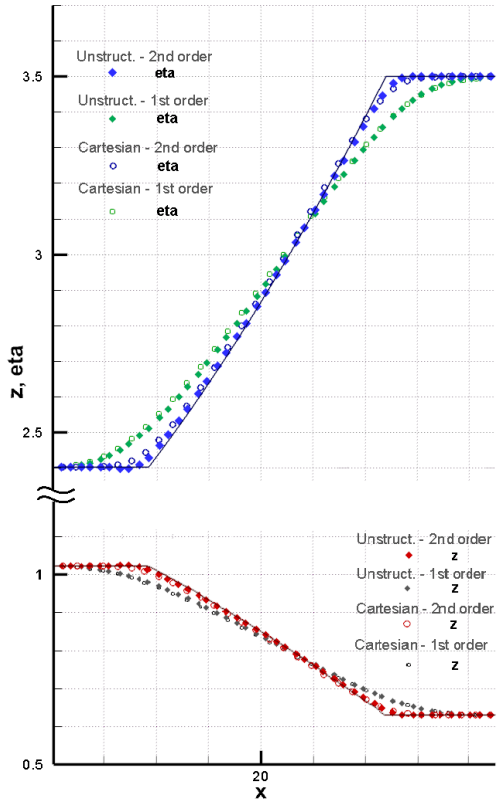

Figure 6.17: Zoom on the third rarefaction wave in the results comparison for the same RP by means of TRENT2D and TRENT2D-UTG considering grids with the same number of cells

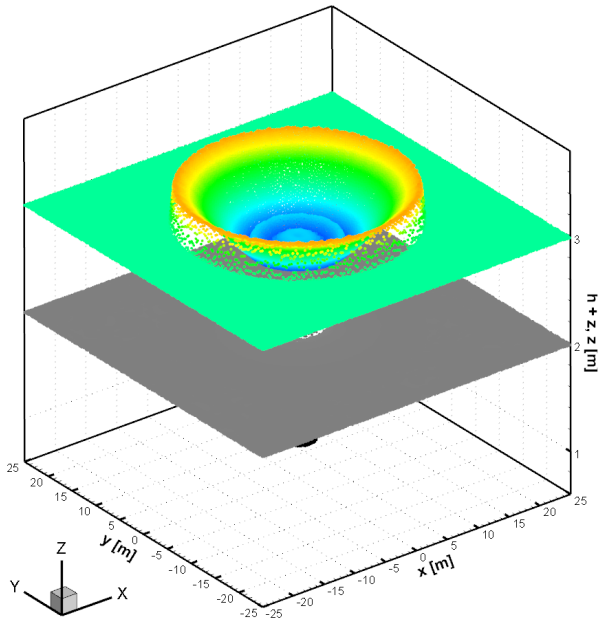

Figure 6.18: 3D view of the circular dam-break results at t =3 s (centroid values).

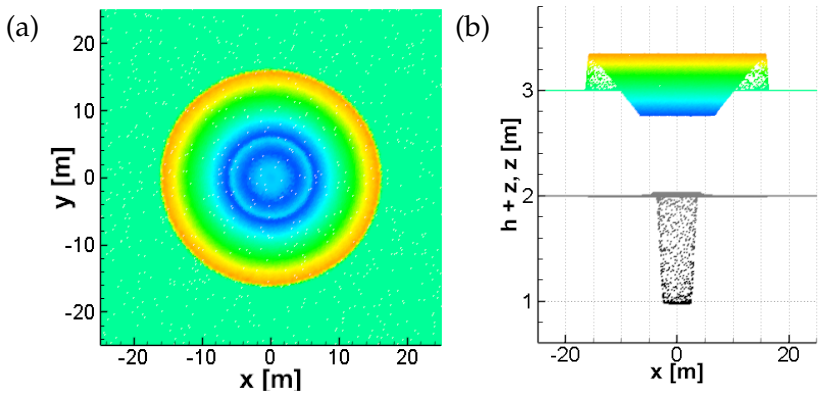

Figure 6.19: 2D view of the circular dam-break results at t =3 s: (a) 2D view in the (x, y) plane (centroid values); (b) 2D view in the (x, z) plane (centroid values).

6.5 A test on realistic morphology

TRENT2D-UTG was used to analyse a realistic case study. A realistic morphology of a hydropower reservoir was created in order to simulate the dynamics of a free-surface sediment-routing process.

For this purpose, an unstructured mesh was used to represent the heterogeneous morphology of the reservoir, introducing a suitable refinement in the outflow area. Furthermore, several

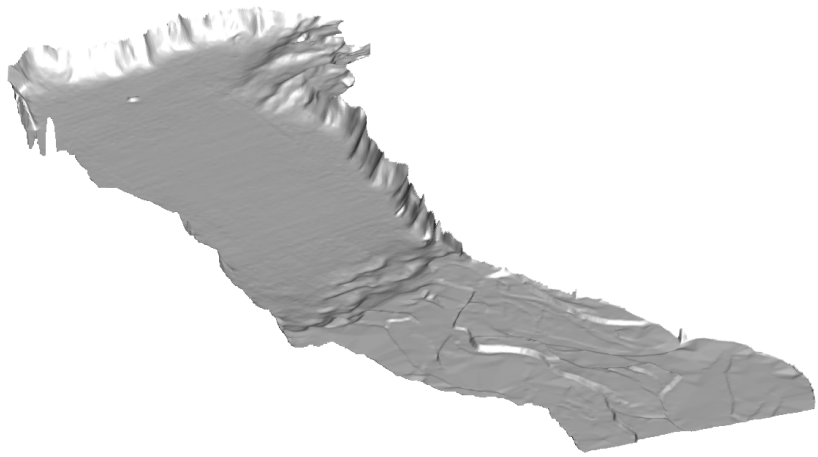

Figure 6.20: 3D view of the reservoir morphology.

types of boundary conditions were introduced to represent properly the hydro- and morphodynamic processes at the inflow section, at the outflow sections and at the lateral walls of the reservoir. Then, a simulation was run, considering the gradient computation and limitation strategy of Barth and Jespersen (1989) computed at locations P_k.

6.5.1 Domain morphology and boundary conditions

To test the TRENT2D-UTG model in real-life conditions, the morphology of a realistic hydropower reservoir was built. The area of the reservoir was set about equal to 105 000 m^2 and its shape was drawn as much realistic as possible, i.e. avoiding trivial shapes (see Figure 6.20). In particular, a significant difference in bed elevation was introduced approximately halfway the reservoir. Since the bed is mobile, the model is expected to simulate erosion and deposition processes in this area, routing eroded sediments towards the outlet section. The outlet cross section was shaped rectangular and its width set equal to 8 m. On the contrary, the inlet cross section was drawn 30 m wide and with an irregular shape.

In order to make geometry more heterogeneous, an irregular channel was introduced inside the reservoir, ending in the outlet section. Two, 20 m long wings canalise the flow into the channel, while the downstream section coincides with the outlet section. This channel is intended to direct reservoir sediments towards the outlet section. In order to increase morphological complexity, also a semi-circular geometrical constraint was introduced along the

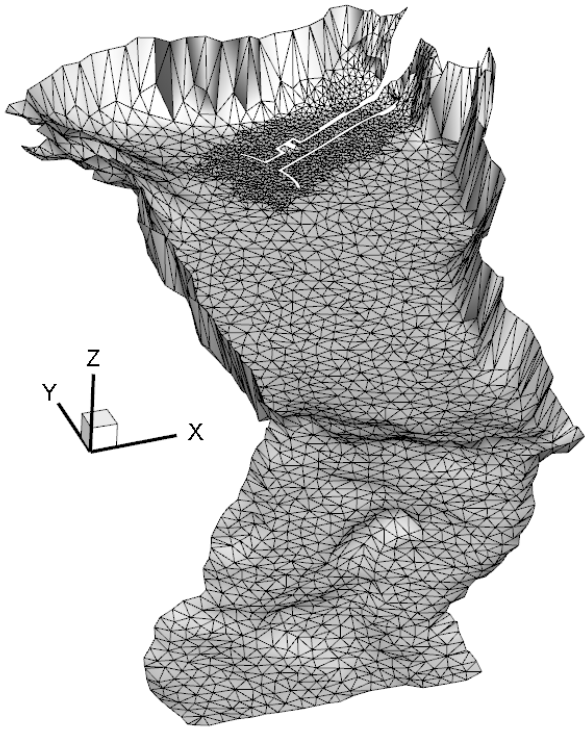

Figure 6.21: 3D view of the unstructured mesh used to discretise the reservoir morphology.

channel at the left bank, obtaining a local variation of the cross-section width. This morphology was used as initial condition for the bed elevation z_b, while the initial condition for the flow depth h was computed assuming the free surface as horizontal and imposing h =10 m above the outlet section. In this way, about the whole reservoir appears wet. Initial velocity is assumed equal to zero.

The domain was discretised by means of a Delaunay triangular mesh obtained by means Triangle (see Figure 6.21, where the vertical scale is amplified of a factor 6). Two different resolution values were used to describe morphology in the computational domain, which includes the whole reservoir. First the whole domain was discretised assuming as maximum cell area a value of 50 m^2. In this way, a grid of 3382 cells was produced, with average cell area of about 35 m^2. The side length of equivalent square cell in a Cartesian mesh would be less than 6 m. Then, a refinement of the mesh was performed in the area near the outlet section, along the channel. In this area, cell area is at most equal to 5 m^2. After the refinement, the mesh turned out to be composed of 4939 cells, which average area is about equal to 1 m^2. In this area, the side

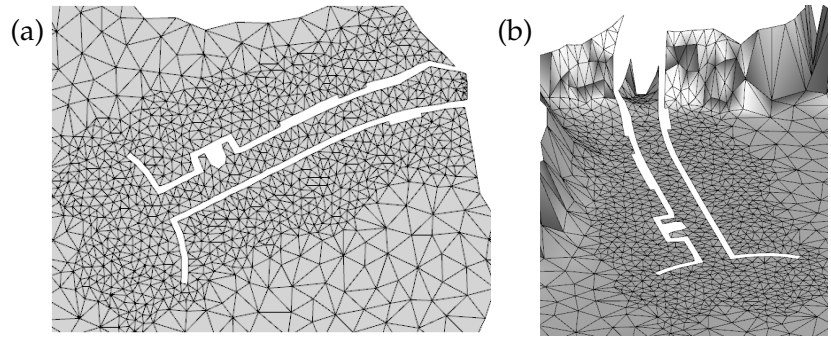

Figure 6.22: (a) 3D and (b) 2D view of the unstructured mesh in the refined area

length equivalent Cartesian cells would be equal to 1 m. Figure 6.22 shows the detail of the mesh in the refined area.

It must be noticed that the walls of the channel are not represented by the mesh, however they are virtually reproduced by the TRENT2D-UTG model by means of the reflecting condition. This condition is set along the whole boundary of the domain, except for the inlet and outlet sections, which are indicated in Figure 6.23. At the inlet bound, the equilibrium condition is imposed, according to the approach used in the original version of TRENT2D. On the other side, at the outlet bound the non-reflecting condition is imposed when the flow is supercritical, while the critical condition is used when the flow is subcritical.

The inflow boundary condition was computed considering the mixture hydrograph plotted in Figure 6.24, which is realistic for the reservoir. The mixture concentration was computed according to the Meyer-Peter and Müller formulation, because of the small slope imposed at the inlet section ($i_F = 0.01$). In uniform flow conditions, the Meyer-Peter and Müller transport formula gives a concentration of slightly higher than $c = 0.002$. Although this value is quite low, this can be accepted, since the aim of the test is the simulation of sediment routing inside the domain, where concentrations are expected to be higher, making the application of TRENT2D-UTG acceptable.

In order to proper represent sediment routing, the Gauckler-Strickler formula for the bed shear stresses was considered. Model parameters were set as follows, choosing realistic values: $c_b = 0.65$, $\Delta = 1.65$, $Ks = 40\,\mathrm{m}^{1/3}\mathrm{s}^{-1}$ and $\beta = 0.0028$.

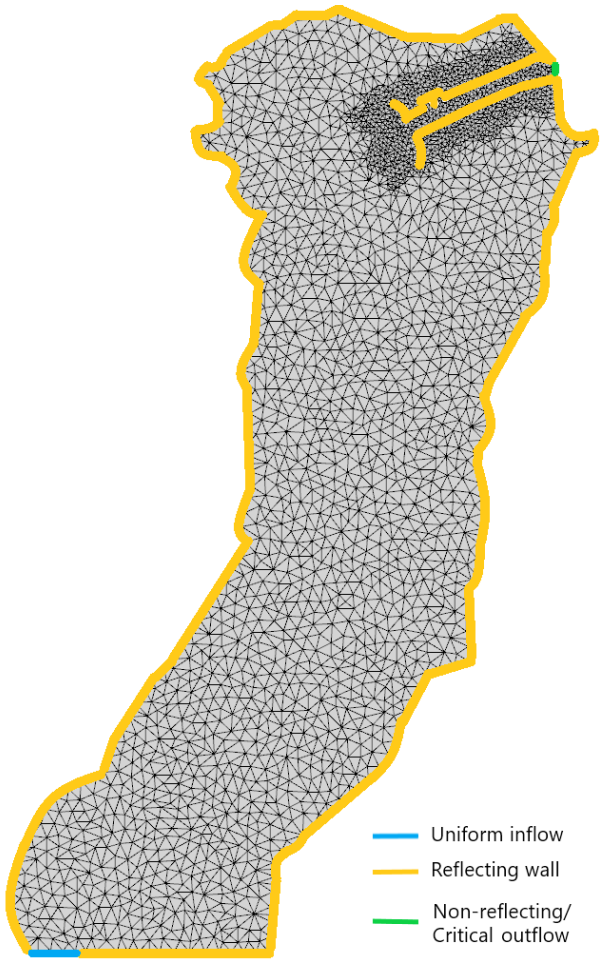

Figure 6.23: Location of the boundary conditions set for the hydropower-reservoir domain.

6.5.2 Model results

Figure 6.25(a) represents the initial condition for the bed elevation, while Figure 6.25(b) shows the bed elevation at the end of the simulation. The sediment-routing phenomenon is quite evident. Erosion processes were observed from the inlet section up to the halfway the reservoir. In particular, a channel 40 m wide took shape by erosion. Eroded sediments were then deposited in the deeper part of the reservoir, with a quite homogeneous spatial distribution, except for the artificial channel area, next to the outlet section. This is even more evident looking at Figure 6.26, where the difference between initial and final bed elevation is shown.

In the refined area, erosion processes are predominant both in-

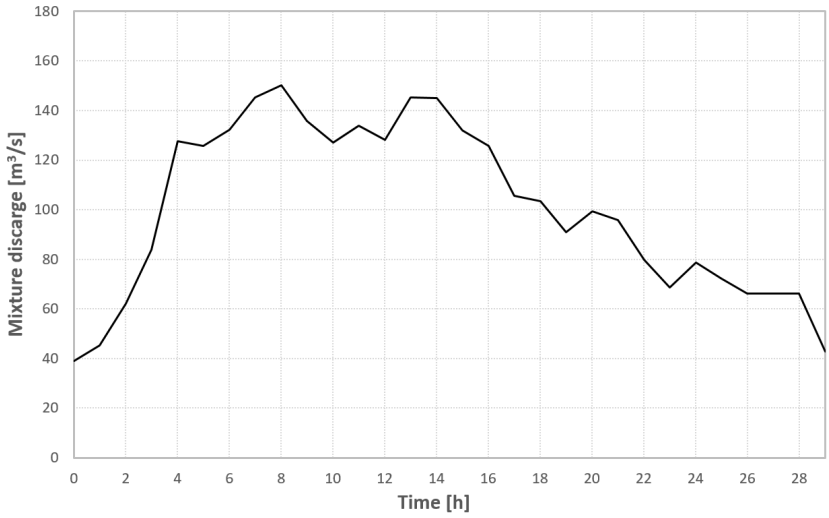

Figure 6.24: Mixture hydrograph supplied at the inflow section of the hydropower reservoir for the sediment-routing test with TRENT2D-UTG

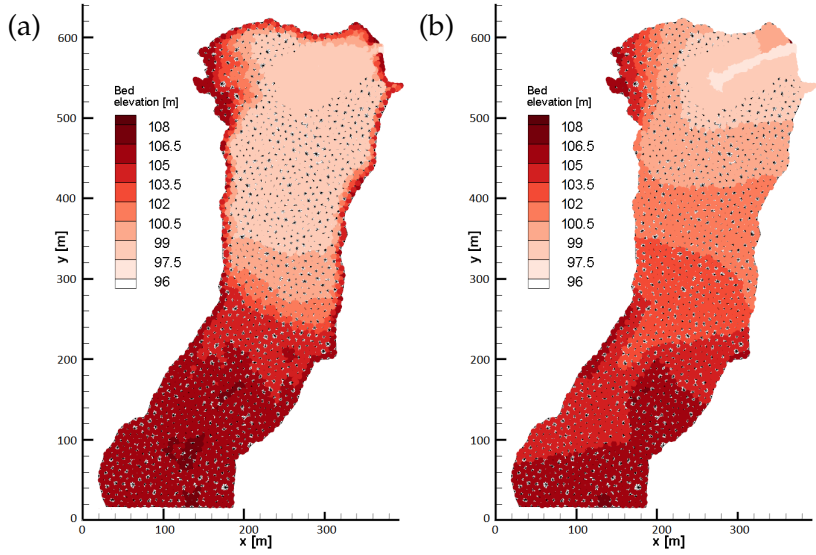

Figure 6.25: (a) Initial and (b) final condition of the bed elevation of the reservoir before and after the TRENT2D-UTG simulation

side and outside the channel (see Figure 6.27). However, erosion timing is different in the two regions. Inside the channel, erosion depth increases continuously during the first part of the simulation, while it decreases during the falling limb of the hydrograph, when the deposition front is approaching the channel. On the other hand, outside the channel, erosion processes appear quite gradual during the whole simulation, except for the region upstream of the channel, where the bed dynamics is more similar to that one of the channel bed.

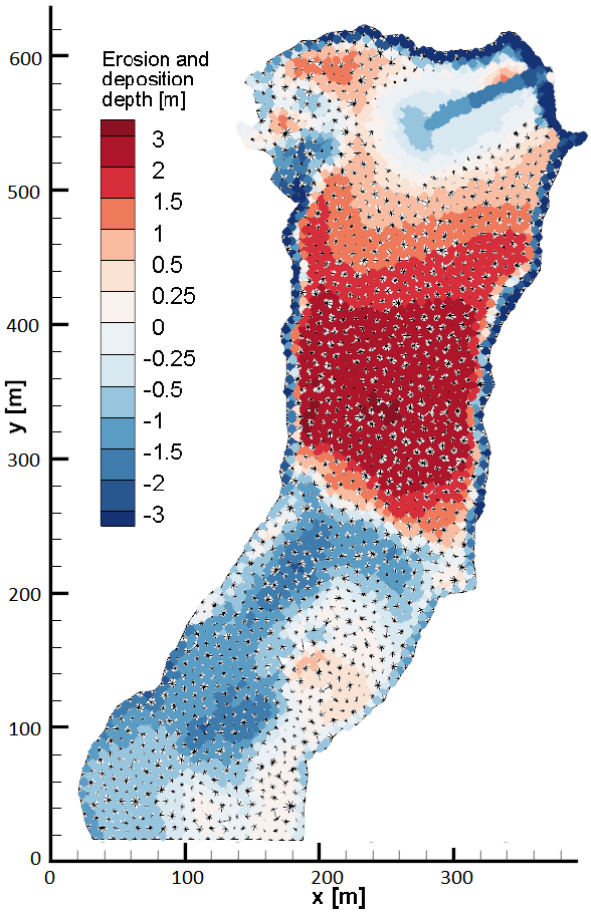

Figure 6.26: Erosion (blue) and deposition (red) depths in the reservoir after the TRENT2D-UTG simulation

The use of different resolution in different areas allows to obtain the *right level* of detail in each area, containing computational costs. Differently, simulating the same phenomenon with the original version of TRENT2D, i.e. over a regular Cartesian, the only possible way to simulate accurately the channel processes is to accept a significant increase in the cell number and, therefore, in computational costs. On the other side, to contain costs, a low level of detail in the channel should be accepted with the original TRENT2D.

On the strength of these results it can be observed that the "geometrical" complexity issue faced in this Chapter is solved. However, the trade-off accepted by the author, i.e. the model developer and user, was a significant effort in model development, especially in the management of geometrical information and in the debugging phases, and in creating and storing suitable

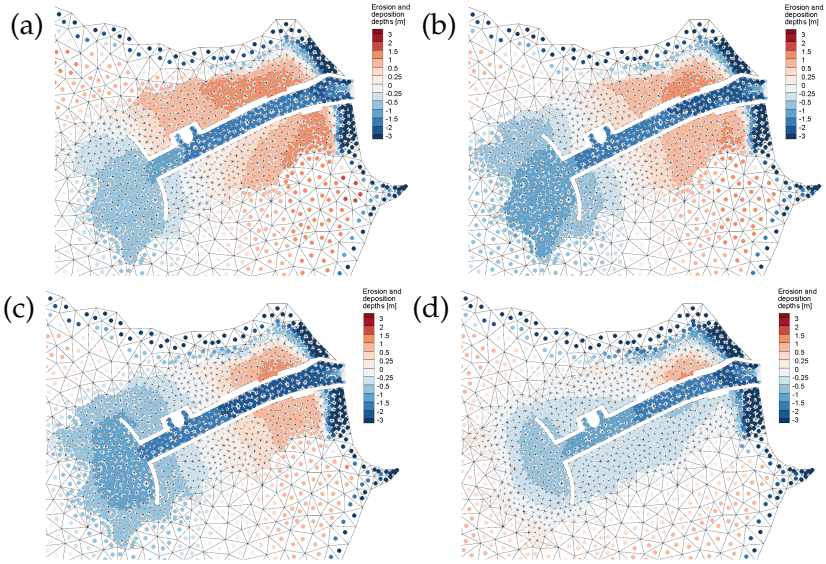

Figure 6.27: Erosion (blue) and deposition (red) depths in the refined area near the reservoir outlet: center cell values for (a) $t = 6h$, (b) $t = 12h$, (c) $t = 18h$ and (d) $t = 29h$.

Delaunay grids. These latter points could be overcome in the future integrating some suitable services in the WEEZARD system, together with the TRENT2D-UTG model, according to the approach presented in the previous Chapter.

Because of its geometrical flexibility, TRENT2D-UTG seems particularly suitable to represent several kinds of flow-controlling structure. Therefore, in perspective, the model could be enriched with further types boundary and internal conditions, to be applied whenever a flow-controlling structure is present in the computational domain. In this way, it would be possible to take into account properly the effects of these structures on the flow and bed dynamics. An example in this sense is presented in the next Chapter.

Chapter 7

Flow-control devices and mobile bed: modelling high-concentration flows conditioned by sluice gates

High-concentration flows show their intrinsic complexity also whenever they interact with flow-control devices, which are artificial structures aimed exactly at conditioning the phenomenon behaviour locally. Common high-concentration flow-control structures and devices are slit check dams, beam dams, weir check dams, deflection walls, block ramps, lateral walls. All these structures are conceived as protection devices, designed to modify high-concentration flow dynamics during flood events, although their effect is sometimes visible also in ordinary conditions. The influence of such geometrical constraints on high-concentration flows has been widely investigated in the literature (e.g. Hungr et al., 1987; VanDine, 1996; Armanini and Larcher, 2001; Chanson, 2004; Takahashi, 2007; Schwindt et al., 2017) and their detailed account, although pertinent, is not within the purpose of this thesis.

Here, attention is paid to another type of flow-control device, which is related especially to river and hydropower plants management: the sluice gate. Sluice gates are installed in hydropower reservoirs, but also along irrigation channels and on river barrages, to control water heights and flow rates by partial or total lifting. In hydropower reservoirs, they may be installed at the outlet bound, on the spillway crest or next to it (Figure 7.1), and activated during floods, in order to maintain the reservoir

Figure 7.1: Sluice gates of the Stramentizzo dam (Italy).

water head under a certain threshold, but sometimes also for sediment-routing purposes against siltation. In the latter case, the hydrodynamic effect produced by the gate is aimed at moving reservoir sediment and possibly discharging a part downstream. This operation generally implies high values of sediment concentration, which lead to tracing these phenomena back to high-concentration flows.

Furthermore, when the slit dam is partially lifted, its effect on the flow dynamics is expected to be quite similar to that one produced by slit check dams. Slit dams are nothing but a local, horizontal shrinkage of the stream cross section, which conditions sediment transport. Typically, the area upstream of the slit check dam is characterised by sediment deposition processes, because of the effects of the dam over the flow hydrodynamics and sediment transport capacity. Different widths of the slit dam opening imply different upstream deposition depths (Armanini and Larcher, 2001). Similarly, because of the shrinkage introduced in the sluice gate on the outflow cross section over the spillway, morphodynamic processes are expected, even if in this case the shrinkage is vertical rather than horizontal. However, since sluice gates are typically studied under the clear-water hypothesis and with a fixed-bed approach (see the short report in Section 7.1), no similar outcomes were found in the literature.

For this reason, a coupled experimental-numerical campaign is being carried out in these months by prof. Luigi Fraccarollo, prof. Giorgio Rosatti, Anna Prati and the author of this work, in order to study the morphodynamic effects of a sluice gate

over a high-concentration flow generated for sediment routing purposes. Some of the results obtained during the experimental study are summarised in Section 7.2 (courtesy of prof. Fraccarollo and Anna Prati), while in Section 7.3 experimental data are processed in order to obtain a mathematical description of gate-controlled flows over mobile bed in the area next to the gate. Outcomes obtained in this Section are then used to implement a suitable, possible outflow boundary condition for the TRENT2D-UTG model, which could be then applied also to study gate-controlled sediment routing in hydropower reservoirs. A realistic example of this application kind is proposed in Section 7.4, where the same reservoir morphology considered in Section 6.5.1 is used. In this application, two complexity sources are therefore considered: morphology and gate-controlled dynamics.

7.1 Studying sluice-gate hydrodynamics: a literature review

Sluice gate hydrodynamics has been studied for more than one century (Montes, 1997), becoming a classical topic in fluid mechanics. However, modern studies have been carried out only in the last decades, starting with the works of Rajaratnam and its co-workers (Roth and Hager, 1999).

Most of the studies present in the literature of the last fifty years are based on a particular schematisation of the problem, referred here as "standard sluice gate" configuration, borrowing the definition proposed in Roth and Hager (1999). The standard sluice-gate configuration considers the gate as vertical, flat and with a sharp crest at the lower bound. The gate is assumed to be inserted in a horizontal channel with rectangular section, negligible roughness and non-erodible bed. Only gates perpendicular to the channel flow are considered. The flow downstream the gate is considered free, although several studies account also for the submerged-flow case (e.g. Franke and Valentin, 1969; Swamee, 1992; Belaud et al., 2009; Cozzolino et al., 2015; Wu and Rajaratnam, 2015). Commonly, steady state conditions are considered.

As far as standard sluice gates are taken into account, some general, qualitative observations can be formulated, especially on the basis of experimental data collected by Rajaratnam and Humphries (1982) and Roth and Hager (1999).

As observed also in Castro-Orgaz and Hager (2014), the flow

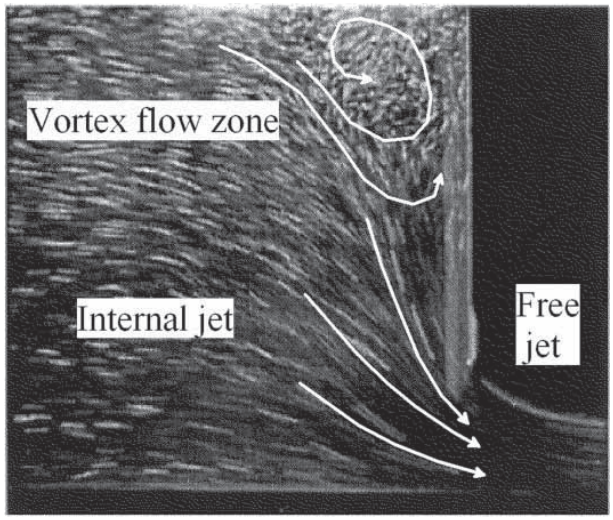

Figure 7.2: Typical internal flow structure upstream the sluice gate (from Castro-Orgaz and Hager, 2014).

(a)

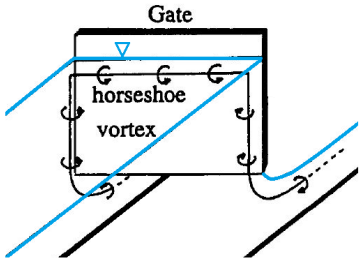

(b)

Figure 7.3: Horseshoe vortex upstream the sluice gate: (a) sketch edited from Montes (1997); (b) side view from Speerli et al. (1999)

approaching the gate, which is typically subcritical, can be divided into two portions: an upper vortex-flow zone and a lower internal-jet zone (Figure 7.2). In the lower zone, acceleration is observed, with the streamlines converging under the gate. The maximum value of velocity is observed slightly above the bed and the pressure distribution appears to be not hydrostatic. In the upper zone, a recirculating flow is observed (Figure 7.2), with a slight increase of the flow depth and the formation of a very thin boundary layer along the sluice gate. In the recirculation zone, some authors (e.g. Montes, 1997; Speerli et al., 1999 and Roth and Hager, 1999) observed the presence of a horseshoe vortex (Figure 7.3). According to Roth and Hager, the narrower is the channel, the larger is the distance between the vortex and the gate.

Downstream, a vertical contraction of the flow section is observed, which is addressed as the phenomenon of the *vena con-*

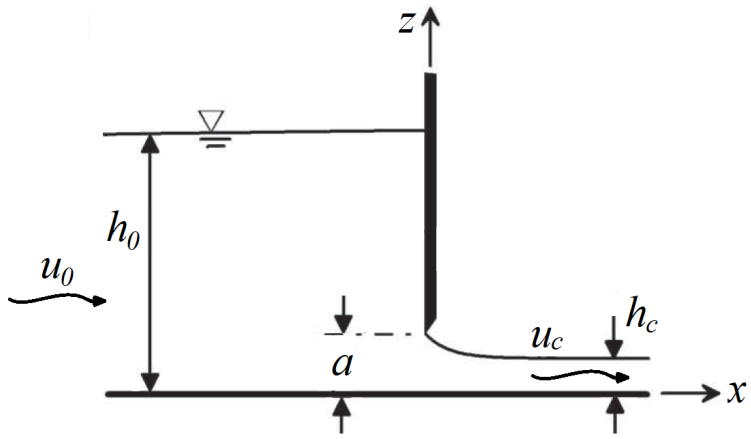

Figure 7.4: Sluice gate notation.

tracta. In the cross section, where the flow depth is the lowest, streamlines are straight and pressure is hydrostatic. Here, the flow is supercritical.

Evidently, sluice gates cause 3D hydrodynamic effects, however there is still not agreement about their description.

Several of the literature contributions assume the flow as irrotational, while the fluid is considered as incompressible and inviscid. Furthermore, most authors assume the upstream free surface as horizontal.

According to this approach, energy can be considered constant from upstream to downstream of the gate and the following energy balance can be written between the upstream undisturbed flow 0 and the *vena contracta* section C (see Figure 7.4 for the notation):

$$h_0 + \frac{u_0^2}{2g} = h_c + \frac{u_c^2}{2g}$$

where h_0 and u_0 are the undisturbed upstream flow depth and velocity, while h_c and u_c are the flow depth and the velocity in the *vena contracta* section. Considering also the mass conservation equation

$$h_0 u_0 = h_c u_c$$

the following relation for the velocity u_c is obtained:

$$u_c = \sqrt{2gh_0}\frac{1}{\sqrt{\frac{h_c}{h_0}+1}} \tag{7.1}$$

The flow depth h_c can be expressed as $h_c = aC_c$, where C_c is the contraction coefficient C_c. Substituting this expression into equation 7.1 and multiplying by h_c, it is possible to obtain a useful relation between the discharge per unit width q, the upstream flow depth h_0 and the gate opening a:

$$q = a\sqrt{2gh_0}\frac{Cc}{\sqrt{\frac{aC_c}{h_0}+1}}$$

Similarly, being C_q the discharge coefficient, the relation becomes (Henry, 1950; Swamee, 1992)

$$q = aC_q\sqrt{2gh_0} \tag{7.2}$$

where (Henderson, 1966)

$$C_q = \frac{C_c}{\sqrt{\frac{aC_c}{h_0}+1}} \tag{7.3}$$

Equation 7.2 is significant, since it allows to compute one among the variables q, a and h_0 once the other two are known, in addition to the discharge (or the contraction) coefficient. However, the estimate of the discharge (or the contraction) coefficient appears to be quite challenging. Most authors observed that C_q depends on the gate opening a and the upstream flow depth h_0, but the dependence is not described univocally. Table 7.1 lists some of the heterogeneous formulations proposed. Most of them were verified experimentally. In all these formulations, the energy loss due to the horseshoe vortex upstream the gate is somehow taken into account, according to observations that indicate the loss as depending on the gate opening (Valentin, 1968).

On the other side, Montes (1997) observed that scale effects introduced by viscosity, roughness and surface tension are significant only if the gate opening and the channel width are small. As a general indication, Roth and Hager (1999) stated that, for a channel of width equal to 1 m, scale effects are negligible if the gate opening is greater than 0.5 m.

Analyses performed by Sepúlveda et al. (2009) showed that formulations produced with reference to the classical theoretical framework are almost all acceptable (with the exception of Swamee, 1992), especially when no calibration can be performed.

Publication	$C_q(h_0, a)$
Rajaratnam and Subramanya (1967)	$C_q = 0.589 + 0.0297\sqrt{\frac{a}{h_0}}$
Garbrecht (1977)	$C_q = 0.6468 - 0.1641\sqrt{\frac{a}{h_0}}$
Noutsopoulos and Fanariotis (1978)	$C_q = 0.62 - 0.15\sqrt{\frac{a}{h_0}}$
Nago (1978)	$C_q = 0.6\exp\left(-0.3\frac{a}{h_0}\right)$
Swamee (1992)[(1)]	$C_q = 0.611\left(\frac{h_0 - a}{h_0 + 15a}\right)^{0.072}$
Roth and Hager (1999)	$C_q = 0.594 + \frac{a/h_0}{\frac{1}{20} + \frac{2}{5}s}\left(\frac{1}{18}s - \frac{3}{500}\right)\left(\frac{a/h_0}{\frac{1}{20} + \frac{2}{5}s} - 2\right)$ with $s = \log\left(\frac{a\sqrt{2ga}}{1000\nu}\right)$
Defina and Susin (2003)	$C_q = \frac{C_c}{\sqrt{C_c\frac{a}{h_0} + 1}}$ with $C_c = 1 - \left(0.153\frac{a^2}{h_0^2} - 0.451\frac{a}{h_0} + 0.727\right)\sin\left(\frac{a}{h_0}\right)$

[(1)] regression on Henry (1950) nomogram

Table 7.1: Some literature formulations for the sluice-gate discharge coefficient C_q.

This leads to the conclusion that, despite the significant uncertainty behind the evaluation of C_q, almost any of the formulations of Table 7.1 can be reasonably applied. Analogously, also the classical Kirchhoff value of $C_c = 0.611$ can used to compute an acceptable value of C_q by means of equation 7.3.

However, it must be noticed that all these results were obtained considering only the steady-state condition, i.e. one of all the possible conditions. Such condition is quite far from the un-

steady processes observed for example during gate-lifting manoeuvre. Nevertheless, experimental analyses carried out in Chanson et al. (2002) regarding flow through a horizontal orifice at the bottom of a tank showed that the difference between unsteady experimental results and classical steady-state theory seem to be very slight. Realistically, this observation can be extended also to gate-controlled flows.

On this basis, relations proposed in Table 7.1 can be profitably used in 2D, shallow-flow models (see for example Zhao et al., 1994 or Cozzolino et al., 2015), in order to properly simulate the gate control effect also in unsteady conditions.

7.2 Sluice gates and high-concentration flows over a mobile bed: some results from an experimental campaign

All the contributions cited in the previous Section refer to the case of a sluice gate controlling a clear-water flow over a fixed bed. However, for the purpose of this Chapter, different conditions must be considered, i.e. a sluice gate controlling a high-concentration flow over a mobile bed. In such conditions, not only hydrodynamics has to be investigated, but also morphodynamics, i.e. bed evolution and sediment transport dynamics. Because of the scarcity of studies in the literature about this problem, an experimental campaign was carried out by prof. Luigi Fraccarollo (University of Trento) and his co-worker Anna Prati, considering steady and unsteady conditions. The main results obtained through the experiments are shortly summarised here (courtesy of prof. Fraccarollo and Anna Prati).

The experimental set up was made of a glass-wall flume 6 m long, with a cross section of 0.1 m $\times$ 0.5 m and adjustable slope. The mixture of water and sediments was supplied by means of a pump, which discharge was adjustable. The sluice gate was positioned at the outflow bound of the flume and its opening was regulated by means of a wheel.

Three materials, characterised by different size and density, were used to simulate the solid phase of the mixture: polymethacrylate (PMMA), polyvinylchloride (PVC) and sand.

With this set-up, two significant problems were studied: the steady-state condition and the gate-opening manoeuvre. Both are

shortly accounted for here below, mainly from a qualitative point of view.

7.2.1 Steady-state conditions

Firstly, the same approach used in the literature to study sluice-gate clear-water flows over fixed bed was applied. On the whole, 35 experiments were performed (13 with PMMA, 17 with PVC and 5 with sand) considering mixture discharge constant during each experiment. For each group of experiments, different configurations were considered, i.e. different values of gate opening (from 0.03 m to 0.1 m), bed slope (from 0.01 to 0.08), mixture discharge (from $5\,\mathrm{ls}^{-1}$ to $12\,\mathrm{ls}^{-1}$) and concentration (from 0.01 to 0.13). For each experiment, a camera was used to acquire videos through the right side-wall of the flume. Furthermore, images of experiments with PMMA and PVC were acquired by Anna Prati with two CCD (Charge Coupled Device) cameras and processed by means of the stereoscopic imaging technique proposed in Spinewine et al. (2003).

Experiments started with the flume in uniform flow conditions, i.e. with the bed slope in equilibrium with the supplied mixture discharge. Then, the gate was inserted at the outlet bound of the flume and lowered through the wheel, setting a certain opening heigh, lower than the upstream flow depth. This operation generated a transient flow, which duration could turn out to be quite long (several minutes). The transient flow led then to another steady-state condition, which is shown in Figure 7.5. In particular, it was observed that the presence of the sluice gate forced the bed to assume a new profile near the gate. The new profile turned out to be very similar to the one observed upstream slit dams when deposition processes occur (Figure 7.6). Such outcome was observed throughout the whole set of experiments.

As in the clear-water case, the free surface raised and a recirculation zone wass observed. However, near the gate, the bed slope increased considerably, if compared to the uniform-flow bed slope associated to the inflow mixture discharge. This variation can be reasonably ascribed to the action of the internal jet on the bed.

Although similarities with the standard case are present, the mobile nature of the bed and the two-phase nature of the flow clearly add complexity to the problem and require a proper description.

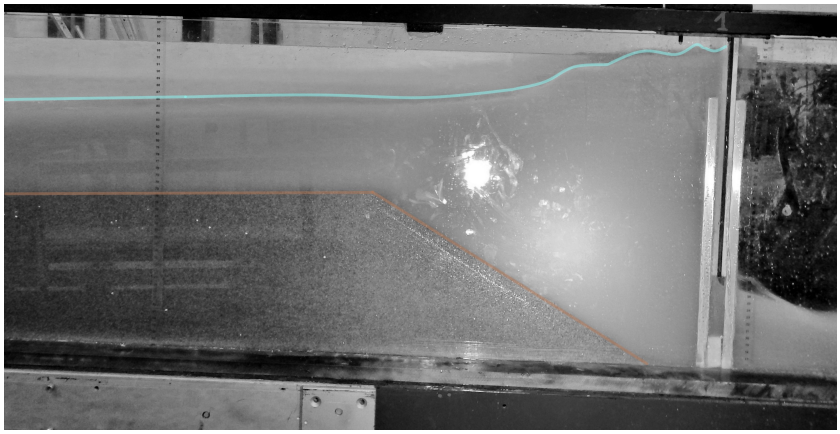

Figure 7.5: Bed (brown) and free-surface (light blue) profiles observed during the high-concentration sluice-gate flow experiments in steady-state condition. Courtesy of prof. Fraccarollo.

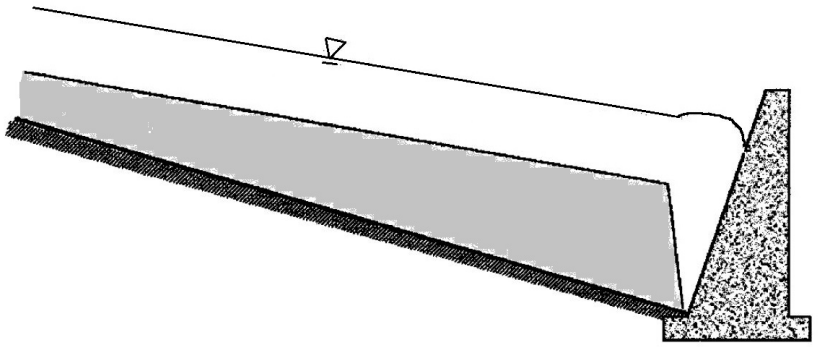

Figure 7.6: Bed profile observed upstream a slit check dam. Pricture edited from Armanini and Larcher (2001).

7.2.2 Gate-opening manoeuvre

Some other qualitative experiments were carried out in order to study the effects of a gradual gate-opening manoeuvre, considering multiple, subsequent partial-opening stages leading to totally free-surface flow conditions. This experiment was intended especially to verify the time duration necessary to flow and bed to adapt to the new boundary conditions. These experiments were carried out only considering sand sediments, which turn out to be the most significant in terms of time scale.

Experiments showed that adaptation processes are quite long as long as the gate is partially open (Figures 7.7(a) and 7.7(b)), while they are extremely rapid when the flow becomes a free-surface flow, i.e. flow depth is lower than the gate opening Figures 7.7(d), 7.7(e) and 7.7(f)). When the flow is free of constraints, the outflow solid discharge increases dramatically and the depos-

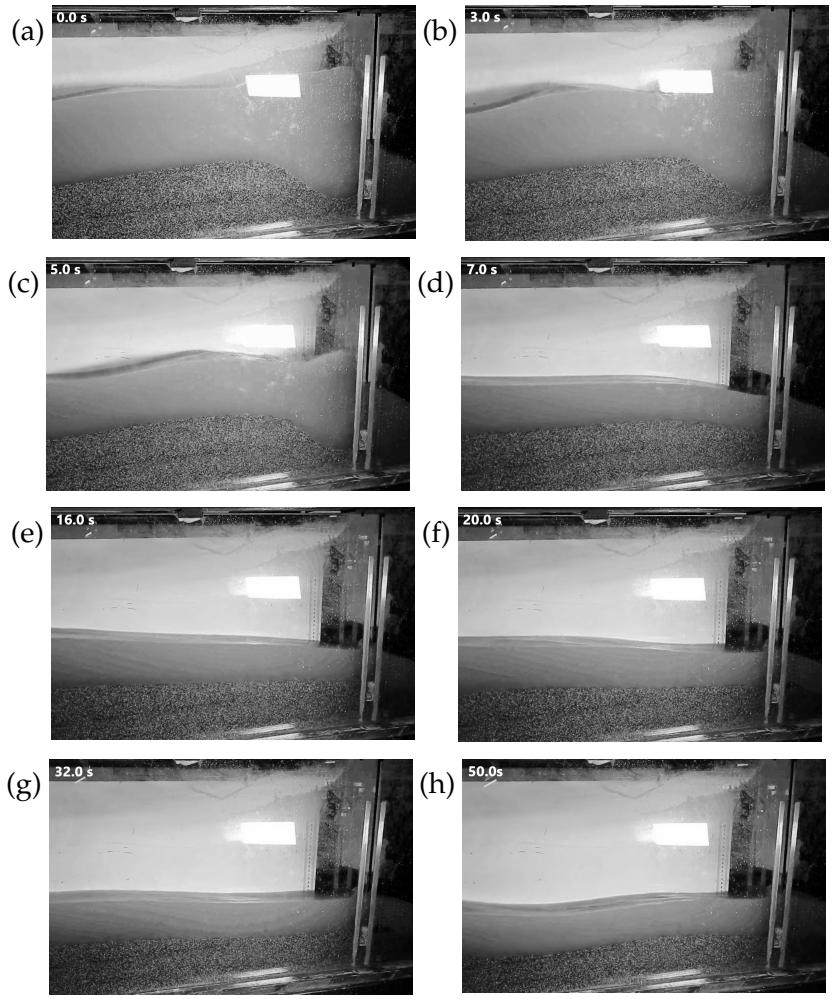

Figure 7.7: Gate lifting experiment with sand: from (a) a partial opening to (h) a total opening. Courtesy of Anna Prati.

ition that was observed just upstream the gate is quickly eroded (Figures 7.7(c)and 7.7(d)).

7.3 Modelling sluice gates over a mobile bed

Data collected during the experimental campaign show clearly that the bed evolution must be described as coupled with the gate hydrodynamics. This task appears not straightforward at all, especially if a depth-average approach is chosen and applied. In this Section a preliminary, very simplified approach was developed only to predict the bed configuration at the morphological equilibrium (see Section 7.2.1), once discharge and gate opening are

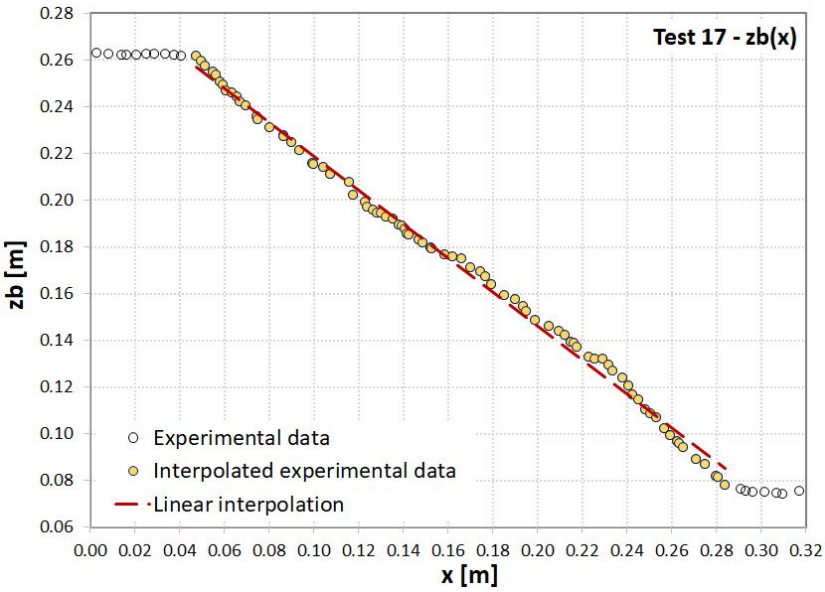

Figure 7.8: Bed profile near the sluice gate: experimental data (PVC) and their interpolation

fixed. Certainly, more detailed and demanding analyses should be carried out to study the dynamic effect of a gradual opening of the gate, however this goal goes beyond the purpose of this thesis.

7.3.1 Mathematical modelling

As a first step, experimental data provided by prof. Fraccarollo and Anna Prati were analysed by the author of this thesis for two purposes: the characterisation of the bed profile at morphological equilibrium and the verification of the validity of the relation 7.2 and of the C_q relations of Table 7.1.

As far as the bed profile is concerned, results obtained through stereoscopic imaging techniques were suitably processed, in order to identify some recurring profile pattern near the gate. For this purpose, non-moving particles were distinguished from the moving ones. Among the non-moving particles, the position of those placed at the upper bed bound was extracted and plotted, as shown in Figure 7.8. It must be noticed that this operation was performed manually, therefore it could be affected by a significant level of subjectivity and uncertainty. Points belonging to the steepest part of the profile were then linearly interpolated, to verify the presence of a common slope trend within the whole experimental set. Some of the results obtained with this proced-

Test	Material	$Q_{mix}\left[\frac{l}{s}\right]$	$a\,[m]$	$i_{F,gate}\,[-]$	$\alpha_{gate}\,[^\circ]$
1	PMMA	5.3	0.028	0.93	42.8
4	PMMA	5.3	0.055	0.76	37.3
6	PMMA	4.8	0.028	0.68	34.3
9	PMMA	4.8	0.045	0.81	39.0
16	PVC	6.0	0.040	0.78	38.0
17	PVC	12.0	0.090	0.73	36.1
18	PVC	12.0	0.095	0.79	38.3
21	PVC	12.0	0.105	0.77	37.6

Table 7.2: Data from some experimental tests about high-concentration flows over mobile bed controlled by sluice gates: bed slope near the gate.

ure are shown in Table 7.2, where $i_{F,gate}$ represents the slope of the steepest bed profile and α_{gate} the corresponding angle in degrees. Looking at the last column in the Table, it must be noticed that the slope angle computed near the gate are quite high and greater than the friction angles of the two materials (31° for PMMA spheres, 32° for PVC spheres). This result could be justified through the difficulty, during image processing, in identifying the right bed profile, i.e. particles whose velocity was almost zero. This identification was particularly problematic in PMMA experiments, since PMMA particles are very light (their density is about equal to $1200\,kgm^{-3}$) and they easily move into suspension because of turbulence. However, also the interpretation of the PVC experiments was partially affected by the same problem because of the particles density, equal to $1510\,kgm^{-3}$). On the basis of this consideration, it seems quite reasonable to assume that the slope of the steepest bed profile is about equal to the friction angle of the material. On the contrary, in the upper part of the flume uniform flow conditions were observed, therefore the slope of this zone can be computed according to uniform flow formulations and considering the two-phase nature of the flow. In this way, both upstream and downstream bed slope appear to be known.

On the basis of the experimental data available, a further important point was investigated, that is the validity of the C_q relations in the case of high-concentration flows over mobile bed. During the experimental campaign, measurements of discharge Q_{mix}, gate opening a and flow depth h_{gate} at the upstream side of the gate were collected. These values were then used by the author of this thesis to estimate the relevant values of discharge coefficient C_q from equation 7.2, being q and a known and substi-

tuting h_0 with h_{gate}:

$$C_q = \frac{q}{a\sqrt{2gh_{gate}}}$$

These values were then compared with the estimates produced by the formulations collected in Table 7.1, performing the same substitution. Only the relation proposed in Defina and Susin (2003) was disregarded, since the authors noticed that reliable results were obtained only for $a/h_0 > 0.3$, while the experiments considered in this Chapter were carried out especially for lower values of the ratio a/h_{gate}.

The comparison between the experimental estimate of C_q and the estimates obtained through formulations was carried out computing the percentage relative error for each experimental test. Results obtained for the 17 PVC experiments are plotted in Figure 7.9.

According to results obtained considering the whole set of experiments, it can be observed that all the considered formulations, except for the one of Rajaratnam and Subramanya (1967), give comparable results. Absolute relative errors are typically lower than 15% and often lower than 10%. Noutsopoulos and Fanariotis (1978) and Nago (1978) seem to produce slightly better results. However, accounting for the uncertainty in measurements, especially in those of h_{gate}, almost all the formulations considered in Table 7.1 can be applied straightforwardly to the case of gate-controlled high-concentration flows over mobile bed.

At this point, it is possible to estimate a further unknown of the problem, i.e. extent of the zone influenced by the gate. For this purpose, the 1D equations reported in Section 2.1.2.1 for QTP modelling were considered and the steady-state hypothesis introduced:

$$\begin{cases} \dfrac{\partial (hu)}{\partial x} = 0 & \text{(7.4a)} \\ \dfrac{\partial (chu)}{\partial x} = 0 & \text{(7.4b)} \\ \dfrac{\partial}{\partial x}\left[(1+c\Delta)\left(hu^2 + \dfrac{1}{2}gh^2\right)\right] + (1+c\Delta)\, gh\dfrac{\partial z_b}{\partial x} = -\dfrac{\tau_b}{\rho_w} & \text{(7.4c)} \end{cases}$$

These mass and momentum conservation equations were applied to the control volume depicted in Figure 7.10. In the schematisation, the raise in free-surface elevation was assumed to be linear.

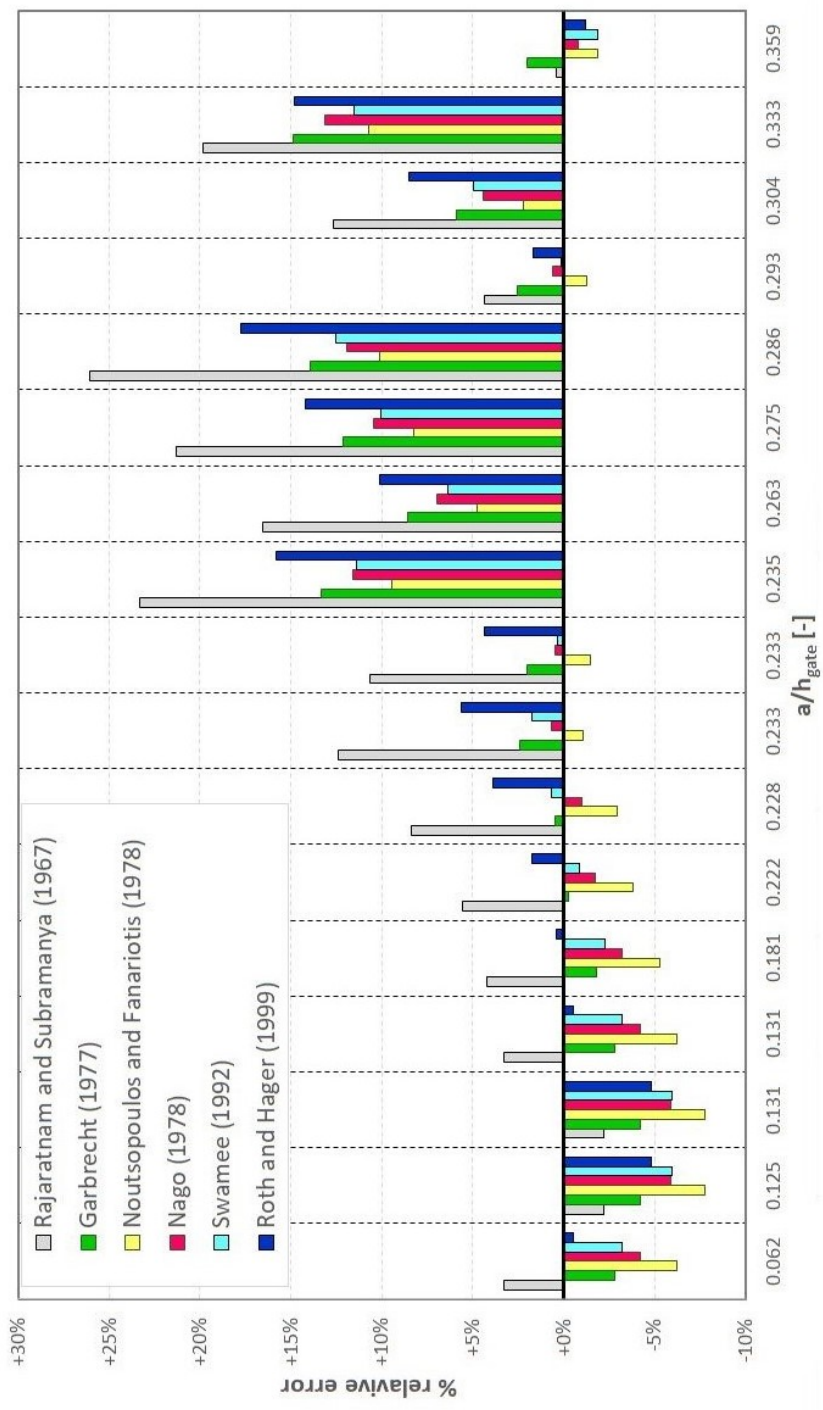

Figure 7.9: Comparison between C_q values obtained experimentally for gate-controlled high-concentration flows over mobile bed and estimates computed according to formulations of Table 7.1: percentage relative error of the PVC set of experiments.

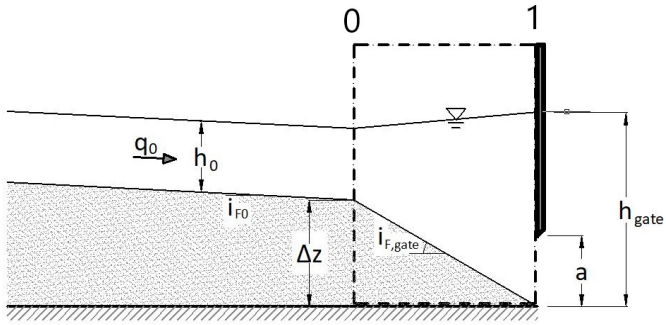

Figure 7.10: Schematisation of a gate-controlled high-concentration flow in steady-state condition over a mobile bed. The hatched line bounds the control volume used in the computations.

In steady-state conditions, mixture and solid mass balances 7.4a and 7.4b can be written as follows over the control volume, i.e. between sections 0 and 1 of Figure 7.10:

$$h_0 u_0 = h_1 u_1 = q_{mix} \tag{7.5}$$

$$c_0 h_0 u_0 = c_1 h_1 u_1 = q_{sol} \tag{7.6}$$

where h_0, u_0 and c_0 are respectively the flow depth, the velocity and the concentration of the upstream steady-state flow, which can be easily computed according to the equilibrium condition, once that q_{mix} and q_{sol} are known. On the other side, h_1, u_1 and c_1 are the flow depth, the average velocity and the average concentration referred to the gate section.

At this stage h_1, u_1 and c_1 are still unknown, however they can be easily quantified closing the problem with the sluice gate equation

$$q_{mix} = a C_q \sqrt{2 g h_1}$$

where C_q is expressed as a function of a and h_1 by means of one of the formulations of Table 7.1. Solving this equation, the h_l is no more an unknown. On this point, it must be noticed that, choosing one among Rajaratnam and Subramanya (1967) and Garbrecht (1977) or Noutsopoulos and Fanariotis (1978) formulations for C_q, an explicit relation can be obtained for h_1. Once h_1 is known, it can be used in equation 7.5 to obtain u_1. Moreover, c_1 can be obtained straightforwardly from equation 7.6, which gives $c_1 = c_0$.

Now, all the near-gate variables are known except for the depth Δz, which represents the height of the bed step shaped by gate effects (Figure 7.10). This variable can be estimated considering the momentum conservation equation, written in the

following form, neglecting shear stresses:

$$(1 + c_0\Delta)\left(\frac{1}{2}gh_0^2 + h_0u_0^2\right) + D_0 = (1 + c_1\Delta)\left(\frac{1}{2}gh_1^2 + h_1u_1^2\right) \quad (7.7)$$

where Δ is the submerged relative density, while D_0 represents the bed pressure term, to be evaluated in the 0 section, over the depth Δz. This last term should be evaluated taking into account the pressure distribution along the steepest slope. However, to date, no detailed information about the distribution is available. Therefore, some assumption were introduced, following the approach used in Rosatti and Fraccarollo (2006), in order to obtain some kind of estimate, although rough. Pressure distribution in the mixture was assumed to be linear and the pressure head was computed with reference to the free-surface level at the gate. Applying the expression proposed in Rosatti and Fraccarollo (2006), the pressure term was written as follows

$$D_0 = g\,(1 + c_0\Delta)\left(h_1 - \frac{\Delta z}{2}\right)\Delta z \quad (7.8)$$

Inserting this expression into the momentum balance 7.7 it is possible to solve the equation in the unknown Δz. In this way, the bed depth conditioned by the gate is known. According to the previous analyses, it can be reasonably assumed that $i_{F,gate} = \tan\Phi$. Therefore, also the horizontal extent X of the area which hydrodynamics is affected by the gate can be evaluated, simply assuming $X = \tan\Phi\Delta z$.

This approach was applied to estimate analytically Δz and X for the experimental test cases, assuming that only the variables values in the 0 section were known and using some of the relations previously investigated to estimate C_q. Results were then compared with Δz and X measurements. Analytical results generally underestimate the experimental values of Δz by 20%. Slightly more accurate results are obtained if the formulations of Noutsopoulos and Fanariotis (1978), Nago (1978) and Swamee (1992) are used in the estimate of h_1, while the the formulation of Rajaratnam and Subramanya (1967) gives the worst results, as expected (underestimation reaches the 60%). However, neglecting results obtained with the Rajaratnam and Subramanya (1967) formulation, analytical estimates appear definitely acceptable at the present of the knowledge.

7.3.2 Implementation in the TRENT2D-UTG model

Results obtained within these analyses may represent an important reference point for numerical modelling aimed at simulating gate-controlled high-concentration flows over a mobile bed. Using these results to set proper boundary or internal conditions at the gate location, not only steady but also unsteady gate-controlled flows could be simulated. For this reason, the possibility of simulating gate-controlled flows was introduced in the TRENT2D-UTG model. However, to date, gates can be located only at domain boundaries. In future, this constraint will probably be removed.

Usually, clear-water shallow-flow models for gate-controlled flows take into account the presence of the gate in three different ways (Cozzolino et al., 2015). The simplest approach is to consider the gate as located at the interface between two cells or at the outlet bound of the boundary cells and evaluate numerical fluxes according to the local flow depth and the sluice-gate equation 7.2. This approach is applied for example in Zhao et al. (1994) and in Cozzolino et al. (2015). Another option is the one used for example in Natale et al. (2004), which requires the evaluation of gate-influenced states upstream, under and downstream the gate. The last approach considers the gate equation coupled with the other equations, using the methods of characteristics. An example of this approach can be found in Jaafar and Merkley (2010).

Because of its simplicity, the first approach was used also in TRENT2D-UTG. The mass fluxes and the momentum fluxes at the gate are computed by means of the local values of the variables and assuming the flow as quasi 1D:

$$\mathbf{F}_{k,gate} = \begin{bmatrix} aC_q\sqrt{2gh_k} \\ c_k\left(aC_q\sqrt{2gh_k}\right) \\ (1+c_k\Delta)\left(\frac{1}{2}gh_k^2 + h_k u_{x,k}^2\right) \\ 0.0 \end{bmatrix} \tag{7.9}$$

The formulation of Noutsopoulos and Fanariotis (1978) was used to compute the discharge coefficient C_q.

The main question in this approach regards the estimate of the concentration c_k. In steady state conditions, concentration should remain constant in the gate-controlled area. This means that it can not be computed by means of transport capacity formulae according to the local values of the hydrodynamic variables.

Different strategies are therefore required. For example, concentration could be kept constant within the gate-controlled area, which extension along the flowing direction could be estimated according to the analytical approach proposed previously. In TRENT2D-UTG, this operation could be performed intervening either directly on the concentration values c_k or on the local value of the transport parameter β. In the latter case, β should assume different values at different locations in order to obtain suitable concentration values by means of the concentration closure relation. This second option seems to be less invasive, however it could cause the lost of hyperbolicity. This question is nothing but another, new complexity issue. Because of the novelty of the problem, it was decided to avoid its investigation in this work, since it appears as a quite demanding issue.

Therefore, in TRENT2D-UTG the problem was circumvented assuming that the gate-controlled boundary cells are large enough to contain the gate-controlled area. In this way, concentration at the gate can be assumed simply equal to the concentration in the upstream cell.

7.4 A realistic case study: simulating a sluice gate controlling sediment-routing in a hydropower reservoir

The TRENT2D-UTG model, upgraded with the sluice-gate boundary condition, was applied to a realistic case study concerning sediment-routing in a hydropower reservoir, with a sluice gate controlling outflow discharges. In particular, the gate was intended to regulate the discharges at the downstream section of the reservoir varying the gate opening in time. The gate regulation is planned in order to avoid too much high values of mixture discharge, which could hypothetically create problems to the river downstream of the reservoir. The gate-opening manoeuvre is set as a model input data.

The case study presented in this Section considers the test performed in Section 6.5 on a realistic morphology as starting point. This means that the domain morphology, the inflow boundary condition, the inflow mixture hydrograph and the model parameters are kept the same, while suitable outflow boundary conditions and further input data are supplied here for the gate section.

Details about these new elements are described in Section 7.4.1, while simulation results are presented in Section 7.4.2.

In this application, the new elements are set so that the outflow discharges are limited and the effects of the gate on the reservoir dynamics and on sediment-routing can be recognised.

Because of the variations in time of the inflow and outflow discharges, the gate opening, the free-surface elevation and the bed morphology, this problem appears markedly unsteady and justifies the use of a sophisticated mathematical and numerical model like TRENT2D-UTG to take into account all these complexity factors.

7.4.1 Model input data

The simulation described in this Section was carried out reusing the input data set for the test case presented in Section 6.5. Therefore, the reservoir and channel morphology was kept equal to the one shown in Figure 6.20; the computational mesh was exactly that one plotted in Figure 6.21; the inflow mixture hydrograph shown in Figure 6.24 was preserved, together with the assumption of uniform flow at the upstream bound of the domain; the values of the model parameters were not modified. Also the choice about the limiter computation was conserved.

The difference between the previous test and the current one lies entirely in the outflow boundary condition. In the previous case, the non-reflecting/critical boundary condition was imposed at the outflow section, i.e. at the end of the channel, for all the simulation duration. On the contrary, in this case study, two alternative boundary conditions were imposed at the outflow section. The first one represents the gate-control condition, assuming that the gate occupies the whole width of the channel section at the outlet bound and its opening can be regulated in time. The gate-control boundary condition coincides with the relations described by expression 7.9, with the discharge coefficient C_q computed according to Noutsopoulos and Fanariotis (1978). This condition is applied whenever the free-surface elevation next to the gate is higher than the gate opening. The second boundary condition is the non-reflecting/ critical boundary condition, already applied in the previous test case. This condition is used in case the flow depth near the gate is lower than the gate opening. Depending on the gate flow depth and opening, the model automatically switches from a condition to the other.

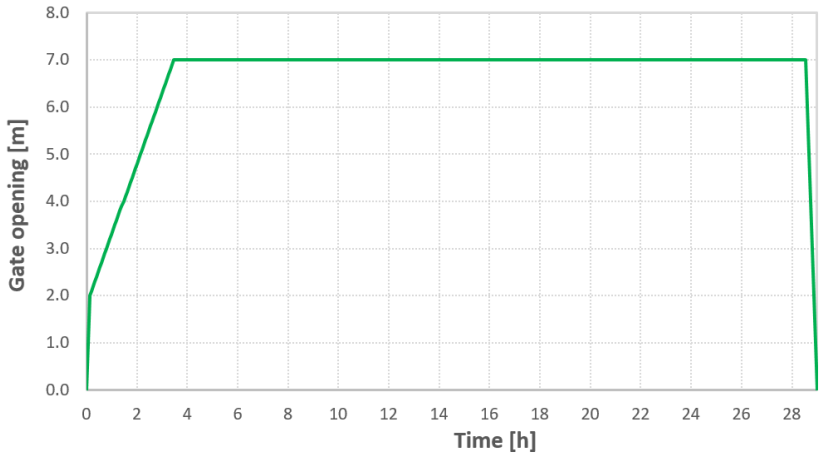

Figure 7.11: Gate manoeuvre: gate openings in time.

The gate opening is set by the user, supplying a suitable manoeuvre file, which describes gate-opening variations in time. For the purposes of this work, the gate was assumed to be initially closed, then it was supposed to be lifted and kept open for almost the entire simulation. It was closed only towards the end of the falling limb of the inflow hydrograph.

The opening manoeuvre was planned according to a couple of criteria:

- avoiding excessive outflow discharges, i.e. maintaining the discharge below the peak value of the inflow hydrograph;
- reaching the free-surface condition quite quickly, in order to avoid the formation of the bed step near the gate, i.e. to be sure that the opening manoeuvre is faster than the bed-step formation process, which is not properly simulated by the model so far.

According to these criteria, the manoeuvre shown in Figure 7.11 was set, which considers both a opening and a closing stage. As the simulation starts, the gate was supposed to be lifted with a velocity of about $0.25\,\mathrm{m\,min^{-1}}$ for the first 8 minutes; then, the velocity was decreased to $0.025\,\mathrm{m\,min^{-1}}$ for the following 200 minutes. In this way, the final gate opening was equal to 7 m, after about 3 hours and a half from the beginning of the manoeuvre. Then, the gate opening was kept constant for almost the entire duration of the simulation. When the inflow discharge dropped below the threshold of $50\,\mathrm{m^3 s^{-1}}$ on the falling limb of the hydrograph, the gate closing manoeuvre eas started. It must

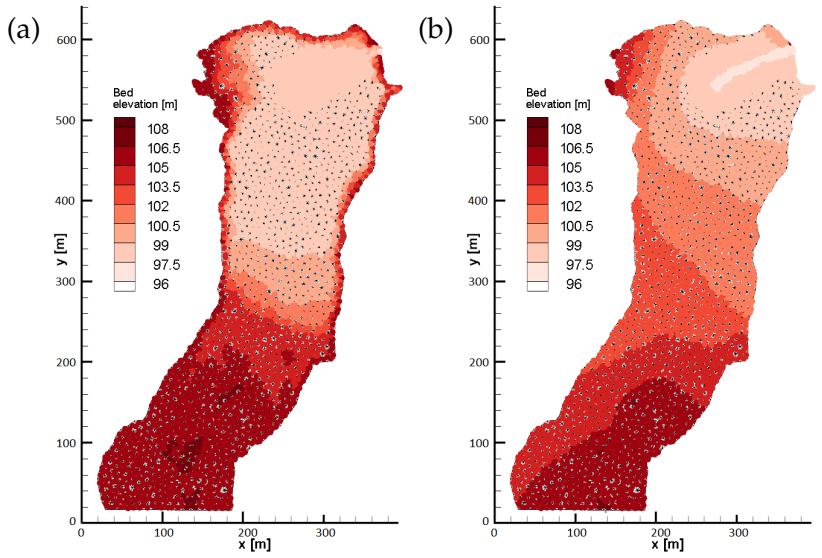

Figure 7.12: (a) Initial and (b) final condition of the bed elevation of the reservoir before and after the TRENT2D-UTG simulation with gate control

be noticed that the value of the discharge threshold value was chosen arbitrarily, just to avoid an excessive reservoir emptying. The closing velocity was set equal to 0.25 m min^{-1}, making the gate completely closed after only 28 minutes.

With these data, a TRENT2D-UTG simulation was run. Results are presented in the next Section.

7.4.2 Model results

Figure 7.12 shows a comparison between the initial and the final state of the reservoir bed elevation. The sediment-routing phenomenon appears quite clear, as for the test of the previous Chapter. However, the final condition is slightly different from that one observed in the previous Chapter, as shown by the comparison of Figure 7.13. The two simulation produce different final bed morphology, especially in the central part of the domain. This difference arises from the morphodynamic processes observed in the first couple of hours, which are different in the two simulations because of the different boundary conditions. In the case study without gate control (Section 6.5), intense erosion process were observed in the channel and a significant fraction of moving sediments was canalised and delivered to the outflow section since the first timesteps. On the contrary, in the current simulation, sediment deposition was observed in the channel as long as the gate was controlling the flow and outflow mixture and

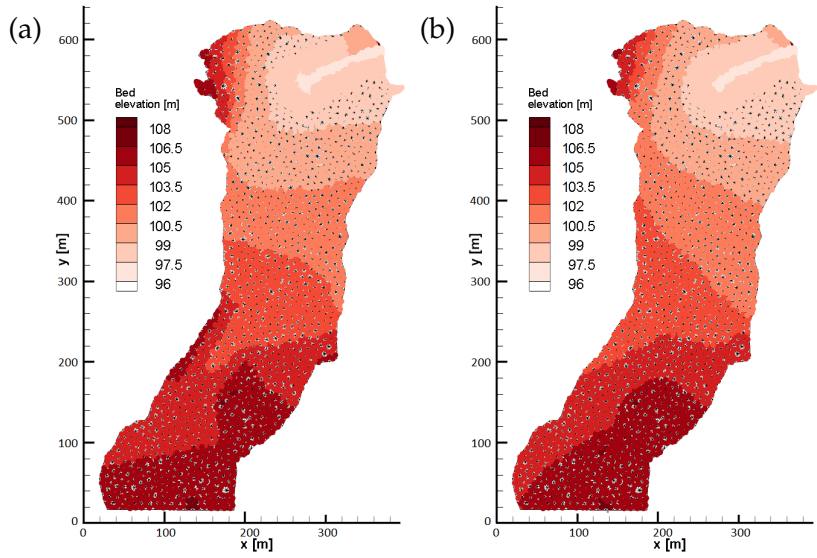

Figure 7.13: Bed elevation inside the reservoir, after the TRENT2D-UTG simulation (a) without gate control and (b) with gate control

solid discharges turned out to be significantly limited by the gate. As a consequence, moving sediments were deposited right inside the reservoir, modifying the domain morphology especially in the downstream part of the domain. Such modification conditioned all the following sediment-routing processes, leading to the morphological state shown in Figure 7.13(b). The effect of the gate on the final bed morphology can be appreciated also through the comparison shown in Figure 7.14, where the difference between the initial and final bed elevation is shown for both the simulation, i.e. without and with gate control.

The effects of the gate on the outflow discharge can be clearly recognised analysing the outflow hydrograph, which is shown in Figure 7.15 together with the inflow hydrograph. In the simulation without the gate, the outflow hydrograph shows a first peak discharge of about $190\,m^3s^{-1}$, which is higher than the peak discharge of the inflow hydrograph. On the contrary, the gate-controlled simulation gives a first peak with a peak discharge value of about $110\,m^3s^{-1}$.

When the gate effect ends, the two outflow mixture hydrographs become overlapped. However, although outflow discharges become similar, the two outflow hydrographs differ in terms of sediment concentration. In both the simulations, outflow sediment concentration is quite high at the very beginning of the simulation, while it decreases during the remaining part of the simulation. However, on average, concentration values in

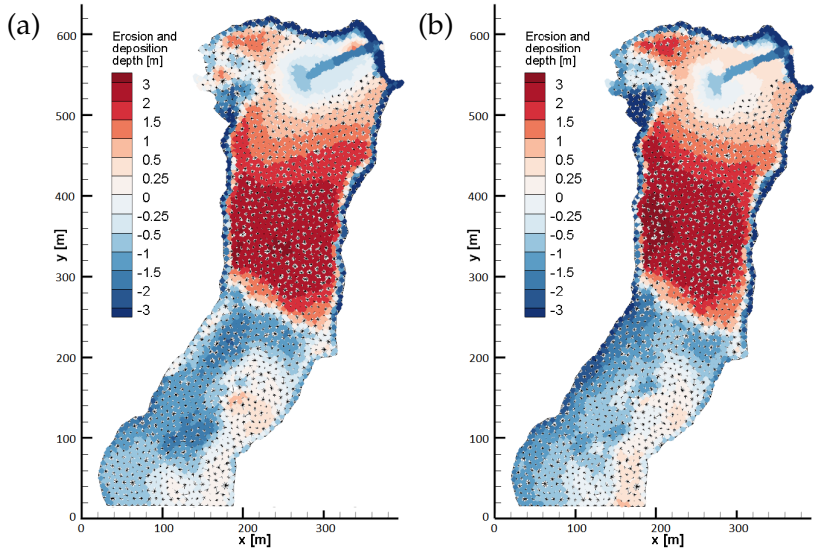

Figure 7.14: Erosion (blue) and deposition (red) depths in the reservoir, after the TRENT2D-UTG simulation (a) without gate control and (b) with gate control.

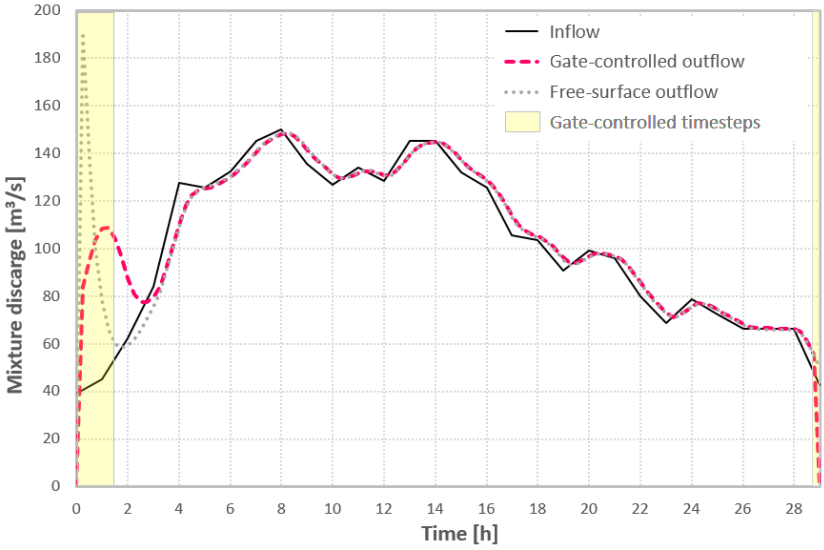

Figure 7.15: Hydropower reservoir: inflow and outflow hydrographs, obtained for the simulations without and with gate control.

the gate-controlled simulation appear slightly higher than those observed in the simulation without the gate. Only during the initial timesteps the situation is reversed. This observation is clearly pointed out by the graph of Figure 7.16, where the cumulative volume of outflow sediments are plotted in time for the two case studies. Except for the very first part of the simulation, the outflow volume in the gate-control case appears always higher than the outflow volume in the case without the gate and the differ-

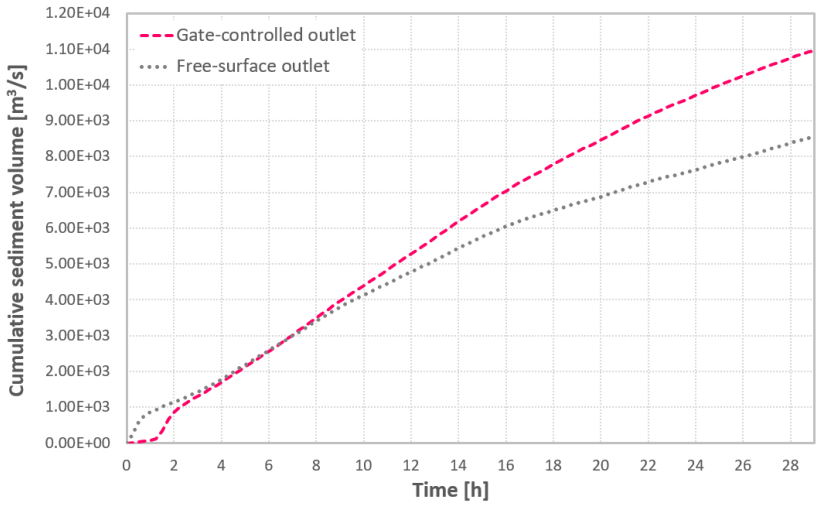

Figure 7.16: Cumulative volume of outflow sediments, obtained for the simulations without and with gate control.

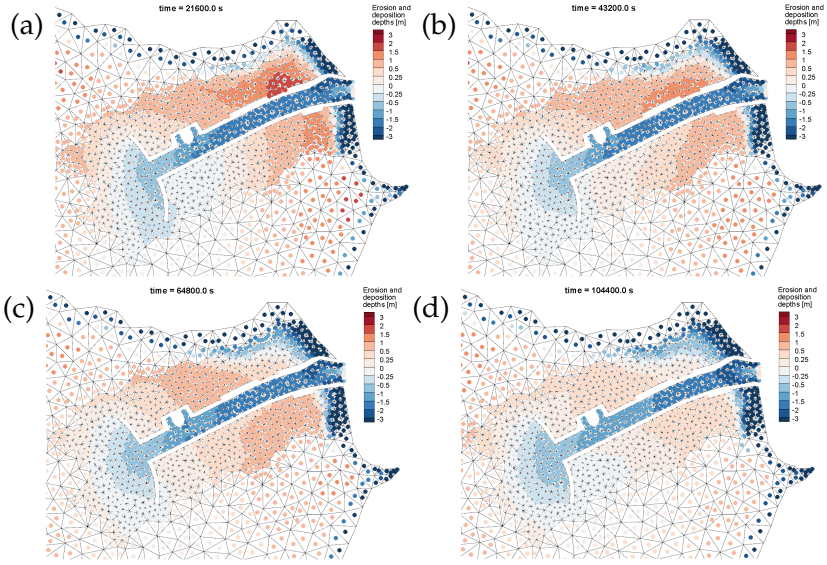

Figure 7.17: Erosion (blue) and deposition (red) depths in the refined area near the reservoir outlet in the gate-controlled case: center cell values for (a) $t = 6h$, (b) $t = 12h$, (c) $t = 18h$ and (d) $t = 29h$.

ence increases in time, also when the gate is no more actively controlling the flow.

The effect of the gate can be recognised also in the channel area, next to the outlet section. Looking at the refined area (Figure 7.17), erosion processes appear not so intense as in the simulation without the gate. The difference appears more evident outside than inside the channel.

In conclusion, according to the upgraded version of TRENT2D-

UTG, the effects of the gate appear quite recognisable for the simulated manoeuvre. It is worth noting that different gate manoeuvre could produce different results, since the effect of the gate on the bed morphology and the sediment-routing dynamics is expected to vary according to opening stages and velocity. Certainly, so far the model does not take into account the 3D effects observed during the experimental campaign and described in this Chapter, because of the obstacles highlighted in the previous Sections. Further analyses should be carried out experimentally and from a mathematical and numerical point of view to account for the whole phenomenon complexity and reach a higher lever of detail in the representation. However, results obtained in this Chapter with a quite simple approach show that some effect of the gate is anyhow taken into account, not only from a hydrodynamic point of view but also for what concerns the global influence on bed morphology.

Chapter 8

Troubles with numerical mass fluxes in TRENT2D: an open issue

One of the most important rules to abide by in natural-hazard modelling is avoiding non-physical solutions or at least solutions that disagree with the hypotheses introduced at the basis the model. This principle applies to both mathematical and numerical modelling.

Certainly, controlling all the possible sources of inconsistent results is not an easy task. A detailed knowledge is required about the phenomenon, the mathematical model and the numerical model. Knowledge helps in identifying inconsistencies, which are not always evident, in finding out their source and, possibly, in fixing the problem, in order to ensure a proper representation of the phenomenon. However, in general, the more sophisticated the model is, the more challenging the task is. For this reason, inconsistencies remain sometimes open or even hidden.

In this Chapter, one of these open issues is discussed. It was identified dealing with the TRENT2D model and its numerical solvers. In fact, some real-world applications of the model, included those presented in Chapter 4, showed an occasional inconsistency in the computation of the numerical mass fluxes at cell interfaces, i.e. solving the Riemann Problems. The inconsistency regarded the sign of mixture-mass flux, that sometimes appeared to be opposite to the sign of the solid-mass flux. This occurrence clashes with the isokinetic hypothesis which the model is based on.

This issue was observed with all the solvers available for TRENT2D, and also with Osher-type solvers (personal communication of Daniel Zugliani, PhD). Therefore, it seems not strictly related to the type of solver.

This observation brought first to the analysis the problem itself (Section 8.1), in order to characterise its manifestation and identify the cause of the inconsistency. The work was not very straightforward, since this fluxes inconsistency does not produce macroscopic effects, i.e. strange behaviours visible to the naked eye. Furthermore, the results of the analysis did not appear sufficient, so some further investigation was carried out, focusing on the numerical solvers that led to the inconsistency (Section 8.2). Attention was paid to the GR solvers because of their higher accuracy in reproducing RP solutions, while the LHLL solver was disregarded. However, although thorny analyses were carried out, no satisfying answer was found and, to date, the issue appears still open (Section 8.3).

8.1 Analysis of the problem

As a first step, a set of 30 Riemann Problems (RPs) leading to inconsistency with both the LHLL and the GR solvers was assembled and analysed, in order to find some recurring pattern and facilitate the identification of the inconsistency source. Among these 30 RPs, also some very simple problems were considered, i.e problems where tangential velocity was equal to zero and bed shear stresses were neglected.

Initially, it was supposed that the problem was caused by opposite velocity directions in the left L and right R states of the RPs, but the first analyses showed that this was seldom the case. Therefore, initial values of the RPs primitive variables were carefully scrutinised, looking at bed-step heights, gaps between L and R free-surface elevations, velocity directions and concentration values, ranges of variables variation. Some of the analysed configurations are sketched in Figure 8.1. However, no recurring trend was found, except for the concentration values, which were typically quite low and sometimes out of the soundness range of the model. On the other side, the inconsistency was observed both with high and low values of the variables, with ascending and descending bed steps, with flat bed, with or without tangential velocity.

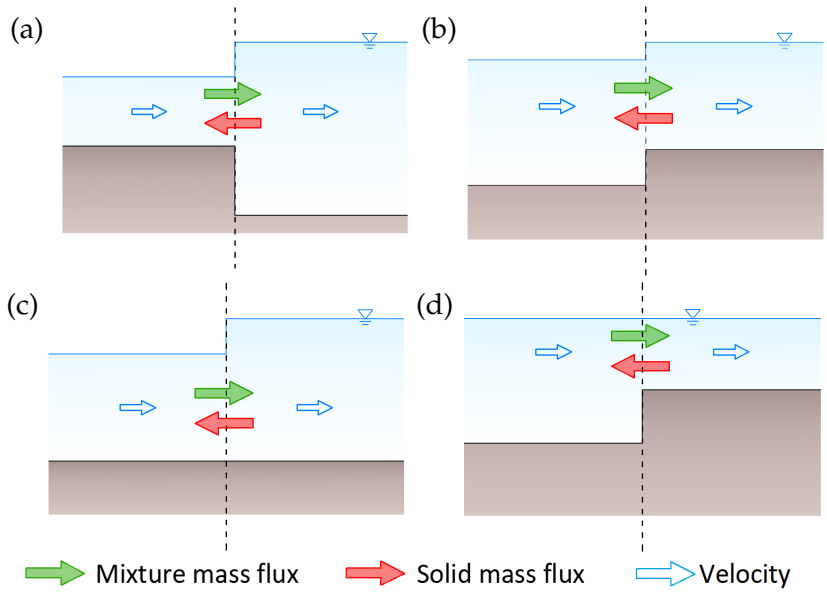

Figure 8.1: Some RP configurations leading to numerical flux inconsistency with the LHLL and the GR solvers.

Further analyses were carried out considering the wave structure of the exact solution obtained for these 30 RPs, always looking for a possible recursive pattern. This investigation showed that typically the second wave is a rather slow rarefaction wave, while the other waves could be either rarefaction waves or shocks. Furthermore, in most cases, the sign of the velocity changed across the wave field. However, no other significant clues were found and the only available observations appear not sufficient to characterise univocally the problem. This outcome represents an obstacle towards the solution of the problem, since it is not possible to identify a priori the issue.

For this reason, a different, more general strategy was considered, investigating possible numerical sources of the problem.

8.2 Dealing with possible numerical sources

Analysing some of the 30 RPs, it was observed that sometimes the fluxes inconsistency occurred only if the problem was solved with the CIGR solver, while it disappeared solving the same problem with the SCGR solver. On the strength of this outcome, further analyses were carried out considering only these two GR solvers. Unlike the LHLL scheme, they do not approximate the wave structure of the solution with a-priori hypotheses

on the type of waves, but rather they are in keeping with the real structure of the solution. In particular, the new analyses were focused first on the term signs in the GR Jacobian matrices (Section 8.2.1) and then on the choice of the multiple averages (Section 8.2.2).

As presented in Section 3.2.2, GR solvers require the computation of the matrix $\mathcal{A}_n$, which can be expressed through the Jacobian matrices $\mathbf{J}_{\mathbf{F_n}}$ and $\mathbf{J}_{\mathbf{U_n}}$. The general expressions of these matrices are written hereafter:

$$\mathbf{J}_{\mathbf{F_n}} = \begin{bmatrix} u_n & h & 0 & 0 \\ cu_n + hu_n\dfrac{\partial c}{\partial h} & ch + hu_n\dfrac{\partial c}{\partial u_n} & hu_n\dfrac{\partial c}{\partial u_t} & 0 \\ (1+c\Delta)\left(gh+u_n^2\right)+ \Delta\left(\frac{1}{2}gh^2+hu_n^2\right)\dfrac{\partial c}{\partial h} & 2(1+c\Delta)hu_n+ \Delta\left(\frac{1}{2}gh^2+hu_n^2\right)\dfrac{\partial c}{\partial u_n} & \Delta\left(\frac{1}{2}gh^2+hu_n^2\right)\dfrac{\partial c}{\partial u_t} & 0 \\ (1+c\Delta)u_nu_t+ \Delta hu_nu_t\dfrac{\partial c}{\partial h} & (1+c\Delta)hu_t+ \Delta hu_nu_t\dfrac{\partial c}{\partial u_n} & (1+c\Delta)hu_n+ \Delta hu_nu_t\dfrac{\partial c}{\partial u_t} & 0 \end{bmatrix} \tag{8.1}$$

$$\mathbf{J}_{\mathbf{U_n}} = \begin{bmatrix} 1 & 0 & 0 & 1 \\ c + h\dfrac{\partial c}{\partial h} & h\dfrac{\partial c}{\partial u_n} & h\dfrac{\partial c}{\partial u_t} & c_b \\ (1+c\Delta)u_n+ \Delta hu_n\dfrac{\partial c}{\partial h} & (1+c\Delta)h+ \Delta hu_n\dfrac{\partial c}{\partial u_n} & \Delta hu_n\dfrac{\partial c}{\partial u_t} & 0 \\ (1+c\Delta)u_t+ \Delta hu_t\dfrac{\partial c}{\partial h} & \Delta hu_t\dfrac{\partial c}{\partial u_n} & (1+c\Delta)h+ \Delta hu_t\dfrac{\partial c}{\partial u_t} & 0 \end{bmatrix} \tag{8.2}$$

These are exactly the matrices considered by the CIGR solver for the application of the multiple-average approach. Choosing for example the following average states for the primitives variables

$$\widetilde{\mathbf{W}_n} = \begin{bmatrix} \widetilde{h} \\ \widetilde{u_n} \\ \widetilde{u_t} \\ \widetilde{z_b} \end{bmatrix} = \frac{1}{2}\begin{bmatrix} h_L + h_R \\ u_{nL} + u_{nR} \\ u_{tL} + u_{tR} \\ z_{bL} + z_{bR} \end{bmatrix} \tag{8.3}$$

the procedure described in Section 3.2.2 was applied. With these average states, only three equations were satisfied: the first con-

cerning $\mathbf{J}_{\mathbf{F_n}}$ and the first and the third concerning $\mathbf{J}_{\mathbf{U_n}}$. Therefore, five unknowns were chosen to populate the sets M_A and M_B: $\widehat{hu_n}$, $\widehat{\frac{1}{2}gh^2 + hu_n^2}$, $\widehat{hu_n u_t}$, $\breve{h}$ and $\widetilde{hu_t}$. Their expression are reported hereafter:

$$\breve{h} = \frac{(\widetilde{c} - \overline{c})(h_R - h_L) + \widetilde{h}(c_R - c_L)}{E}$$

$$\widehat{hu_n} = \frac{(\widetilde{c} - \overline{c})(h_R u_{nR} - h_L u_{nL}) + \widetilde{hu_n}(c_R - c_L)}{E}$$

$$\widetilde{hu_t} = \frac{(\widetilde{c} - \overline{c})(h_R u_{tR} - h_L u_{tL}) + \widetilde{hu_t}(c_R - c_L)}{E}$$

$$\widehat{\frac{1}{2}gh^2 + hu_n^2} = \frac{(\widetilde{c} - \overline{c})\left(h_R u_{nR} u_{tR} - h_L u_{nL} u_{tL}\right) + \frac{1}{2}(c_R - c_L)\left(h_R u_{nR} u_{tR} + h_L u_{nL} u_{tL}\right)}{E}$$

$$\widehat{hu_n u_t} = \frac{(1 + \Delta c_R) h_R u_{nR} u_{tR} - (1 + \Delta c_L) h_L u_{nL} u_{nL} - (1 + \overline{c}\Delta)\left(\widetilde{u_n}\widetilde{u_t}\Delta_1 - \widetilde{hu_t}\Delta_2 - \widetilde{hu_n}\Delta_3\right)}{E\Delta}$$

where

$$c_L = c\left(h_L, u_{nL}, u_{nL}\right); \quad c_R = c\left(h_R, u_{nR}, u_{nR}\right);$$

$$\widetilde{c} = 0.5\left(c_L + c_R\right); \qquad \overline{c} = c\left(\tilde{h}, \tilde{u_n}, \tilde{u_t}\right);$$

$$\Delta_1 = h_R - h_L; \qquad \Delta_2 = u_{nR} - u_{nL};$$

$$\Delta_3 = u_{tR} - u_{tL}; \qquad E = \left.\frac{\partial c}{\partial h}\right|_{\widetilde{\mathbf{W_n}}} \Delta_1 + \left.\frac{\partial c}{\partial u_n}\right|_{\widetilde{\mathbf{W_n}}} \Delta_2 + \left.\frac{\partial c}{\partial u_t}\right|_{\widetilde{\mathbf{W_n}}} \Delta_3.$$

These quantities, together with the vector $\widetilde{\mathbf{W_n}}$, can be used to compute the matrix $\mathcal{A}_n$ and the inter-cell fluxes.

Differently from the CIGR, the SCGR solver considers $\mathbf{J}_{\mathbf{F_n}}$ and $\mathbf{J}_{\mathbf{U_n}}$ Jacobian matrices where the concentration derivatives are substituted with their exact expression, according to the TRENT2D closure $c = c_b\beta\left(u_n^2 + u_t^2\right)/(gh)$:

$$\mathbf{J_{F_n}} = \begin{bmatrix} u_n & h & 0 & 0 \\ 0 & \frac{c_b\beta}{g}\left(3u_n^2+u_t^2\right) & 2\frac{c_b\beta}{g}u_nu_t & 0 \\ (gh+u_n^2)+\frac{1}{2}c_b\beta\Delta\left(u_n^2+u_t^2\right) & (2+\Delta c_b\beta)hu_n+2\Delta\frac{c_b\beta}{g}u_n\left(2u_n^2+u_t^2\right) & 2\Delta\frac{c_b\beta}{g}u_t\left(\frac{1}{2}gh+u_n^2\right) & 0 \\ u_nu_t & u_t\left(h+\Delta\frac{c_b\beta}{g}\left(3u_t^2+u_n^2\right)\right) & u_n\left(h+\Delta\frac{c_b\beta}{g}\left(u_n^2+3u_t^2\right)\right) & 0 \end{bmatrix} \tag{8.4}$$

$$\mathbf{J_{U_n}} = \begin{bmatrix} 1 & 0 & 0 & 1 \\ 0 & 2\frac{c_b\beta}{g}u_n & 2\frac{c_b\beta}{g}u_t & c_b \\ u_n & h+\Delta\frac{c_b\beta}{g}\left(3u_n^2+u_t^2\right) & 2\Delta\frac{c_b\beta}{g}u_nu_t & 0 \\ u_t & 2\Delta\frac{c_b\beta}{g}u_nu_t & h+\Delta\frac{c_b\beta}{g}\left(u_n^2+3u_t^2\right) & 0 \end{bmatrix} \tag{8.5}$$

Also in this case, the multiple-average procedure was applied, starting from the same averaged vector of primitive variables $\widetilde{\mathbf{W_n}}$, but introducing also other convenient average variables, set according to a trial-and-error procedure (Rosatti and Begnudelli, 2013b). Once again, five equations were not satisfied, therefore five unknowns were identified. The set of unknowns and supporting variables is listed hereafter:

$$\widetilde{u_n^2} = \frac{u_{nR}^2+u_{nL}^2}{2}; \qquad \widetilde{u_t^2} = \frac{u_{tR}^2+u_{tL}^2}{2};$$

$$\overline{u_n^2} = u_{nL}^2+u_{nR}^2-u_{nL}u_{nR}; \quad \overline{u_t^2} = u_{tL}^2+u_{tR}^2-u_{tL}u_{tR};$$

$$\widehat{u_n} = \sqrt{u_{nL}u_{nR}}; \qquad \widehat{u_t} = \sqrt{u_{tL}u_{tR}};$$

$$\widehat{u_nu_t} = \frac{u_{nL}u_{tL}+u_{nR}u_{tR}}{2};$$

$$\breve{u_n^2} = \frac{u_{nL}^2+u_{nR}^2+u_{nL}u_{nR}}{3}; \quad \breve{u_t^2} = \frac{u_{tL}^2+u_{tR}^2+u_{tL}u_{tR}}{3}.$$

These terms are intended to be substituted in the Jacobian matrices as shown hereafter:

$$\mathbf{J_{F_n}} = \begin{bmatrix} \widetilde{u_n} & \widetilde{h} & 0 & 0 \\ 0 & \frac{c_b\beta}{g}\left(3\widetilde{u_n^2} + \widetilde{u_t^2}\right) & 2\frac{c_b\beta}{g}\widehat{u_n u_t} & 0 \\ \left(g\widetilde{h} + \widetilde{u_n^2}\right) + \frac{1}{2}c_b\beta\Delta\left(\widetilde{u_n^2} + \widetilde{u_t^2}\right) & \left(2\widetilde{u_n} + \Delta c_b\beta\widehat{u_n}\right)\widetilde{h} + 2\Delta\frac{c_b\beta}{g}\widehat{u_n}\left(2\widetilde{u_n^2} + \widetilde{u_t^2}\right) & 2\Delta\frac{c_b\beta}{g}\widehat{u_t}\left(\frac{1}{2}g\widetilde{h} + \widetilde{u_n^2}\right) & 0 \\ \widehat{u_n u_t} & \widehat{u_t}\left(\widetilde{h} + \Delta\frac{c_b\beta}{g}\left(3\widetilde{u_t^2} + \widetilde{u_n^2}\right)\right) & \widehat{u_n}\left(\widetilde{h} + \Delta\frac{c_b\beta}{g}\left(\widetilde{u_n^2} + 3\widetilde{u_t^2}\right)\right) & 0 \end{bmatrix} \tag{8.6}$$

$$\mathbf{J_{U_n}} = \begin{bmatrix} 1 & 0 & 0 & 1 \\ 0 & 2\frac{c_b\beta}{g}\widetilde{u_n} & 2\frac{c_b\beta}{g}\widetilde{u_t} & c_b \\ \widetilde{u_n} & \widetilde{h} + \Delta\frac{c_b\beta}{g}\left(3\widetilde{u_n^2} + \widehat{u_t^2}\right) & 2\Delta\frac{c_b\beta}{g}\widehat{u_n u_t} & 0 \\ \widetilde{u_t} & 2\Delta\frac{c_b\beta}{g}\widehat{u_n u_t} & \widetilde{h} + \Delta\frac{c_b\beta}{g}\left(\widehat{u_n^2} + 3\widetilde{u_t^2}\right) & 0 \end{bmatrix} \tag{8.7}$$

Comparing the Jacobian obtained by means of the two GR approaches, very similar matrices should be obtained. In particular, the matrix terms of the CIGR matrices are expected to have the same sign observed in the SCGR matrices for the same terms. Furthermore, zero terms of the SCGR matrices are expected to be zero also in the CIGR matrices. However, when the numerical-fluxes inconsistency is observed, these are not always the cases. This result was taken into account as a possible source of inconsistency and possible ad hoc solutions were studied, as reported in the next Sections.

8.2.1 Sign analysis and possible constraints on zero-value terms

Because of the occasional sign discordance between the CIGR and SCGR matrices in case of numerical-fluxes inconsistency, an analysis was carried out to identify which are the expected signs of the terms in $\mathbf{J_{F_n}}$ and $\mathbf{J_{U_n}}$. For this purpose, the SCGR matrices were taken into account as reference matrices, since they are obtained for the specific concentration closure relation implemented in the TRENT2D model. In the matrices, the only variables that can

assume both positive and negative values are the velocities u_n and u_t. Starting from this observation, it was possible to identify some terms that are necessarily positive and other which sign depends on the velocity sign. Matrices 8.8 and 8.9 show the result of the sign analysis:

$$\text{sign}\left(\mathbf{J}_{\mathbf{F_n}}\right) = \begin{bmatrix} \text{sign}\left(u_n\right) & > 0 & = 0 & = 0 \\ = 0 & > 0 & \text{sign}\left(u_n u_t\right) & = 0 \\ > 0 & \text{sign}\left(u_n\right) & \text{sign}\left(u_t\right) & = 0 \\ \text{sign}\left(u_n u_t\right) & \text{sign}\left(u_t\right) & \text{sign}\left(u_n\right) & = 0 \end{bmatrix} \tag{8.8}$$

$$\text{sign}\left(\mathbf{J}_{\mathbf{U_n}}\right) = \begin{bmatrix} = 1 & = 0 & = 0 & = 1 \\ = 0 & \text{sign}\left(u_n\right) & \text{sign}\left(u_t\right) & = c_0 \\ \text{sign}\left(u_n\right) & > 0 & \text{sign}\left(u_n u_t\right) & = 0 \\ \text{sign}\left(u_t\right) & \text{sign}\left(u_n u_t\right) & > 0 & = 0 \end{bmatrix} \tag{8.9}$$

Comparing these matrices with the CIGR matrices computed for the inconsistency cases, it was shown that sometimes there was no full agreement between the matrices. In particular, in the CIGR matrices it was observed that:

1) the derivative of the solid mass flux *chu* with respect to *h* was always different from zero, while it is necessarily equal to zero in the SCGR matrix;

2) similarly, the derivative of the conserved variable $ch + c_b z_b$ with respect to *h* was always different from zero, although this term is zero in the SCGR;

3) among the 30 RPs, in seven cases some of the signs of the CIGR terms depending on the velocity sign were opposite to those expected. This outcome was observed in the following terms: the u_t derivative of the solid-mass flux, the u_t derivative of the momentum flux in the velocity derivatives of the third and the fourth conserved variables.

Since the third point was observed only for some of the test cases, it was considered not very relevant. On the contrary, an attempt was made to fix the other two points, simply forcing the two critical terms of CIGR matrices to be identically equal to zero. However, this solution did not lead to the expected outcome and

the fluxes inconsistency was not resolved. Therefore, a further different approach was used, based on a different choice of the unknown averages. The new analysis is discussed in the next Section.

8.2.2 The choice of the unknowns averages

Since the only constraint on the zero terms turned out to be not sufficient to fix the problem, a further attempt was made choosing the unknown averages differently from what presented previously. This modification was added to the constraint on the zero terms.

As a first attempt, the set M_A was populated with the unknown averages $\widehat{u_n}$, $\widehat{u_t}$ and $\widehat{u_n^2}$, identified as follows in the $\mathbf{J_{F_n}}$ CIGR matrix:

$$\mathbf{J_{F_n}} = \begin{bmatrix} u_n & h & 0 & 0 \\ 0 & ch + h\widehat{u_n}\dfrac{\partial c}{\partial u_n} & h\widehat{u_n}\dfrac{\partial c}{\partial u_t} & 0 \\ (1+c\Delta)\left(gh + \widehat{u_n^2}\right) + \Delta\left(\frac{1}{2}gh^2 + h\widehat{u_n^2}\right)\dfrac{\partial c}{\partial h} & 2(1+c\Delta)hu_n + \Delta\left(\frac{1}{2}gh^2 + h\widehat{u_n^2}\right)\dfrac{\partial c}{\partial u_n} & \Delta\left(\frac{1}{2}gh^2 + h\widehat{u_n^2}\right)\dfrac{\partial c}{\partial u_t} & 0 \\ (1+c\Delta)u_n\widehat{u_t} + \Delta hu_n\widehat{u_t}\dfrac{\partial c}{\partial h} & (1+c\Delta)h\widehat{u_t} + \Delta hu_n\widehat{u_t}\dfrac{\partial c}{\partial u_n} & (1+c\Delta)hu_n + \Delta hu_n\widehat{u_t}\dfrac{\partial c}{\partial u_t} & 0 \end{bmatrix} \tag{8.10}$$

The other terms of the matrix were computed according to the averages collected in the vector $\widetilde{\mathbf{W_n}}$, included c and its derivatives.

The set M_B was populated with the unknown averages $\breve{u_n}$ and $\breve{u_t}$, identified as follows:

$$\mathbf{J_{U_n}} = \begin{bmatrix} 1 & 0 & 0 & 1 \\ c + h\dfrac{\partial c}{\partial h} & h\dfrac{\partial c}{\partial u_n} & h\dfrac{\partial c}{\partial u_t} & c_b \\ (1+c\Delta)\breve{u_n} + \Delta h\breve{u_n}\dfrac{\partial c}{\partial h} & (1+c\Delta)h + \Delta h\breve{u_n}\dfrac{\partial c}{\partial u_n} & \Delta h\breve{u_n}\dfrac{\partial c}{\partial u_t} & 0 \\ (1+c\Delta)\breve{u_t} + \Delta h\breve{u_t}\dfrac{\partial c}{\partial h} & \Delta h\breve{u_t}\dfrac{\partial c}{\partial u_n} & (1+c\Delta)h + \Delta h\breve{u_t}\dfrac{\partial c}{\partial u_t} & 0 \end{bmatrix} \tag{8.11}$$

Also in this case the other terms of the matrix were computed according to $\widetilde{\mathbf{W_n}}$.

The expressions of these new unknown terms are written hereafter:

$$\widehat{u_n} = \frac{c_R h_R u_{tR} - c_L h_L u_{tL} - \widetilde{c}\widetilde{h}\Delta_2}{\widetilde{h}\left(\left.\frac{\partial c}{\partial u_n}\right|_{\widetilde{\mathbf{W_n}}}\Delta_2 + \left.\frac{\partial c}{\partial u_t}\right|_{\widetilde{\mathbf{W_n}}}\Delta_3\right)}$$

$$\widehat{u_t} = \frac{(1+c_R\Delta)\,h_R u_{nR} u_{tR} - (1+c_L\Delta)\,h_L u_{nL} u_{tL} - (1+\widetilde{c}\Delta)\,\widetilde{h}\widetilde{u_n}\Delta_3}{(1+\widetilde{c}\Delta)\left(\widetilde{u_n}\Delta_1 + \widetilde{h}\Delta_2\right) + \widetilde{h}\widetilde{u_n}\Delta E}$$

$$\widehat{u_n^2} = \frac{F_{3R} - F_{3L} - (1+\widetilde{c}\Delta)\,\widetilde{h}\,(g\Delta_1 + 2\widetilde{u_n}\Delta_2) - \frac{1}{2}\Delta g\widetilde{h^2}E}{(1+\widetilde{c}\Delta)\,\Delta_1 + \widetilde{h}\Delta E}$$

$$\widecheck{u_n} = \frac{h_R u_{nR} - h_L u_{nL} + \Delta\,(c_R h_R u_{nR} - c_L h_L u_{nL}) - (1+\widetilde{c}\Delta)\,\widetilde{h}\Delta_2}{(1+\widetilde{c}\Delta)\,\Delta_1 + \Delta\widetilde{h}E}$$

$$\widecheck{u_t} = \frac{h_R u_{tR} - h_L u_{tL} + \Delta\,(c_R h_R u_{tR} - c_L h_L u_{tL}) - (1+\widetilde{c}\Delta)\,\widetilde{h}\Delta_3}{(1+\widetilde{c}\Delta)\,\Delta_1 + \Delta\widetilde{h}E}$$

where

$$F_{3L/R} = \left(1 + c_{L/R}\Delta\right)\left(h_{R/L}u_{nR/L}^2 + \frac{1}{2}gh_{R/L}^2\right)$$

However, also using this new set of averages the problem on the numerical fluxes did not disappear.

An additional attempt was performed using the same set of unknowns, except for the second term in M_A, $\widehat{u_t}$, which was substituted with $\widehat{u_n u_t}$. The expression for the new unknown is:

$$\widehat{u_n u_t} = \frac{(1+c_R\Delta)\,h_R u_{nR} u_{tR} - (1+c_L\Delta)\,h_L u_{nL} u_{tL} - (1+\widetilde{c}\Delta)\,\widetilde{h}\,(\widetilde{u_n}\Delta_3 + \widetilde{u_t}\Delta_2)}{(1+\widetilde{c}\Delta)\,\Delta_1 + \Delta\widetilde{h}E}$$

However, also this approach did not lead to the solution of the inconsistency.

Each time a different set of unknowns is used in computing the Jacobian matrices, slightly different values of the matrix terms are found. However, differences typically showed a order of magnitude equal to or lower than 10^{-2}, never sufficient to cause a change of sign in the solid mass flux.

8.3 An open issue

Although the issue was not resolved, no further attempts were carried out to reach its solution, because of the laborious work required for each try, which appears quite high if compared to the dimension of the problem and its effects on the solution.

Furthermore, it must be stressed that in this analysis attention was paid only to the GR solvers, and especially to the CIGR solver, but also other solvers showed the same inconsistency. It is possible that, turning the attention on other solvers, more profitable results could be obtained. However, similar analyses could be carried out only once knowledge of these other solvers appears in-depth enough.

Anyhow, whichever the numerical solver considered, the key point remains the characterisation of the problem. As long as no recurring pattern is found, it seems quite difficult that further analyses on the solvers could lead to the solution of the issue. Therefore, to date the question remains open.

Despite the poor operational result, this complexity issue revealed itself as a useful occasion to deal with sophisticated numerical models and experience their intricacy. Although in this case the use of a sophisticated numerical approach did not bring to the solution of the question, in general sophisticated numerical schemes lead to more accurate results. This is true also for the GR solvers, as clearly shown in Rosatti and Begnudelli (2013a). However, the price to pay for this higher accuracy is a large effort in numerical implementation and in scouting possible issues like the one discussed in this Chapter.

Conclusions

In this work, some effects of high-concentration flow complexity on modelling aimed at hazard assessment were experienced and faced. By means of some gained experience (Chapters 1 and 2) and some case studies (Chapter 4), it was shown that natural complexity may affect a very large variety of aspects related to the entire hazard assessment procedure. Focusing on the modelling stage, some specific points were disclosed and discussed, trying to understand, for each one of them, how is it possible to reach the *right level* of detail in high-concentration flow description and reduce the gap between the phenomenon and its representation.

The first point, tackled in Chapter 5, regarded difficulties in using a sophisticated model in the hazard-assessment process. Although often disregarded by model developers, the model use is one of the key factors that move closer or distance practitioners and model developers, supporting or hindering the Transfer of Technology. Furthermore, if the model use and, more in general, the entire hazard-assessment procedure are complicated, demanding and entail fragmentation, it is possible that results are affected by unintentional errors, undermining the accuracy of the global hazard-assessment outcome. Therefore, avoiding complicatedness is essential and is primarily a developer duty. Model developers should implement user-friendly modelling solution that allow the user to focus attention on the physical meaning of the operations, rather than on their number or sequence. Integrated solutions for modelling based on the SOA approach, as for example WEEZARD, may represent profitable solutions, especially if they are conceived as end-to-end systems. Furthermore, in perspective, such kind of systems can turn out to be useful not only for technicians and practitioners involved in hazard assessment, but also for other categories, as for example stakeholders and policy makers. This is exactly one of the future perspectives of WEEZARD, which appears to be suited for the integration of

further services and also for itself integration in existing Decision Support System. This perspective widens much the scope of the system within and also beyond modelling. Anyhow, achieving the goal of unburdening model users and involve different subjects and roles is possible only if a larger development responsibility is accepted by modellers and if multi-disciplinary partnerships are undertaken.

The question about how to reach the proper level of detail in high-concentration flow description was then discussed focusing on another important point: morphology representation. Reaching the *right level* of detail in this task means that all the relevant geometrical features of the computational domain must be taken discretised properly, i.e. with a sufficient resolution, whichever the position and the orientation. This requirement is particularly important in heterogeneous context as mountain areas, where flow dynamics depends largely on the flow interaction with morphology. Accurate morphology representation can be obtained by means of unstructured meshes, as shown in Chapter 6, where the TRENT2D-UTG model was presented. However, although the use of unstructured meshes is quite diffused and consolidated in the research community, it is not possible to overlook the fact that their use requires to model developers a sizeable effort in managing and organising geometric information, as well as in the implementation suitable numerical models. Besides, the use of unstructured meshes results demanding also for users. Therefore, in compliance with the reasons that led to the development of WEEZARD, TRENT2D-UTG is planned to be redeveloped as a service and integrated in WEEZARD, as well as some suitable applications for grid management and display. Moreover, in perspective more efficient numerical approaches could be applied or developed to manage gradient computation and limitation.

As the third point of the discussion, the problem of how to describe the effects induced by sluice gates on high-concentration flow and sediment routing was tackled in Chapter 7. In particular, it was shown that the *right level* of detail in the description can be reached with difficulty to the present levels of knowledge and understanding. Specific attention must be paid to the interaction of the gate with the flow and its effects on the sediment transport and the bed dynamics, since without understanding this aspects no reliable modelling approach can be developed. In this case, experimental activity and abstraction turn out to be essential to overcome the actual limit of knowledge and develop

suitable mathematical models. In perspective, better knowledge and understanding of the phenomenon could lead to the development of a more accurate numerical description, able to take into account the 3D effects induced by the gate preserving hyperbolicity in the governing system of equation. In this way, models could be used more effectively to support decisions also in the field of hydropower-reservoir management. Also in this case, the final destination could be WEEZARD, according to the purpose of widening the modelling capabilities of the system.

The last point was maybe the most arduous, since it had to deal with unwanted effects of complexity on numerical modelling (Chapter 8). Sometimes, great efforts made to develop accurate numerical schemes lead to unexpected, non-physical results, which appear hard to be understood and fixed. This outcome can be considered as the possible other side of the coin of sophisticated modelling products, which development is quite demanding, and, in addition, requires large efforts in finding the sources of possible incoherent results. In the future, further analysis are intended to investigate the issue thoroughly, considering different solvers and different systems of equations and possibly proposing a relief to avoid non-physical solutions.

These four points showed clearly that, dealing with high-concentration flow complexity, some kind of compromise is indispensable to reach the *right level* of detail and often the "quid pro quo" required to model developers is a significant increase in development efforts. Therefore, it can be concluded that it is not possible to face high-concentration flow complexity without compromising over the details to be included in its representation. However, if the necessary existence of trade-offs is accepted, a solution is often available to reach the *right level* of detail and avoid "spherical cows".

References

Abbott, M., J. Bathurst, J. Cunge, P. O'Connell and J. Rasmussen (1986). 'An introduction to the European Hydrological System âĂŤ Systeme Hydrologique Europeen, âĂIJSHEâĂİ, 1: History and philosophy of a physically-based, distributed modelling system'. In: *Journal of Hydrology* 87.1-2, pp. 45–59. DOI: 10.1016/0022-1694(86)90114-9.

Albano, R., A. Sole and J. Adamowski (2015). 'READY: a web-based geographical information system for enhanced flood resilience through raising awareness in citizens.' In: *Natural Hazards and Earth System Science* 15.7, pp. 1645–1658. DOI: 10.5194/nhess-15-1645-2015.

Ammann, W. J. (2006). 'Risk concept, integral risk management and risk governance'. In: *RISK21 - Coping with Risks due to Natural Hazards in the 21st Century*. Ed. by W. J. Ammann, S. Dannenmann and L. Vulliet. Taylor & Francis, pp. 2–23. DOI: 10.1201/9780203963562.pt1.

Anastasiou, K and C. T. Chan (1997). 'Solution of the 2D shallow water equations using the finite volume method on unstructured triangular meshes'. In: 24.April 1996, pp. 1225–1245.

APAT, A. p. l. p. d. e. p. i. servizi tecnici) and Agenzie Regionali e delle Province Autonome per la Protezione Ambientale (2004). *SISTAN, Sistema Statistico Nazionale: annuario dei dati ambientali*. Tech. rep. Roma: APAT, p. 1192.

Arattano, M. and L. Franzi (2003). 'On the evaluation of debris flows dynamics by means of mathematical models'. In: *Natural Hazards and Earth System Science* 3.6, pp. 539–544. DOI: 10.5194/nhess-3-539-2003.

Armanini, A. (2013). 'Granular flows driven by gravity'. In: *Journal of Hydraulic Research* 51.2, pp. 111–120. DOI: 10.1080/00221686.2013.788080.

Armanini, A. (2015). 'Closure relations for mobile bed debris flows in a wide range of slopes and concentrations'. In: *Advances in*

Water Resources 81, pp. 75–83. DOI: 10.1016/j.advwatres.2014.11.003.

Armanini, A. and M. Larcher (2001). 'Rational criterion for designing opening of slit-check dam'. In: *Journal of Hydraulic Engineering* 127.2, pp. 94–104. DOI: 10.1061/(ASCE)0733-9429(2001)127:2(94).

Armanini, A., L. Fraccarollo and M. Larcher (2005). 'Debris Flow'. In: *Encyclopedia of Hydrological Sciences*. Ed. by M. G. Anderson. Chichester, UK: John Wiley & Sons, Ltd, pp. 2173–2186. DOI: 10.1002/0470848944.hsa149.

Armanini, A., M. Larcher and L. Fraccarollo (2009a). 'Intermittency of rheological regimes in uniform liquid-granular flows'. In: *Physical Review E - Statistical, Nonlinear, and Soft Matter Physics* 79.5, pp. 1–7. DOI: 10.1103/PhysRevE.79.051306.

Armanini, A., L. Fraccarollo and G. Rosatti (2009b). 'Two-dimensional simulation of debris flows in erodible channels'. In: *Computers & Geosciences* 35.5, pp. 993–1006. DOI: 10.1016/j.cageo.2007.11.008.

Armanini, A., G. Rosatti and N. Zorzi (2014). *Studio dei fenomeni torrentizi avvenuti nel 2010 sul versante pinetano di Costalta compreso tra la Val Regnana e il Rio Le Giare: elaborazione di possibili miglioramenti nella redazione della Carta della Pericolosità*. Tech. rep. Trento, pp. 1–159.

Atkins, D. E., K. K. Droegemeier, S. I. Feldman, H. García Molina, M. L. Klein, D. G. Messerschmitt, P. Messina, J. P. Ostriker, M. H. Wright, H. Garcia-molina, M. L. Klein, D. G. Messerschmitt, P. Messina, J. P. Ostriker and M. H. Wright (2003). *Revolutionizing Science and Engineering Through Cyberinfrastructure: Report of the National Science Foundation Blue-Ribbon Advisory Panel on Cyberinfrastructure*. Tech. rep. Washington, pp. 1–124.

Bacchini, M. and a. Zannoni (2003). 'Relations between rainfall and triggering of debris-flow: case study of Cancia (Dolomites, Northeastern Italy)'. In: *Natural Hazards and Earth System Science* 3.1/2, pp. 71–79. DOI: 10.5194/nhess-3-71-2003.

Bagnold, R. A. (1954). 'Experiments on a Gravity-Free Dispersion of Large Solid Spheres in a Newtonian Fluid under Shear'. In: *Proceedings of the Royal Society A: Mathematical, Physical and Engineering Sciences*. A 225.1160, pp. 49–63. DOI: 10.1098/rspa.1954.0186.

Balsara, D. S., M. Dumbser and R. Abgrall (2014). 'Multidimensional HLLC Riemann solver for unstructured meshes âĂŞ With application to Euler and MHD flows'. In: *Journal of Com-*

putational Physics 261, pp. 172–208. DOI: 10.1016/j.jcp.2013.12.029.

Bar-Yam, Y. (1997). *Dynamics of complex systems*. Vol. 213. Addison-Wesley Reading, pp. 1–498.

Barth, T. and D. Jespersen (1989). 'The design and application of upwind schemes on unstructured meshes'. In: *27th Aerospace Sciences Meeting*. Vol. AIAA-89-03. AIAA paper: 89-0366. Reston, Virigina: American Institute of Aeronautics and Astronautics. DOI: 10.2514/6.1989-366.

Barth, T. J. (1990). 'On unstructured grids and solvers'. In: *VKI, Computational Fluid Dynamics*. Vol. 2. (SEE N90-27933), pp. 1–66.

Barth, T. J. and P. O. Fredrickson (1990). 'Higher order solution of the Euler equations on unstructured grids using quadratic reconstruction'. In: *AIAA, Aerospace Sciences Meeting, 28th, Reno, NV, Jan. 8-11, 1990* 13.

Beck, K., M. Beedle, A. van Bennekum, A. Cockburn, W. Cunnigham, M. Flowler, J. Grenning, J. Highsmith, A. Hunt, J. Kern, B. Marick, R. C. Martin, S. Mellor, K. Schwaber, J. Sutherland and D. Thomas (2001). *Manifesto for agile software development*. URL: http://agilemanifesto.org.

Belaud, G., L. Cassan and J.-P. Baume (2009). 'Calculation of Contraction Coefficient under Sluice Gates and Application to Discharge Measurement'. In: *Journal of Hydraulic Engineering* 135.12, pp. 1086–1091. DOI: 10.1061/(ASCE)HY.1943-7900.0000122.

Belete, G. F., A. Voinov and G. F. Laniak (2017). 'An overview of the model integration process: From pre-integration assessment to testing'. In: *Environmental Modelling & Software* 87, pp. 49–63. DOI: 10.1016/j.envsoft.2016.10.013.

Benkhaldoun, F., I. Elmahi, S. Sari and M. Seaid (2013). 'An unstructured finite-volume method for coupled models of suspended sediment and bed load transport in shallow-water flows'. In: *International Journal for Numerical Methods in Fluids* 72.9, pp. 967–993. DOI: 10.1002/fld.3771.

Bern, M., D. Eppstein and J. Gilbert (1994). 'Provably good mesh generation'. In: *Journal of Computer and System Sciences* 48.3, pp. 384–409. DOI: 10.1016/S0022-0000(05)80059-5.

Berti, M., R. Genevois, R. LaHusen, A. Simoni and P. Tecca (2000). 'Debris flow monitoring in the acquabona watershed on the Dolomites (Italian alps)'. In: *Physics and Chemistry of the Earth,*

Part B: Hydrology, Oceans and Atmosphere 25.9, pp. 707–715. DOI: 10.1016/S1464-1909(00)00090-3.

Beven, K. J. (2009). *Environmental modelling: an uncertain future?* London: Routledge, pp. 1–310.

Billett, S. and E. F. Toro (1997). 'On WAF-Type Schemes for Multidimensional Hyperbolic Conservation Laws'. In: *Journal of Computational Physics* 130.1, pp. 1–24. DOI: 10.1006/jcph.1996.5470.

Borga, M. and D. Zoccatelli (2010). *Esame del carattere di eccezionalità delle precipitazioni misurate dalla stazione di S. Orsola nel periodo 14-15 agosto 2010 - versione preliminare*. Tech. rep. Padova: University of Padova.

Bruner, C. and R. Walters (1997). 'Parallelization of the Euler equations on unstructured grids'. In: *13th Computational Fluid Dynamics Conference*. Reston, Virigina: American Institute of Aeronautics and Astronautics. DOI: 10.2514/6.1997-1894.

Buffard, T. and S. Clain (2010). 'Monoslope and multislope MUSCL methods for unstructured meshes'. In: *Journal of Computational Physics* 229.10, pp. 3745–3776. DOI: 10.1016/j.jcp.2010.01.026.

Cao, Z., G. Pender and P. Carling (2006). 'Shallow water hydrodynamic models for hyperconcentrated sediment-laden floods over erodible bed'. In: *Advances in Water Resources* 29.4, pp. 546–557. DOI: 10.1016/j.advwatres.2005.06.011.

Casti, J. (1979). 'Connectivity, Complexity and Catastrophe in Large-scale Systems'. In: *International Series on Applied Systems Analysis* 7, p. 203. DOI: 10.1016/0377-2217(80)90118-6.

Castro-Orgaz, O. and W. H. Hager (2014). 'Transitional flow at standard sluice gate'. In: *Journal of Hydraulic Research* 52.2, pp. 264–273. DOI: 10.1080/00221686.2013.855951.

Chanson, H., Miahr, S. Aoki and M. Maruyama (2002). 'Unsteady two-dimensional orifice flow: A large-size experimental investigation | Ecoulement non-permanent dans un orifice rectangulaire: Une étude experimentale de grande taille'. In: *Journal of Hydraulic Research* 40.1, pp. 63–71.

Chanson, H. (2004). 'Sabo check dams âĂŘ mountain protection systems in Japan'. In: *International Journal of River Basin Management* 2.4, pp. 301–307. DOI: 10.1080/15715124.2004.9635240.

Chern, I.-L. and P. Colella (1987). *A conservative front tracking method for hyperbolic conservation laws*.

Christen, M., Y. Bühler, P. Bartelt, R. Leine, J. Glover, A. Schweizer, C. Graf, B. W. McArdell, W. Gerber, Y. Deubelbeiss, T. Feistl, A. Volkwein, B. W. McArdell, W. Gerber, Y. Deubelbeiss, T. Feistl and A. Volkwein (2012). 'Integral hazard management using a unified software environment. Numerical simulation tool "RAMMS" for gravitational natural hazardS'. In: *Conference Proceedings of the 12th Congress INTERPRAEVENT 2012 - Grenoble / France*, pp. 77–86. DOI: ISBN978-3-901164-19-4.

Coe, J. A., D. A. Kinner and J. W. Godt (2008). 'Initiation conditions for debris flows generated by runoff at Chalk Cliffs, central Colorado'. In: *Geomorphology* 96.3-4, pp. 270–297. DOI: 10.1016/j.geomorph.2007.03.017.

Cordier, S., M. H. Le and T. Morales de Luna (2011). 'Bedload transport in shallow water models: Why splitting (may) fail, how hyperbolicity (can) help'. In: *Advances in Water Resources* 34.8, pp. 980–989. DOI: 10.1016/j.advwatres.2011.05.002.

Corominas, J., H. Einstein, T. Davis, A. Strom, G. Zuccario, F. Nadim and T Verdel (2015). 'Glossary of terms of landslide hazard and risk'. In: *Engineering Geology for Society and Territory - Volume 2, Acts of: International Association of Engineering Geology and the Environment IAEG XII Congress*. Ed. by G. Lollino, D. Giordan, G. Crosta, J. Corominas, R. Azzam, J. Wasowski and N. Sciarra. Vol. 2. Torino / Italy: Springer International Publishing, pp. 1775–1779. DOI: 10.1007/978-3-319-09057-3_314.

Courant, R., K. Friedrichs and H. Lewy (1928). 'Über die partiellen Differenzengleiehungen der mathematischen Physik'. In: *Mathematische Annalen* 100.1, pp. 32–74.

Coussot, P and M Meunier (1996). 'Recognition, classification and mechanical description of debris flows'. In: *Earth-Science Reviews* 40, pp. 209–227. DOI: 10.1016/0012-8252(95)00065-8.

Cozzolino, L., L. Cimorelli, C. Covelli, R. Della Morte and D. Pianese (2015). 'The analytic solution of the Shallow-Water Equations with partially open sluice-gates: The dam-break problem'. In: *Advances in Water Resources* 80, pp. 90–102. DOI: 10.1016/j.advwatres.2015.03.010.

Darwish, M. and F. Moukalled (2003). 'TVD schemes for unstructured grids'. In: *International Journal of Heat and Mass Transfer* 46.4, pp. 599–611. DOI: 10.1016/S0017-9310(02)00330-7.

De Zolt, S., P. Lionello, A. Nuhu and A. Tomasin (2006). 'The disastrous storm of 4 November 1966 on Italy'. In: *Natural*

Hazards and Earth System Science 6.5, pp. 861–879. DOI: 10.5194/nhess-6-861-2006.

Defina, A. and F. M. Susin (2003). 'Hysteretic behavior of the flow under a vertical sluice gate'. In: *Physics of Fluids* 15.9, pp. 2541–2548. DOI: 10.1063/1.1596193.

Della Lucia, D., S. Fattorelli and S. Provasi (1979). 'Determinazione delle zone omogenee per le piogge intense nel Trentino'. In: *Memorie del Museo Tridentino di Scienze naturali - Volume XXI, fascicolo 2*. Trento.

DMA (2000). *Disaster Mitigation Act of 2000*. U.S.A. Public Law 106-390.

Dottori, F and E Todini (2010). 'A 2D flood inundation model based on cellular automata approach.' In: *Proc. computer methods water resources (CMWR)*.

Dubois, F. and M. Guillame (1993). 'Nonparameterized 'entropy fix' for Roe's method'. In: *AIAA Journal* 31.1, pp. 199–200. DOI: 10.2514/3.11339.

Dumbser, M., A. Hidalgo, M. Castro, C. Parés and E. F. Toro (2010). 'FORCE schemes on unstructured meshes II: Non-conservative hyperbolic systems'. In: *Computer Methods in Applied Mechanics and Engineering* 199.9-12, pp. 625–647. DOI: 10.1016/j.cma.2009.10.016.

Durlofsky, L. J., B. Engquist and S. Osher (1992). 'Triangle based adaptive stencils for the solution of hyperbolic conservation laws'. In: *Journal of Computational Physics* 98.1, pp. 64–73. DOI: 10.1016/0021-9991(92)90173-V.

Dyn, N., D. Levin and S. Rippa (1990). 'Data Dependent Triangulations for Piecewise Linear Interpolation'. In: *IMA Journal of Numerical Analysis* 10.1, pp. 137–154. DOI: 10.1093/imanum/10.1.137.

Edelsbrunner, H. and T. S. Tan (1993). 'A Quadratic Time Algorithm for the Minmax Length Triangulation'. In: *SIAM Journal on Computing* 22.3, pp. 527–551. DOI: 10.1137/0222036.

Egashira, S. and K. Ashida (1987). 'Sediment transport in steep slope flumes'. In: *RoC Japan Joint Seminar on Water Resources*.

Einfeldt, B, C. Munz, P. Roe and B Sjögreen (1991). 'On Godunov-type methods near low densities'. In: *Journal of Computational Physics* 92.2, pp. 273–295. DOI: 10.1016/0021-9991(91)90211-3.

Einfeldt, B. (1988). *On Godunov-Type Methods for Gas Dynamics*. DOI: 10.1137/0725021.

Engquist, B. B. and S. Osher (1981). 'One-Sided Difference Approximations for Nonlinear Conservation Laws'. In: 36.154, pp. 321–351.

Eppstein, D. (1994). 'Approximating the minimum weight Steiner triangulation'. In: *Discrete & Computational Geometry* 11.2, pp. 163–191. DOI: 10.1007/BF02574002.

Fagherazzi, S. and T. Sun (2003). 'Numerical simulations of transportational cyclic steps'. In: *Computers and Geosciences* 29.9, pp. 1143–1154. DOI: 10.1016/S0098-3004(03)00133-X.

Favis-Mortlock, D. (2013). 'Non-linear dynamics, self-organization and cellular automata models'. In: *Environmental Modelling: Finding Simplicity in Complexity*. Ed. by J. Wainwright and M. Mulligan. Second Edi. John Wiley & Sons, Ltd, pp. 45–67.

Feng, L., C. Wang, C. Li and Z. Li (2011). 'A research for 3D WebGIS based on WebGL'. In: *Computer Science and Network Technology (ICCSNT), 2011 International Conference on*. Vol. 1, pp. 348–351.

Fernandez Luque, R. and R. Van Beek (1976). 'Erosion And Transport Of Bed-Load Sediment'. In: *Journal of Hydraulic Research* 14.2, pp. 127–144. DOI: 10.1080/00221687609499677.

Fernandez-Nieto, E. D., F. Bouchut, D. Bresch, M. J. Castro Diaz and A. Mangeney (2008). 'A new Savage-Hutter type model for submarine avalanches and generated tsunami'. In: *Journal of Computational Physics* 227.16, pp. 7720–7754. DOI: 10.1016/j.jcp.2008.04.039.

Filippi Gilli, E. (2016). *Cambiamenti climatici nelle Valli di Primiero. Eventi naturali estremi*. La Bottega del Nord Est, pp. 1–223.

Fraccarollo, L. and H. Capart (2002). 'Riemann wave description of erosional dam-break flows'. In: *Journal of Fluid Mechanics* 461, pp. 183–228. DOI: 10.1017/S0022112002008455.

Fraccarollo, L, H Capart and Y Zech (2003). 'A Godunov method for the computation of erosional shallow water transients'. In: *International Journal for Numerical Methods in Fluids* 41.9, pp. 951–976. DOI: 10.1002/fld.475.

Franke, P.-G. and F. Valentin (1969). 'The Determination Of Discharge Below Gates In Case Of Tailwater Conditions'. In: *Journal of Hydraulic Research* 7.4, pp. 433–447. DOI: 10.1080/00221686909500280.

Garbrecht, G. (1977). 'Discharge computations at river control structures'. In: *Journal of the Hydraulics Division* 103.12, pp. 1481–1484.

Garegnani, G., G. Rosatti and L. Bonaventura (2013). 'On the range of validity of the Exner-based models for mobile-bed

river flow simulations'. In: *Journal of Hydraulic Research* 51.4, pp. 380–391. DOI: 10.1080/00221686.2013.791647.

Gell-Mann, M. (1995). 'Plectics'. In: *The third culture: beyond the scientific revolution*. Ed. by J. Brockman. New York: Simon & Schuster, pp. 316–332.

George, D. L. and R. M. Iverson (2014). 'A depth-averaged debris-flow model that includes the effects of evolving dilatancy. II. Numerical predictions and experimental tests'. In: *Proceedings of the Royal Society A: Mathematical, Physical and Engineering Sciences* 470.2170, p. 20130820. DOI: 10.1098/rspa.2013.0820.

Giupponi, C., J. Mysiak, Y. Depietri and M. Tamaro (2011). 'Decision Support Systems for water resources management: current state and guidelines for tool development'. In: *Decision Support for water framework directive implementation*. Ed. by P. A. Vanrolleghem. London, UK: IWA Publishing. Chap. 2, pp. 107–202.

Glimm, J., J. W. Grove, X. L. Li, K.-m. Shyue, Y. Zeng and Q. Zhang (1998). 'Three-Dimensional Front Tracking'. In: *SIAM Journal on Scientific Computing* 19.3, pp. 703–727. DOI: 10.1137/S1064827595293600.

Greco, M., M. Iervolino, A. Leopardi and A. Vacca (2012). 'A two-phase model for fast geomorphic shallow flows'. In: *International Journal of Sediment Research* 27.4, pp. 409–425. DOI: 10.1016/S1001-6279(13)60001-3.

Gregoretti, C., M. Degetto and M. Boreggio (2016). 'GIS-based cell model for simulating debris flow runout on a fan'. In: *Journal of Hydrology* 534, pp. 326–340. DOI: 10.1016/j.jhydrol.2015.12.054. URL: http://dx.doi.org/10.1016/j.jhydrol.2015.12.054.

Hagemeier-Klose, M. and K. Wagner (2009). 'Evaluation of flood hazard maps in print and web mapping services as information tools in flood risk communication'. In: *Natural Hazards and Earth System Science* 9.2, pp. 563–574. DOI: 10.5194/nhess-9-563-2009.

Harte, J. (1988). *Consider a spherical cow: a course in environmental problem solving*, pp. 1–283.

Harten, A., P. D. Lax, B van Leer and B. Vanleer (1983). 'On upstream differencing and Godunov-type schemes for hyperbolic conservation laws'. In: *SIAM Review* 25.1, pp. 35–61. DOI: 10.1137/1025002.

Hashimoto, H., T. Tsubaki and H. Nakayama (1978). 'Experimental consideration on debris flow'. In: *33rd National Meeting of JSCE*, pp. 574–575.

Heinimann, H. R., K. Hollenstein, H. Kienholz, B. Krummenacher and P. Mani (1998). *Methoden zur Analyse und Bewertung von Naturgefahren*. Tech. rep. 85. Bern: Bundesamt für Umwelt, p. 248.

Henderson, F. (1966). *Open channel flow*. New York: Macmillan, pp. 1–522.

Henry, H. (1950). 'Discussion of Diffusion of Submerged Jets'. In: *Journal of Irrigation and Drainage Engineering* 115, pp. 687–694.

Honglian, L. and C. Xiangxing (1988). 'Some characteristics of debris flow in mountain areas of Western China'. In: *Internationales Symposion INTERPRAEVENT 1988*, pp. 157–172.

Hubbard, M. E. (1999). 'Multidimensional Slope Limiters for MUSCL-Type Finite Volume Schemes on Unstructured Grids'. In: 74, pp. 54–74.

Hungr, O. (2005). 'Classification and terminology'. In: *Debris-flow Hazards and Related Phenomena*. Berlin, Heidelberg: Springer, pp. 9–23. DOI: 10.1007/3-540-27129-5_2.

Hungr, O., G. C. Morgan, D. F. VanDine and D. R. Lister (1987). 'Debris flow defenses in British Columbia'. In: *Reviews in Engineering Geology*. Ed. by J. E. Costa and G. F. Wieczorek. Geological Society of America, pp. 201–222. DOI: 10.1130/REG7-p201.

Hungr, O., S. G. Evans, M. J. Bovis and J. N. Hutchinson (2001). 'A review of the classification of landslides of the flow type'. In: *Environmental & Engineering Geoscience* 7.3, pp. 221–238. DOI: 10.2113/gseegeosci.7.3.221.

Hürlimann, M, D Rickenmann and C Graf (2003). 'Field and monitoring data of debris-flow events in the Swiss Alps'. In: *Canadian Geotechnical Journal* 40.1, pp. 161–175. DOI: 10.1139/t02-087.

Hürlimann, M., D. Rickenmann, V. Medina and A. Bateman (2008). 'Evaluation of approaches to calculate debris-flow parameters for hazard assessment'. In: *Engineering Geology* 102.3-4, pp. 152–163. DOI: 10.1016/j.enggeo.2008.03.012.

Hutchinson, J. N. (1988). 'General report: morphological and geotechnical parameters of landslides in relation to geology and hydrogeology'. In: *Fifth International Symposium on Landslides*. Ed. by C. Bonnard. Vol. 1. Rotterdam: Balkema, pp. 3–35.

Ingram, D. M., D. M. Causon and C. G. Mingham (2003). 'Developments in Cartesian cut cell methods'. In: *Mathematics and Computers in Simulation* 61.3-6, pp. 561–572. DOI: 10.1016/S0378-4754(02)00107-6.

Iverson, R. M. and C. Ouyang (2015). 'Entrainment of bed material by Earth-surface mass flows: Review and reformulation of depth-integrated theory'. In: *Reviews of Geophysics* 53.1, pp. 27–58. DOI: 10.1002/2013RG000447.

Jaafar, H. H. and G. P. Merkley (2010). 'High-Resolution Method for Modeling Hydraulic Regime Changes at Canal Gate Structures.' In: *Journal of Irrigation & Drainage Engineering* 136.12, pp. 795–808. DOI: 10.1061/(ASCE)IR.1943-4774.0000263.

Jakob, M. (2005a). 'A size classification for debris flows'. In: *Engineering Geology* 79.3-4, pp. 151–161. DOI: 10.1016/j.enggeo.2005.01.006.

Jakob, M. (2005b). 'Debris-flow hazard analysis'. In: *Debris-flow Hazards and Related Phenomena*. Ed. by M. Jakob and O. Hungr. Berlin, Heidelberg: Springer, pp. 411–443. DOI: 10.1007/3-540-27129-5_17.

Jia, Y., H. Zhao, C. Niu, Y. Jiang, H. Gan, Z. Xing, X. Zhao and Z. Zhao (2009). 'A WebGIS-based system for rainfall-runoff prediction and real-time water resources assessment for Beijing'. In: *Compters & Geosciences* 35.7, pp. 1517–1528. DOI: 10.1016/j.cageo.2008.10.004.

Jones, S. (2005). 'Toward an acceptable definition of service'. In: *IEEE Software* 22.3, pp. 87–93. DOI: 10.1109/MS.2005.80.

Julien, P. (1997). 'Introduction to chapter 2'. In: *Recent developments on debris flows*. Ed. by A. Armanini and M. Michiue. Springer. Chap. 2, pp. 65–69.

Kulkarni, A. T., J. Mohanty, T. I. Eldho, E. P. Rao and B. K. Mohan (2014). 'A web GIS based integrated flood assessment modeling tool for coastal urban watersheds'. In: *Computers and Geosciences* 64, pp. 7–14. DOI: 10.1016/j.cageo.2013.11.002.

Kunz, M. and L. Hurni (2008). 'Hazard Maps in Switzerland State-of-the-Art and Potential Improvements'. In: *Proceedings of 6th ICA Mountain Cartography Workshop Mountain Mapping and Visualisation*. Ed. by L. Hurni and K. Kriz. Lenk / Switzerland: ETH Zurich Institute of Cartography, pp. 133–138.

Laigle, D. (1997). 'A two-dimensional model for the study of debris-flow spreading on a torrent debris fan'. In: *Debris-Flow Hazards Mitigation: Mechanics, Prediction, and Assessment, Proc.*

1st International DFHM Conference. Ed. by C. Chen. San Francisco, CA, USA, pp. 123–132.

Lambert, C., D. M. Causon, P. Batten, C. Lambert and D. M. Causon (1996). 'Positively conservative high-resolution convection schemes for unstructured elements'. In: *International Journal for Numerical Methods in Engineering* 39.11, pp. 1821–1838. DOI: 10.1002/(SICI)1097-0207(19960615)39:11<1821::AID-NME929>3.0.CO;2-E.

Lanni, C., B. Mazzorana, P. Macconi and R. Bertagnolli (2015). 'Suitability of mono- and Two-Phase Modeling of Debris Flows for the Assessment of Granular Debris Flow Hazards: Insights from a Case Study'. In: *Engineering Geology for Society and Territory - Volume 2, Acts of: International Association of Engineering Geology and the Environment IAEG XII Congress*. Ed. by G. Lollino. Torino / Italy: Springer International Publishing, pp. 1629–1633. DOI: 10.1007/978-3-319-09057-3_89.

Lenzi, M. and P. Paterno (1997). *La progettazione e la valutazione di impatto ambiental degli interventi di sistemazioni idraulico-forestali. Uno studio di caso sul Rio Lazer*. Ed. by E. Progetto. Padova, p. 158.

Leskens, J. G., M. Brugnach, A. Y. Hoekstra and W. Schuurmans (2014). 'Why are decisions in flood disaster management so poorly supported by information from flood models?' In: *Environmental Modelling and Software* 53, pp. 53–61. DOI: 10.1016/j.envsoft.2013.11.003. URL: http://dx.doi.org/10.1016/j.envsoft.2013.11.003.

LeVeque, R. J. (1992). *Numerical methods for conservation laws*. Ed. by O. E. Lanford. Second edi, pp. 1–228.

LeVeque, R. J. (2002). *Finite Volume Methods for Hyperbolic Problems*. Cambridge University Press, pp. 129–138. DOI: 10.1017/CBO9780511791253.

LeVeque, R. J. and K.-M. Shyue (1996). 'Two-dimensional front tracking based on high resolution wave propagation methods'. In: *Journal of Computational Physics* 123.2, pp. 354–368. DOI: 10.1006/jcph.1996.0029.

Liu, G. R. and M. B. Liu (2003). *Smoothed Particle Hydrodynamics - A Meshfree Particle Method*. World Scientific Publishing Co. Pte. Ltd. DOI: 10.1142/9789812564405.

Marchelli, M., M. Pirulli, C. Scavia and G. Rosatti (2016). 'TRENT2D, a quasi-two-phase numerical code to simulate debris flow dynamics'. In: *Landslides and Engineered Slopes. Experience, Theory*

and Practice. CRC Press, pp. 1353–1360. DOI: 10.1201/b21520-165.

Marchi, L., M. Arattano and A. M. Deganutti (2002). 'Ten years of debris-flow monitoring in the Moscardo Torrent (Italian Alps)'. In: *Geomorphology* 46.1-2, pp. 1–17. DOI: 10.1016/S0169-555X(01)00162-3.

Marra, F., E. I. Nikolopoulos, J. D. Creutin and M. Borga (2016). 'SpaceâĂŞtime organization of debris flows-triggering rainfall and its effect on the identification of the rainfall threshold relationship'. In: *Journal of Hydrology* 541, pp. 246–255. DOI: 10.1016/j.jhydrol.2015.10.010.

Mathys, N., S. Brochot, M. Meunier and D. Richard (2003). 'Erosion quantification in the small marly experimental catchments of Draix (Alpes de Haute Provence, France). Calibration of the ETC rainfall-runoff-erosion model'. In: *Catena* 50.2-4, pp. 527–548. DOI: 10.1016/S0341-8162(02)00122-4.

Mavriplis, D. J. (1997). 'Unstructured grid techniques'. In: *Annual Review of Fluid Mechanics* 29.1, pp. 473–514. DOI: 10.1146/annurev.fluid.29.1.473.

McGuire, K. J., J. J. McDonnell, M. Weiler, C. Kendall, B. L. McGlynn, J. M. Welker and J. Seibert (2005). 'The role of topography on catchment-scale water residence time'. In: *Water Resources Research* 41.5, pp. 1–14. DOI: 10.1029/2004WR003657.

Medina, V., M. Hürlimann and A. Bateman (2008). 'Application of FLATModel, a 2D finite volume code, to debris flows in the northeastern part of the Iberian Peninsula'. In: *Landslides* 5.1, pp. 127–142. DOI: 10.1007/s10346-007-0102-3.

Mergili, M. and W. Fellin (2007). 'GRASS GIS and Modelling of Natural Hazards. An Integrated Approach for Debris Flow Simulation.' In: *OSGeo Journal* 3, pp. 53–59.

Meyer-Peter, E. and R. Müller (1948). 'Formulas for bed-load transport'. In: ed. by IAHR. Stockholm, pp. 39–64.

Montes, J. S. (1997). 'Irrotational Flow and Real Fluid Effects Under Planar Sluice Gates'. In: *Journal of Hydraulic Engineering* 123.3, pp. 219–232. DOI: 10.1061/(ASCE)0733-9429(1997)123:3(219).

Mulligan, M. and J. Wainwright (2013). 'Modelling and model building'. In: *Environmental Modelling: Finding Simplicity in Complexity*. Ed. by J. Wainwright and M. Mulligan. Second Edi. John Wiley & Sons, Ltd, pp. 7–26.

Mure-Ravaud, M., G. Binet, M. Bracq, J.-J. Perarnaud, A. Fradin and X. Litrico (2016). 'A web based tool for operational real-

time flood forecasting using data assimilation to update hydraulic states'. In: *Environmental Modelling & Software* 84, pp. 35–49. DOI: 10.1016/j.envsoft.2016.06.002.

Murillo, J. M. and P. García-Navarro (2010). 'An Exner-based coupled model for two-dimensional transient flow over erodible bed'. In: *Journal of Computational Physics* 229.23, pp. 8704–8732. DOI: 10.1016/j.jcp.2010.08.006.

Muste, M. V. and A. R. Firoozfar (2016). 'Toward generalized decision support systems for flood risk management'. In: *E3S Web of Conferences* 7. Ed. by M. Lang, F. Klijn and P. Samuels, p. 20017. DOI: 10.1051/e3sconf/20160720017.

Nago, H. (1978). 'Influence of gate-shapes on discharge coefficients'. In: *Proceedings of Japan Society of Civil Engineers*. Ed. by J. S. o. C. Engineers, pp. 59–71.

Natale, L, G Petaccia and F Savi (2004). 'Mathematical simulation of the effects of bridges and structures on flood waves propagation'. In: *River Flow 2004*. CRC Press, pp. 895–901. DOI: 10.1201/b16998-114.

Nativi, S., P. Mazzetti and G. N. Geller (2013). 'Environmental model access and interoperability: The GEO Model Web initiative'. In: *Environmental Modelling & Software* 39, pp. 214–228. DOI: 10.1016/j.envsoft.2012.03.007.

Nielsen, P. (1992). *Coastal bottom boundary layers and sediment transport*. World Scientific Publishing Co. Inc., pp. 1–324.

Noutsopoulos, G. and S. Fanariotis (1978). 'Discussion of: Free flow immediately below sluice gates'. In: *Journal of the Hydraulics Division* 124.3, pp. 451–454.

Nsom, B., S. Longo, D. Laigle and M. Arattano (1998). *Debris flow rheology and flow resistance, Thematic Report*. Tech. rep. U.E. contract Debris Flow Risk n. ENV4 - CT96 - 0253, pp. 1–49.

O'Brien, J. S. and P. Y. Julien (1988). 'Laboratory Analysis of Mudflow Properties'. In: *Journal of Hydraulic Engineering* 114.8, pp. 877–887. DOI: 10.1061/(ASCE)0733-9429(1988)114:8(877).

O'Brien, J. S., P. Y. Julien and W. T. Fullerton (1993). 'Two-dimensional water flood and mudflow simulation'. In: *Journal of Hydraulic Engineering* 119.2, pp. 244–261. DOI: 10.1061/(ASCE)0733-9429(1993)119:2(244).

OpenStreetMap (2016). *No Title*. URL: http://www.openstreetmap.org.

Osher, S. and F. Solomon (1982). 'Upwind difference schemes for hyperbolic systems of conservation laws'. In: *Mathematics of*

Computation 38.158, pp. 339–374. DOI: 10.1090/S0025-5718-1982-0645656-0.

Pelanti, M., F. Bouchut and A. Mangeney (2008). *A Roe-type scheme for two-phase shallow granular flows over variable topography*. DOI: 10.1051/m2an:2008029. arXiv: 0608007 [math].

Petrascheck, A. and H. Kienholz (2003). 'Hazard assessment and mapping of mountain risks in Switzerland'. In: *Debris-Flow Mitigation: mechanics, prediction and assessment*. Ed. by D. Rickenmann and Chen. Davos / Switzerland: Millpress, Rotterdam, pp. 25–38.

Pitman, E. B. and L. Le (2005). 'A two-fluid model for avalanche and debris flows.' In: *Philosophical transactions. Series A, Mathematical, physical, and engineering sciences* 363.1832, pp. 1573–1601. DOI: 10.1098/rsta.2005.1596.

Pitman, E. B., C. C. Nichita, A. Patra, A. Bauer, M. Sheridan and M. Bursik (2003). 'Computing granular avalanches and landslides'. In: *Physics of Fluids* 15.12, pp. 3638–3646. DOI: 10.1063/1.1614253.

Power, D. J. (1997). 'What is a DSS?' In: *DSstar, The On-Line Executive Journal for Data-Intensive Decision Support* 1.3, pp. 1–4.

Power, D. J. (2004). *Free Decision Support System Glossary*.

Preparata, F. P. and M. I. Shamos (1985). *Computational Geometry*. New York, NY: Springer New York, p. 400. DOI: 10.1007/978-1-4612-1098-6.

Provincia Autonoma di Trento (2017). *Criteri e metodologia per la redazione e l'aggiornamento delle carte della pericolosità*.

Rajaratnam, N. and J. A. Humphries (1982). 'Free Flow Upstream Of Vertical Sluice Gates'. In: *Journal of Hydraulic Research* 20.5, pp. 427–437. DOI: 10.1080/00221688209499471.

Rajaratnam, N. and K. Subramanya (1967). 'Flow equation for the sluice gate'. In: *Journal of the Irrigation and Drainage Division* 93.3, pp. 167–186.

Rickenmann, D. and B. W. McArdell (2007). 'Continuous measurement of sediment transport in the Erlenbach stream using piezoelectric bedload impact sensors'. In: *Earth Surface Processes and Landforms* 32.9, pp. 1362–1378. DOI: 10.1002/esp.1478. arXiv: bhmic00033.

Rickenmann, D. (1999). 'Empirical relationships for debris flows'. In: *Natural Hazards* 19.1, pp. 47–77. DOI: 10.1023/A:1008064220727.

Rigon, R., P. D'Odorico and G. Bertoldi (2011). 'The geomorphic structure of the runoff peak'. In: *Hydrology and Earth System Sciences* 15, pp. 1853–1863. DOI: 10.5194/hessd-8-1031-2011.

Rigon, R., G. Monacelli, S. Franceschi, G. Formetta, G. Monacelli and G. Formetta (2012). *The triggering of landslides and debris flow and their mapping*. Tech. rep. Sofia, pp. 1–57.

Roe, P. L. (1981). 'Approximate Riemann solvers, parameter vectors, and difference schemes'. In: *Journal of Computational Physics* 43.2, pp. 357–372. DOI: 10.1016/0021-9991(81)90128-5.

Roering, J. J., B. H. Mackey, J. A. Marshall, K. E. Sweeney, N. I. Deligne, A. M. Booth, A. L. Handwerger and C. Cerovski-Darriau (2013). ''You are HERE': Connecting the dots with airborne lidar for geomorphic fieldwork'. In: *Geomorphology* 200, pp. 172–183. DOI: 10.1016/j.geomorph.2013.04.009.

Rosatti, G. and L. Begnudelli (2013a). 'A closure-independent Generalized Roe solver for free-surface, two-phase flows over mobile bed'. In: *Journal of Computational Physics* 255, pp. 362–383. DOI: 10.1016/j.jcp.2013.08.020.

Rosatti, G. and L. Begnudelli (2013b). 'Two-dimensional simulation of debris flows over mobile bed: enhancing the TRENT2D model by using a well-balanced Generalized Roe-type solver'. In: *Computers & Fluids* 71, pp. 179–195. DOI: 10.1016/j.compfluid.2012.10.006.

Rosatti, G. and L. Fraccarollo (2006). 'A well-balanced approach for flows over mobile-bed with high sediment-transport'. In: *Journal of Computational Physics* 220.1, pp. 312–338. DOI: 10.1016/j.jcp.2006.05.012.

Rosatti, G. and D. Zugliani (2015). 'Modelling the transition between fixed and mobile bed conditions in two-phase free-surface flows: The Composite Riemann Problem and its numerical solution'. In: *Journal of Computational Physics* 285, pp. 226–250. DOI: 10.1016/j.jcp.2015.01.011.

Rosatti, G., N. Zorzi, L. Begnudelli and A. Armanini (2015). 'Evaluation of the Trent2D model capabilities to reproduce and forecast debris-flow deposition patterns through a back analysis of a real event'. In: *Engineering Geology for Society and Territory - Volume 2, Acts of: International Association of Engineering Geology and the Environment IAEG XII Congress*. Ed. by G. Lollino, D. Giordan, G. Crosta, J. Corominas, R. Azzam, J. Wasowski and N. Sciarra. Torino / Italy: Springer International Publishing, pp. 1629–1633. DOI: 10.1007/978-3-319-09057-3_290.

Rosatti, G., N. Zorzi, D. Zugliani, A. Rizzi, S. Piffer and L. Rech (2016). 'TRENT2D WG : a smart, web-based modelling solution to assess debris-flow hazard in mountain regions'. In: *XXXV Convegno Nazionale di Idraulica e costruzioni Idrauliche*.

Ed. by A. Castellarin, R. Archetti, E. Baratti, M. Cappelletti, F. Carisi, A. Domeneghetti, M. G. Gaeta, A. Paci, S. Persiano, A. Pugliese and A. Samaras. Bologna / Italy: Department of Civil, Chemical, Environmental, Material Engineering of the University of Bologna, pp. 1067–1070. DOI: 10.6092/unibo/amsacta/5400.

Rosatti, G., N. Zorzi, D. Zugliani, S. Piffer and A. Rizzi (2017). 'A Web service ecosystem for high-quality, cost-effective debris-flow hazard assessment'. In: *Environmental Modelling & Software* (in press).

Roth, A. and W. H. Hager (1999). 'Underflow of standard sluice gate'. In: *Experiments in Fluids* 27.4, pp. 339–350. DOI: 10.1007/s003480050358.

Rulot, F., B. Dewals, S. Erpicum, P. Archambeau and M. Pirotton (2012). 'Modelling sediment transport over partially non-erodible bottoms'. In: *International Journal for Numerical Methods in Fluids* 70.2, pp. 186–199. DOI: 10.1002/fld.2684. arXiv: fld.2684Modelling [10.1002].

Sanders, B. F., A Luke, J. E. Schubert, H. R. Moftakhari, A Agha Kouchak, R. A. Matthew, K Goodrich, W Cheung, D. L. Feldman, V Basolo, D Houston, K Serrano, D Boudreau and A Eguiarte (2016). 'Co-development of coastal flood models: Making the leap from expert analysis to decision support.' In: *Sustainable Hydraulics in the Era of Global Change. Advances in Water Engineering and Research*.

Scheidl, C. and D. Rickenmann (2011). 'TopFlowDF - A simple gis based model to simulate debris-flow runout on the fan'. In: *Italian Journal of Engineering Geology and Environment*, pp. 253–262.

Schwindt, S., M. Franca, G. De Cesare and A. Schleiss (2017). 'Analysis of mechanical-hydraulic bedload deposition control measures'. In: *Geomorphology* 295, pp. 467–479. DOI: 10.1016/j.geomorph.2017.07.020.

Sepúlveda, C., M. Gómez and J. Rodellar (2009). 'Benchmark of discharge calibration methods for submerged sluice gates'. In: *Journal of Irrigation and Drainage Engineering* 135.5, pp. 676–682. DOI: 10.1061/(ASCE)IR.1943-4774.0000013.

Shan, T. and W. Hua (2006). 'Solution Architecture for N-Tier Applications'. In: *2006 IEEE International Conference on Services Computing (SCC'06)*. IEEE, pp. 349–356. DOI: 10.1109/SCC.2006.99.

Shewchuk, J. R. (1996). 'Triangle: Engineering a 2D Quality Mesh Generator and Delaunay Triangulator'. In: *Applied Computational Geometry: Towards Geometric Engineering* 1148, pp. 203–222. DOI: 10.1007/BFb0014497.

Shewchuk, J. R. (2002). 'Delaunay refinement algorithms for triangular mesh generation.' In: *Computational Geometry* 22, pp. 21–74. DOI: doi:10.1016/S0925-7721(01)00047-5.

Speerli, J., W. H. Hager, M. G. Webby and J. S. Montes (1999). 'Discussions and Closure: Irrotational Flow and Real Fluid Effects under Planar Sluice Gates'. In: *Journal of Hydraulic Engineering* 125.2, pp. 208–213. DOI: 10.1061/(ASCE)0733-9429(1999)125:2(208).

Spinewine, B., H. Capart, M. Larcher and Y. Zech (2003). 'Three-dimensional Voronoi Imaging Methods For The Measurement Of Near-wall Particulate Flows'. In: *Experiments In Fluids* 34.2, pp. 227–241. DOI: 10.1007/S00348-002-0550-4.

Stancanelli, L. M. and E. Foti (2015). 'A comparative assessment of two different debris flow propagation approaches âĂŞ blind simulations on a real debris flow event'. In: *Natural Hazards and Earth System Science* 15.11, pp. 735–746. DOI: 10.5194/nhess-15-735-2015.

Stoffel, M., D. Tiranti and C. Huggel (2014). 'Climate change impacts on mass movements - Case studies from the European Alps'. In: *Science of the Total Environment* 493, pp. 1255–1266. DOI: 10.1016/j.scitotenv.2014.02.102.

Sun, Z., I. Lorscheid, J. D. Millington, S. Lauf, N. R. Magliocca, J. Groeneveld, S. Balbi, H. Nolzen, B. Müller, J. Schulze and C. M. Buchmann (2016). 'Simple or complicated agent-based models? A complicated issue'. In: *Environmental Modelling & Software* 86.3, pp. 56–67. DOI: 10.1016/j.envsoft.2016.09.006.

Swamee, P. K. (1992). 'Sluice-Gate Discharge Equations'. In: *Journal of Irrigation and Drainage Engineering* 118.1, p. 56. DOI: 10.1061/(ASCE)0733-9437(1992)118:1(56).

Takahashi, T. (1978). 'Mechanical characteristics of debris flow'. In: *Journal of the Hydraulics Division* 104.HY8, pp. 1153–1169.

Takahashi, T. (1987). 'High velocity flow in steep erodible channels'. In: *Proceedings of the 22nd Congress of IAHR*. Lausanne, pp. 42–53.

Takahashi, T. (2007). *Debris Flow: mechanics, prediction and countermeasures*. London, UK: Taylor & Francis, pp. 1–465. DOI: 10.1201/9780203946282.

Tan, X., L. Di, M. Deng, F. Huang, X. Ye, Z. Sha, Z. Sun, W. Gong, Y. Shao and C. Huang (2016). 'Agent-as-a-service-based geospatial service aggregation in the cloud: A case study of flood response'. In: *Environmental Modelling & Software* 84, pp. 210–225. DOI: 10.1016/j.envsoft.2016.07.001.

Toro, E. F. (1989). 'A Weighted Average Flux Method for Hyperbolic Conservation Laws'. In: *Proceedings of the Royal Society A: Mathematical, Physical and Engineering Sciences* 423.1865, pp. 401–418. DOI: 10.1098/rspa.1989.0062.

Toro, E. F. (2001). *Shock-capturing methods for free-surface shallow flows*. John Wiley & Sons, pp. 1–309.

Toro, E. F. (2009). *Riemann solvers and numerical methods for fluid dynamics*, p. 724. DOI: 10.1007/978-3-540-49834-6.

Toro, E. F., M Spruce and W Speares (1994). 'Restoration of the contact surface in the HLL-Riemann solver'. In: *Shock Waves* 4.1, pp. 25–34. DOI: 10.1007/BF01414629.

Tsubaki (1972). 'Keikoku taiseki dosha no ryndo'. In: *XXVII Japanese National Congress on Civil Engineering*.

UE (2007). *Flood Directive*. 2007/60/EC.

Valentin, F. (1968). *Eingluss des Unterwasserstandes auf die Strömungsverhältnisse beim Ausfluss unter einer Schütze*.

van Leer, B. (1979). 'Towards the ultimate conservative difference scheme. V. A second-order sequel to Godunov's method'. In: *Journal of Computational Physics* 32.1, pp. 101–136. DOI: 10.1016/0021-9991(79)90145-1.

VanDine, D. F. (1996). 'Debris Flow Control Structures for Forest Engineering'.

Varnes, D. J. (1978). 'Slope Movement Types and Processes'. In: *Transportation Research Board Special Report* 176, pp. 11 –33.

Venkatakrishnan, V. (1995). 'Convergence to steady state solutions of the euler equations on unstructured grids with limiters.pdf'. In: *Journal of Computational Physics* 118, pp. 120–130.

Veronesi, E. (2017). 'Problematiche nella ricostruzione modellistica di eventi di colate detritiche: il caso del Rio Lazer del 1966'. MSc thesis (in Italian). University of Trento.

Wang, C., S. Li and T. Esaki (2008). 'GIS-based two-dimensional numerical simulation of rainfall-induced debris flow'. In: *Natural Hazards and Earth System Science* 8.1, pp. 47–58. DOI: 10.5194/nhess-8-47-2008.

Wolfram, S. (1984). 'Cellular automata as models of complexity'. In: *Nature* 311.5985, pp. 419–424. DOI: 10.1038/311419a0.

Wright, N. G. and D. Hargreaves (2013). 'Environmental applications of Computational Fluid Dynamics'. In: *Environmental Modelling: Finding Simplicity in Complexity*. Ed. by J. Wainwright and M. Mulligan. Second Edi. John Wiley & Sons, Ltd, pp. 91–109.

Wu, J., G. Chen, L. Zheng and Y. Zhang (2013). 'GIS-based numerical simulation of Amamioshima debris flow in Japan'. In: *Frontiers of Structural and Civil Engineering* 7.2, pp. 206–214.

Wu, S. and N. Rajaratnam (2015). 'Solutions to Rectangular Sluice Gate Flow Problems'. In: *Journal of Irrigation and Drainage Engineering* 141.12, p. 06015003. DOI: 10.1061/(ASCE)IR.1943-4774.0000922.

Wu, W. and S. Wang (2008). 'One-dimensional explicit finite-volume model for sediment transport'. In: *Journal of Hydraulic Research* 46.1, pp. 87–98. DOI: 10.1080/00221686.2008.9521846.

Yin, L., J. Zhu, X. Zhang, Y. Li, J. Wang, H. Zhang, X. Yang2 and X. Yang (2015). 'Visual analysis and simulation of dam-break flood spatiotemporal process in a network environment'. In: *Environmental Earth Sciences* 74.10, pp. 7133–7146. DOI: 10.1007/s12665-015-4418-3.

Zasso, M. (2015). 'La colata detritica del torrente Grand Valey (AO): dal caso di studio alla derivazione di criteri metodologici per la ricostruzione modellistica'. MSc thesis (in Italian). University of Trento.

Zhang, S. (1993). 'A Comprehensive Approach to the Observation and Prevention of Debris Flows in China'. In: *Natural Hazards* 7.1, pp. 1–23. DOI: 10.1007/BF00595676.

Zhang, Y. (2011). 'Web-Based Spatial Decision Support System and Watershed Management with a Case Study'. In: *International Journal of Geosciences* 02.03, pp. 195–203. DOI: 10.4236/ijg.2011.23021.

Zhao, D. H., H. W. Shen, G. Q. Tabios, J. S. Lai and W. Y. Tan (1994). 'Finite-volume two-dimensional unsteady-flow model for river basins'. In: *Journal of Hydraulic Engineering* 120.7, pp. 863–883. DOI: 10.1061/(ASCE)0733-9429(1994)120:7(863).

Zimmermann, M. N. (2005). 'Analysis and management of debris-flow risks at Sörenberg (Switzerland)'. In: *Debris-flow Hazards and Related Phenomena*. Ed. by M. Jakob and O. Hungr. Berlin, Heidelberg: Springer, pp. 615–634. DOI: 10.1007/3-540-27129-5_24.

Zorzi, N., A. Rizzi, D. Zugliani, S. Piffer and G. Rosatti (2015). 'Strumenti per la modellazione di colate detritiche e la mappatura del pericolo: sviluppo di una SDI con servizi di elaborazione, basata sul modello numerico TRENT2D'. In: *ASITA 2015*. Ed. by ASITA. Lecco (Italy), pp. 787–794.

Zorzi, N., G. Rosatti, D. Zugliani, A. Rizzi and S. Piffer (2016a). 'Equipping the TRENT2D model with aWebGIS infrastructure: A smart tool for hazard management in mountain regions'. In: *Sustainable Hydraulics in the Era of Global Change*. Ed. by S. Erpicum, B. Dewals, P. Archambeau and M. Pirotton. London, UK: CRC Press, pp. 819–826. DOI: 10.1201/b21902-137.

Zorzi, N., G. Rosatti, D. Zugliani, A. Rizzi and S. Piffer (2016b). 'New technology in debris-flow modelling: A WebGIS integrated solution for TRENT2D'. In: *River Flow 2016*. Ed. by G. Constantinescu, M. Garcia and D. Hanes. St. Louis: CRC Press, pp. 1924–1931. DOI: 10.1201/9781315644479-301.

Zugliani, D. (2015). 'Two-phase modelling of debris flow over composite topography : theoretical and numerical aspects'. PhD thesis. University of Trento.

Zugliani, D., M. Pasqualini and G. Rosatti (2017). 'Dynamic transition between fixed- and mobile-bed : mathematical and numerical aspects'. In: *EGU General Assembly 2017*. Vol. 19. Vienna, p. 7512.